ENHANCING THE HEAT AND INTERPARTICLE MASS TRANSFER OF ADSORPTION COOLING AND DESALINATION SYSTEMS

HANDSOME BANDA

Doctor of Philosophy

ASTON UNIVERSITY

February 2024

ABSTRACT

Enhancing the Heat and Interparticle Mass Transfer of Adsorption Cooling and Desalination Systems

Handsome Banda

Doctor of Philosophy

2024

Adsorption systems which utilise low-temperature renewable and waste heat sources, have emerged as a feasible alternative to conventional water desalination and cooling systems, despite their poor heat and mass transfer performance. This PHD project experimentally and computationally studies the utilisation of graphene oxide (GO) of a few atomic layers as a parent adsorbent material owing to its reported high thermal performance potential, the development and investigation of new composites employing few-layered graphene platelets GNP and ionic liquids (IL), namely ethyl-methylimidazolium methane sulfonate ($EMIMCH_3SO_3$) and Ethyl-methylimidazolium-chloride (EMIM Cl) and new consolidated composite synthesised from GNP, (EMIMCl) / ($EMIMCH_3SO_3$) and binder Polyvinyl alcohol (PVA).

The impact of the Graphene oxide, few-layered graphene platelets, and the developed composites thermal properties (thermal diffusivity) and water adsorption properties of were experimentally investigated. Benchmarking them against the widely investigated silica gel (SG) adsorbent, emphasising adsorption cooling cum desalination application. Besides, the overall cyclic performance was studied experimentally at the material level. A 2D computational dynamic model was developed and employed to envisage the dynamic heat and mass transfer of a packed bed (component level) configuration. The thermal diffusivities and adsorption characterisation of the adsorbents were experimentally investigated and empirically modelled. The results showed that GO enhances thermal performance by 44% compared to silica gel and adsorption uptake by up to 57%. Furthermore, GO compared to silica gel, enhanced the system's SDWP by 44.4%, SCP by 29.5%, COP by 17.2% and exergy efficiency by 15.8%.

The GP/IL composites showed higher thermal diffusivities and the highest thermal diffusivity was 11.84 mm^2/s for GP-CH_3SO_3-10, 394 times higher than silica gel. The cumulative advanced adsorption and thermal characteristics of the developed composites resulted in higher cyclic performance by up to 82% and 85% than silica gel. At system level the SDWP, SCP, COP and exergy efficiency for the GP-CL-30 based system was 60%, 70.5 %, 38.5% and 30% higher than the SG-based system. The consolidated composite GP-CL-30-CP7 showed the highest thermal diffusivity of 4.652 mm^2/s which was 12.7 times higher than SG. System level performance of the highest performing consolidated composite GP-CL-30-CP1 based system for SDWP, SCP, COP, and exergy efficiency was 95%, 75%, 76% and 68% higher than the SG-based system.

Keywords: Graphene Oxide, Silica gel, Graphene, Composite sorbents. Ionic liquids, Exergy analysis, adsorption cooling, Desalination, Water, computational modelling

ACKNOWLEDGMENT

First and foremost, I would like to express my humble gratitude to God, the source of wisdom and enlightenment, without whom this great achievement would not been possible. His abundant love has constantly sustained me in time of challenges and illuminated my path in pursuit of knowledge and fulfilment of academic aspirations.

I would like to express my profound gratitude to my supervisor DR A Rezk for his support and invaluable guidance throughout the research process. His expertise and insightful feedback have been instrumental in shaping this thesis.

I am also grateful to my associate supervisor DR A.K Hossain for his support, valuable support, and constructive feedback during this research.

I extend my heartfelt appreciation to my parents Rev J.C Banda and Mrs M Banda for their unwavering love, prayers, and support in moments of doubt which provided me with the confidence to navigate the complexities of academia. Special thanks to my siblings Emmanuel, Thokozani and Shadreck for their words of encouragement and support which have been a constant source of inspiration throughout my studies.

I extend my deepest gratitude to my wife Chipo and children Tinayeishe and Nia for their endless patience, unwavering love, encouragement, and sacrifice that have fuelled my determination to excel.

Special thanks to Prof B.B Saha, Dr T Rupam, Dr Z. Visak, Dr Q. Yuan, J. Hammerton and S. Mwangi for their assistance and collaboration during my research.

Lastly, I am indebted to the Royal Society for their financial support.

PUBLICATION

Banda, H., Rupam, T. H., Rezk, A., Visak, Z., Hammerton, J., Yuan, Q., & Saha, B. B. (2024). Preparation and assessment of ionic liquid and few-layered graphene composites to enhance heat and mass transfer in adsorption cooling and desalination systems. *International Journal of Heat and Mass Transfer*, *221*, Article 125095. Advance online publication.

Banda, H., Rezk, A., Elsayed, E., & Askalany, A. (2023). Experimental and computational study on utilising graphene oxide for adsorption cooling and water desalination. *Applied Thermal Engineering*, *229*, Article120631.

Banda, H., Rezk, A., & Hossain, A. K. (2021). Investigation of few-layered Graphene based adsorbents for hybrid adsorption cooling and water desalination. In *16th Conference on Sustainable Development of Energy, Water and Environment Systems (SDEWES)*

TABLE OF CONTENTS

LIST OF ABBREVIATIONS

Nomenclature

C_p	Specific heat capacity	[kJ kg^{-1}K^{-1}]
d	Tube diameter	[m]
D_h	Hydraulic diameter	[m]
D_s	Surface diffusivity	[m^2 s^{-1}]
D_{so}	Pre-exponential coefficient	[m^2 s^{-1}]
E_a	Activation energy	[kJ mol^{-1}]
h	Enthalpy	[kJ kg^{-1}]
h	Height	[m]
l	Tube length	[m]
k	Thermal conductivity	[W m^{-1} K^{-1}]
K_o	Adsorption constant	[KPa^{-1}]
$k_s\alpha_v$	Diffusion time constant	[-]
M	Mass	[kg]
$\dot{m}$	Mass flowrate	[kg/s]
P	Pressure	[Pa]
p	Fin pitch	[m]
Pr	Prandtl number	[-]
Q	Heat transmitted	[J]
Q_{st}	Heat of adsorption	[*kJ kg^{-1}*]
R	Gas law constant	[kJ kmol^{-1}K^{-1}]
t	Time	[s]
T	Temperature	[K] [℃]
q	Uptake	[kg kg^{-1}]
q_o	Equilibrium uptake	[kg kg^{-1}]
R_p	Particle radius	[m]
Re	Reynolds number	[-]

Greek

μ	Dynamic viscosity	*[Pa s]*
ρ	Density	*[kg m^{-3}]*
α	Thermal diffusivity	*[mm^2 s^{-1}]*
δ	Fin thickness	*[m]*
v_g	specific volume	*[m^3 kg^{-1}]*
η	Efficiency	

Subscripts

ad	adsorbent
ads	adsorption
cw	cooling water.
chw	chilled water
cond	condenser
des	desorption
evap	evaporator
f	Fin
hex	heat exchanger
hw	heating water
i	inner
in	inlet
o	outer
out	outlet
sat	saturation

Nomenclature

COP	Coefficient of performance
CFD	Computational fluid dynamics
CNT	Carbon Nanotubes
FDM	Finite element method
FEM	Finite difference method
FVM	Finite volume Method
GCI	Grid Convergence Index
GP/IL	Graphene nanoplatelets/Ionic liquid
GN	Graphene nano platelets
GO	Graphene oxide.
IL	Ionic liquid
HCFC	Hydrochlorofluorocarbon
HTF	Heat transfer fluid
PDM	Partial differential equation
SCP	Specific colling power
SDWP	Specific daily water production
SG	Silica gel
UDF	User defined functions
Wt%	Percentage weight ratio

LIST OF TABLES

LIST OF FIGURES

CHAPTER 1: INTRODUCTION

1.1 Introduction

The increasing scarcity of clean water sources for human consumption and economic development of countries is an issue that needs to be seriously addressed. Increasing world population and the effects of climate change is not helping the situation. About 36% of the world's population lives in areas that encounter high degree of water stress and the increasing water scarcity has resulted in over 2 billion people not having access to fresh water supplies globally [1]. Several countries face water scarcity especially in the Gulf cooperation council (GCC) also heat stressed of ambient temperature above 40℃ [1]. Therefore, there has been an increasing demand for brackish and seawater desalination to address such challenges [2]. Most countries facing water scarcity are focussing on desalination of both sea water and brackish water [3]. Desalination is a water treatment process by which dissolved salts and impurities are removed from seawater and brackish water to produce fresh water.

Currently most of the desalinated water is produced through the conventional desalination processes such as Multi-stage Flash, Multi-Effect Desalination, Reverse Osmosis, and the Electro-dialysis. These traditional desalinations are linked to direct consumption of fossil fuel as a primary energy source even for generating electricity for their operation. More interestingly, societies facing water scarcity and heat stressed require sustainable cooling for comfort and food preservation [1]. Like conventional water desalination systems (e.g., Multi-effect desalination, reverse osmosis and multistage flash), vapour compression cooling systems are predominantly employed that is energy intensive and utilise high global warming potential refrigerants such as R410a and R134a for residential and mobile air conditioning cooling [4, 5].

Considering the Montreal Protocol and the Kigali amendment of the Montreal protocol, measures have been put in place to phase out the use of the refrigerants that have long-lasting adverse environmental impacts, such as hydrochlorofluorocarbon (HCFC) and Chlorofluorocarbon (CFC) by 2030 in developed countries and 2040 in developing counties. However, a considerable number of applications in highly populated and developing countries are still utilising these refrigerants [6]. The increase in urbanisation in developing countries and other countries like Nigeria, India and China, has seen an increase in cooling services for space cooling and products refrigeration. In 2018, the global cooling service electricity consumption was 3900 TW, about 17% of the global electricity and is expected to increase threefold by 2050 [6]. Moreover, the increasing energy consumption for cooling raises major environmental concerns related to energy production and thermal pollution [1, 7].

To curb the impact of fluorinated gas emissions and restrict the use of the fluoride refrigerants, regulations such as the European Union regulation EU No. 517/2014 were established to ban the

use of vapour compression equipment using these refrigerants[8]. Of late several refrigerants with low GWP <1 and zero ozone depletion potential (ODP) such as ammonia (R717) carbon dioxide R744, propane (R209) and isobutene (R600a) have emerged as alternatives for HCFC and CFC. While these refrigerants are known to possess excellent thermodynamic properties, low GWP and zero ODP, they have high flammability levels, high toxicity and low compatibility with other materials which results in high initial costs of equipment [8, 9].

Therefore, using environmentally friendly refrigerants, such as water, methanol and ethanol, and the ability to utilise low-grade waste and renewable heat makes the adsorption system one of the most feasible alternatives to conventional desalination and cooling systems [10-13]. The thermally driven Adsorption desalination technology (AD) is becoming more feasible as an alternative process to conventional desalination processes due to its ability to produce fresh water and cooling effect. This means AD has an advantage of not consuming high energy associated with conventional desalination and at the same time efficiently utilises low temperature renewable heat sources. This means in areas where more cooling is needed than water desalination or vice versa, the AD system can control the operating conditions to either maximise water or cooling production according to the end user requirement. This dual effect is most beneficial to rural and arid locations.

Bulkiness, low heat and mass transfer in the current adsorption beds–the core component in adsorption systems – lead to low energy conversion efficiency, hence poor clean water and cooling production for the given thermal energy source [13-15]. Most recorded studies on adsorption systems focussed on enhancing the adsorption system performance by applying new adsorbents, adsorbent-bed heat exchange designs and adsorption cycle layouts [16-18]. However, the poor heat transfer, specifically at the material level remains challenging. In response to such challenges, this thesis contributes to the current knowledge standing by:

(a) investigating the utilisation and applicability of a highly thermal diffusive graphene oxide (GO) as an adsorbent to improve the heat and mass transfer in the adsorption bed for adsorption cooling and water desalination process.
(b) developing novel sorption composites consisting of host matrix Graphene platelets and sorbent hydrophilic ionic liquids (IL) Ethyl-methylimidazolium-chloride (EMIM Cl) and Ethyl-methylimidazolium methane sulfonate (EMIM CH_3SO_3) to understand their applicability in sorption cooling and desalination.
(c) Developing novel sorption consolidated composites comprising of GP, IL, and Polyvinyl alcohol (PVA) binder, to cultivate an understanding of utilising consolidated composites for sorption cooling and desalination application.

The thesis focuses initially on the adsorbent material level development and then assessing their impact on improving the heat and mass transfer properties of the sorption and desorption processes.

The material and component cyclic level performances were determined experimentally and by employing a 2D computational heat and mass transfer modelling tool.

1.2 Objectives.

To achieve the thesis contribution outlined above, the following objectives are set out**:**

1 Experimentally investigate the thermal and adsorption characteristics of a few layered Graphene Oxide and assess its performance as a substitute for traditional adsorbents for application in adsorption cooling and desalination.

2 Develop new Graphene nanoplatelets and Ionic liquid composites and investigate the adsorption and thermal characteristics of the developed composites benchmarking against traditional baseline adsorbent silica gel.

3 Develop consolidated composites using IL/GP and a binder and investigate the impact of various binder concentration and compressional pressure on the adsorption and thermal characteristics compared to baseline adsorbent silica gel.

4 To develop and validate a 2D computational heat transfer modelling tool to predict the heat and mass transfer during adsorption/desorption processes in the adsorbent bed.

5 Perform further studies on the capabilities of the developed composites to replace traditional adsorbent silica gel based on the performance indicators such as SDWP, SCP, COP and exergy analysis at both component and system levels.

1.3 Thesis outline

The thesis consists of seven chapters. The first chapter covers the research topic introduction including the aims, objectives, and thesis outline.

Chapter Two presents the up-to-date literature review on the improvement of heat and mass transfer in adsorption systems focussing on cooling and water desalination application to identify the knowledge gap. A review of the adsorbents and comparison of their performance.

Chapter Three presents the methodology used in investigating the novel adsorbent materials including the development of a CFD modelling tool to simulate the adsorption process in the packed adsorbent bed/reactor of a two-bed system employing graphene oxide, silica gel, developed graphene nano-platelets/ionic liquid composites and the developed consolidated graphene nano-platelets/ionic liquid composites as the adsorbent bed. The tool will be used to envisage the thermal and adsorption response of the adsorbents under various operating conditions. The validation of the computational modelling will be presented at the end of this Chapter.

Chapter Four presents the experimental investigation of the thermal and adsorption properties of graphene oxide as a new adsorbent for desalination and cooling systems. The chapter includes the

experimental and computational modelling of the adsorbent packed bed utilising graphene oxide in comparison to silica gel baseline adsorbent. A study on the effect of varying the evaporator temperature, cycle time and heating source temperature on the adsorbent bed was carried out to assess the component level performance. The system level performance was assessed through the energy and exergy study.

Chapter Five presents the experimental investigation of the developed graphene nano-platelets/ionic liquid composite for cooling and desalination application. This includes material level experimental findings and the utilisation of the 2D computational modelling to investigate the adsorbent bed performance based on different cycle time, evaporator temperature and heating source temperature. Further studies on the impact of varying the ionic liquid concentrations on performance of the composite are reported.

Chapter Six presents the experimental investigation of the consolidated GNP/IL composites for cooling and desalination systems. The chapter includes the thermal and adsorption characterization findings of the consolidated composites and benchmark them against baseline adsorbent silica gel. The effect of varying compressional pressure and binder concentration on the performance of the consolidated composite is investigated. An analysis on the packed adsorbent bed performance based on varying the cycle time, heating source temperature and evaporator temperatures was presented.

Chapter Seven presents the conclusions from the thesis addressing the research objectives. The recommendation for further research work were also outlined.

CHAPTER 2 LITERATURE REVIEW

2.1 Introduction

Of all the water in the world, fresh water only makes up 2.5 % while 97.5% is salty water as shown in Figure 2.1 [19]. The water scarcity is expected to worsen due to increasing population such that by 2050, clean water demand is also expected to increase by 40% [3, 20]. Many areas that suffer from water scarcity also experience high temperatures; the demand for cooling is also increasing due to global temperature rise, urbanisation and economic growth [6].

Adsorption desalination and cooling technology utilising renewable and low temperature waste heat below 100 ℃ is emerging as the most promising method to solve the fresh water scarcity and also provide the much needed cooling in areas experiencing high temperatures [1, 3, 21]. There has been an increasing interest in the development of adsorption technology for different application because of its environmental friendliness, low cost and ability to produce high quality fresh water and chilled water for cooling at the same time [22, 23].This chapter presents a review of the adsorption system and how it can act as an alternative to conventional systems. Nevertheless, the commonly used adsorbents, their low heat and mass transfer properties leading to low specific daily water production (SDWP), specific cooling power (SCP) and coefficient of performance (COP) and applicability for adsorption cooling and desalination have been reviewed. Furthermore, the techniques used to enhance the inherently poor heat and mass transfer at adsorbent (material) and adsorber bed (component) levels during adsorption/desorption processes have been reviewed in order to establish novel approaches to enhance adsorption/desorption processes at component level.

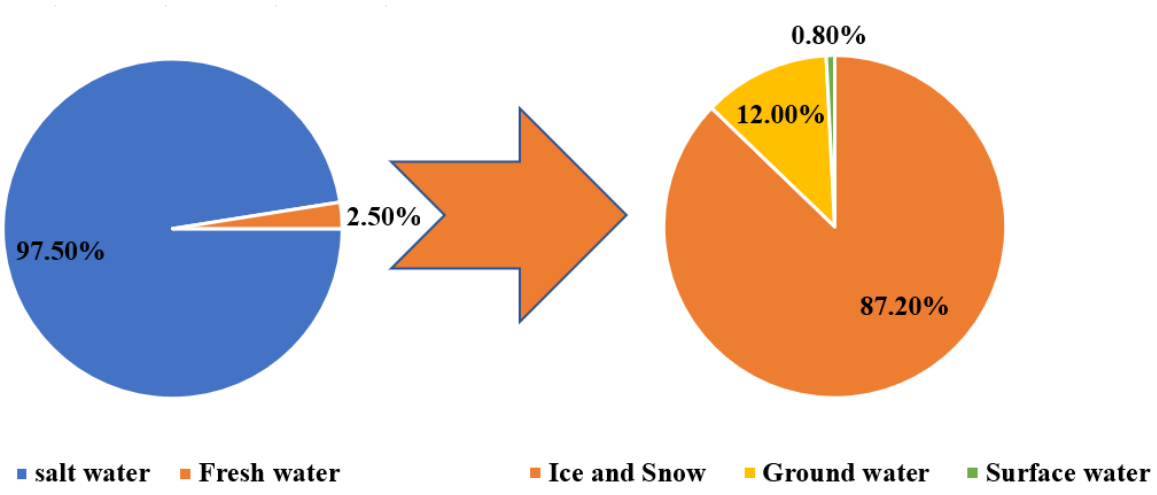

Figure 2.1: Water distribution

2.2 Adsorption phenomenon

Adsorption is defined as a physicochemical process that generally involves the mass transfer of an adsorbate i.e., liquid or gas to a surface of an adsorbent. An adsorbent is the substance on which on its surface the adsorption occurs. An adsorbate is a substance that is adsorbed by the adsorbent surfaces. Generally, the adsorption process takes place in four steps (i) bulk diffusion, (ii) external mass or film diffusion hereby the diffusion transportation from the bulk solution to the adsorbent occurs through a boundary layer, (iii) intraparticle/pore diffusion whereby mass transportation through diffusion is from external surfaces into the adsorbent's pores and (iv) chemical reaction or physical adsorption, in this cases an adsorbate molecule travels through the surrounding fluid by diffusion until it finds a vacant adsorption site on the surface of the solid adsorbent[24]. For adsorption to take place an adsorbent and adsorbate are subjected to appropriate thermodynamic conditions of temperature, partial pressure, or concentration. Figure 2.2 is a schematic diagram showing the adsorption and desorption processes. In an adsorption process energy is released when adsorbate molecules (e.g., water vapour) is adsorbed on the surface of the adsorbent. Similar amount of heat must be added when moisture is desorbed from the adsorbent surface, a process called desorption [25].

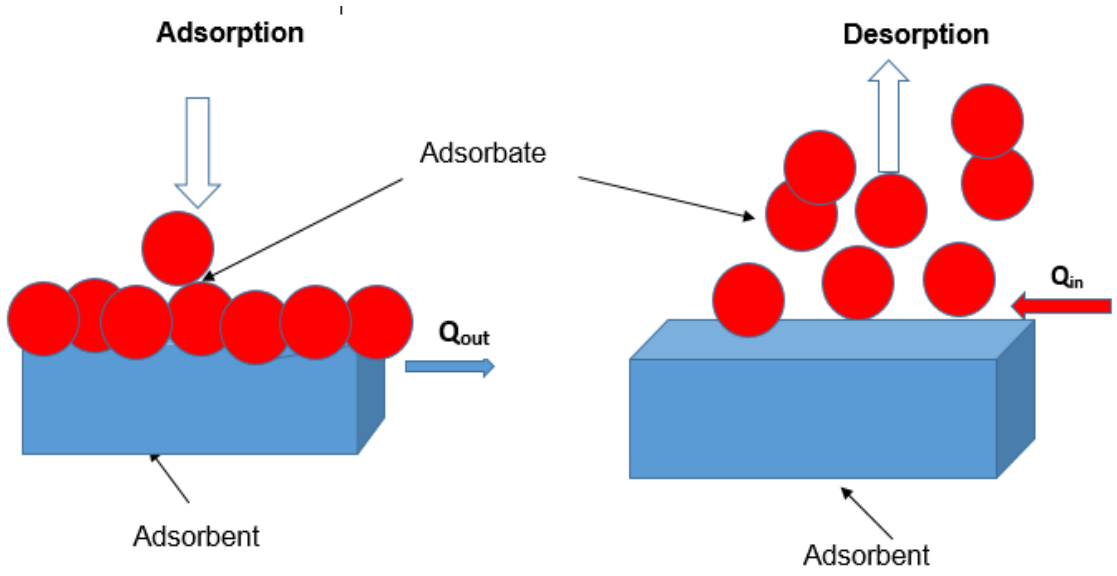

Figure 2.2 Adsorption - desorption principle

2.2.1 Types of Adsorptions

Adsorption is divided into two categories, chemical and physical adsorption. Chemical adsorption is derived from forces that make up the chemical bonds of the substance it is distinguished by the formation of chemical bonds between the adsorbent and adsorbate. Through electron pairing or transfer on the inner region surface network [24].

Physical adsorption involves the attraction of molecules of the adsorbate onto the surface of the adsorbent. Physical adsorption can be divided into three sub-categories namely: monomolecular, multi-molecular and condensation in pores or capillaries [26]. Water vapour Physical adsorption's main driving forces are van der Waal forces, hydrogen bonding, electrostatic. interaction, **π -π** interaction which involve the outer region surface networks [24]. The adsorption/desorption energy in physical adsorption ranges from 20 to 40 kJ/mol, compared to chemical adsorption which is in the range from 40 to 800 kJ/mol.

The type of physical or chemical adsorption mechanism that takes place for example the electrostatic interactions between different charged surfaces, hydrogen bonding formed by functional groups, the hydrophobic and hydrophilic interaction depend on the nature of the adsorbent and adsorbate. In physical interactions pore filling is the most prevalent adsorption mechanism in porous adsorbents whereby larger and meso-pores are initially saturated within a short time and the micropores will then be saturated after taking a longer time because of strong diffusion resistance. This means pores with sizes more than 10nm will show faster adsorption kinetics compared to micropores of less than 2 nm capillaries [24].

2.3 Adsorption cooling and desalination technology.

Adsorption cooling and desalination system (AD) can employ low temperature waste or renewable heat (e.g., solar, geothermal), typically below 100℃ to produce both desalinated water and cooling. The adsorption desalination and cooling involve evaporation/adsorption and desorption/condensation processes. The adsorbent material is responsible for adsorbing the water vapour generated in the evaporator. A typical adsorption desalination and cooling systems consists of an evaporator, condenser, and adsorbent beds. The adsorbent bed is the main part of the adsorption system that is normally packed or coated in a thin layer form. A two-bed adsorption system is a basic component that is simple and can be used to produce continuous desalinated water and cooling intermittently as shown in a two bed adsorption desalination system Figure 2.3a.

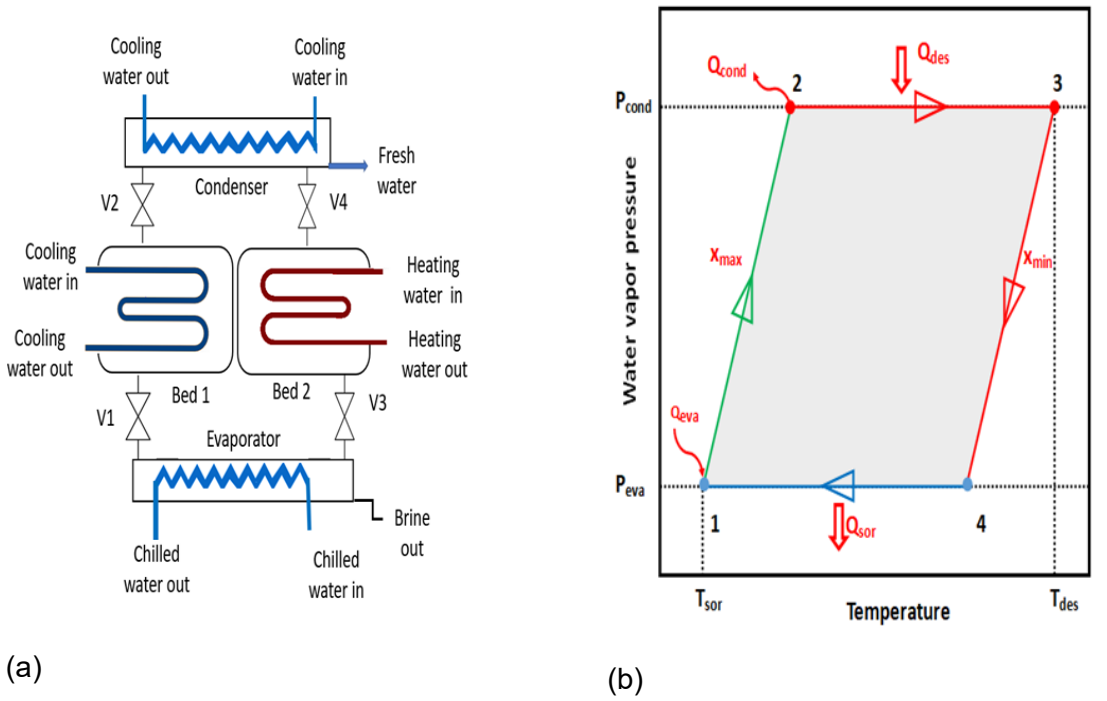

Figure 2.3: (a)A two bed adsorption cooling /desalination system (b) adsorption /desorption Cycle plot

In the adsorption desalination and cooling cycle, the driving force is adsorption and desorption reactions that take place between the adsorbent material and water vapour, Saline or brackish water is supplied to the evaporator from an external source. Valve 1 opens to allow water vapour into the adsorbent bed 1 by suction effect. The adsorbent bed which is a heat exchanger packed with adsorbents. The vapour is adsorbed by the adsorbent material until it is saturated, during this process cooling water is supplied to reduce the heat produced by the adsorption process. Once the adsorption is complete valve 1 is closed and hot water is supplied to the adsorbent material to regenerate the saturated adsorbent bed and bring the bed pressure to condenser pressure (desorption process). As desorption starts valve 2 linking the adsorbent bed and condenser opens to allow desorbed water vapour to enter the condenser where it is cooled by the cold water supplied to the condenser. When most of the water is driven off the adsorbent material cold water is circulated in bed to reduce the pressure to evaporator pressure. The cooling effect is obtained at the evaporation process as a by-product of water desalination. This means while the adsorption and desorption processes produce the desalinated water, the evaporation process produces the cooling effect at temperature ranging from 10 to 30°C [27]. For continuous process vapour from evaporator enters the adsorbent bed 2 through valve 3 when valve 1 is in closed mode. The cycle continues as explained for bed 1. The adsorption /desorption cycle consist of four operations as shown in Figure 2.3b. 1→2 isosteric heating process, 2→3 isobaric desorption process, 3→4 isosteric cooling process and 4→1 isobaric adsorption process.

2.3.1 Impact of operating conditions on the performance of adsorption system

The performance of the adsorption systems depends on various operating conditions: hot water temperature , chilled water temperature , cooling water temperature , cycle time and switching time [28]

(a) Hot water temperature

Increasing the hot water temperatures gives rise to the amount of water vapour desorbed during the desorption process hence increases the SDWP, SCP and COP [29]. Zhang et al [28] reviewed the influence of factors affecting the performance of adsorption desalination. They reported that employing a 2 bed system utilising Silica gel with heat source temperature change from 65 to 95 ^{o}C yielded an SDWP increase of 124%, SCP of 376 and 548 W/kg at 95 ^{o}C using multistage evaporators and mass recovery respectively and the COP reaching 1.6 at 95^{o}C. This information on the factors affecting adsorption desalination systems would be used to assess the performance of the new materials at component and systems levels.

(b) Chilled water

Increasing the chilled water which is the inlet temperature of the HTF to the evaporator has the effect of increasing the SDWP,SCP and COP in adsorption systems [28]. The increase in evaporation temperature also increases the evaporation pressure resulting in increased sorption capacity, hence high SDWP. On the other hand, increasing chilled water temperature increases heat of adsorption (evaporation heat), hence increase the corresponding SCP and COP [28].

(c) Cooling water Temperature

An increase in sorption and condensation temperatures reduces the sorption capacity and amount of water desorbed. Therefore, cooling water for the condensation and adsorption process in the adsorbent bed influences the SDWP, SCP and COP. Raising the cooling water temperature for the adsorption process and condensation results in low sorption heat hence, low sorption uptake exchange in the adsorbent bed and the condenser which effectively decreases the SDWP,SCP and COP [28].

(d) Switching time

The switching time is the time taken to switch saturated adsorber to desorption mode for the water vapour to be released to the condenser to complete the adsorber regeneration at the same time preparing the adsorber for sorption mode to get water vapour and cooling effect. A longer switching time allows the adsorbent bed pressure to be equal or close to evaporator pressure or condenser pressure to increase the system performance, while a shorter switching time results in insufficient precooling or preheating and reduced system performance. However, the optimal switching time depends on other operating conditions, and evaporator/condenser and adsorber configurations [28].

(e) Cycle time

The cycle time consists of the desorption, sorption and switching operation time and has a great influence on the SDWP, SCP and COP of adsorption systems. A longer cycle time allows for a higher sorption capacity attributable to higher water exchange taking place from adsorption to desorption process [28]. An increase in sorption capacity as a result of longer cycle has the effect of reducing the sorption enthalpy and thus increase COP .The optimal cycle time influences the number of cycles that can be achieved per day and varies with system configuration, working conditions and adsorbent type resulting in attaining the highest SDWP Most of the adsorption systems reported employed equal operating cycle time adsorption and desorption with switching time taking a small proportion of the cycle time [28].

2.3.2 Advantages of Adsorption cooling and desalination systems

The adsorption cooling cum desalination systems presents many advantages in comparison to traditional desalination and cooling technologies apart from mainly due to minimal electrical power usage. These include:

1. Despite its low COP, adsorption cooling and desalination system is regarded as an attractive option because it can employ low-temperature heat source such as industrial waste heat , and solar energy resulting in significant reduction of the carbon footprint of air conditioning and pure water production [28, 30].
2. It has low maintenance cost since it has few moving parts [31].
3. Its ability to be operated at low temperature prevents fouling and scaling [32].
4. It does not need a pre-treatment process which requires the use of chemicals as in reverse osmosis desalination [1].
5. Use environmentally friendly refrigerants [28].
6. Can produce both cooling and clean water simultaneously [28].
7. It has high adaptability to different feed water quality and produce high quality clean water [28].

2.4 Performance and drawback of the adsorption systems

Although AD is regarded as an efficient low energy consumption system, one of the main drawbacks is the poor heat and mass transfer. This issue results in low efficiency and less water production and poor cooling efficiency [1]. The coefficient of performance (COP) of adsorption system in cooling is very low because of very large thermal mass of the adsorbent material coupled with the intermittency of heating and cooling during the adsorption/ desorption cycle [33]. The shortcomings of adsorption systems, make the system bulky and heavy which limits its application. Table 2-1 shows the reported SDWP, SCP and COP of some adsorption cooling and desalination systems using different adsorbents which is still low for commercialisation of adsorption systems. The thermal conductivity

of materials indicates the ability of the adsorbent to conduct heat which is important in the heat transfer performance of the adsorption systems. The performance of adsorption cooling and desalination systems is greatly limited due to low thermal conductivity of the adsorbent material and their low thermal diffusivity [34-36].The recorded thermal conductivity of commonly used adsorbent pairs of Silica, Zeolites and activated carbon is approximately 0.1 to 0.4W/m/K while that of composite adsorbents ranges from 0.24 to 0.28W/m/K. The mass diffusivity of adsorbate pairs is approximately 10^{-8} to 10^{-14}m ^{2}/s [36]. This showed the need to explore new materials with higher thermal properties to improve heat transfer in adsorption systems. Table 2-2 shows the thermal conductivities of some adsorbent materials used in adsorption systems.

Table 2-1 Reported SDWP, COP and SCP adsorption cooling desalination water output.

Adsorbent	**SDWP (m^3/tonne/day)**	**COP**	**SCP (W/Kg)**	**Ref**
Activated Carbon fibre	N/a	0.6	330	[37]
$CaCl_2$ /Activated Carbon	N/A	0.41	241	[38]
Silica gel	N/A	0.4	85	[39]
Zeolite	N/A	0.9	250	[40]
$CaCl_2$/graphite	N/A	0.3	1000	[41]
Activated carbon	N/A	0.36	627.7	[42]
RD Silica gel	7.5	0.64	175	[43]
CPO-27 (Ni) MOF	22.8	N/A	760	[44]
MIL-100(Fe)	19	N/A	226	[45]
Aluminium Fumarate	13	N/A	136	[45]
AQSOA FAM-Z02	5.8	N/A	.50.1	[46]
MWCNT-embedded Zeolite 13X/$Cacl_2$	25.3	0.34	548.4	[13]
Maxsorb/$(NH_2)_4CO_3$	13.2	0.63	373	[47]

Table 2-2: The Thermal conductivities of the adsorbent in use for adsorption systems

Adsorbent	**Thermal conductivity W/m/K**	**Ref**
Silica gel- $CACl_2$	0.12	[35]
Zeolite 13X	0.1	[34]
Carbon activated	0.44	[48]
Powdered graphite / $CaCl_2$	0.3-0.4	[49]
Expanded Graphite / metal chloride	10-40	[50]
Expanded graphite/Zeolite 13 X	5-15	[51]
Expanded graphite silica gel	10-20.1	[52]

2.4.1 Current improvement on the Adsorption cooling and desalination systems

The problems associated with the adsorption systems highlights the motivation for research and innovative ways to improve the freshwater output and cooling. Various current investigations at component and material levels on enhancing the heat transfer and mass transfer in the adsorbent bed include:

(a) Component level

(i) Eliminating thermal contact resistance of heat exchanger metal part and adsorbent granules approach

Coating a heat exchanger, metal tube and metal foam with the adsorbent material was proved to enhance the heat and mass transfer. This method is effective in reducing the contact resistance between the adsorbent and the metal surface resulting in increased heat transfer rate. A coated adsorbent bed is associated with high cooling powers up to 600W/Kg [53].

(ii) The use of Fins in the reactor

The use of fins to enhance the heat transfer performance of the adsorption systems by improving the contact surface between the metallic wall of the reactor and the solid adsorbent. Al Mers et al [54], studied the optimising of cylindrical finned reactor working with activated carbon and ammonia pair. Their findings showed that increasing the number of fins reduces the heat loss to the environment. The use of fins increased the COP from 0.072 to 0.105. The recommended optimum number of fins is five or six over 250mm [54, 55]. This will help to optimise adsorbent bed design to improve its performance.

(b) Material level

(i) Adding metal particles to adsorbent granules (additives approach).

Another way of enhancing the heat transfer in adsorbent bed is the metal filling or addition approach whereby metals with higher thermal conductivity than the adsorbent material in the adsorber bed is known to increase the overall thermal conductivity of the adsorbent material [28]. Metals used as additives include copper, stainless steel, brass and Aluminium[56]. Sztekler et al [57], investigated the performance of a two-bed adsorption chiller utilising silica gel and copper additives. The results indicated that copper at 15% mass fraction showed a quick temperature stabilisation during cooling and preheating. This reduced the cooling and preheating period by 17.4% and 13.1 % respectively in comparison with beds utilising pure silica gel. The SCP and COP were increased by 3.5 and 4 times respectively. Metal with high thermal conductivity such a copper when added to the adsorbent can help quickly transfer heat within the adsorbent bed, therefore when the chiller begins the cooling or preheating, the copper will absorb or release the heat faster resulting in a quick temperature stabilisation of the adsorbent bed. Pino et al [58], investigated a composite material made from zeolite, graphite and aluminium hydroxide binder. The results showed between 3-8 times

improvement in thermal conductivity and the specific cooling power improved from 100 to 400 W/kg. This information will help to explore ways which can be used to improve adsorbents' heat transfer properties.

(ii) The development of consolidated composites

The consolidated method involves forming or moulding the composites into a suitable form such as pellets and sheets. The use of the consolidated method in developing the Graphite-$CaCl_2$ composite managed to improve the conductivity of the composite from 0.3 to 0.4W m^{-1} K^{-1} to 7.05$Wm^{-1}K^{-1}$ [59]. Experimental and numerical studies on AFI type Zeolites using the consolidated method showed that, AFI Zeolites had high specific cooling power of 500W/kg and a COP of 0.42 at regeneration temperature of 60°C. However, the drawback of the consolidated method is the increasing resistance of the mass transfer in the adsorbent bed [60].

(iii) The use of highly porous crystalline materials to improve the mass transfer performance.

The use of highly porous materials on the adsorbent bed has been proved to enhance heat transfer and mass transfer in the adsorbent bed. Metal organic framework have large surface area of 5500m^2 /g have high porosity and showed high water adsorption performance giving specific daily water production of 19m^3 /ton day^{-1} and an increase in specific cooling power by 22% [45].

(iv) Developing composites to improve the thermal properties of the adsorbents.

The use of composite adsorbents which are powders from solid adsorbents mixed/blended with other materials with high thermal conductivity improve the thermal properties of the adsorbents. Wang et al [42], developed a composite from $CaCl_2$ and Expanded graphite. The results showed an improvement in the thermal conductivity by 32 times compared to pure $CaCl_2$.

2.5 Working substances in adsorption systems

In an adsorption process, the performance of the system depends on how the solid adsorbent performs in both equilibrium and kinetic terms. The adsorption cycle efficiency in water production and cooling is dependent on the sorption characteristics of adsorbent and adsorbate. The affinity of an adsorbate for a certain adsorbent depends on the adsorbent characteristics such as shape, size and polarity, the fluid concentration or partial pressure and the system temperature [61]. While there are many materials that could be considered for adsorption not all are viable for adsorption process [33]. For desalination and cooling, the adsorbent should have the following qualities [62, 63] at (a) Material level and (b) component level.

a. Material level

- Non-corrosive and non-toxic to the environment
- Widely available and low cost
- Durable and stable under repetitive cycles to show their operability.

- High level of Hydrophilicity at low regeneration temperature

b. Component level

- High level of adsorption equilibrium uptake, preferably at low partial pressure to adsorb large amount of adsorbate at low partial pressure.
- High level of desorption of adsorbate during the regeneration when heat or thermal energy is applied to have a maximum water output.
- Not deteriorate easily in use to inhibit the convective heat transfer and diffusion of adsorbate molecules in the adsorbent.

2.5.1 Types of Adsorbents

There are three main groups of adsorbents used in adsorption systems namely chemical, composites and physical adsorbents. There are also other materials such as graphene derivatives which have been introduced as novel adsorbents for purifying waste water [64].

Chemical adsorbents are mainly metallic compounds that are used either as oxides or salts. Examples of chemical adsorbents are metal chlorides, metal hydrides and metal oxides.

The chemical adsorbents use valence forces to sorb the adsorbate chemically. They are known to sorb more adsorbate than physical adsorbent [65]. However, they have lower stability compared to physical adsorbents and hence cannot keep their original state which limits their use for adsorption application. Another downside of chemical adsorbents is their susceptibility to swelling and agglomeration which impacts negatively to their heat and mass transfer [65].

2.5.1.1 Metal oxides

Metal oxides have been used as adsorbent especially for chemisorption applications [66]. They have been widely used in water purification since the early 1950s and are regarded as promising adsorbent due to their excellent adsorption performance, ease to modify and low cost in mass production. Metal oxides adsorbents are mostly used in ions sorption. They characteristically possess a wide range of functional groups onto their surfaces. There is a wide range of metal oxide adsorbents that are in use for water purification including iron oxides, aluminium oxides, titanium oxide, magnesium oxide [24]. Just as in chemical adsorbents metal oxides experience swelling and agglomeration issues.

2.5.1.2 Metal hydrides

Metal hydrides are materials composed of metalloid or metals bonded with hydrogen and are classified by the nature of the chemical bond between the metal and hydrogen [67]. The existence of the of hydrides ions in the metal hydrides with equilibrium temperature range of 113^{o}C to above 527^{o}C, under equilibrium pressure of 1bar, provides the metal hydrides with a wide range of potential for adsorption cooling application [68].The down side of using metal hydrides/hydrogen pair is the

bulkiness of the system which has a weight almost twice that of a system operating with an evaporator and condenser [68].

2.5.1.3 Metal chlorides

Metal chlorides are mostly used in adsorption refrigeration using ammonia refrigerant. The main metal chlorides for adsorption refrigeration are barium chloride, magnesium chloride, calcium chloride, nickel chloride. The limitation of metal chlorides in adsorption application is the swelling and agglomeration associated with them which have a negative effect on the heat and mass transfer [68].

2.5.2 Physical adsorbents

The behaviour of adsorbents in adsorption differs with porous structure and the size of adsorbate. This means materials having a microporous structure are regarded as effective adsorbents for small molecules and ions [24]. Physical adsorbents are porous in nature characterised by different pore sizes and adsorb the adsorbate through Vander Waals forces whilst maintaining their original properties during adsorption/desorption processes. There are three categories namely:

(i) Microporous materials (0.2 – 2nm)

(ii) Mesoporous materials (2 - 50 nm)

(iii) Macro porous materials (> 50 nm)

Most adsorbents used commercially are porous materials with pore surface areas ranging from 100 to 1200m^2/g. This large surface area permits a large amount of adsorption to take place relative to the adsorbent [25]. They adsorb the adsorbate using Van der Waals forces. One of the attributes of physical adsorbents is their ability to retain their original properties after the desorption process. However, they experience low adsorption kinetics which results in low adsorption capacity. Examples of physical adsorbents include zeolites, mesoporous silicates, porous carbons (Activated carbon), metal organic frameworks and metal-alumino phosphates [69] .

2.5.2.1 Silica Gel

Silica gel is a commercially available adsorbent material which is usually used as a benchmark adsorbent material in adsorption desalination systems [70]. SG is a polymeric porous material with a colloidal silicic acid structure and has SiOH and SiOSi functional groups which allows it to absorb water and alcohol adsorbates. One of the attributes of SG is the ability to adsorb water 35-40 % of its dry mass and has an adsorption capacity regarded as highly stable under long operation periods at high vapour pressure [66, 71, 72]. When heated at temperature up to 120°C it loses its adsorption capacity [66]. Its regenerative capability at low temperature of 50-90°C makes it suitable for adsorption application utilising a low temperature heat source. There are three type of Silica Gel type A type B and type C [73]. Type A has particle sizes of 2-3nm (microporous)while type B has pore

size of 7-8nm (mesoporous)and type C with 9-10nm (mesoporous). Type A is used in cooling due to its large internal surface area which can allow high moisture adsorbing at low humidity. Type B and types C has larger pores which enables it to adsorb water at low temperature and desorbs it at high temperature [73]

2.5.2.2 Activated Carbon (AC)

ACs are made by a process of pyrolyzing and carbonising wood, coal, synthetic polymers, and nutshells at very high temperature between 700-800°C. The ACs from coal is the most preferred because of its physicochemical properties It is available in various forms such as granulated, microporous, carbon fibres and molecular sieves [74]. AC is known to have large porous surface area a controllable pore structure, thermal stability, a low adsorption heat and is regarded as a very flexible material in removing different type organic and inorganic substances from aqueous media [74]. Powdered activated carbon (PAC) of particles size 15-25μm is mostly used for liquid adsorption and has high diffusion resistance of adsorbed molecules [74]. The granulated activated carbon (GAC) of particle size of 0.8 to 3mm or pellet for forms has low surface area and low gas /liquid resistance are used for gas separation and water purification [66, 74]. The mesoporous AC is mainly used for the separation of nitrogen and oxygen in air [66] Despite its good properties in adsorption, it is expensive and has regeneration problem associated with high temperatures which affects its ability to regain adsorption capacity [74].

2.5.2.3 Zeolites

Zeolites also known as molecular sieves are regarded to have high potential as excellent adsorbent material and are known to maintain their structure even after adsorbing molecules during adsorption/desorption cycle [66, 75]. Zeolites belong to the group of Alumina-Silicates with high porosity. It is made from crystals to form a crystallographic structure. They have porosity of between 0.2 and 0.5. There are many types of Zeolites with different adsorption capacity named by a letter or group of letters including Zeolite X, Y and A [76]. Zeolite A and X are the commonly used adsorbents in adsorption cooling applications. They adsorb variety of adsorbates due to the inlet necks of their pores which are large [66]. Zeolites water pairs are known to have high adsorption capacity with equilibrium water uptake high at 100℃ [77]. The regeneration of zeolites can be achieved at temperatures above 350℃ [76]. Therefore, they are not suitable for application in low generation temperature sources.

2.5.2.4 Metal organic frameworks.

Conventional adsorbents, such as silica gel and zeolite, have limited adsorption capacity and poor thermal characteristics [78, 79]. Therefore, researchers devoted their efforts to developing new parent adsorbents and composites of advanced adsorption and thermal characteristics. An example of advanced tuneable parent adsorbents is metal-organic frameworks (MOF). Metal organic

frameworks (MOFs) also known as metal organic coordination polymers are crystalline microporous hybrid organic/inorganic materials formed through coordinate bonds between metal ions and organic ligands or linkers [80, 81]. MOFs show excellent tuneable functionality and exceptional surface area of up to 5500m^2/g and defined molecular adsorption sites[82, 83]. Essentially MOFs can easily adjust their physical and chemical properties by modifying organic ligands, metal centres and active functional groups compared to other solid state materials [84, 85]. However, despite these qualities, many MOFs are highly unstable, making them problematic to utilise in real-life applications. Besides, MOF's mass production is not financially viable [83, 86].

2.5.2.5 Graphene

Graphene and its derivates such as graphene oxide (GO), reduced graphene Oxide (rGO). produced from further GO treatment and graphene platelets (GNP) have recently drawn the attention of many researchers due to their advanced thermophysical characteristics, such as a large specific surface area of 2630m^2 /g and high thermal conductivity of 3000-5000W/mK [87]. Figure 2.4 shows a comparison of the structure of graphene and its derivatives. Graphene is a two-dimensional monoatomic sheet of carbon atoms arranged in a hexagonal structure with a sp^2 hybridised orbit. The carbon atoms in graphene are bonded by covalent bonds in a plane, forming monolayer sheets connected by van der Waals forces. Compared to graphite, the latter is a graphene allotrope of several atomic layers [87, 88]. Generally, graphene is produced by two methods: the top-down method and the bottom-up method. The top-down method involves graphite's structural breakdown and separating the interlayers to form graphene sheets [88]. The bottom-up method uses chemical vapour synthesis and carbon source gas to synthesise graphene substrate [87, 88]. With such attractive properties the capability of graphene derivative GO will be discussed in detail in this thesis Chapter 4, where its thermophysical properties and adsorption characteristics are experimentally investigated.

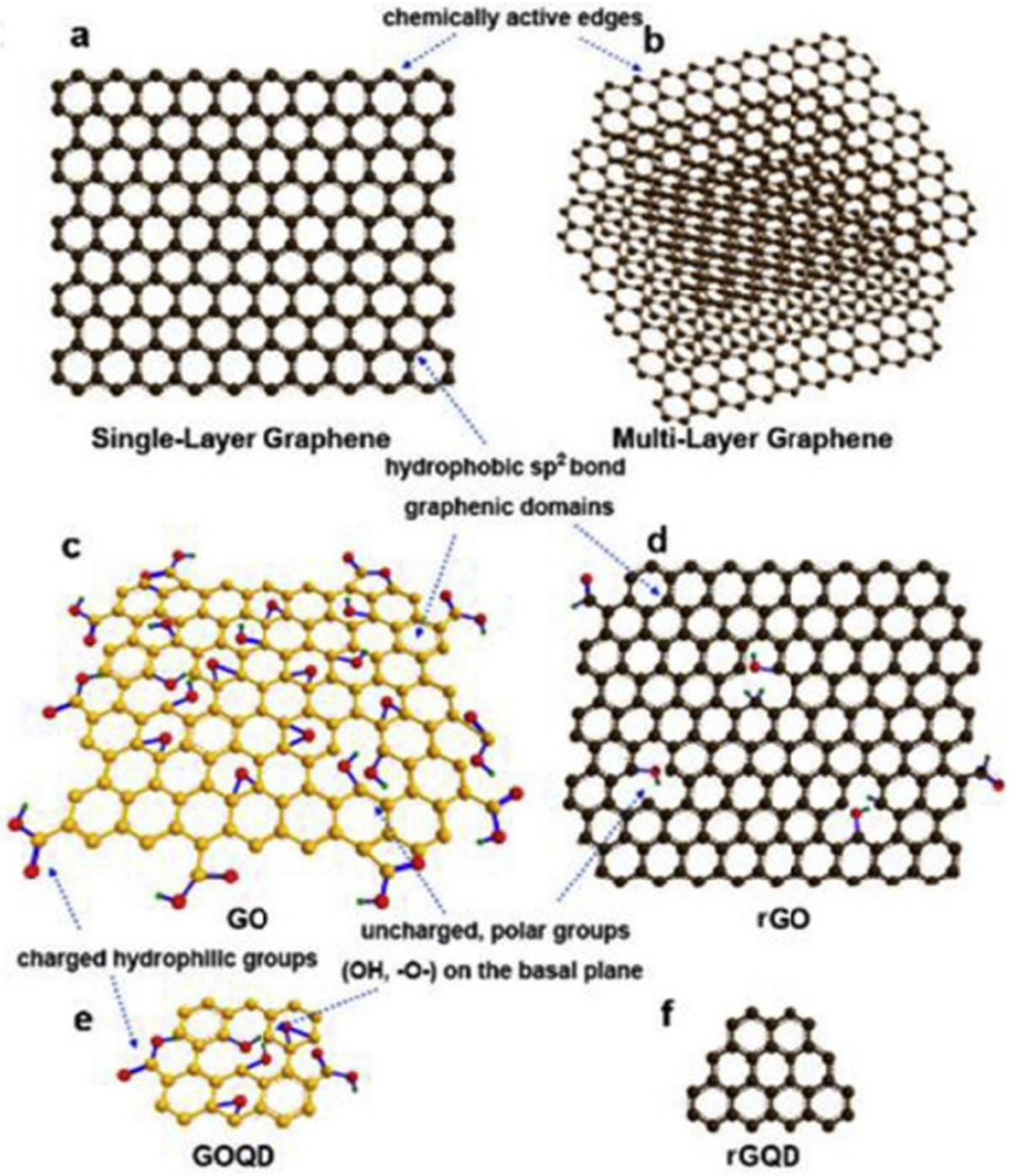

Figure 2.4: Structure of Single and Multilayer Graphene and its derivatives[89]

2.6 Composite adsorbents

The adsorption capacity of adsorbents depends on their surface chemistry and surface area. This means the availability of surface area for adsorption and the pore volume can be improved by developing a composite structure. The use of composites is designed to address the problems associated with chemical adsorbents such as agglomeration, swelling and poor heat conductivity while at the same time improve the adsorption capacity and thermal properties of physical adsorbents [66]. Conventionally, Composites are a mixture of chemical and physical adsorbents.

Researchers have developed composite adsorbents using metal salts supported by porous materials and graphite derivatives as thermal conductivity enhancers to improve the adsorbents' heat and mass transfer properties. Examples of such composites are calcium chloride / silica gel / expanded graphite, sodium bromide / expanded graphite, calcium chloride / activated carbon with expanded graphite, and Lithium chloride / activated carbon / expanded graphite. All the composites showed higher thermal conductivity and adsorption capacity than the sole parent adsorbent [51, 68, 75, 90-93]. Furthermore, adding chemical adsorbent materials with high thermal conductivity and porous structure such as expanded graphite contributed massively to enhancing the composites' thermal resistance [94]. Blending or integrating the porous adsorbent material with metal additives can be classified as composite. Examples of utilising metal additives are blending silica gel adsorbent with aluminium, stainless steel, brass and copper [56], [77, 95-97]. For instance, Aristov et al [98], studied silica gel impregnated with $LiNO_3$ as a new adsorbent composite $LiNO_3$/silica KSK (SWS-9L) for cooling and reported a 6% increase in cooling capacity compared to SG/water pair. Tanashev et al [96], investigated Silica gel KSK impregnated with three salts $CaCl_2$, $MgCl_2$ and LiBr. The three composites increased thermal conductivity 3-4 times compared to silica gel, and water adsorption increased from 0.05 to 0.7-0.9kg/kg. Tso et al [97], investigated composites for adsorption cooling by impregnating AC and Silica with $CaCl_2$ at different concentrations. Their results showed an enhancement of SCP by 372% and COP by 92%. Apart from composite from conventional adsorbents, researchers have developed composite composed of carbon nanotubes (CNT) [71]. CNT are lightweight cylindrical molecules composed of hexagonal hybridized carbon atoms which can be formed by either rolling a single sheet or multi sheets of graphene [99]. CNT is regarded to have unique properties including high thermal conductivity ranging from 1600-6000 W/mK, thermal stability, efficient heat transfer resistance, a well-developed pore structure and possesses attractive functional water transport capability [100-102]. Kulakowska et al [71], investigated the impact of aluminium, copper and CNT additives on silica gel adsorption bed. Their findings showed that all the three additives blended with silica gel improved the thermal diffusivity significantly compared to pure silica gel adsorbent.

Although the metal additives enhanced the thermal performance of the blends, a considerable amount of the effective adsorbent materials were replaced by additives that negatively affected the overall adsorption capacity [56, 103]. The most highly regarded and promising composites due to their improved sorption for commonly used adsorbate including water, ammonia and methanol are composite salts inside porous matrix (CSPM)[104]. Graphene nanoplatelets (GNP) and Ionic liquid (IL)composite synthesis, characterisation and capability as an adsorbent for cooling and desalination will be investigated and discussed in Chapter 5 of this thesis.

2.6.1 Composites inside porous matrix (CSPM)

The CSPM are made up of two material components, one is the host matrix and the other a salt deposited inside the pores of the matrix. It is this salt that reacts with the adsorbate (water or ammonia) to form a complex molecule of the salt. Many researchers have worked on improving the performance of adsorbents by developing composites with different compositions either by impregnating the hygroscopic salts into host matrix or blending the porous adsorbent such as silica gel, zeolites and activated carbon with heat transfer enhancing material. The porous matrix plays an important role in dispersing the salt particles which influences the sorption properties of the salts. This results in the heat and mass transfer to the salt particles within the matrix [104]. Restuccia et al [105], investigated a composite of silica gel and $CaCl_2$ called selective water sorbent and it was reported that an adsorption capacity of 0.7g/g, a COP of 0.6 and SCP of 20W/kg were achieved. It was concluded that the silica gel may not be a suitable host since it attains low water uptake when operating at low pressure adsorption and high-pressure desorption resulting in low COP [77]. Chan et al [77], developed and investigated a zeolite13X and $CaCl_2$ composite. Their findings showed an uptake to 0.48kg/kg. The reported enhancement on the uptake, COP and SCP were 320%, 80% and 35% respectively. While the zeolite13X /$CaCl_2$ composite has an improved performance, there is an ion exchange that takes place between the Na^+ in zeolite and Ca^{2+} which may cause changes in the composite adsorbent properties and hence reduces its performance in cooling application [77]. Zeolite is also known to have limitations in the thermal conductivity which results in poor heat transfer [106-108].

2.6.2 Consolidated composites

Consolidated composites adsorbents are a combination of porous adsorbent, thermal enhancer such as expanded graphite and a binder [4]. Consolidation usually involves the application of heat and pressure to achieve a desired structure or geometry. There are many types of binders that are in use for composite synthesis including Polyvinyl alcohol (PVA), Hydroxyethyl cellulose (HEC), Polyvinyl pyrrolidone (PVP, gelatine, Polytetrafluoroethylene (PTFE), and polymerised ionic liquid (PIL) [109, 110]. Sharafian et al [36], investigated composites made from silica gel and PVP binder. The results showed a thermal conductivity of 0.26$Wm^{-1}K^{-1}$, which was a 78% increase compared to pure Silica gel. Copper nano powder was blended with silica gel to improve its thermal performance and compressed at 2MPa. The results showed a 20% increase in thermal conductivity compared to pure silica gel. This information reported on composite development would be used for synthesis of consolidated GNP/IL composites, characterisation and adsorption capability assessment for cooling and water desalination application in Chapter 6.

2.7 Adsorption Isotherms

The equilibrium relationship between the adsorbate in the surrounding phase and the adsorbate adsorbed on the adsorbent surface at constant temperature is known as the adsorption isotherm [111]. Adsorption isotherm, adsorption kinetics and isosteric heat of adsorption are important characteristics that affects the performance of adsorption systems and provide more detail about the adsorption material properties. The adsorption isotherm characteristics are measured using two methods namely the gravimetric method and the volumetric method. Both methods are used to obtain experimental data pertaining to the uptake of water vapour at given temperatures and range of equilibrium pressures.

Adsorption isotherms present the adsorbed amount on the adsorbent as a function of its pressure or concentration at a given temperature. In adsorption systems, the interaction of adsorbates with adsorbents varies from material to material. Hence, there is a wide range adsorption isotherm models in use. The physicochemical parameters involved in the adsorption process shown in the models, could be obtained directly from the experimental isotherms. Therefore, adsorption isotherms are used to compare the adsorption capacity of adsorbents for various substances. In order to get more information about the material characteristics, it is important to measure and fit the adsorption isotherm data to the appropriate model [26].

2.7.1 Types of Adsorption isotherms

The International union of pure and applied chemistry (IUPAC) classified the physical adsorption isotherms into six types shown in Figure 2.5 [112]. The overall shape of the isotherm is determined by the nature of the gas-solid system, the pore or intermolecular spacing structure of the adsorbent and the temperature of operation [113].

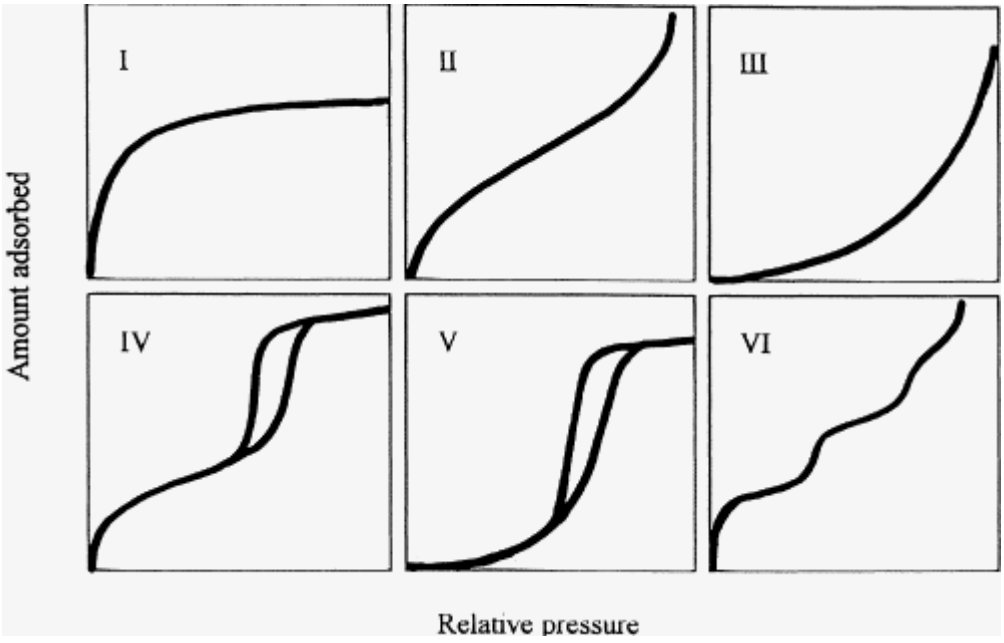

Figure 2.5: Six Isotherm types by IUPAC [112]

2.7.1.1 Type I

Type I reversible isotherms generally show a concave relationship between the adsorbed amount and the relative pressure. It applies microporous solids with small external surfaces such as molecular sieve zeolites, metal organic frameworks and activated carbons. They are usually monolayer adsorption and easy to explain with the Langmuir adsorption isotherm. The monolayer adsorption is the formation a single layer of adsorbate molecules on the adsorbent. This takes place when the adsorbate molecules interact with adsorbent surface and settles there due to the action of various forces such as van der Waals forces and chemical interactions. In a monolayer adsorption, the adsorbate molecules are closely packed, and each molecule occupies a specific site on the adsorbent surface. The rate of adsorption decreases with time as the adsorption progresses until equilibrium is attained. At equilibrium point the adsorption rate is equal to the desorption rate and the adsorbent surface will be saturated with the adsorbate molecules [114, 115].

2.7.1.2 Type II Isotherms

A reversible type II Isotherm is usually linked with monolayer – multilayer adsorption on a stable external surface of a non-porous powder and allows for monolayer – multilayer adsorption to take place at higher relative pressure. Multilayer adsorption is a process by which the adsorbate molecules adhere to the surface of the adsorbent forming multiple layers. It involves the addition of molecules on top of the initial monolayer and settle on active sites on the surface either directly or by adsorbing onto an existing molecule to form a second layer. Each subsequent layer is added as adsorption progresses and is dependent on the temperature and the strength of adsorbent adsorbate interactions. Equilibrium in multilayer adsorption is reached when the surface is covered with adsorbate molecules and the rate of adsorption is equal to rate of desorption [114, 115]. As shown in Figure 2.6, at the beginning of the adsorption process, monolayer adsorption occurs at a faster rate due to the availability of many active sites on the adsorbent surface as indicated by the concave shape. As multilayer adsorption starts, the adsorption rate slows down, and the curve slope will change from positive to negative (point of inflection) indicating the transition point from rapid monolayer adsorption to slow multilayer adsorption. The isotherm curve has an inflection point A which normally occurs near the completion of the first adsorbed monolayer followed by second and higher layers with increasing relative pressure until saturation point. At saturation point the number of layers becomes infinite [116].

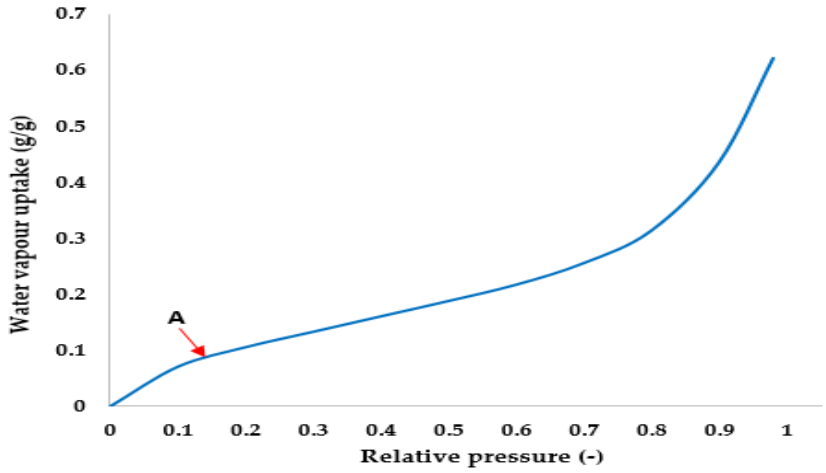

Figure 2.6: Type ii isotherm

2.7.1.3 Type III

A reversible type III is linked to unrestricted multilayer adsorption. The curve takes a convex shape over the entire adsorption range. The shape explains the strong interaction between the adsorbed molecules compared to the interactions of the adsorbent and adsorbate [114, 115].

2.7.1.4 Type IV and V

Type IV just as in type II has nonporous monolayer and multilayer adsorption taking place on the same surface area of the adsorbent. However, in both type IV and V, the isotherm, mesoporous solid adsorption involves limited multilayer adsorption then capillary condensation [115]. Type V just like type III comes from small adsorbent -adsorbate interaction [116].The capillary condensation is linked to the hysteresis loop on both curves as shown in Figure 2.5.

2.7.1.5 Type VI

It is a rare isotherm with profile steps that are dependent on the temperature and the system. it is linked to a stepwise multilayer adsorption on surfaces that are non-porous. The monolayer capacity of each adsorbed layer is represented by the step height and is constant for the next two or three layers.

2.7.2 Adsorption isotherm models

Generally, isotherm models are developed using two fundamental approaches: the kinetic approach and the thermodynamic approach [117]. In the kinetic approach, the equilibrium is considered as a state of dynamic equilibrium where both adsorption and desorption are equal. The thermodynamic approach provides the framework for deriving various forms of adsorption Isotherm models convenient to fit data and their applicability to numerical computation [118].

Choosing the adsorption isotherm model is dependent on the characteristics of the adsorption process, the application, and the nature of the adsorbate and adsorbent characteristics. There are

several adsorption isotherm models in use to model adsorption isotherms such as the Langmuir, Freundlich, Tóth, Dubnin Asthakov and Sips. These isotherms have been selected based on their wide use and flexibility in describing adsorption processes showing monolayer and multilayer characteristics.

2.7.2.1 Langmuir Isotherm

It is regarded as one of the most used models in describing adsorption data because it is suitable for various adsorption systems. Langmuir has the minimum number of parameters required for fitting a non-linear isotherm, which are adsorption equilibrium, saturation loading and heat of adsorption [117]. The formulation of this empirical model assumed monolayer adsorption i.e, the adsorbed layer is one molecule thick and occurs at definite identical fixed localised adsorption sites. Its derivation is based on homogeneous adsorption whereby each site has the same affinity for the adsorbate[119]. Langmuir isotherm is designed to fit gas- solid adsorption isotherm data [120]. To account for the surface coverage of the adsorbent, Langmuir isotherm balances the rate of adsorption and desorption. This means adsorption is proportional to the fraction of the adsorbent surface that is open, and desorption is proportional to the surface that is closed [121]. The linear expression of the Langmuir is given in Equation (2.1).

$$C_e / q_e = 1/q_m K_e + C_e/q_m \quad (2.1)$$

Where K_e is Langmuir constant, C_e is concentration of adsorbate at equilibrium[122]

2.7.2.2 Freundlich isotherm

Freundlich isotherm is an empirical model used to describe non ideal and reversible adsorption. It is widely used for organic compounds or species that are highly interactive on activated carbon. It is mostly applicable for multi-layer adsorption processes that occur on heterogeneous surfaces with non-uniform distribution of adsorption heat. The adsorbed amount is given as the summation of all adsorptions at each site and each site have its own bond energy. The distribution of the site energy decreases exponentially and those sites with stronger bond energy are first to be occupied [119].The Freundlich expression is given in equation (2.2). The expression defines the surface heterogeneity, the exponential distribution, and active sites[123].

$$\text{Log } q_e = \textit{log } K_p + \textit{1/n log } C_e \quad (2.2)$$

Where K_p is adsorption capacity and 1/n is adsorption intensity.

2.7.2.3 Sips isotherm

Sips is used to predict heterogeneous adsorption systems. Heterogeneous adsorption is whereby a gas phase adsorbate sticks or binds onto a solid surface adsorbent. It is regarded as a combined

form of Langmuir and Freundlich expressions. It reduces to Freundlich isotherm at low adsorbate while it predicts a monolayer adsorption characteristic of the Langmuir isotherm at high adsorbate concentrations. The equation parameters are dependent on temperature, pH, and concentration [119].The Sips expression is given as equation (2.3):

$$q_e = K_s\, C_e^{\beta s} / 1 + \alpha_s\, C_e^{\beta s} \quad (2.3)$$

Where K_s is Sips constant, β_s is Sips isotherm exponent and α_s is Sips isotherm model constant [119].

2.7.2.4 Tóth, equation

The Toth equation is an empirical equation(2.4) developed as an improvement of the Langmuir equation. Its development was to reduce errors between experimental and predicted equilibrium data. It is used to describe heterogeneous desorption systems this allows isotherm modelling of both high and low end boundaries of adsorbate concentration [119]. Unlike the Langmuir isotherm model which has three parameters to fit a nonlinear isotherm, the Tóth, isotherm model possesses four independent parameters which gives it extra degree of freedom [117].

$$q_e = \frac{K_T C_e}{(\alpha_T + C_e)^{\frac{1}{t}}} \quad (2.4)$$

2.7.2.5 Dubinin-Astakhov (D-A)

The D-A is origins is traced back to the Polanyi adsorption potential for micro pore filling and derived from the Dubinin theory. It is applied to describe adsorption data in microporous sorbents mostly in the micropore volume be it in liquid -solid or gas-solid adsorption systems. It can accurately linearise adsorption data over a varied range of relative pressure. This make its application more suitable where the pressure range is very low between 10^{-5} to 0.8Pa. It is most suitable to apply the D-A where the whole range of the micro filling adsorption isotherm is required unlike where data over a limited relative range [124].

$$V = V_o \exp\left(-\left[\frac{A}{\beta E_0}\right]^n\right) \quad (2.5)$$

Where V_o is the material's limiting micropore uptake, V is the gas uptake at a given adsorption potential A, E_0 is the characteristic adsorption potential related to size of pores and $\boldsymbol{\beta}$ is the affinity coefficient that permits the correlation of results from other different adsorbates [124].

2.8 Enhancing the heat and mass transfer in adsorbent bed

The main aims in utilising the heat exchangers in adsorber bed are to enlarge and improve heat transfer surface area between adsorbent particles and heat transfer fluid (HTF) during

adsorption/desorption processes, while decreasing the mass transfer resistance between the adsorbent particles and adsorbate [125]. There are many adsorbent beds that have been adopted to increase the heat transfer in adsorbent bed which are heat exchanger design, adsorbent coating and metal filling and using polyaniline net.

2.8.1 Adsorbent bed design

The adsorbent bed is the main component of any adsorption system and its configuration and design have a huge influence on the mass and heat transfer to fully realise the potential of the adsorbent materials [28]. There are various adsorber beds design used in adsorption applications including finned tube heat exchanger (rectangular/square or annular), finned double tube heat exchanger, plate heat exchanger and metal foam [125-127].

2.8.1.1 Finned tube heat Exchanger

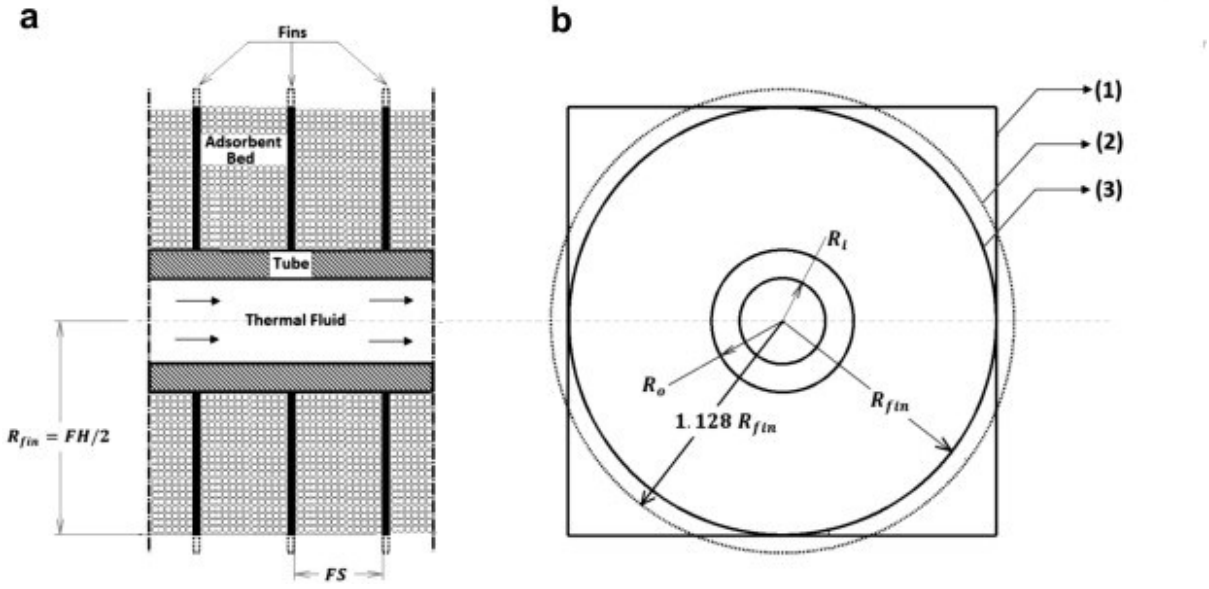

Figure 2.7: (a) adsorbent bed (b) Finned tube geometries (1) squarer (2) annular (3) annular with same volume as square fins[128]

A finned tube heat exchanger Figure 2.7 is composed of a metal tube on which a series of fins have been added on the outside of the tube and porous media is placed in between the fins [128]. The heat transfer fluid (HTF) flows through the tube across the length of the tube. The finned tube heat exchanger provides a large surface area due to the presence of fins and that improves the heat and mass transfer in the bed significantly. This has an effect of reducing cycle time. Hence, the finned tube heat exchangers are the most used heat exchangers in adsorption systems. A finned tube heat exchanger utilising $CaCl_2$ in silica gel sorbent gave a COP of 0.5 and SCP of 600W/kg compared to COP of 0.4119 and SCP of 429.8W/kg of a plate heat exchanger using the same adsorbent [129]. Further improvements on the adsorbent bed can be realised by optimisation of bed configurations

such as fin length, fin spacing and fin length. For these reasons Finned tube heat exchangers are considered to perform better than other adsorbent bed designs [125].

2.8.1.2 Finned double tube heat exchanger (FDHX).

The finned double tube heat exchanger Figure 2.8 has two tubes the inner tube and the outside tube. The HTF passes through the inner tube to provide or remove the heat to the adsorbent bed which is insulated outside the outer tube. The adsorbent material is packed and covered with a net between the welded fins which are symmetrically distributed on the inner tube. The water vapour is allowed to flow through the space between the outer tube and net. The transfer of the water vapour in the adsorber through the net can occur either axially or radially and this reduces the mass transfer resistance in adsorbent. FDHX has an insulation layer which prevents heat loss. The performance of finned double tube can be improved by applying various fin geometries such as straight, helical, parabolic, and triangular fins to be attached to outer surface area of the inner and provide a large heat transfer area which improves the heat transfer efficiency between the bed and the surrounding fluid. The enhanced rate of heat transfer and large heat transfer area allows for precise temperature control within the adsorbent bed. Other measures taken to improve the heat transfer efficiency and durability of the finned double tubes included constructing them using alloys and coatings with enhanced heat transfer properties [130].

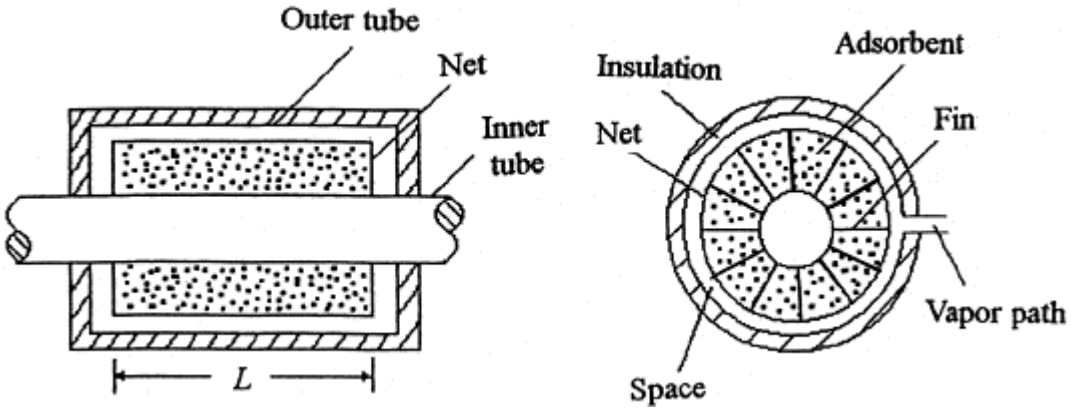

Figure 2.8: finned double tube annulus heat exchanger[126].

2.8.1.3 Plate heat exchanger (Plate HX)

The plate HX Figure 2.9 is a compact size adsorbent bed made up of many thin plates with engraved patterns. The adsorbent particles are overlayed between the thin plate's channels created by the engraved patterns. HTF and vapour flows orthogonally in the bed. The HTF flow in the gap between two plates is interrupted by engrave patterns on the plates. This has an effect of enhancing the heat transfer capacity [129]. Hong et al [129], applied a Plate on adsorption chiller utilising SWS-IL and water pair which resulted in a COP of 0.5118 and a SCP of 662.8W/kg. in comparison with a finned tube HX, the plate HX's COP was 19.9% lower while the SCP was 15.7% higher than the finned HX.

The plate HX has the advantage of improved heat transfer within the adsorbent bed and compactness which reduces the bulkiness of the adsorption systems [129].

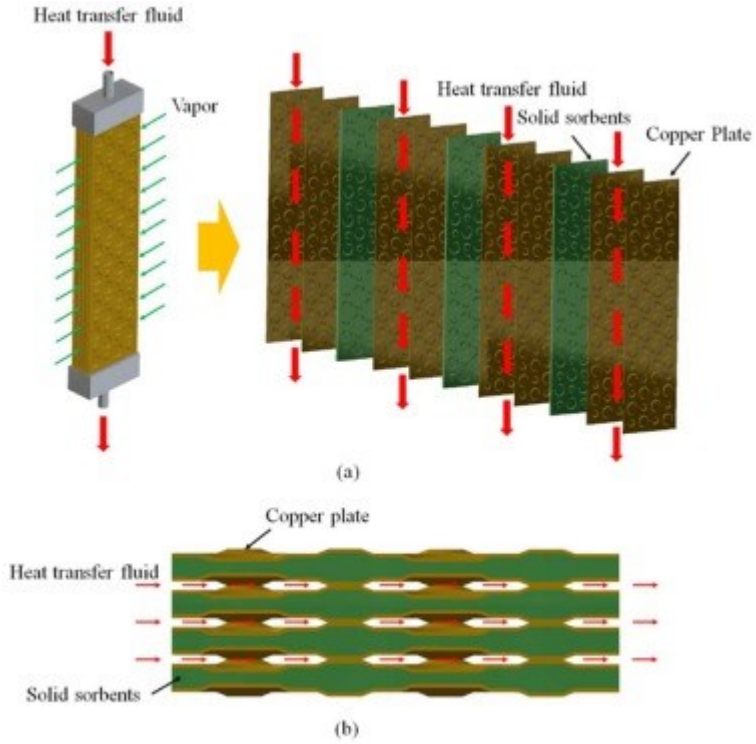

Figure 2.9::Plate heat exchanger adsorbent bed[129]

2.8.2 Adsorbent bed coating

Most commercial adsorption systems utilise packed bed. Packed adsorbent beds Figure 2.10 are designed so that adsorbent particles are packed between the fins as a way of integrating adsorbent material inside an adsorbent bed and is the most widely used method in adsorption systems.[28]. Packed beds are considered to have high mass transfer rate obtained from the high permeability within the bed. However, packed beds been characterised by poor heat transfer due to high thermal resistance caused by the void space that exist between adsorbent particles which acts like thermal insulators and reduces the contact area between the adsorbent particles and the heat exchanger surfaces. In some cases, the thermal resistance is caused by limited contact area between adjacent particles resulting in restricted heat transfer between them [28, 53]. To reduce the contact thermal resistance between the heat exchanger and adsorbents, researchers proposed coating the adsorbent bed and packing the adsorbent bed [28]. McCague et al [131], investigated a sorption chiller using two methods coating a heat exchanger (HX) with AQSOA FAM-Z02 (Z02) and packing HX with Z02 pellets. The results showed a SCP of 90 kW/m^3 for coated HX compared to 59 kW/m^3 for HX packed with Z02 pellets. Investigation by Saleh et al [132], on lab scale adsorption desalination system using a wire finned HX coated with AL-Fum MOF showed a higher SDWP ,SCP and COP of 23.5m^3/ton/day, 682W/kg and 0.32 in comparison to 12.7m^3/ton/day, 318.5W/kg and COP of 0.23 for a packed finned HX.

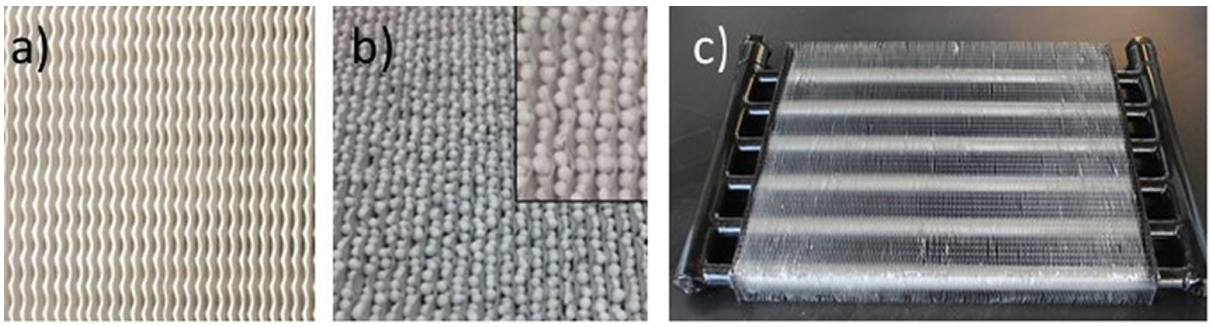

Figure 2.10:Coated HX (b) packed HX (c) empty HX[131]

2.8.3 Adsorbent deposition on Metal foam

In adsorbent deposition over metal foam, Figure 2.11, the metal foam is employed to create an adsorbent bed where, the adsorbent particles are filled in the gaps of metal walls such that the heat transfer within the bed is effected by three means ; grain to the metal wall, inside the metal framework, and particle to particle [127]. This type of bed maximises heat transfer process by minimising largest resistance caused by the particle to particle heat transfer. Investigation on the adsorbent deposition over metallic foam has shown an increase in the heat transfer within the adsorbent bed leading to improved adsorption uptake. Performance of a single adsorbent bed with Silica gel packed in Aluminium foam was investigated and the results showed a total cooling power of 8.74kW and total daily water production of 300m^3 per day [127].

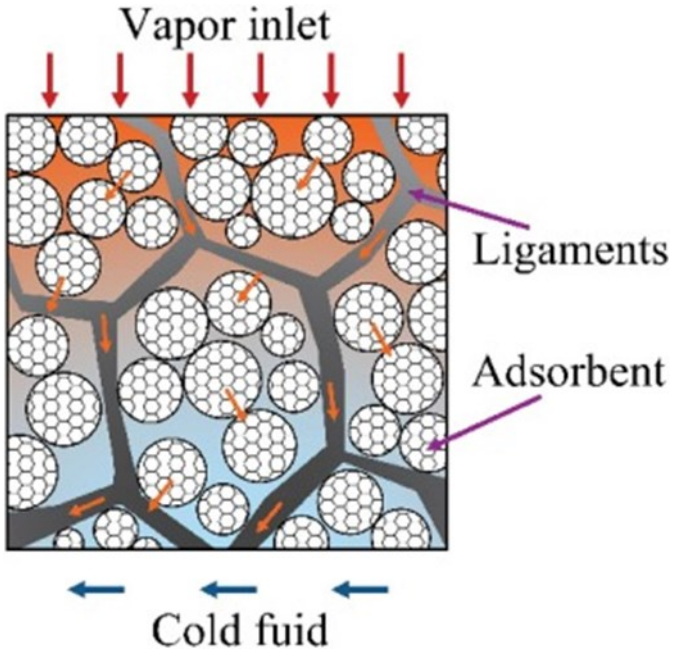

Figure 2.11: Heat transfer in Metal foam adsorbent bed[127]

2.8.4 Use of polyaniline to cover adsorbent particles.

Polyaniline polymer has amongst its attributes, high electrical conductivity, thermal stability and is simple to prepare. Employing the polyaniline net to cover the adsorbent particles has the effect of

increasing their thermal conductivity and thus increase the heat transfer within the adsorbent bed. A thin thermal conductive net was build up on the zeolite particles using the chemical oxidative in situ polymerisation of aniline and this improved the thermal conductivity within the adsorbent bed by 4 times [133].

2.9 Knowledge Gap and Contributions of the thesis

There has been much research on investigation and utilisation of porous media as adsorbent and the development of composites to enhance the heat and mass transfer of the adsorbents. Most composites reported are composites in porous media (CSPM), in which the porous media is the host matrix. However, there is hardly any literature on utilising non-porous material such as highly thermal diffusive graphene derivatives such as graphene oxide as adsorbent and better still graphene nanoplatelets as host matrix for hydrophilic ionic liquids sorbates in composite development for application in adsorption cooling and desalination. The introduction of new adsorbent materials will help to explore novel materials with superior thermal and adsorption properties that will revolutionise adsorption system performance in terms of heat and mass transfer. It is found out from the literature that there is no computational dynamic modelling done on GO, GP/IL composites to investigate the impact of the thermal and adsorption properties adsorbents on the heat and mass transfer at component level (adsorbent bed) leading to the overall system performance. Employing the computational dynamics tool will increase knowledge on the dynamic temperature and uptake changes within the adsorbent bed and allow for novel approaches to enhance the adsorption/desorption processes at the adsorption reactor/bed. There has not been energy conversion performance and exergy efficiency studies at component and system levels involving graphene derivative adsorbents. Understanding of the energy conversion will increase knowledge on the energy conversion of the components and allows adsorption system performance optimisation and design of more energy efficient systems which minimise waste and maximise the utilisation of energy. This could play a significant role in reducing the bulkiness of the adsorption systems and eliminate some of the barriers for its commercialisation.

2.10 Systems Summary

From the above literature review, it can be concluded that:

- Water scarcity and demand for space cooling is a worldwide issue and is expected to rise due to urbanisation and population growth. In some cases, people in high water stress areas experience high temperatures and require cooling. The conventional systems for producing fresh water and cooling are causing harm to the environment. This calls for more research to come up with environmentally friendly materials and systems to solve the water scarcity and meet the rising colling demand.

- Adsorption cooling and water desalination has emerged as a perfect alternative to the conventional systems in terms of energy conservation and mitigating climate change through using user friendly refrigerants such as water and the utilisation of low temperature waste heat, renewable solar and geothermal energy. However, their low performance in terms of the COP, SDWP and SCP due to the adsorbent materials' poor heat and mass transfer has stalled their widespread use.
- The sorption characteristics of adsorbent and adsorbate are key to the efficiency of the adsorption cooling and water desalination systems. Silica gel on the other hand is regarded a baseline adsorbent widely used in commercial adsorption application due to its regenerative capability at low temperature, however its low thermal and adsorption properties stall the commercialisation of adsorption cooling and water desalination systems. This has created the need to find new adsorbents with improved thermal properties such as graphene and its derivatives to outperform Silica gel and other conventional adsorbents.
- The thermal properties of the adsorbents is crucial in solving the poor heat and mass transfer associated with the adsorption cooling and water desalination systems. Therefore, at material level, composites are regarded as the most viable adsorbents to improve the heat transfer and adsorption properties for application in adsorption cooling and water desalination systems.
- Adsorbent bed is the main component of the adsorption cooling and water desalination. Its design and enhancement techniques for the heat and mass transfer is key to the system level performance. A two-bed cooling and water desalination system is regarded as the simplest design to provide continuous water and cooling. Therefore, it is the most used.

CHAPTER 3 : METHODOLOGY.

3.1 Introduction

To establish and develop novel materials as adsorbent materials for cooling and desalination applications, it was imperative to carry out the investigation through experimentation and computational modelling to fully understand their capability. This Chapter gives an insight into the methodology used to fulfil the fundamental objectives of the study made up of three aspects: (1) the experimental investigation of the thermal and adsorption characteristics of the novel adsorbents. (2) the development of a computational dynamics modelling tool used to predict the heat and mass transfer to investigate their impact at component and system levels. (3) the performance assessment of the adsorption cooling and desalination at system level including the energy and exergy analysis. The Chapter presents the experimental thermal and adsorption characteristics test methodology, the computational dynamics methodology and the energy and exergy methodology.

3.2 Materials thermophysical properties experimental assessment

The bulk thermal diffusivity for all the investigated materials in Chapters 4, 5 and 6 were experimentally determined using laser flash analyser apparatus (LFA) NETZSCH LFA 467™, schematically illustrated in Figure 3.1. LFA consists of a laser source, a furnace for temperature control, a sample holder, an infrared detector, and a data control unit. For each measurement, a laser pulse strikes the sample's front face, and the sample's adsorbed heat increases the rear face's temperature. The infrared detector determines the increase in the temperature, and the Data control unit records the measured data. The thermal diffusivities of the materials were measured at a room temperature of 25°C. The experiments were performed three times with five laser shots at each trial to determine repeatability. The rise in temperature at the rear face of the test sample is measured as a function of time and is used to mathematically determine the thermal diffusivity (α) [134]. Equation (3.1) was derived by Parker et al [135] and used for determining the thermal diffusivity.

$$\alpha = 0.1388.\ l^2/t_0 \tag{3.1}$$

where l is the thickness of the sample and t_0, is time required for the sample's rear face to reach half the maximum temperature. The sample holder in the apparatus is round and suitable for 12.7mm diameter samples of thickness in the range of 1-3mm. To improve the accuracy of the measurement, it is important to maintain the same distance between IR detector and both the reference sample and test sample. The test sample thickness in this study was 2.5mm the same as reference sample. The thermal conductivity is then calculated from the thermal diffusivity using equation (3.2).

$$K(T) = \alpha(T)\ \rho\ (T) C_p\ (T) \tag{3.2}$$

Where α is the thermal diffusivity; K is the thermal conductivity; C_p is the Specific heat capacity; ρ is the density of the material. (T) is the temperature.

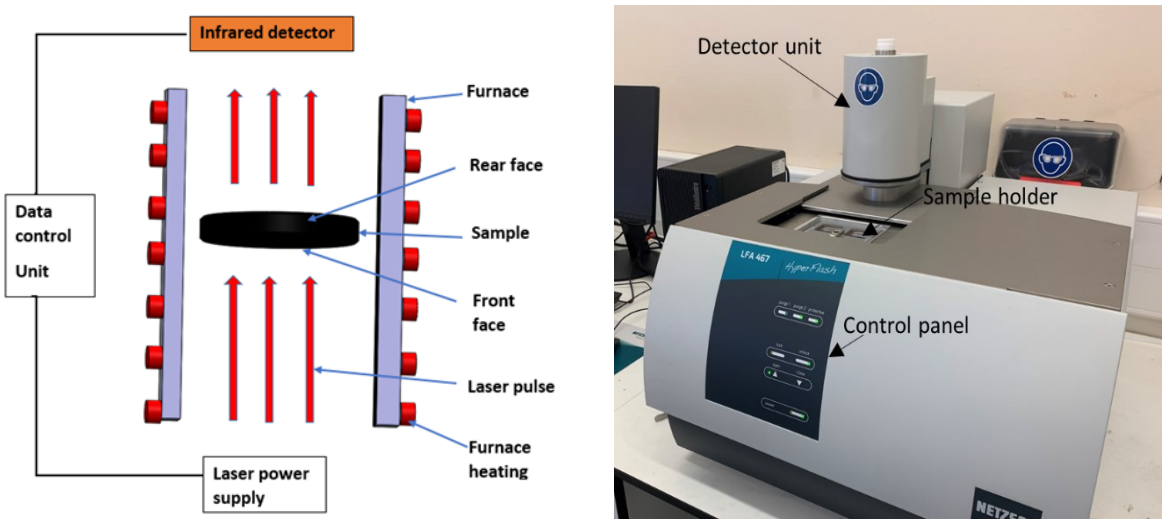

(a) (b)

Figure 3.1: (a) Schematic diagram of LFA operation (b) pictorial view

3.3 Adsorption characteristics experimental assessment

The measuring of adsorption characteristics can be achieved through two methods, the volumetric method, and the gravimetric method [136, 137] The materials' adsorption characteristics for this study were determined using the dynamic vapour sorption (DVS) gravimetric analyser DVS Resolution™, as shown in Figure 3.2. The DVS resolution incorporates a dual balance design that provides high precision sorption measurement for a wide range of materials. The equipment includes a microbalance (SMS Ultrabalance™) that measures the adsorbent mass to determine the instantaneous water vapour uptake/offtake during adsorption/desorption processes while varying the pressure ratio between the adsorbent and water vapour equivalent to Pevap/Pbed. The accuracy of the DVS analyser microbalance was verified at ±0.05mg by using 100mg standard calibration mass before the test. The DVS can determine sorption behaviour of sample sizes as small as 10mg accurately hence minimises the equilibration time taken by providing a rapid sorption equilibrium. The instrument employs dry carrier Nitrogen gas and incorporates digital mass flow controllers for regulating the dry gas flow. Dry nitrogen purges the reaction and microbalance chambers before every test.

The water vapour uptake corresponding to the vapour pressure values that form adsorption isotherms was developed by measuring the adsorbent mass at the condition of no change in mass at a defined water vapour pressure ratio and adsorption temperature. Having an automated in-built control software package, the DVS provides a user-friendly interface to set up and run sorption and desorption experiments. Available is also a platform for quick plotting and data analysis.

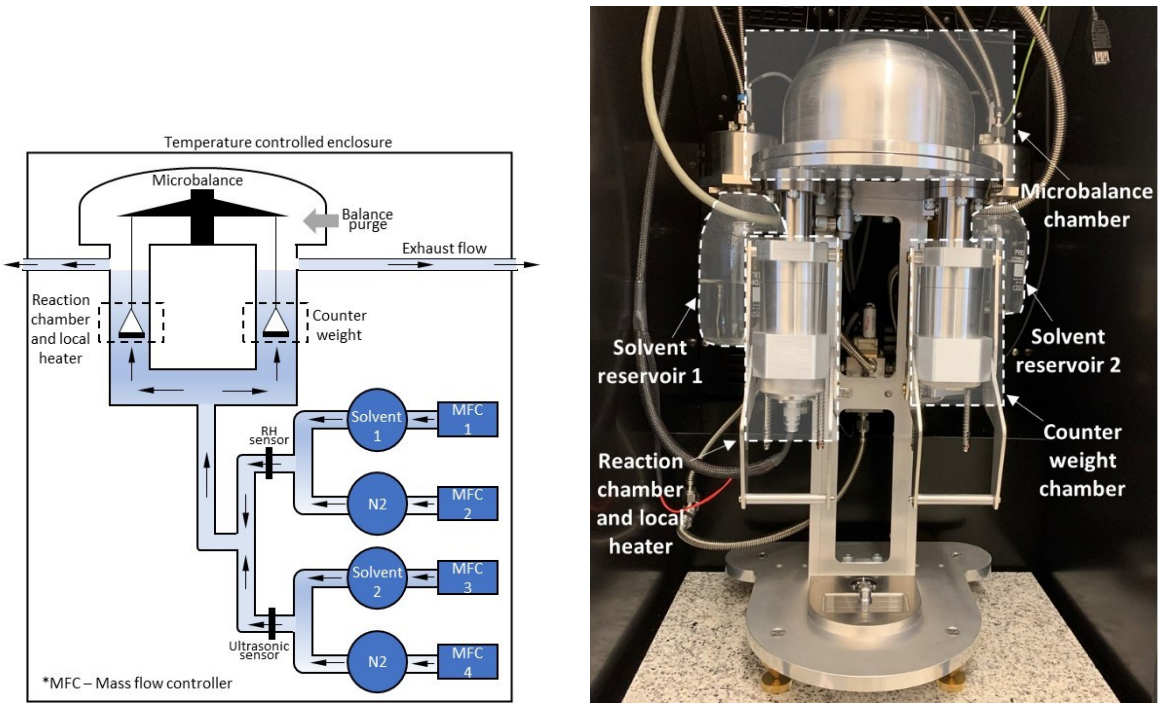

(a) (b)

Figure 3.2:Dynamic Vapor Sorption Analyser (a) schematic diagram and (b) pictorial view

The Several empirical isotherm models are available to determine the isotherms primarily based on the heat of adsorption, solid saturation loading (i.e., amount of loading to create a monolayer coverage per unit volume of the packing media), adsorption equilibrium constant and temperature-dependent saturation [138-141]. Examples of such models are, Langmuir, Freundlich, Sips, Dubinin-Astakhov (D-A), Tóth, Temkin and Hill-de Boer [119]. Some of these isotherm models were used to model isotherms of the investigated adsorbent materials in Chapters 4, 5 and 6.

3.4 Adsorption kinetics

The adsorption kinetics is the rate at which adsorption occurs, which describes how fast the fluid phase molecules are adsorbed on the adsorbent surface. The adsorption kinetics are described by mathematical models representing the relationship between adsorption rate and factors such as surface properties, time, temperature, and concentration. The Linear driving force model (LDF) is regarded as a simplified representation of complicated adsorption process which is widely used to describe adsorption rate in porous media and is used to analyse data from dynamic experiments to determine the parameters that characterise the adsorption process. The adsorption kinetics in this study were calculated using the linear driving force LDF model, where the water particles can reach all the adsorbent granules, neglecting the inter-particle mass transfer resistance. The LDF is described by equation (3.3).

$$\frac{\partial \omega}{\partial t} = k_s\, \alpha_v\, (w^*\text{-}w) \tag{3.3}$$

Where w [kg/kg] is the uptake at any given time; The equilibrium uptake w^* kg/kg; $k_s\alpha_v$ [s^{-1}] is the diffusion time constant and is calculated based on the Arrhenius equation (3.4).

$$k_s\alpha_v = D_{so} exp\left(-\frac{E_a}{RT}\right) \tag{3.4}$$

Where, D_{so} is the pre-exponential factor; E_a (kJ/kg) is the activation energy ; R (kJ. $kmol^{-1}K^{-1}$) is the universal gas constant;); T (K) is the adsorbent temperature.

$$k_s\alpha_v = 15\frac{D_s}{R_p^2} \tag{3.5}$$

Where D_s ($m^2\ s^{-1}$) is the surface diffusivity; R_p is the particle radius (m). The constant 15 was used since the adsorbent particles are spherical in shape. The values of D_{so} and E_a can approximated and obtained by the Arrhenius plot in which ln D_s is plotted against (1/T). the slope of the plot gives $\frac{E_a}{R}$ and the intercept gives the constant D_{so}. Rearranging the equation (3.3)(3.4)(3.5) to give the LDF equation (3.6).

$$\frac{\partial \omega}{\partial t} = \left(15\frac{D_{so}}{R_p^2}\right) exp^{\frac{-E_a}{RT}}(w^*\text{-}w) \tag{3.6}$$

3.5 Isosteric heat of adsorption

Isosteric heat of sorption is defined as the heat released at a constant adsorbate loading and represents the quantity of heat exchanged between adsorption and desorption. It is a critical thermodynamic property for estimating the energy involved in the adsorption system [142]., Chakraborty et al. [143], proposed a Chakraborty-Saha-Koyama equation (C-S-K) for calculating isosteric heat of adsorption (Q_{st}). The C-S-K was developed based on the principle of equilibrium chemical potential between the adsorbed and the gaseous phase, the equations of state and the Maxwell relations [142]. The Q_{st} for the investigated composite adsorbents was calculated as a function of the sorption potential gradients of pressure and temperature concerning entropy and specific volume. Equation (3.7) defines the C-S-K equation to calculate the isosteric heat or adsorption enthalpy Q_{st}.

$$Q_{ST=}\ RT^2\left[\left(\frac{\partial(lnP)}{\partial T}\right)_q\right] + Tv_g\frac{dP}{dT}(P,T) \quad (3.7)$$

Where R (J g^{-1} K^{-1}) denotes the gas constant; v_g (m^3 kg^{-1}) is the specific volume of the adsorbate; q is the Uptake kg/kg; T (K) is the adsorption temperature at corresponding pressure P (kPa).

3.6 Computational modelling

3.6.1 Dynamic heat and mass transfer modelling

Computational dynamics tool is a numerical tool that is used to envisage dynamic systems beyond fluid flow such as chemical reactions, heat and mass transfer through solving a series of governing mathematical equations for discretised cells over a stated time and space domains employing computational power [144, 145]. Claude-Louis Navier and George Gabriel Stokes developed the viscous transport into the Euler equations to derive the Navier-Stokes equations found in the computational fluid dynamics CFD and also included within computational dynamics [146]. With Computational dynamics, it is possible to obtain specific results about heat transfer, water vapour uptake and velocity which is not easy to predict experimentally. Generally, computational dynamics has played a key role to facilitate the evaluation of the performance of dynamic systems at less time and low cost and it was used to evaluate the developed new materials, existing materials, and new reactor bed design in adsorption systems in this study. The ability to visualise different parameters in the Computational dynamics simulation contributed to the breadth and depth of the component-level investigations [147]. On reflection, Niazmand et al, [147] used computational dynamics simulation to investigate the physics in the transfer process in an adsorbent bed with annular fins using silica gel/water pair. The computational dynamics modelling enabled assessing the effect of various parameters such as the physical structure of the adsorbent bed and its influence on the heat and mass transfer performance. Jribi et al, [5] numerically investigated the adsorption rate of a model using activated carbon and ethanol pair using CFD simulation, which enabled evaluating the non-isothermal time diffusion constant.

The advantages and limitation of computational dynamic modelling

While CFD cannot replace experiments, it has many advantages over experiments. However, it also has some limitations. The advantages and limitations of computational are listed below:

3.6.2 Advantages of computational modelling

- It provides a cost effective and alternative approach to compliment experimental approaches by simulating real fluids flow [148, 149].
- It reduces lead time, design, and production costs in comparison to experimental approaches [149].

- It enables solving of complicated flow problems which cannot be achieved by analytical approaches [148].
- It is capable of simulating flow conditions non- reproduceable in experimental tests that are too huge or cannot be envisaged experimentally [148, 149].
- It can provide visual, and detailed information in comparison to experimental and analytical fluid dynamics [148, 149].

3.6.3 Limitations of computational modelling

- Modelling complex designs can be difficult and getting accurate results can be compromised by using unknown or incorrect boundary conditions[150].
- Numerical errors due to finite difference approximation computations can cause differences between reality and computed results[149, 150].

3.7 Commercial CFD

The use of commercial CFD increased in the early 1980s [146]. There are several commercial packages that are widely used in CFD, which include COMSOL MULTIPHYSICS, COSMOS FLO, Solid Works and ANSYS Fluent, ANSYS CFX, ADINA, OpenFoam and STAR-CD. ANSYS Fluent was used in this study for several reasons which include its ability to simulate heat transfer, laminar flow, turbulent flow, compressible flow, incompressible flow, multiphase flow with high accuracy. It uses to good advantage high performance computing to solve complex large simulations in a short time and it can be easily integrated with various software such as computer aided design to facilitate exporting of geometric models from one design environment to simulation environment.

Solving CFD equations requires the discretization of the numerical data i.e., every term of the flow equation should be written in a programmable way to solve the equations. There are three principle numerical approaches used in CFD namely the Finite Element method (FEM), Finite difference (FDM) and Finite volume (FVM). The FDM is regarded as the oldest numerical approach based on the use an approximation of the polynomials, Fourier, and Taylor series expansion to provide solution for differential equations at discreet points in a flow field. This method is mainly applied to structured uniform mesh. The FDM method stimulated the application of partial differential equations (PDE) leading to the evolution of the FVM and FEM methods. FDM has limitations in handling geometries which are complicated hence the FVM and FEM are the main methods used in CFD [146]. The FEM is a numerical method to solve PDEs by discretising the flow region into smaller regions or finite elements of the computational domain. The main advantage is application on coarse mesh to give high accuracy and is mainly applicable to diffusion problems. The discretisation in FVM is based on solving the PDEs and averaging the values of variables across the volume. The PDE are written in a way that can be solved for each finite volume/cell. Since the FVM is discretised into finite volumes, the governing equations are solved for each volume.

3.8 Ansys Fluent Modelling

ANSYS workbench Fluent 2019 R2 was used to simulate the flow in porous media to envisage the heat and mass transfer. It allows employing the User defined functions (UDF) to simulate the undefined phenomenon in the simulation package. ANSYS Fluent has two types of solvers, the pressure-based solver, and the density-based solver. The pressure-based solver was preferred in this study since it is used for simulating low speed incompressible and weak compressible flows. Since Ansys is one of versatile simulation tools that can model several modes of heat transfer such as convection, conduction, radiation, and phase change by activating the energy equation in the Fluent solver. It enables solving the flow in porous media to solve single and multiphase flow including heat transfer through filter papers, perforated plates, tubes, and packed bed. Adsorption is a time dependent process, and the boundary conditions always vary during the adsorption/desorption process. While ANSYS has the mass, momentum, and energy parameters in its database, it does not include the physics specified for the adsorption process. Therefore, UDFs are developed and incorporated onto the governing equations for energy, momentum, mass transfer, heat transfer and multiphase boundary conditions to complement the missing physics and enable the modelling of the adsorption process [145].

3.9 computational solving procedure

ANSYS provides user friendly graphical user interface (GUI) platforms to input parameters and check out the computed results. These platforms include the pre-processor, solver, and post processor. The ANSYS simulation process has three main domains namely spatial domain (geometry), temporal domain (time) and parameter domain. Three main interfaces and the simulation procedure for the adsorption process in this study is shown in Figure 3.3.

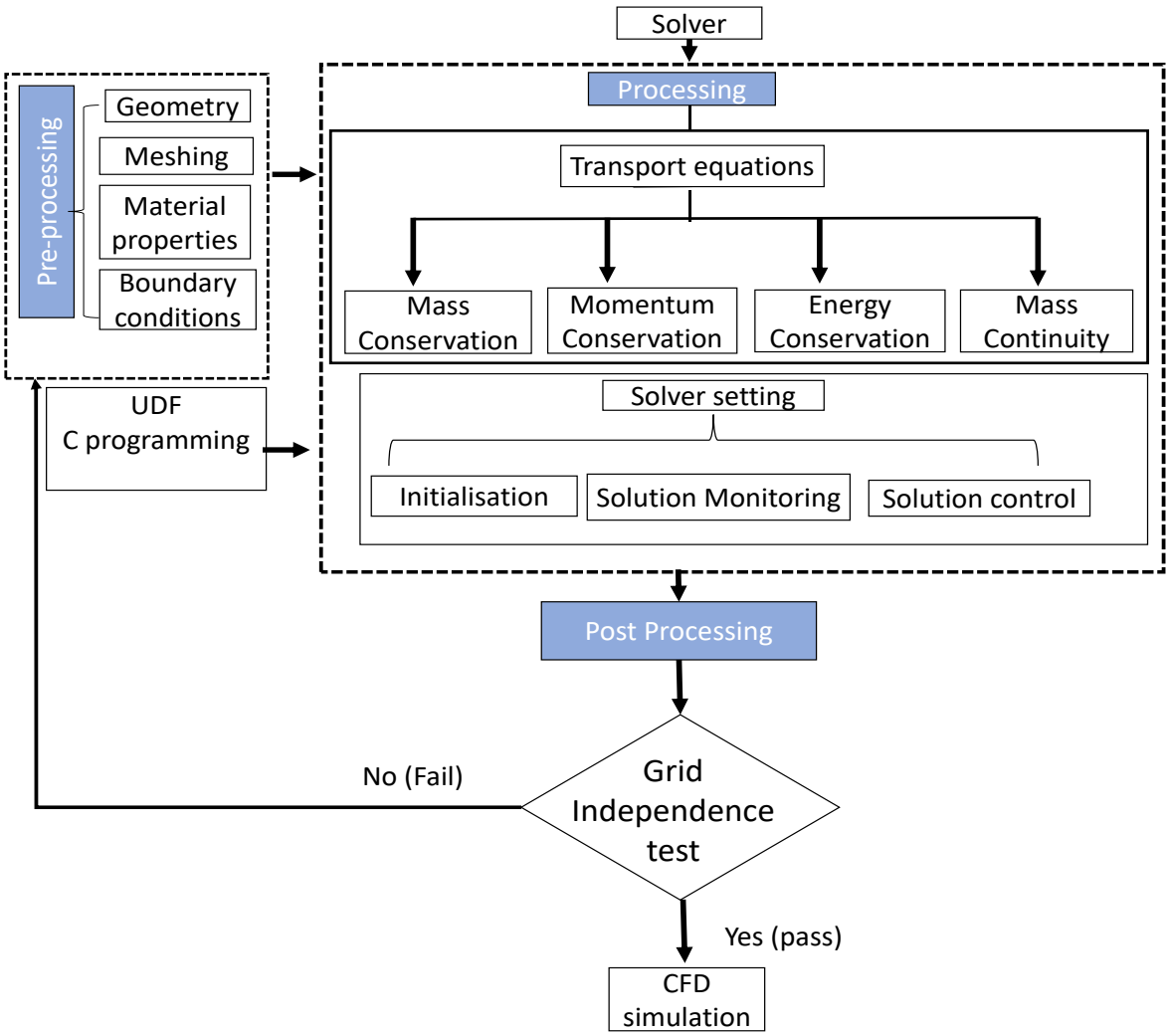

Figure 3.3: Simulation procedure and interconnectivity of the GUI platforms

3.10 Governing equations

The fundamental physical principles of energy, mass and momentum conservations were used to govern the multi-phase flow of adsorbate in porous media using a finite-volume solver. Jin and Kuznetsov [151] considered the fluid flow in porous media laminar, given the low flow velocity from 0.15- 2m/s than (i.e., low Reynolds number less than 100). However, other researchers have used a macroscopic approach for low Reynolds numbers and considered the turbulence effect [152]. In this research, the macroscopic approach was employed considering that any turbulence that might occur in the porous medium is minimal. The relevant physics of the governing equations in computational modelling of adsorption phenomena include the adsorbate diffusion, mass conservation, adsorbate mass balance continuity, momentum conservation and energy.

3.10.1 Adsorbate diffusion

Equation (3.8) is the widely used Darcy equation that governs the diffusion process of the adsorbate in finite volume modelling. It models the packed adsorbent material as a block of porous medium [153, 154].

$$\frac{\partial}{\partial t}(\rho_w \gamma) + \nabla\left[\rho_w\left(-\frac{k_\varepsilon}{\mu}\nabla P_{ads}\right)\right] = \frac{\partial}{\partial t}(\rho_{ads} w) \tag{3.8}$$

Where γ is the adsorbent's porosity (m^2/g); μ (Pa.s) is the dynamic viscosity; ρ_w and ρ_{ads} (kg/m^3) are the densities of water and adsorbent. P_{ads} is the adsorption saturation pressure at the given adsorption temperature; w is water vapour uptake; and k_ε (m^2) is the permeability of the adsorbent material. The permeability is a function of the adsorbent particles' radius (R_p) and adsorbent porosity, as shown in Equation (3.9) [55].

$$k_\varepsilon = \frac{4\gamma^2 {R_p}^2}{150(1-\gamma)^2} R_p \tag{3.9}$$

3.10.2 Mass conservation equation

Equation(3.10). presents the differential form of the Mass conservation.

$$\frac{\partial \rho}{\partial t} + \nabla .(\rho \vec{v}) = s_m \tag{3.10}$$

Where S_m ($kg.m^{-3}s^{-1}$) denotes the mass source term corresponding to the amount of vapour adsorbed onto the adsorbent material porous surfaces, which is governed by equation (3.11).

$$S_m = -(1-\gamma)\rho\frac{\partial \omega}{\partial t} \tag{3.11}$$

Where the term $\frac{\partial \omega}{\partial t}$ is the adsorption rate of the adsorbate determined from the above mentioned LDF adsorption kinetics model.

3.10.3 The adsorbate mass balance continuity

Equation (3.12)governs the continuity of mass of the adsorbate into the porous media during the adsorption/desorption processes.

$$\frac{\partial(\gamma\rho_w)}{\partial t} + \nabla.(\rho_w \vec{v}\gamma) + (1-)\rho_{ads}\frac{\partial \omega}{\partial t} = 0 \tag{3.12}$$

The term $\frac{\partial(\gamma\rho_w)}{\partial t}$ denotes the change of density over time in the pores volume; $\nabla.(\rho_w\vec{v})$ is the mass transfer within the adsorbent boundaries; $(1-\gamma)\rho_{ads}\frac{\partial\omega}{\partial t}$ is the unsteady source term of the adsorption process; γ is the porosity of the adsorbent bed.

3.10.4 Momentum conservation

The porous media model (PMM) approach was used to simulate the flow through the adsorbent material within ANSYS Fluent platform. The PMM introduces properties that considers the flow and resistance characteristics within the porous media. The viscous and inertial losses in the porous medium are accounted for by the momentum source term (F) in Equation (3.13).

$$\frac{\partial}{\partial t}(\rho_w\vec{v})+\nabla.(\rho\vec{v}\vec{v})=-\nabla p+\nabla.(\bar{\bar{\tau}})+\rho_w\vec{g}+\vec{F} \quad (3.13)$$

Where, ρ_w (kg/m^3) denotes the density of adsorbate; $\vec{v}$ (m.s^{-1}) is the velocity vector; $\rho\vec{g}$ (N) the gravitational forces [155].

3.10.5 Energy conservation

Equation (3.14) is the general form of energy conservation, assuming the thermal equilibrium between the fluid and the porous medium [7].

$$\frac{\partial}{\partial t}(\rho_w E)+\nabla.(u(\rho_w U+p)) = \nabla.(K_{eff}\nabla T-\sum h J)+\nabla.(\bar{\bar{\tau}}.\vec{v})+S_h \quad (3.14)$$

Where K_{eff} (W/mK) denotes the effective thermal conductivity of the adsorbent; h (J/kg) is the enthalpy of adsorption, J (kgm^{-1}) is the diffusion flux; U (kJ) is the internal energy obtained from $E = h - p/\rho + v^2/2$; $\nabla.(K_{eff}\nabla T)$ is the energy transfer by conduction in the porous medium; $\sum hJ$ is the diffusion flux; $\nabla.(\bar{\bar{\tau}}.\vec{v})$ is the viscous dissipation; S_h (Wm^{-3}) is the heat source term that correlates to the heat of adsorption (Q_{st}) during the adsorption/desorption process [155]. The energy source term is determined using Equation (3.15).

$$S_h = -(1-\gamma)\rho Qst\frac{\partial\omega}{\partial t} \quad (3.15)$$

3.11 Simulation Geometry

The geometry can be created using two approaches the solid modelling and the direct generation. The solid modelling uses predefined geometric shapes created from various drawing software platforms linked to the CFD software such computational tool as SolidWorks, CATIA, Auto CAD, etc. and imported into ANSYS. It requires the user to have good knowledge of meshing to be able to create the finite element mesh. Whereas the direct generation method allows the user to generate a geometry within the same modelling software. It is very easy to use for generating simple 2D

geometries and gives the user complete control of nodes and elements placements and numbering [156]. It is also regarded as the shortest way to create finite element meshing. Albaik et al [157] investigated the use of a 2D and 3D axisymmetric models to simulate heat and mass transfer for cooling and desalination, their findings showed that a 2D axisymmetric model can give the same performance and results as a 3D axisymmetric model at 70% less computational time. The direct generation approach of creating a model was undertaken using design modeler, the software inbuilt drawing platform as shown in Figure 3.4. This stage requires a computer with a suitable processer speed to enable the input of boundary conditions and allow the simulation to run until convergence is attained.

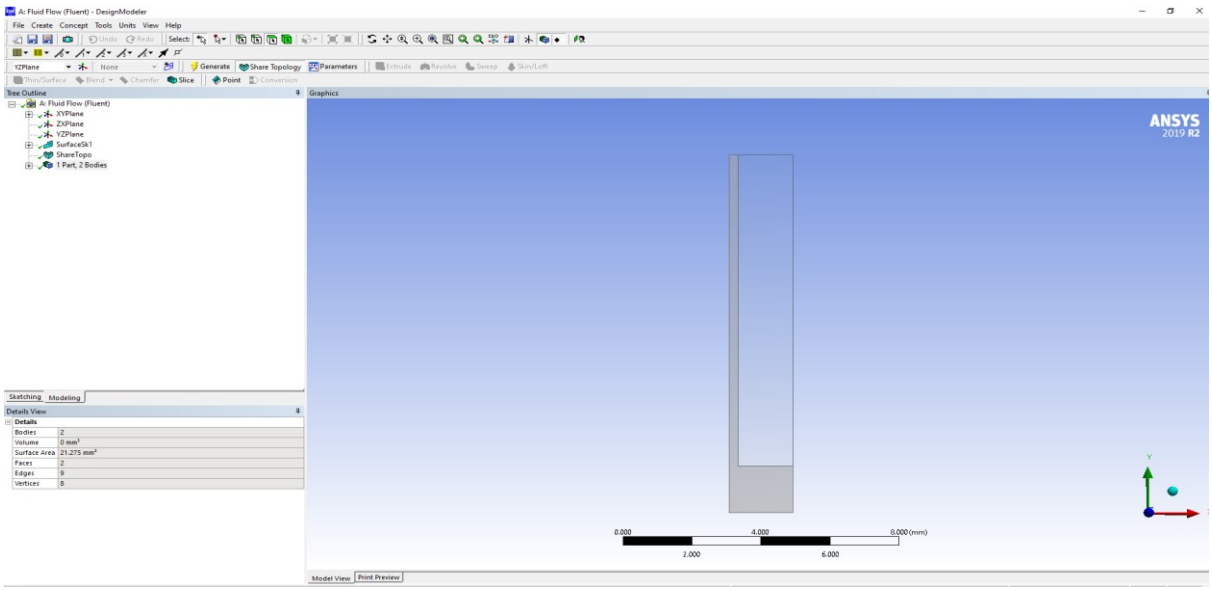

Figure 3.4: Design modeller for geometry generation

The geometry employed in this study is a circular finned tube heat exchanger packed with adsorbent materials Figure 3.5a. Given the symmetry of the heat exchanger, the geometry was reduced to a 2D-axisymmetry model and created on the X-Y plane. The computational domain was considered half the space between two fins, as shown in Figure 3.5b to reduce computational time since geometry has many fins and symmetry planes. The dimensions of the baseline geometry are given in Table 3-1.

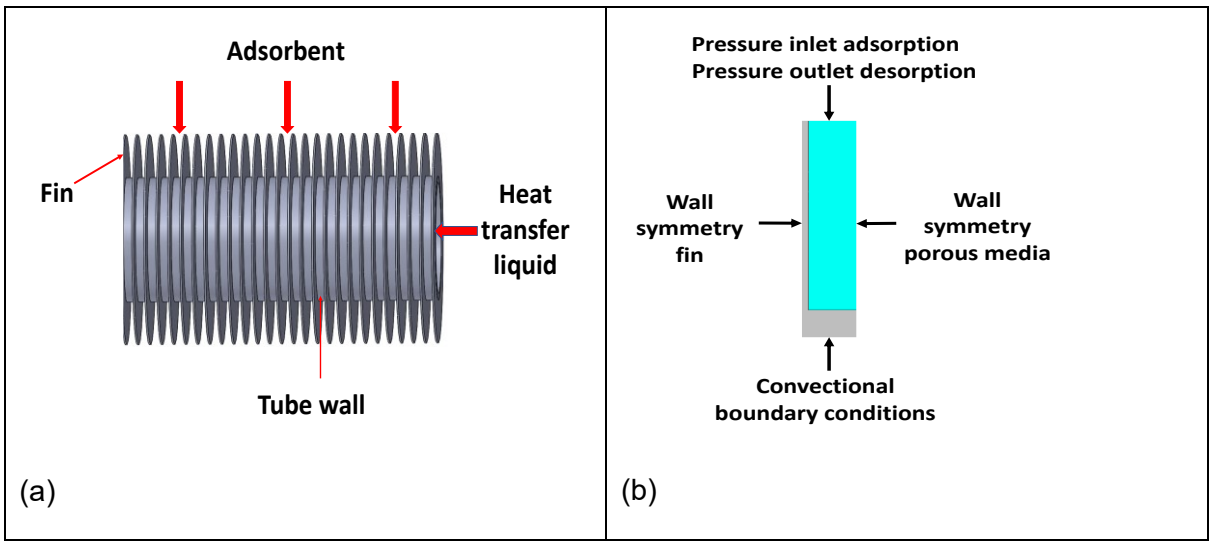

Figure 3.5; (a) Finned tube geometry and (b) the Axisymmetric segment

Table 3-1 Dimensions of Finned Tube

Parameter	Value
Tube outer diameter (d_0)	27 mm
Tube inner diameter (d_i)	24 mm
Fin height (h_f)	10 mm
Fin thickness (δ)	0.54 mm
Fin pitch (p)	3.8 mm
length of the finned tube (l)	500 mm

3.12 Mesh generation

Following the geometry development is the generation of mesh The mesh replicates the simulated geometry in a discretised form to give finite set of elements. The developed Mesh enables solving the flow equations at the developed nodes. The computational accuracy and stability of the CFD modelling is greatly influenced by the quality of the mesh [145]. The general meshing procedure is given in Figure 3.6

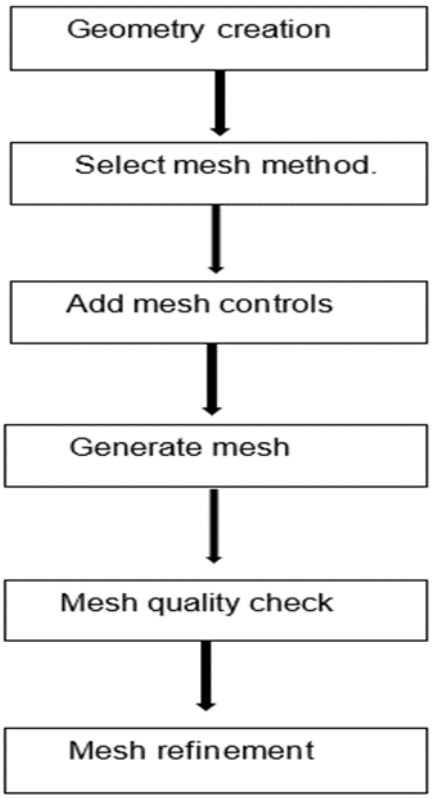

Figure 3.6 Mesh generation process

3.12.1 Meshing

There are several mesh types used in CFD solvers: structured, unstructured and hybrid meshes. These meshes are comprised of triangle, quadrilateral, tetrahedron, hexahedron, pyramid, and prism/wedge. The choice of mesh type to apply is dependent on the application for example triangular and quadrilateral or their combination can be used on 2D design and tetrahedral, polyhedral, hexahedral and pyramids can be effectively used on 3D design.

3.12.2 Structured Mesh

Figure 3.7 shows a structured mesh model. In a structured mesh model for both 2D and 3D designs there is an orderly or regular connectivity and the nodes' locations are well defined and predictable in terms of programming. The structured mesh solvers employ quadrilateral and hexahedral mesh codes in 2D and 3D respectively. While the structured mesh is efficient in terms of memory usage and computational time, it is only effective for simple geometries and the element choice is limited to quadrilaterals in 2D and hexahedral for 3D.

Figure 3.7: Structured Mesh

3.12.3 Unstructured mesh

Unlike the structured mesh, the unstructured mesh is irregular in either 2D, or 3D models, as shown in Figure 3.8. The unstructured mesh solvers employ triangles and tetrahedral in 2D and 3D respectively [145]. The unstructured mesh has an advantage of replicating complex geometries. This emanate from the fact that some control volumes of complex geometries will require unstructured mesh to be generated.

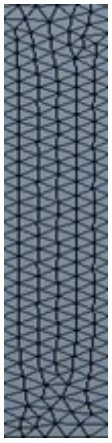

Figure 3.8:Unstructured mesh

3.12.4 Hybrid Mesh

Hybrid mesh employs both structured and unstructured mesh on the same geometry. This type of meshes combines the advantages of both structured and unstructured meshes to produce high quality mesh and improve the accuracy of the simulation. Hybrid meshing comprises of hexahedral, tetrahedral and pyramid element in 3D geometries while 2D contain quadrilaterals and triangles. In this study, the triangular mesh in Figure 3.8 was developed to replicate the computational domain, which was bounded by the pressure inlet/outlet, fin wall symmetry, porous medium's wall symmetry

and tube wall. The water vapour flow in the adsorbent bed was considered laminar flow, which required near-wall meshing near the fin to resolve the near-wall domain and reduce the y^+ values.

Mesh quality

The mesh quality is crucial to the accuracy of the simulation results. The pre-processing step can affect a model's convergence and numerical stability under CFD analysis. Therefore, it was essential to select mesh parameters that give reliable results and reduce mesh-induced errors, as reported by Sosnowski et al [158].

The mesh quality was determined by mesh orthogonality and skewness. The minimum orthogonality observed from the mesh was 0.9999. The orthogonality value is assessed on a scale from 0 to 1, with values close to zero indicating poor quality. The maximum skewness was 0.242, with values from 0 to 0.25 generally considered reasonable in analogues modelling by Ozen [159].

The flow of adsorbate in the adsorbent bed is considered a low Re flow and requires fine near wall mesh able to resolve the near wall area. Therefore, enhanced wall treatment was preferred as it would be able to handle both fine and coarse near wall mesh. Local mesh controls such as inflation and sizing were applied for making some global mesh adjustments to the model. The symmetry porous media domain uses its edges in contact with the fin and tube as boundary conditions, so five inflation layers were applied on meshing the edges in contact. This was intended to capture boundary layer gradients by creating thin cells adjacent to wall boundaries sufficient to resolve viscous sublayers associated with the first near wall node. To resolve the viscous layer the first layer should have a y^+ equal to 1. However, a wall function was used and a y^+ in the range $30 < y^+ < 300$ would be sufficient to resolve the wall viscous layer. Meshing was performed until the y^+ criteria was met. Since fin wall and porous media domains had different dimensions, face sizing was applied to specify the number of divisions.

Table 3-2 Mesh quality guideline [159]

Skewness mesh metrics spectrum

Excellent	Very good	Good	Acceptable	Bad	Unacceptable
0-0.25	0.25-0.50	0.50-0.80	0.80-0.94	0.95-0.97	0.98-1.00

Orthogonal Quality mesh metrics spectrum

Unacceptable	Bad	Acceptable	Good	Very good	Excellent
0-0.001	0.001-0.14	0.15-0.20	0.20-0.69	0.70-0.95	0.95-1.00

3.13 Mesh independency

This study used the grid convergence index (GCI) method to scrutinise mesh independency [158]. It requires analysing the CFD results of the same case at least (3) three times with different mesh resolutions. One of the recommended steps in meshing is to apply a coarse mesh first as this allows the evaluation of computer code's storage and running time. Above all a coarse mesh offers the

opportunity to carry out several test runs aimed at assessing the convergence behaviour. Having achieved a convergence, mesh refinement in the domain can be performed to attain the desired CFD solution [149]. The first mesh generated was a coarse mesh followed by two refined meshes using a scaling factor of 0.7 and 0.5 using the Equation (3.16)(3.17)(3.18)(3.19)(3.20) [158].

$$h = \left[\frac{1}{N}\ \sum_{i=1}^{N}(\Delta A_i)\right]^{\frac{1}{2}} \tag{3.16}$$

Where N is the total number of cells in the computational domain; ΔA_i is the area of the ith cell. The calculation of the mesh refinement factor (r) was performed as a quotient of the size of coarse and fine mesh, as in Equation (3.17):

$$r = \frac{h_{coarse}}{h_{fine}} \tag{3.17}$$

For the calculation of r, the assumption of $h_1 < h_2 < h3$ was made, where $r_{21} = \frac{h_2}{h_1}$ and $r_{32} = \frac{h_3}{h_2}$. Accordingly, calculating the order of convergence p was performed using Equations (3.18)(3.19)(3.20). Employing the fixed-point iteration with the initial approximation equal to the first term:

$$P = \left| \frac{ln\left|\frac{\varepsilon_{32}}{\varepsilon_{21}}\right| + ln\left(\frac{r_{21}^{p}\text{-}1.sgn\left(\frac{\varepsilon_{32}}{\varepsilon_{21}}\right)}{r_{32}^{p}\text{-}1.sgn\left(\frac{\varepsilon_{32}}{\varepsilon_{21}}\right)}\right)}{ln(r_{21})} \right| \tag{3.18}$$

$$\varepsilon_{32} = \emptyset_3 - \emptyset_2 \tag{3.19}$$

$$\varepsilon_{21} = \emptyset_2 - \emptyset_1 \tag{3.20}$$

$\emptyset_k$ represents the value of the simulation's most concerned variable, of which a solution is obtained with the kth mesh; the water uptake was the selected variable in this study. The calculation of the extrapolated values was based on Equations(3.20)(3.21) and (3.22).

$$\emptyset_{ext}^{21} = \frac{r_{21}^{p}\ \emptyset_1 - \emptyset_2}{r_{21}^{p} - 1} \tag{3.21}$$

$$\emptyset_{ext}^{32} = \frac{r_{32}^{p}\ \emptyset_2 - \emptyset_1}{r_{32}^{p} - 1} \tag{3.22}$$

The calculation of the approximate relative error was based on Equations (3.23) and (3.24).

$$e_a^{21} = \left| \frac{\emptyset_1 - \emptyset_2}{\emptyset_1} \right| \tag{3.23}$$

$$e_a^{32} = \left| \frac{\emptyset_2 - \emptyset_3}{\emptyset_2} \right| \tag{3.24}$$

Calculating the relative extrapolated errors was based on Equations (3.25) and (3.26).

$$e_{ext}^{21} = \left| \frac{\emptyset_{ext}^{12} - \emptyset_1}{\emptyset_{ext}^{12}} \right| \tag{3.25}$$

$$e_{ext}^{32} = \left| \frac{\emptyset_{ext}^{23} - \emptyset_2}{\emptyset_{ext}^{23}} \right| \tag{3.26}$$

The mesh convergence index GCI calculation was based on Equations (3.27) and (3.28).

$$GCI_{21} = \frac{1.25 \cdot e_a^{21}}{r_{21}^p - 1} \tag{3.27}$$

$$GCI_{32} = \frac{1.25 \cdot e_a^{32}}{r_{32}^p - 1} \tag{3.28}$$

The convergence type was evaluated using Equation (3.29)

$$\frac{\varepsilon_{course}}{\varepsilon_{fine}} = \begin{cases} <0 & \text{oscilatory converged} \\ >1 & \text{not converged} \\ [0.1] & \text{converged} \end{cases} \tag{3.29}$$

The mesh parameters and values calculated with Equations (3.16 - (3.29) are in Table 3-3. The obtained mesh independency study showed a mesh convergence with a GCI of 0.54%.

Table 3-3:The calculated mesh parameters

N(-)	∅ (-)	h(-)	r(-)	ε(-)	$\varepsilon_{course}/\varepsilon_{fine}$	P (-)	$\emptyset_{ext}$(-)	e_a (%)	e_{ext} (%)	GCI (%)
714	0.736	0.0025	1.4	-0.36	-	-	-	-	-	-
357	0.7235	0.0035	1.43	-0.1	converged	4.46	0.739	1.17	0.40	0.54
152	0.707	0.0050	-	-	-	-	-	-	-	-

3.14 Boundary conditions

The finned tube walls and the adsorbent domains have matching surfaces with different mesh topologies, and an interface was created (region-src.) to exchange heat between them numerically. The no-slip boundary condition was imposed between the adsorbent and the finned tube walls. The water vapour flow to the adsorbent is a function of the pressure and temperature. Accordingly, the pressure inlet was the most suitable boundary condition at the interface between the porous medium and the surrounding water vapour.

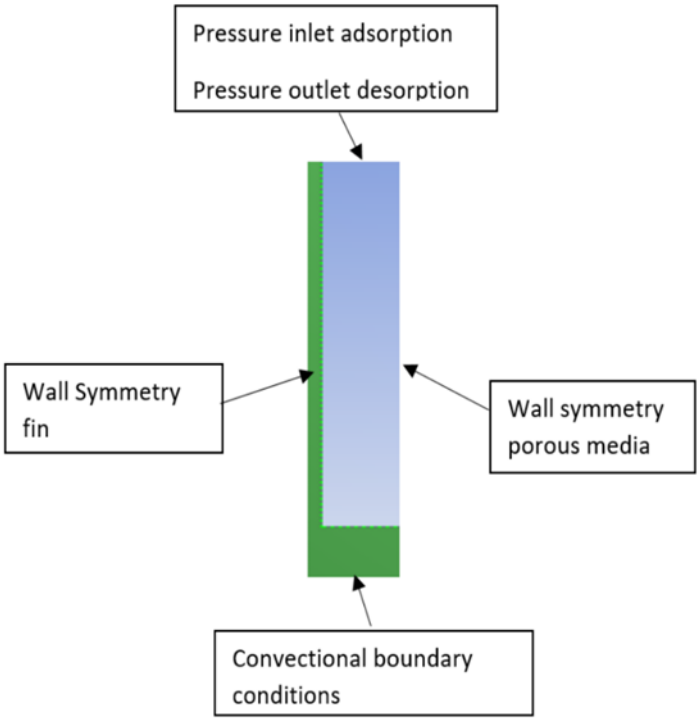

Figure 3.9: Simulation domain boundary conditions

To simulate the adsorbent bed, four computational domains in Figure 3.9 were developed to represent the packed adsorbent, the reactor bed the adsorbent vapour and the heating and cooling domains. To link up all the cell zones in the system the walls were changed to interfaces and coupled with adjacent cell zones. The contact regions between the tube wall and the adsorbent and that between the fin wall and the adsorbent were developed. The interfaces were created to allow exchange of heat between the coupled zones. For the wall to remain at constant temperature, the temperature was set in the solid domain. The finned tube heat exchanger material was used to model the shell conduction and wall thermal resistance. The fin and tube thickness of 0.00053 and 0.0015m are small and assumed to have little influence on the heat-transfer in the heat exchanger. The adsorbent was considered as a solid body whereby the adsorbate particles move in and around it. Therefore, a no-slip boundary condition was assumed between the adsorbent and wall interface. There was no friction and no relative movement between the fluid layer and boundary layer adsorbate molecules would stick to the adsorbent. The flow of the adsorbate to the adsorbent is a

function of the pressure and temperature. Hence the pressure inlet was chosen at the interface between the adsorbent and the adsorbate.

The boundary condition for the vapour to the adsorbent upper surfaces during adsorption was considered as a pressure inlet and pressure outlet for the desorption process. The pressure boundary conditions are known to give a better convergence Convection heat transfer occurs between heating/cooling water (heat transfer fluid) and the inner tube walls. The calculated heating/cooling water flow rate to maintain adsorption and desorption temperature was 0.036 kg/s. The water temperature in the tube was input as polynomial function and introduced onto fluent as free stream temperature using UDFs. The heat transfer coefficient for the convection heat transfer was determined using Dittus and Boelter correlation, as shown in Equation (3.30), and imported into the solver as a parameter in the thermal boundary conditions [160]. Computationally, the heating and cooling processes assumed no friction or relative movement between the heat transfer fluid layer and the boundary wall.

3.14.1 Dittus Boelter equation

The calculation of the convective heat transfer coefficient using the Dittus and Boelter correlation involved calculating the Nusselt number in smooth circular tubes. The Nusselt number is a dimensionless parameter that measures the ratio of convective heat transfer and conductive heat transfer determines the boundary film coefficient for heat transfer. It is a function of the Reynolds and Prandtl number Equation (3.30)

$$h = \frac{0.023\, Re_{Dh}^{0.8}\, Pr^{0.4}\, .k_f}{D_h} \tag{3.30}$$

Where Dh denotes the hydraulic diameter (m); Re is Reynolds number; Pr is Prandtl number; k_f is the thermal conductivity of the heating/cooling water (i.e., heat transfer fluid). The Dittus Boelter parameters are presented in Table 3-4.

Table 3-4: Dittus Boelter parameters

D_h (m)	ρ (kg/m^3)	μ (N.s/m)	C_p (KJ.kg.K)	k_w (W/m.K)	Nu_{Dh}	Re_{Dh}	Pr	h (kW/m.K)
0.027	995	0.0000798	4.184	0.614	218.9	127928	0.54	4.98

3.15 Modelling Validation

The validated baseline model was carefully modified to investigate different sorbent pairs. The material used for the solid porous material zone for the validation of the simulation tool was activated

carbon regarded as a versatile adsorbent with large surface area, high porous structure and high adsorption capacity and has been used in investigating adsorption cooling systems performance [14, 155, 161]. Ethanol was the adsorbate fluid and the gas phase zone. The fins and tube were made from copper. The properties of copper and ethanol were obtained from the Ansys fluent data base. The activated carbon properties were obtained from a solid porous material Maxsorb III and input into Ansys. The Dubinin- Astakhov model (D-A) Equation (3.31) was used to govern the equilibrium uptake for activated carbon/ ethanol [162].

$$\omega^0 = \omega_s exp\left(\left(\frac{RT}{E} ln\left(\frac{P_s}{P}\right)\right)^n\right) \tag{3.31}$$

Where ω^0 is the equilibrium constant, ω_s is the maximum uptake, n is the heterogeneity constant, E characteristic energy, R is the universal gas constant and P_s is the saturated pressure of ethanol at temperature T. The validation range of the temperature T according to the Antoine equation is within 292.7 and 366.63 K.

P_s , as expressed by the Antoine equation(3.32) for ethanol is given as

$$log_{10} P_s = A + \frac{B}{T+C} \tag{3.32}$$

Where A = 5.214, B = 1598.673, C = -46.424 Khanam et al [155]. The data used for the simulation was furnished in Table 3-5..

Table 3-5: Data Used for the Simulation

Parameter values	Unit	Description
Adsorbent AC properties		
464.1	Kgm^{-3}	Particle density
0.2	$W\ m^{-1}K^{-1}$	Thermal conductivity
1.375	$kJkg^{-1}K^{-1}$	Specific heat capacity
0.4345		Porosity (´Y)
8.379×10^{-12}	m^2	Permeability
3.447×10^{5}	m^{-1}	Inertial loss coefficient
3.5×10^{-4}	m	Particle radius
Cycle parameters		
800	s	Total Cycle time
20	s	Flow time / change time
400	s	Cycle counts
Temperatures		
15	℃	Evaporator temperature
20	℃	Cooling temperature
29.8	℃	Condenser temperature
80	℃	Heating temperature
Adsorption parameters		
1002	$kJkg^{-1}$	Heat of adsorption
22.97	$kJmol^{-1}$	Activation energy
139.5	$kJkg^{-1}$	Characteristic energy
132.89	s^{-1}	Pre-exponential factor
1.8		D-A,Heterogeneity parameter

Figure 3.10 compares the predicted temporal adsorbent bed temperature, water vapour uptake developed from the Multiphysics 2D model, and their analogues experimental values obtained from Khanam et al. [155], during an entire adsorption/desorption cycle. A good agreement between the predicted and experimental data was observed with a mean absolute standard error of 3%. This showed that the data obtained was reliable and meaningful to be used for assessing the dynamic temperature and water uptake changes taking place in the adsorbent bed during adsorption and

desorption. On the other hand, simulating many cycles until steady cycles are obtained could be time consuming given the time taken for the simulation of one cycle. Therefore, a decision to use a single cycle analysis based on the literature and simulation time was adopted for this study.

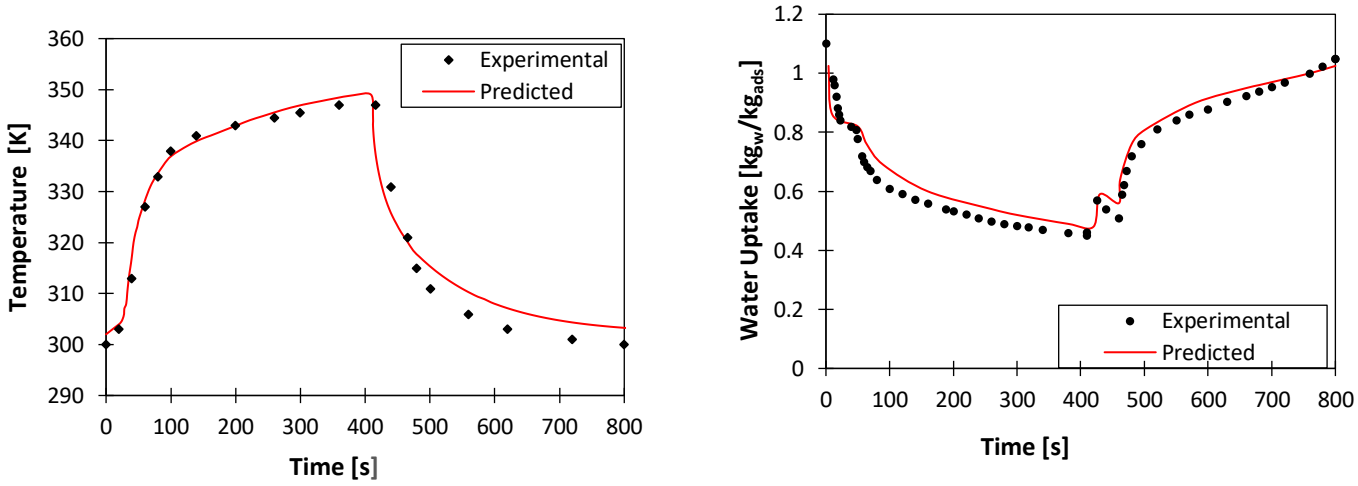

(a) (b)

Figure 3.10: 2D Multiphysics model validation (a) cyclic temperature profile and (b) cyclic water uptake profile

3.16 Adsorbent material performance assessment system level

The adsorption cooling and desalination system's performance utilising the adsorbents under investigation in this study was assessed based on the specific daily water production (SDWP), specific cooling power (SCP), coefficient of performance (COP) and exergy efficiency (ηex).

$$SDWP = N \int_0^{t_{cycle}} \frac{\dot{Q}_c}{\rho_w . h_{fg.} M_{ad}} \, dt \tag{3.33}$$

Where t_{cycle} is cycle time; h_{fg} is the latent heat of condensation of water; M_{ad} is the adsorbent mass; ρ_w is density of water 1tonne /m^3; N (day^{-1}) is number of cycles per day defined by N= 86400[s/d]/t_{cycle}; $\dot{Q}_c$(kW) is the condensation heat flux.

$$SCP = \frac{\int_0^{t_{cycle}} \frac{\dot{Q}_e}{M_{ad}} \, dt}{t_{cycle}} \tag{3.34}$$

$$COP = \frac{\int_0^{t_{cycle}} \dot{Q}_e \, dt}{\int_0^{t_{cycle}} \dot{Q}_{des} \, dt} \tag{3.35}$$

$$\eta_{ex} = \frac{\int_0^{tcycle} E_x \dot{Q}_e dt}{\int_0^{tcycle} E_x \dot{Q}_{in} dt} \quad (3.36)$$

Where,

$$Q_c = \int_0^{t_{cycle}} \dot{m}_c c_p(T_c)(T_{c\,out} - T_{c\,in})\, dt \quad (3.37)$$

$$Q_{des} = \int_0^{t_{cycle}} \dot{m}_{hw} c_p(T_{hw\,in} - T_{hw\,out})\, dt \quad (3.38)$$

$$Q_e = \int_0^{t_{cycle}} \dot{m}_{chw} c_p(T_e)(T_{chw\,in} - T_{chw\,out})\, dt \quad (3.39)$$

3.16.1 Exergy

The exergy efficiency is crucial to assessing the impact of the entropy generated (i.e., the irreversibility) in the adsorbent bed alongside the energy conversion efficiency represented by the COP. While the COP determines the ratio of the produced cooling and the heat supplied, the exergy efficiency quantify how much of the applied heat was effectively utilised in the actual production of water and cooling.

Heat transfer through a finite temperature difference generate entropy and causes some Irreversibility resulting in exergy destruction. The exergy destroyed is always proportional to the entropy generated as shown in Equation (3.40). The irreversibility coming about from the thermodynamic non-equilibrium found in system components are explained by the entropy or exergy analysis based on the second law of Thermodynamics. There are also external irreversibility that exist as a result of the temperature difference between HTF and heat source during heat input and the temperature difference between adsorbent bed and the HTF during heat rejection [163]. Exergy analysis enables the finding of the exergy destruction for each process and component and hence determine accurate magnitudes of the exergy losses [164].

Chua et al [165], performed an entropy study on a two bed non -regenerative chiller. Their findings showed that the largest entropy generation was in the adsorbent bed and the least losses were in the condenser. In their study of the dissipative loses in batch operated adsorption cycles, Thu et al

[166], concluded that there was an increase in cycle entropy generation with increase in heat source temperature and the highest entropy generation was in the adsorption process.

The exergy analysis was performed based on the detailed results obtained from the CFD simulation of the investigated adsorbents in this study. The general rate of exergy balance for adsorption cycle is expressed in equation (3.40).

$$X_{dest} = T_{\circ}\, S_{gen} \geq 0 \tag{3.40}$$

Where X_{dest} is exergy destruction, $T_{\circ}$ is the temperature of the environment and S_{gen} is the entropy generated during the irreversible processes. The exergy destruction of components in the adsorption system is performed by applying the exergy balance equation (3.41).

$$\Delta U - T_{\circ}\Delta S = \sum\left(1-\frac{T_{\circ}}{T_i}\right)Q_i + \sum_{in} m(h-T_{\circ}s) - \sum_{out} m(h-T_{\circ}s) - T_{\circ}\cdot\Delta S_{gen} \tag{3.41}$$

Where $\Delta U - T_{\circ}\Delta S$ denotes the maximum potential which correspond to change in internal energy U and entropy S of the system. $\sum\left(1-\frac{T_{\circ}}{T_i}\right)Q_i = \sum E_x Q_i$ denotes the exergy due to heat transfer to the environment, the second and third terms $\sum_{in} m(h-T_{\circ}s) = \epsilon_i$ and $\sum_{out} m(h-T_{\circ}s) = \epsilon_f$ denotes mass exergy variation between the initial state (inlet) and final state (outlet) of the system The last term . $T_{\circ}\cdot\Delta S_{gen}$ denotes exergy destruction proportional to the entropy generated as result of the irreversible processes. s denotes the specific entropy J $kg^{-1}K^{-1}$, h is the specific enthalpy (J kg^{-1}, Q is the heat transfer (J) and $T_{\circ}$ is the dead state temperature.

Rewriting Equation (3.41) to find the rate exergy loss/destruction, we get equation (3.42).

$$\dot{X}_{dest} = \sum E_x Q_i + \sum \epsilon_i - \sum \epsilon_f - (\Delta U - T_{\circ}\cdot\Delta S_{gen}) \tag{3.42}$$

Where ϵ denotes the specific flow exergy.

Applying Eq (3.42) to the adsorbent bed for calculating exergy destruction during adsorption and desorption processes.

3.16.2 Desorption

During the desorption process, the vapour produced during the heating process goes to the condenser. The supplied heat to system is for supporting the endothermic process associated with desorption while some of it will heat up the reactor bed and the adsorbent material resulting in exergy destruction. The exergy destruction X_{des} during desorption is expressed as

$$X_{des} = \sum E_x Q_{des} - (\epsilon_f - \epsilon_{in}) - (\Delta U_{des} - T_{\circ}\cdot\Delta S_{des}) \tag{3.43}$$

Where,

$$E_xQ_{des} = \sum\left(1-\frac{T_o}{T_i}\right)Q_{des} = \left(1-\frac{T_o}{T_H}\right)\left(\int_{T_{sa}}^{T_g} c_{sa}\,(T)dT + \int_{T_{sa}}^{T_g} m\,(T)c_l(T)dT + \int_{T_{sa}}^{T_g} q_{st}\,(T)|dm(T)|\right) \quad (3.44)$$

$$\epsilon_f - \epsilon_{in} = \int_{T_s}^{T_g} q_{st}\,(T)|dm(T)| - T_o \int_{T_s}^{T_g} \frac{q_{st}(T)}{T}|dm(T)| \quad (3.45)$$

$$\Delta U_{des} = \left(\int_{T_s}^{T_g} c_{sa}\,(T)dT + \int_{T_{sa}}^{T_g} m\,(T)c_l(T)dT\right) \quad (3.46)$$

$$\Delta S_{des} = \left(\int_{T_s}^{T_g} c_{sa}\,(T)\frac{dT}{T} + \int_{T_{sa}}^{T_g} m\,(T)c_l(T)\frac{dT}{T}\right) \quad (3.47)$$

Where $E_x\,Q_{des}$ denotes exergy due to the heat supplied during the desorption process, c is the specific heat capacity of the adsorbed phase, T (K) is the desorption temperature, sa denotes adsorbent, g denotes gaseous state, l denotes liquid state. q_{st} is the adsorption uptake (kg/kg).

3.16.3 Adsorption process

During the adsorption process the water vapour moves to the reactor bed and adsorbed there causing an increase in the adsorbate mass in the bed. The adsorber reactor is cooled to remove the heat generated by the adsorption process. The exergy destruction during this process can be denoted by equation (3.48):

$$X_{ads} = \sum E_xQ_{ads} - (\epsilon_f - \epsilon_{in}) - (\Delta U_{ads} - T_o \cdot \Delta S_{ads}) \quad (3.48)$$

Where,

$$E_xQ_{ads} = \sum\left(1-\frac{T_o}{T_i}\right)Q_{ads} = 0 \quad (3.49)$$

$$\epsilon_f - \epsilon_{in} = -\left[\int_{T_s}^{T_g} q_{st}\,(T)dm(T) - T_o \int_{T_s}^{T_g} \frac{q_{st}(T)}{T}dm(T)\right] \quad (3.50)$$

$$\Delta U_{ads} = \left(\int_{T_s}^{T_g} c_s\,(T)dT + \int_{T_s}^{T_g} m\,(T)c_l(T)dT\right) \quad (3.51)$$

$$\Delta S_{ads} = \left(\int_{T_s}^{T_g} c_s(T)\frac{dT}{T} + \int_{T_s}^{T_g} m(T)c_l(T)\frac{dT}{T}\right) \quad (3.52)$$

Where $E_x Q_{ads}$ denotes exergy due to the heat generated during the adsorption process, Q is the heat (J).

3.16.4 Condenser

The exergy destruction in the evaporator and condenser took into consideration the partially stationary contents in these components. The exergy destruction in the condenser is expressed as

$$X_c = \sum E_x Q_c - (\epsilon_f - \epsilon_{in}) \quad (3.53)$$

Where,

$$E_x Q_c = \left(1 - \frac{T_\circ}{T_c}\right) Q_c = 0 \quad (3.54)$$

$$(\epsilon_f - \epsilon_{in}) = m_a \left[h_g(T_c) - h_v(T_c)\right] - m_a \cdot T_\circ \left[s_g(T_c) - s_v(T_c)\right] \quad (3.55)$$

Where T_c is the condenser temperature, v denotes the vapor phase, m_a is mass of adsorbed phase.

3.16.5 Evaporator

The exergy for evaporator is modelled similar to the condenser modelling and is expressed as

$$X_e = \sum E_x Q_c - (\epsilon_f - \epsilon_i) \quad (3.56)$$

$$E_x Q_e = \left(1 - \frac{T_\circ}{T_e}\right) Q_e \quad (3.57)$$

$$(\epsilon_f - \epsilon_i) = m_a \left[h_v(T_e) - h_g(T_e)\right] - m_a \cdot T_\circ \left[s_v(T_e) - s_g(T_e)\right] \quad (3.58)$$

3.17 Exergy efficiency

Summation of the exergy destruction for each component will give the total exergy destruction for whole system and is expressed as equation (3.59).

$$X_{Dest} = X_{des} + X_{ads} + X_c + X_e + X_{tv} \quad (3.59)$$

Applying the exergy balance to the whole system gives the following equation(3.60)

$$E_x\, Q_{in} = E_x Q_e + X_{Dest} \quad (3.60)$$

Where, $E_x\, Q_{in}$ denotes the exergy due to heat supplied to the system.

$$E_x\, Q_{in} = E_x\, Q_{des} \quad (3.61)$$

The exergy efficiency is denoted by equation (3.62)

$$\eta_{ex} = \frac{\int_0^{tcycle} E_x\, \dot{Q}_e\, dt}{\int_0^{tcycle} E_x\, \dot{Q}_{in} dt} = 1 - \frac{\int_0^{tcycle} X_{Dest}\, dt}{\int_0^{tcycle} E_x\, \dot{Q}_{in} dt} \quad (3.62)$$

CHAPTER 4: STUDYING GRAPHENE OXIDE AS A PARENT ADSORBENT

4.1 Introduction

This chapter builds on the attractive thermal performance of graphene allotropes and revolves around studying the viability of graphene oxide as a new sorbent. Graphene oxide (GO) is a derivative of graphene with a similar structure and is produced by graphite oxidation using the Hummers method and the exfoliation of graphite oxide into thin sheets by reducing the number of layers [167, 168]. GO sheets are separated from graphite oxide easier than graphene can be separated from graphite, meaning that GO's production is potentially scalable [89]. GO has expandable inter-layer spacing, and active oxygen functional groups, such as epoxy, phenolic hydroxyl and carboxylic, on its surface that act as active sites interacting with water vapour molecules. GO has similar properties to graphene such as high surface area, high electrical conductivity, and high mechanical strength. Furthermore, its swift water transport mechanism attributed to oxygenated functional group has attracted interest in utilising it in dehumidification applications [167, 168]. Although GO has attractive properties, what has not yet been studied is using it as high thermal diffusive parent adsorbents to address the material-level poor heat and mass transfer in adsorption systems. Therefore, this chapter covers the quantitative and qualitative analysis that was undertaken to understand utilising graphene oxide as a parent adsorbent for cooling and desalination and its influence on the system level's energy conversion potential – via exergy analysis and overall performance–via energy analysis–under various operating conditions. As such, the objectives are to (1) experimentally investigate the adsorption and thermal characteristics of Graphene Oxide and benchmark it against the baseline silica gel adsorbent; (2) use the developed 2D Multiphysics computational model to envisage the heat and mass transfer performance at the adsorbent bed level; (3) study the influence of varying the heat source temperature, cycle time and evaporation temperature on the adsorbent bed and overall system performance by undertaking energy and exergy analyses when utilising graphene oxide and silica gel.

4.2 Materials

The investigated GO as a new water sorbent for cooling cum desalination application was benchmarked against the widely used RD Silica gel (RD 2060 of 0.18-1mm particle size) and porosity of 0.36. GO of 1-3 carbon atomic layers, and a particle size of 0.5-20μm was utilised and sourced from Graphitene ltd. Figure 4.1 shows SEM images for the employed GO and silica gel samples.

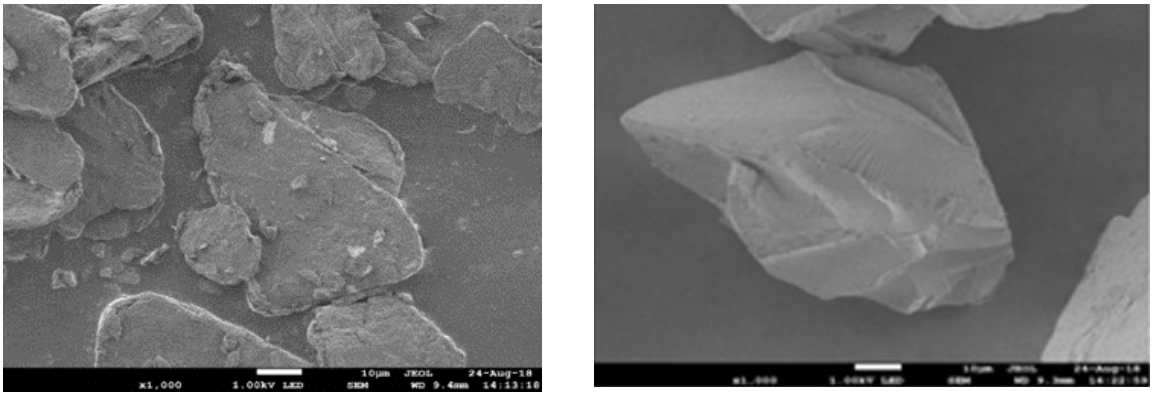

(a) (b)

Figure 4.1: SEM images for (a) Graphene Oxide and (b) Silica gel

4.3 Adsorption characteristics modelling

Figure 4.2 shows the adsorption isotherms of GO and SG measured at 15 and 35°C. It can be observed that the sorption equilibrium uptake for GO increased by increasing the temperature indicating the chemisorption phenomenon, unlike that for silica gel, decreased by increasing the temperature due to the physical sorption [169] .

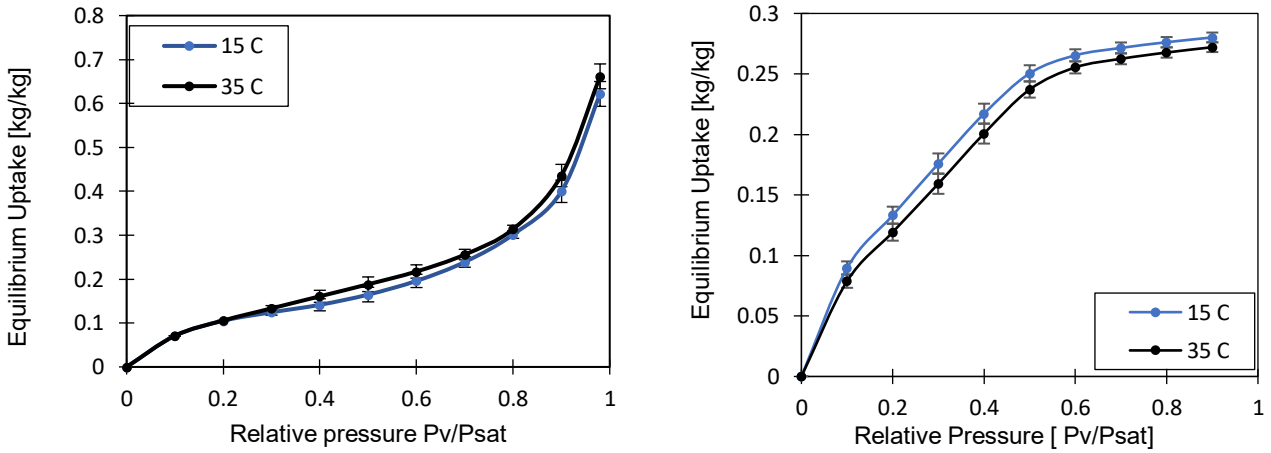

(a) (b)

Figure 4.2: Experimental isotherms for(a)graphene oxide and(b) silica gel at 15°C and 35°C

4.3.1 Isotherms modelling

The Tóth model was the most suitable for mathematically imitating the experimentally determined isotherms for GO, especially at low vapour pressure isotherms. Therefore, empirically, equation (4.1) was developed to model GO based on the Tóth equation, dubbed the GO-modified Tóth model.

$$W^{*}=\frac{Ko\times exp\left(\frac{Q_{st}}{(RT)}\right)\times\frac{P_v}{P_{sat}}}{1+\left[\frac{exp\left(\frac{Q_{st}}{(RT)}\right)}{q_m}\times\frac{P_v}{P_{ads}}\right]^{(t)\,1/t}\times 1-m\times\left(\frac{P_v}{P_{sat}}\right)^{n}} \quad (4.1)$$

Where W*(kg_w/kg_{ads}) denotes the equilibrium uptake; Ko (KPa^{-1}) is the adsorption constant; R is the universal gas constant; T (K) is adsorption temperature; P_v (kPa) is the vapour pressure for the adsorbed vapour; P_{sat} (kPa) is the saturation pressure of the adsorbent at the given operating temperature; q_m (kg/kg) is the monolayer adsorption capacity; t, n and m are empirical dimensionless indexes; Q_{st} (kJ/kg) is the heat of adsorption.

The heat of adsorption is estimated by employing the Clausius-Clapeyron equation (4.2) using equilibrium isotherm data for at least three temperatures. Table 4-1 shows the parameters of the modified-GO Tóth model developed from experimental data with a regression parameter (R2) of 0.989 and the isosteric heat of adsorption. The developed isotherm model agrees well with the experimental adsorption isotherm of 0.07 mean deviation, as shown in Figure 4.3.

$$Q_{st} = - R\frac{\partial (\ln P)}{\partial \frac{1}{T}} \quad (4.2)$$

Table 4-1: GO-Modified Tóth model's coefficients.

Q_{st} (kJ/kg)	K_0 (KPa-1)	R (kJ/kg K)	q_m (kg/kg)	t	m	n
2740	0.2476	8.31	0.612	3.7	1.360	2

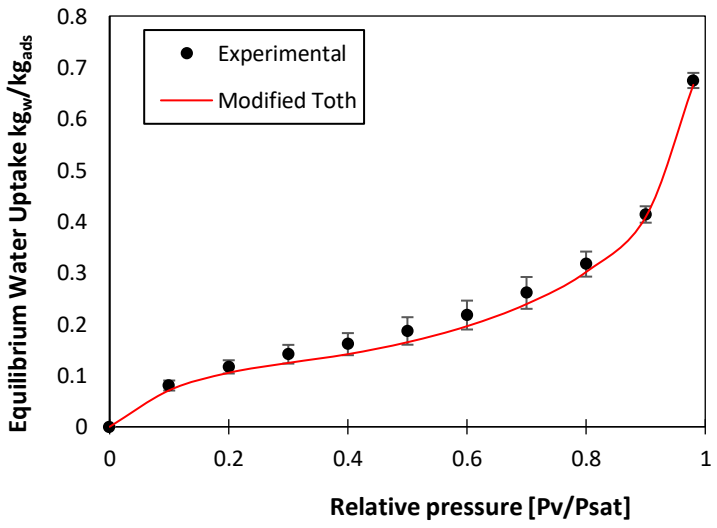

Figure 4.3: Isotherms model for GO - modified Tóth

The widely known modified Freundlich model was employed to imitate the adsorption isotherms for the Silica gel baseline adsorbent – as recommended by Youssef et al. [46]. The modified Freundlich model equation can be described by equations (4.3), (4.4) and (4.5)and it was employed to develop the SG's isotherms, where the isotherms model's constants are furnished in Table 4-2. Figure 4.4 shows the SG's isotherm model.

$$w^{*}=A(T_{ads})\left[\frac{P_{sat}(T_{ref})}{P_{sat}(T_{ads})}\right]^{B(T_{ads})} \tag{4.3}$$

$$A(T_{ads})=A_0+A_1T_{ads}+A_2T_{ads}^2+A_3T_{ads}^3 \tag{4.4}$$

$$B(T_{ads})=B_0+BT_{ads}+B_2T_{ads}^2+B_3T_{ads}^3 \tag{4.5}$$

Table 4-2 - Modified Freundlich model's coefficients

Constant	Value	Constant	value
A_0	-6.5314	B_0	-15.587
A_1	0.72452E	B_1	0.15915
A_2	-0.23951E-3	B_2	-050612E-3
A_3	0.25493E-6	B_3	0.53290E-6
ΔH_{ads}	2.939E6		

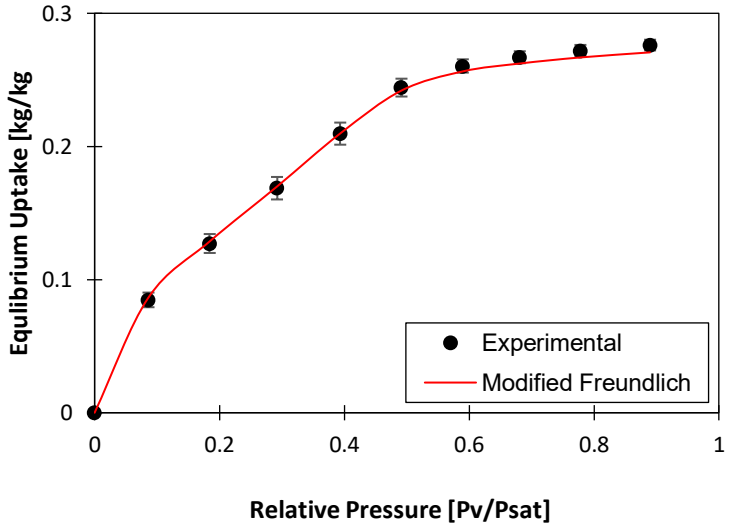

Figure 4.4: Isotherm model for SG - modified Freundlich

4.3.2 Adsorption kinetics modelling

Utilising the LDF model for adsorption kinetics modelling as introduced in Chapter 3 and using equation (4.6).

$$\frac{\partial \omega}{\partial t} = \left(15 \frac{D_{so}}{R_p^2} \right) exp^{\frac{-E_a}{RT}} (w^* - w) \tag{4.6}$$

The model's coefficients are shown in Table 4-3.

Table 4-3 - The empirical constants for the LDF model

Parameter	value		Unit
	Graphene Oxide	**Silica gel**	
D_{so}	4.4E-4	2.54E-4	m^2/s
E_a	32000	42000	J/mol
R_p	1E-6	0.16E-5	m

4.4 Computational modelling

A 2D Multiphysics simulation model developed in Chapter 3 was employed to envisage adsorption/desorption in an adsorbent bed utilising GO/water working pair and benchmark its performance against Silica gel/water. The influence of the operating conditions (i.e., temperature and pressure) on the thermo-physical properties of GO and SG during the adsorption/desorption processes were considered. The development of the modelling tool and simulation procedure is given in Chapter 3. The thermophysical properties are added to the simulation pre-processing as material properties and are found within the Fluent database [5].

4.5 Material /system Performance

The performance of GO as an adsorbent is based on its material level, component and system level performance obtained from the experimental and computational modelling investigation performed. This section presents the isotherm cyclic performance of GO at material level, its impact on the heat and mass transfer at the adsorbent bed level and consequently the overall system performance benchmarking them against those of Silica gel. Furthermore, the exergy analysis to ascertain the impact of enhancing the heat and mass transfer on the system energy conversion performance was carried out. The adsorbent bed and overall cycle performance analysis was based on primary operating conditions heat source temperature and cycle time centred on two evaporator temperatures 12°C and 30°C.

4.5.1 Cyclic performance

The cyclic analysis based on the experimentally developed isotherms was undertaken to determine the cyclic equilibrium water uptake potential (i.e., the material level figure of merit) for GO and benchmark it against SG, as shown in Figure 4.5. In such analysis, the condensation and regeneration temperatures were maintained at 35°C and 85°C respectively. At 12°C evaporator temperature, corresponding to 1 kPa vapour pressure, the net cyclic water vapour uptake was 0.07kg_w/kg_{ads} for SG and 0.05kg_w/kg_{ads} for GO water, while at 30℃, corresponding to 4.2kPa vapour pressure [170], the net cyclic equilibrium uptake of GO outperformed that of SG by 36%, as the isotherms for both materials' isotherms intersect at 4.2kPa. It is noteworthy that low evaporator temperature might not be demanded when freshwater production is prioritised over cooling. These findings align with the previously reported results by Lian et al [86].

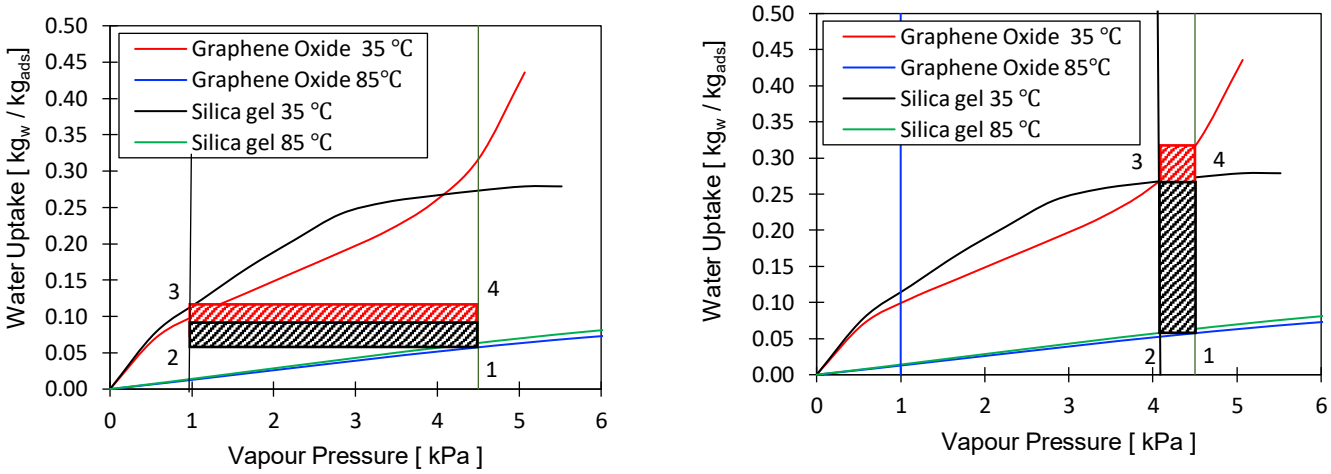

Figure 4.5: Comparison of GO and SG at 35℃, condensation and 85℃, regeneration temperatures (a) 12 ℃ evaporation temperature and (b) 30℃ evaporation temperature

The isotherm-based cyclic analysis did not consider the impact of the thermal performance of either material at the adsorbent bed level. Therefore, the Multiphysics model for the adsorbent bed was employed to study the combined effect of adsorption and thermal characteristics for GO and SG at the component level. 800s cycle time, including 30s switching (preheating/precooling) time, was considered. Figure 4.6 shows the cyclic dynamic changes in the adsorbent bed's temperature at evaporator temperatures 12°C and 30°C. Though the outstanding performance of silica gel from the isotherm-based cyclic performance perspective at low evaporator temperature, its low thermal diffusivity hindered the utilisation of such an adsorption capacity. Accordingly, the cyclic uptake of GO outperformed SG at the component level at evaporator temperature below 12℃ by 69.7% over the entire cycle, owing to its relatively faster thermal response, as confirmed by the dynamic temperature profiles in Figure 4.6-a and b. The findings align with Elsheniti et al. [2]; the material's

low thermal diffusivity negatively impacts the component and system level's performance. At an evaporator temperature of 30℃, while the cooling water temperature was 35°C, GO's compound advances in adsorption and thermal characteristics led to higher water uptake by 60% over the entire cycle, as shown in Figure 4.7. The colourmaps contours for the dynamic temperature profiles and dynamic water uptake shown in Figure 4.6 and Figure 4.7 respectively, are indicating the average sorbent temperature and uptake for a full cycle which include the adsorption/desorption process. The time allocated for each colourmap are for the full adsorption and desorption cycle rather than the half cycle time.

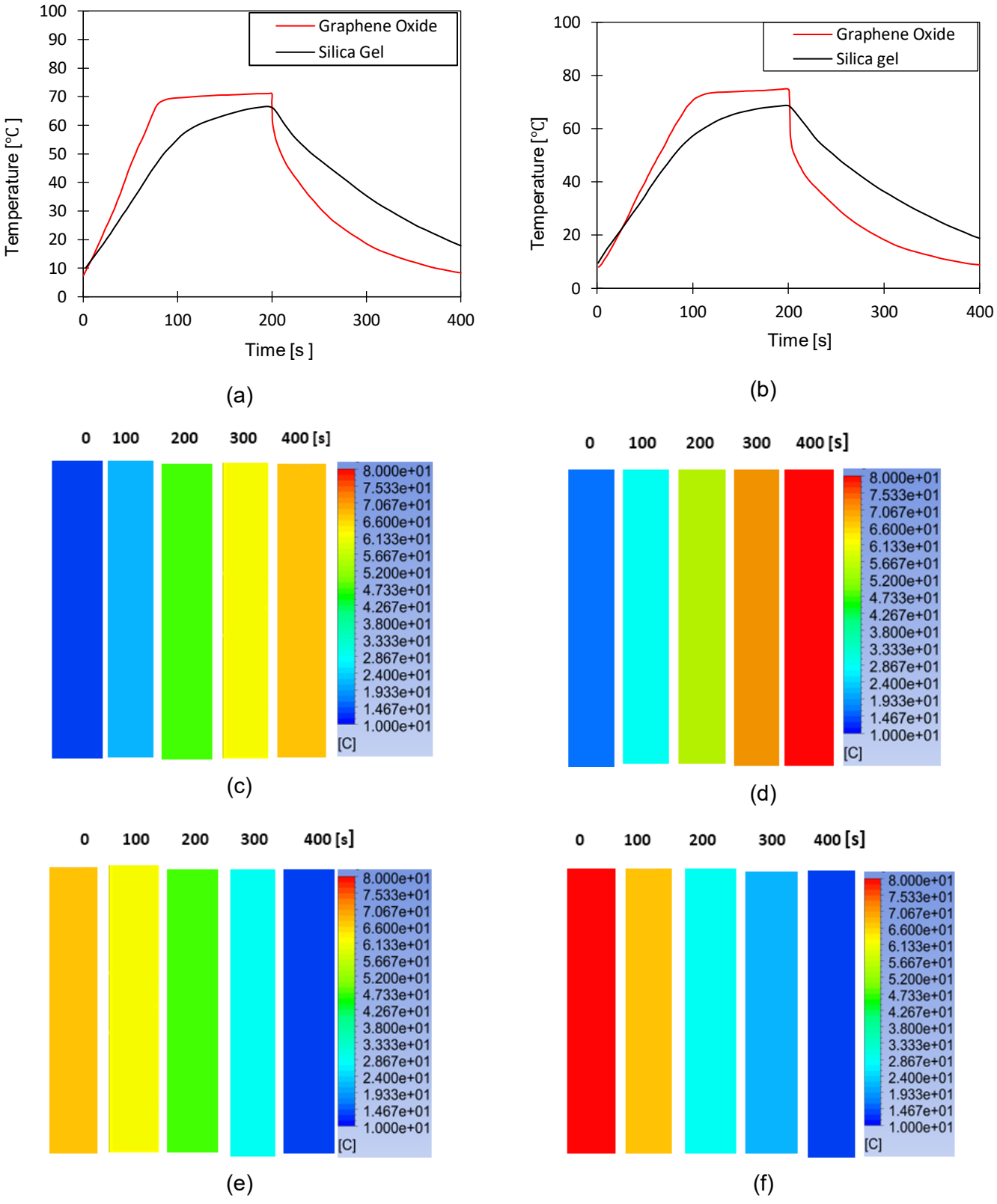

Figure 4.6: Dynamic temperature profiles for GO and SG at (a) 12°C evaporator temperature and (b) 30°C evaporator temperature; adsorption bed temperature for (c) SG and (d) GO at evaporator temperature 12 °C; (e) desorption bed temperature for (e) SG and (f) GO at evaporator temperature 12 °C

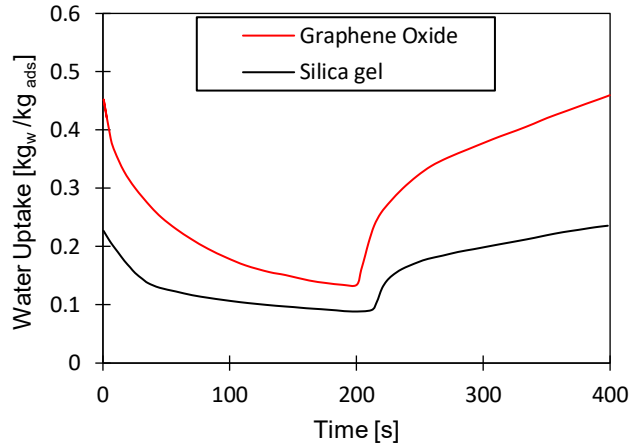

(a)

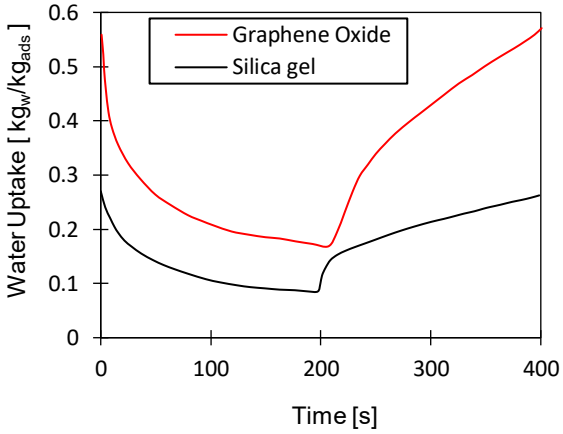

(b)

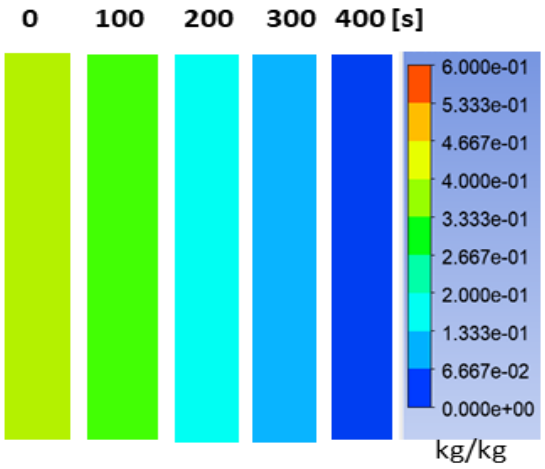

(c)

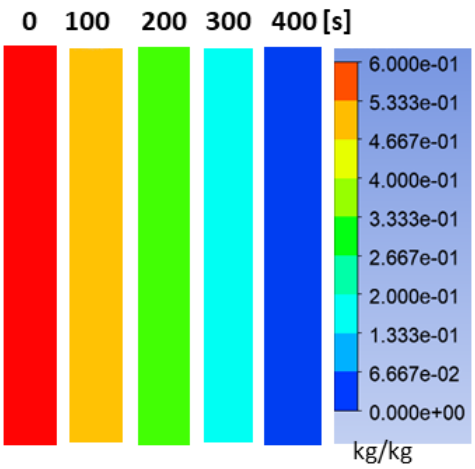

(d)

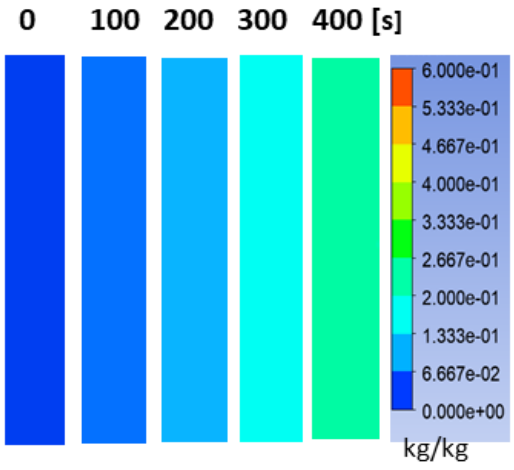

(e)

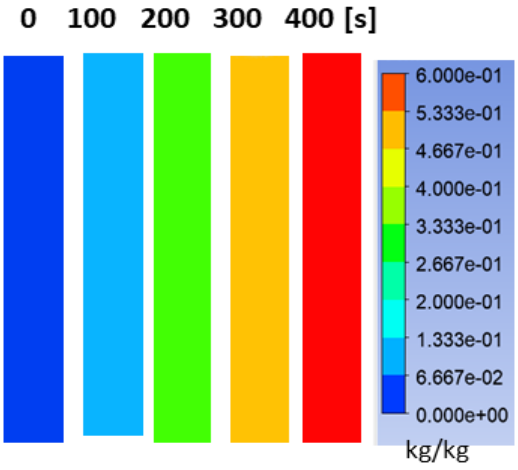

(f)

Figure 4.7: Dynamic uptake profiles for GO and SG at (a) 12°C evaporator temperature and (b) 30°C evaporator temperature; adsorption uptake for (c) SG and (d) GO at evaporator temperature 12 °C; (e) desorption uptake for (e) SG and (f) GO at evaporator temperature 12 °C.

The simulation operating conditions parameter used in this study are shown in Table 4-4.

Table 4-4: Parameters and operating conditions

Parameter	Value	Unit
M_{GO}	0.4	kg
M_{SG}	0.22	kg
M_{hex}	2.02	kg
T_{evap}	12-30	℃
T_{cond}	35	℃
T_{cw}	35	℃
T_{des}	65-85	℃
T_{ads}	35	℃
T_{chw}	35	℃
Ads/des bed flow rate	0.036	kg/s
Evap flow rate	0.018	kg/s
Cond flow rat	0.048	kg/s
Cycle time	400 -800	s

4.5.2 Exergy destruction

The exergy analysis was undertaken to understand the degradation of energy in each component during the adsorption/desorption processes using GO/water and benchmarked against SG/water. Table 4-5 shows the exergy destruction and exergy efficiency for the GO- and SG-based systems. It was observed that the highest exergy destruction occurred in the adsorbent beds. For the investigated operating conditions, the exergy destruction during desorption and adsorption was 9.861kW and 11.247kW for the GO-based system at 85 and 30°C, respectively. The same trend was observed in the SG-based system, as the exergy destruction during the desorption and adsorption were 6.165 kW and 7.523kW, respectively. These results agree with Cao et al [164] using the SG/water adsorption pair.

The high exergy destruction in the adsorbent bed is attributed primarily to the substantial temperature differences between the heat transfer fluid and adsorbent at the beginning of the adsorption/desorption processes. These temperature differences comprise most of the irreversibility quantified by the high exergy destruction during the entire cycle. The exergy destruction in desorption is higher than the adsorption due to the relatively higher regeneration temperature levels.

The fractional contributions of each component to the overall exergy destruction in the systems are shown in Figure 4.8. On the one hand, the GO-based system showed higher exergy destruction, which is attributed to the fact that GO has high thermal diffusivity that increases the heat transfer

rate hence higher temperature levels in the adsorbent beds. On the other hand, the same heating water inlet temperature caused the opposite effect in the SG-based system but at the expense of the mass transfer hence the cooling and clean water production. Therefore, the system's exergy efficiency was determined to understand the exergy destruction on the energy conversion quality. As a result, the GO-based system showed a higher overall exergy efficiency of 21.2% than the SG-based system of 16.6%. Such a higher exergy efficiency means more thermal energy was effectively utilised to produce clean water and cooling, which is attributed to GO's superior heat transfer characteristics to SG. In other words, the thermal energy consumed by the metal and the adsorbent material comprises the exergy deficiency in the form of irreversibility [171].

Table 4-5 - Exergy destruction for adsorption system components

Component/Process	**Graphene Oxide**	**Silica Gel**
	Exergy destruction (kW)	
Adsorption at 35 °C	9.861	6.165
Desorption at 85 °C	11.247	7.523
Condenser at 35 °C	1.223	1.202
Evaporator at 30 °C	1.475	1.385
System overall	22.264	14.099
	Exergy efficiency (%)	
	21.2%	16.6%

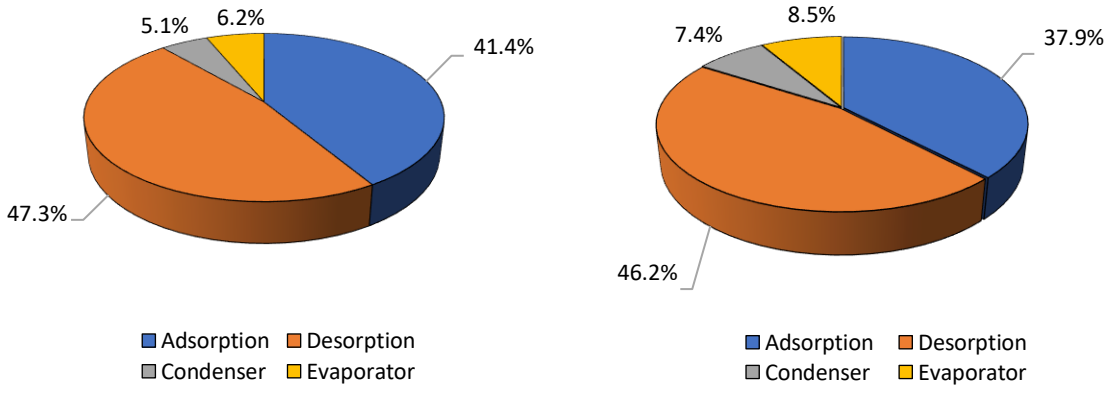

(a) (b)

Figure 4.8: Exergy destruction fraction for components utilising (a) GO and (b) SG.

4.5.3 The effect of cycle time

The effect of cycle time on the adsorbent bed's performance was investigated for two cycles, 800s and 400s, including 30s switching time each and evaporation temperatures of 12℃ and 30℃, as shown in Figure 4.9 - Figure 4.10. The heating and cooling water inlet temperatures were maintained at 85°C and 35°C, respectively. At 400s cycle time and 30°C evaporation temperature, the net cyclic water uptake was 0.45kg_w/kg_{ads} and 0.2kg_w/kg_{ads} in GO and SG-based systems. Similarly, at 800s cycle time, the net cyclic water uptake was 0.57kg_w/kg_{ads} while SG 0.24kg_w/kg_{ads} in GO- and SG-based systems, respectively. The higher cyclic water uptake reflects the faster thermal response of GO than SG. At 400s cycle time and 30°C evaporation temperature, the net cyclic temperature rise was 60°C and 51°C in GO- and SG-based systems, respectively. At 800s cycle time, the net cyclic temperature rise was 70°C and 58°C in GO and SG-based systems, respectively. A steep rise in the temperature was observed during the first 100s and 200s for 400s and 800s cycle times, followed by a plateau in the GO-based system, whereas the temperature rise was gradual in the case of the SG-based system.

At 400s cycle time and 12°C evaporation temperature, the net cyclic water uptake was 0.32kg_w/kg_{ads} and 0.10kg_w/kg_{ads} in GO- and SG-based systems. At 800 s cycle time, the net cyclic water uptake was 0.352kg_w/kg_{ads} while SG was 0.12kg_w/kg_{ads} in GO and SG-based systems. At 400s cycle time and 12°C evaporation temperature, the net cyclic temperature rise was 60°C and 55°C in GO- and SG-based systems, respectively. At 800 s cycle time, the net cyclic temperature rise was 71°C and 57°C in GO- and SG-based systems, respectively. Similarly, a steep rise was observed in the temperature almost during the first 100s and 200s for 400s and 800s cycle times, followed by a plateau in the GO-based system. However, the temperature rise was gradual in the case of the SG-based system. The observed plateau in the GO-based system was due to the build-up of heat in the adsorbent bed. During the adsorption process, the temperature drop was faster in the first few seconds in the case of the GO-based system than in the SG-based system, followed by a gradual reduction in temperature. Such observation was for the GO-based system under various evaporation temperatures and cycle times. The influence of cycle time observed in this investigation agree with Li et al [172].

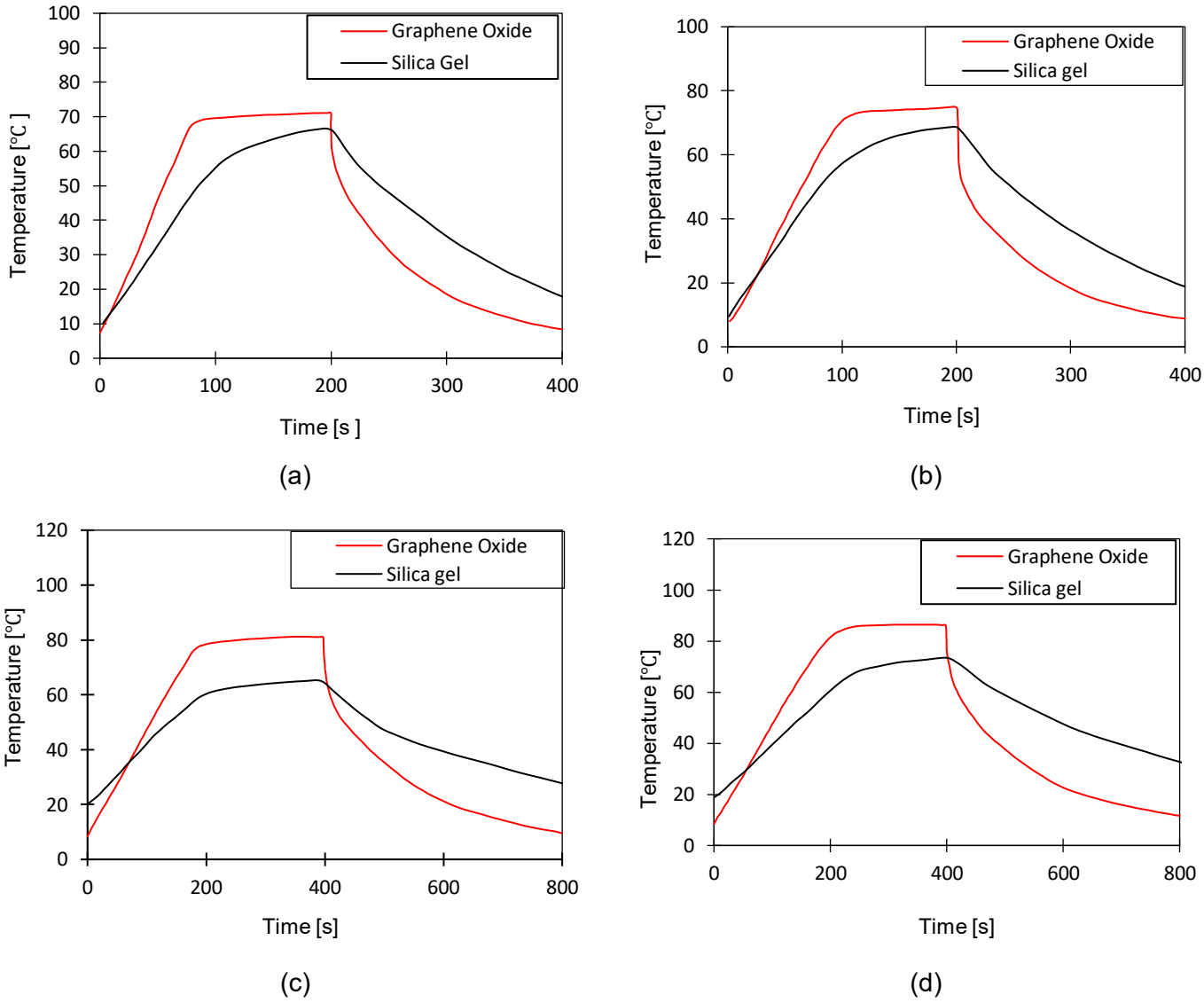

Figure 4.9: Dynamic temperature profiles for SG and GO at (a) Tev=12°C temperature tcycle=400s; (b) Tev=30°C temperature tcycle=400s; (c) Tev=12°C temperature tcycle=800s; (d) Tev=30°C temperature tcycle=800s.

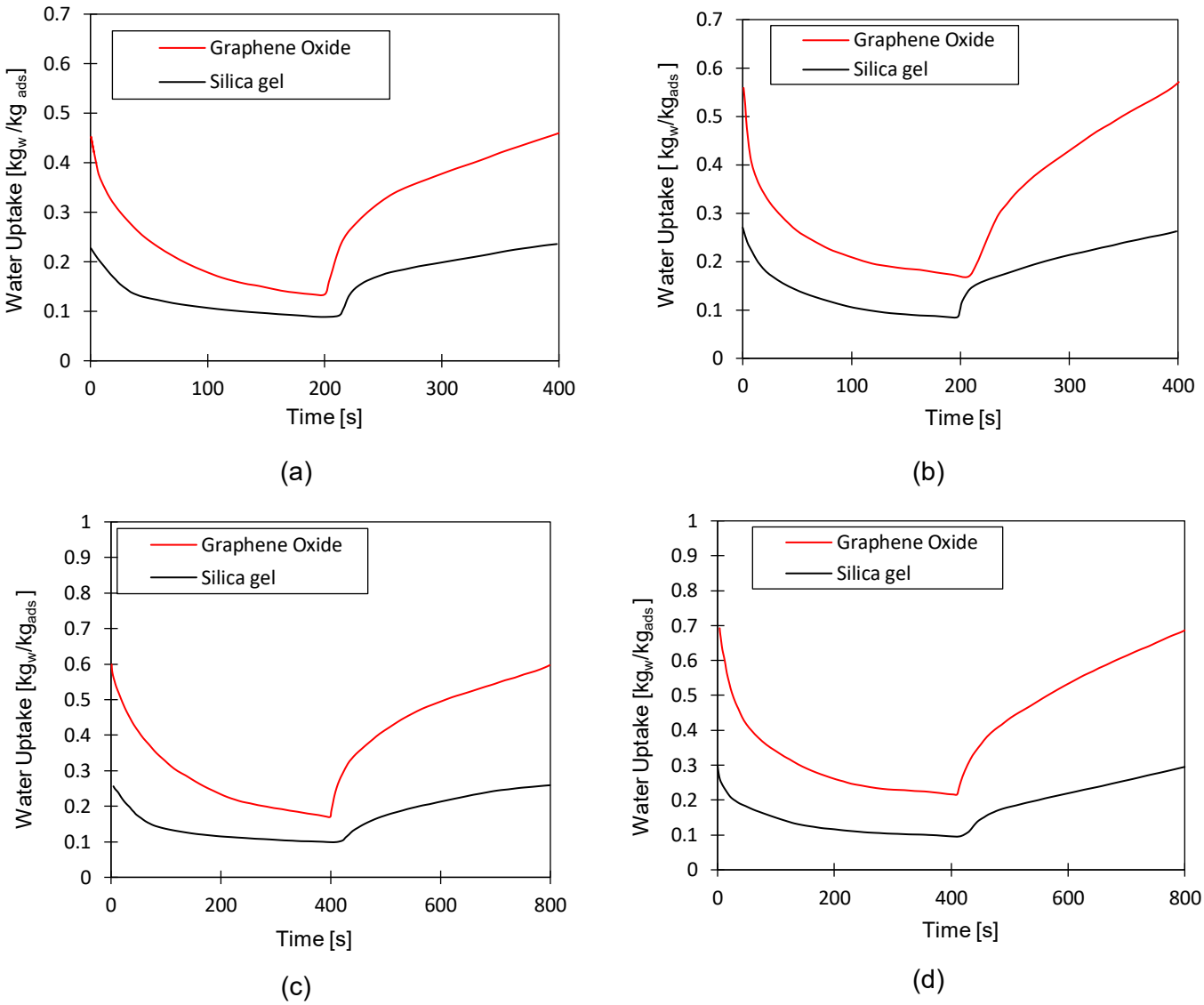

Figure 4.10: Dynamic water uptake profiles for SG and GO at (a) Tev=12°C temperature tcycle=400s; (b) Tev=30°C temperature tcycle=400s; (c) Tev=12°C temperature tcycle=800s; (d) Tev=30°C temperature tcycle=800s.

The investigation was extended to include the influence of varying the cycle time on the overall system performance, as shown in Figure 4.11, Figure 4.12, Figure 4.13 and Figure 4.14 Generally, it was observed that SDWP, SCP, COP, and exergy efficiency in both GO-based and SG-based systems increased by increasing the cycle time as the systems approached the equilibrium conditions. The overall system performance enhancement was attributed to increasing the cyclic water uptake by extending the adsorption/desorption time, which positively influenced the clean water and cooling production. The GO-based system operated at 12°C evaporation temperature showed SDWP, SCP, COP, and exergy efficiency averagely higher than the SG-based system by 46%, 25%, 13% and 15.8%. The average increase in SDWP, SCP, COP and exergy efficiency were 41%, 27%, 15% and 19% when utilising GO compared to SG at 30°C evaporation temperature. The increase in the overall system performance reflects a faster thermal response of GO that enhanced

the overall cyclic water uptake/offtake hence the water and cooling production. Moreover, the GO-based system's exergy efficiency outperformed the SG-based system due to the better energy conversion from the heat input to producing cooling and clean water, as mentioned above. Figure 14 shows that GO has a higher thermal response resulting in higher temperatures attained during desorption than SG using the existing finned tube heat exchanger (HE). However, using different HE designs might develop different heat transfer profiles, better utilising GO, improving the desorption process and hence the overall system performance (e.g., cooling and water production). It is noteworthy that investigating different bed designs is out of the scope of this study.

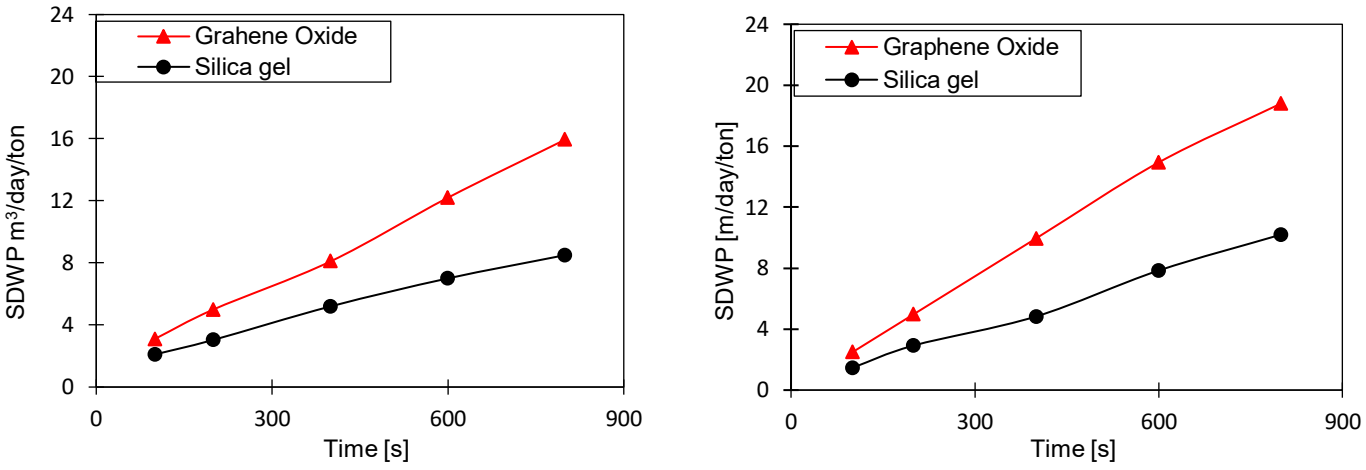

Figure 4.11:The effect of changing cycle time on SDWP for GO and SG at (a) Tev=12 ℃ and (b) Tev=30 ℃

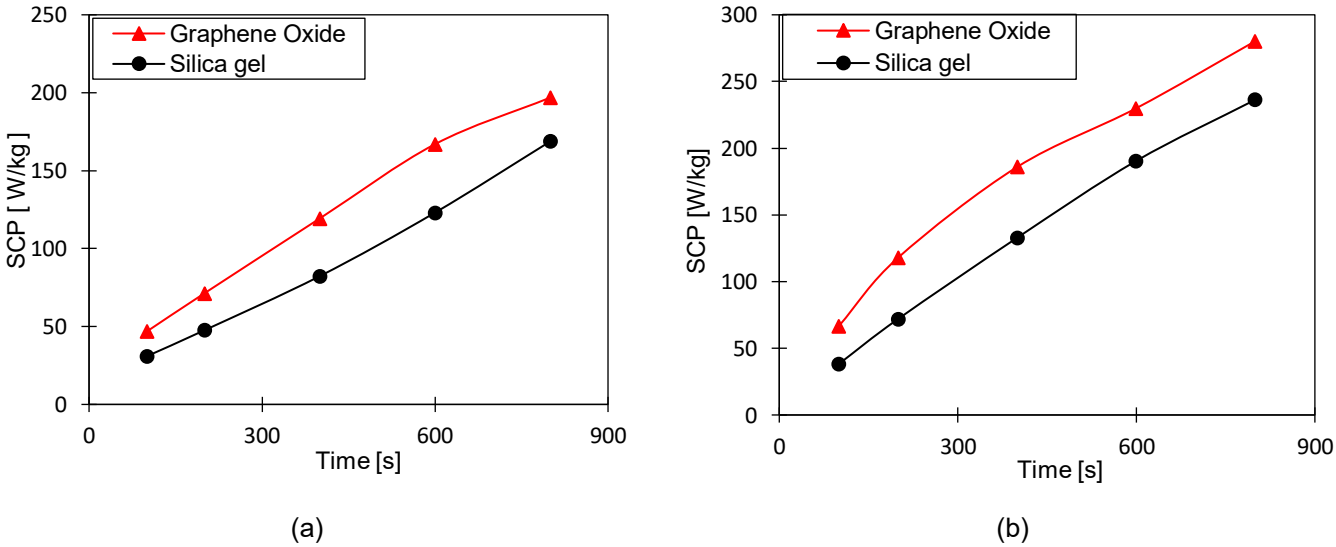

Figure 4.12: The effect of changing cycle time on SCP for GO and SG time at (a) Tev=12 ℃ and (b) Tev= 30℃

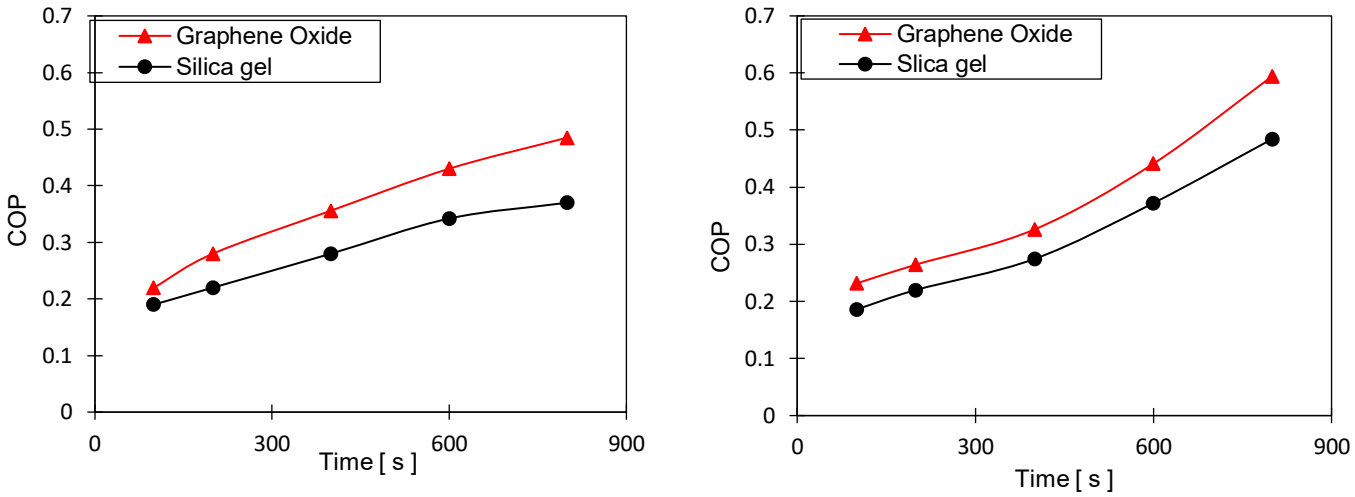

Figure 4.13: The effect of changing cycle time on COP for GO and SG time at (a) Tev=12 ℃ and (b) Tev=30 ℃

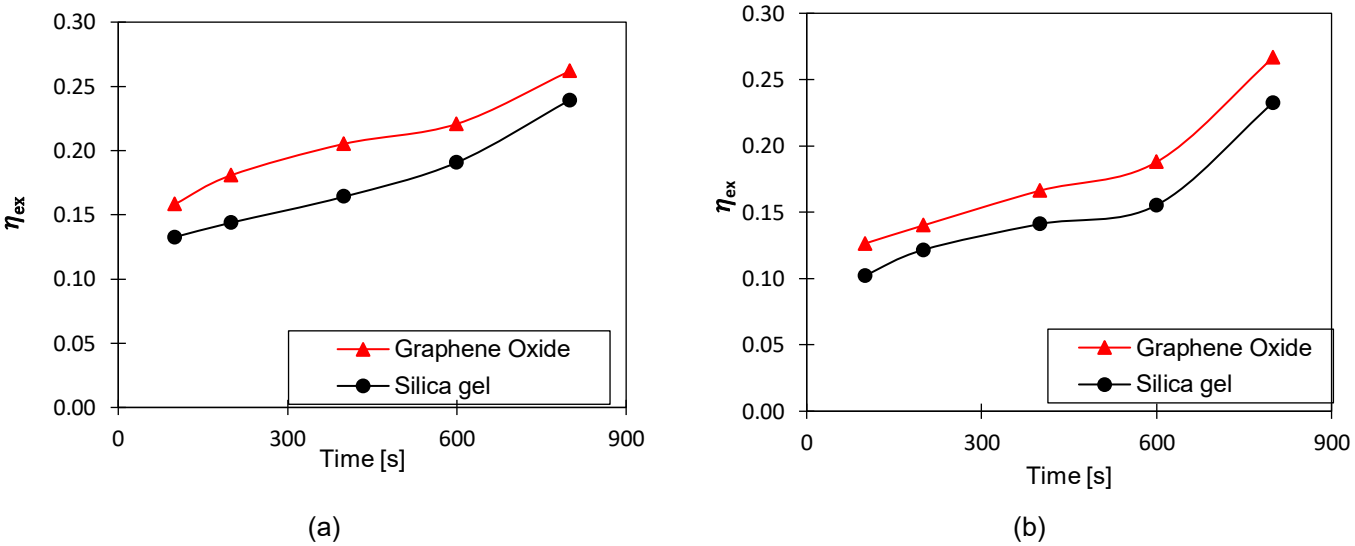

Figure 4.14:– The effect of changing cycle time on Exergy efficiency for GO and SG time at (a) Tev=12 ℃ and (b) Tev=30 ℃

The effect of increasing the cycle time on SDWP and SCP was more influential in the GO-based system than in the SG-based system at evaporation temperatures of 12°C and 30°C. However, the increase in the cooling and water production was accompanied by an increase in the heat added to the system, which caused almost the same change in the COP of the system. A similar change in the exergy efficiency was observed as a function of the ratio between useful outcomes and heat added to the system. The observed results agree with previous work by Cao and Chung [164], which studied the influence of cycle time on the performance of the silica gel/water adsorption cooling system. The changes in the system performance by varying the cycle time from 400s to 800s and across the investigated range (100 - 800s) are quantified and summarised in Table 4-6.

Table 4-6 - The percentage change in the system performance by employing GO and SG

Performance indicator	The material employed and evaporation temperatures				Cycle time change	
	GO		SG		From	To
	T_{ev}=12 °C	T_{ev}=30 °C	T_{ev}=12 °C	T_{ev}=30 °C		
SDWP [m^3/day ton]	76.3%	75.5%	70%	72%	100 s	800 s
	40.7%	47 %	41%	5.8%	400 s	
SCP [W/kg]	76%	76.2%	51.4%	56%	100 s	
	39.4%	52.6%	38.8%	44%	400 s	
COP [-]	55.6%	33.5%	51.3%	61.6%	100 s	
	26.5%	45 %	24.3%	43.3%	400 s	
η_{ex}	39.4%	52.5%	44.7%	50.5%	100 s	
	21.4%	37.6%	23.6%	39.3 %	400 s	

4.5.4 Effect of heat source temperature

In this investigation, the heat source temperature varied from 65℃ to 85℃ considering evaporation temperatures of 12℃ and 30°C, while the cooling water temperature, condensation temperature and cycle time remained 35 °C, 35°C and 800s. Figure 4.15 shows the effect of increasing heating water temperature on the SDWP. Increasing the heat source temperature from 65℃ to 85℃ increased the SDWP for the GO-based system by 30% (from 6 to 8.6 m^3/day/ton) and the SG-based system by 53% (from 3.1 to 6.6 m/day/ton) at 12℃ evaporation temperature. The same trend was observed for the 30℃-evaporation temperature, as increasing the heating water temperature from 65℃ to 85°C increased the SDWP for the GO-based system by 77% (from 5.5 to 24.6m^3/day/ton), and SG-based system by 73% (from 5.2 to 19.5m^3/day/ton). The GO-based system showed SDWP higher than the SG-based system on average by 34%.

Figure 4.16 shows the effect of increasing heating water temperature on the SCP. In alignment with the SDWP trends, the GO-based system outperformed the SG-based averagely by 27.7% at an evaporator temperature of 12℃ and by 24% at a 30℃ evaporator temperature, assuring the advancement of the GO-based system for water desalination at high evaporation temperature, as previously investigated. Generally, the better performance of the GO-based system across the investigated temperature range is attributed to the advanced thermal diffusivity, hence the higher thermal response at the component level compared to the SG-based system resulting in a higher cyclic water uptake/offtake rate at the system level. Increasing the heat source temperature from 65℃ to 85℃ increased the SCP for the GO-based system by 87.5% (from 17.05 to 137.2W/kg) and the SG-based system by 87.8% (from 9.2 to 75.47 W/kg) at 12℃ evaporation temperature. Besides, increasing the heating water temperature from 65℃ to 85°C increased the SDWP for the GO-based system by 30% (from 6 to 8.6 m^3/day/ton) and the SG-based system by 43.5% (from 3.13 to 6.6m^3/day/ton). These findings agree with the study by Youssef et al [46], who investigated the

influence of the heating water temperature on the SDWP for the water adsorption desalination system.

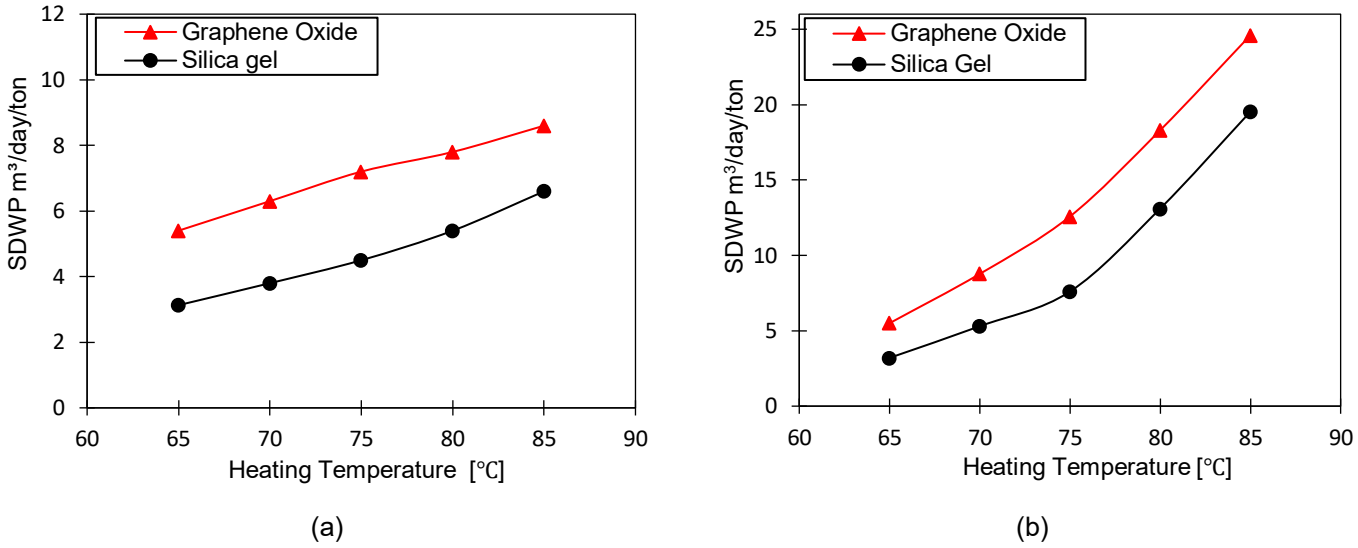

Figure 4.15: SDWP at different heating water temperatures at (a) Tev=12 ℃ and (b) Tev=25 ℃

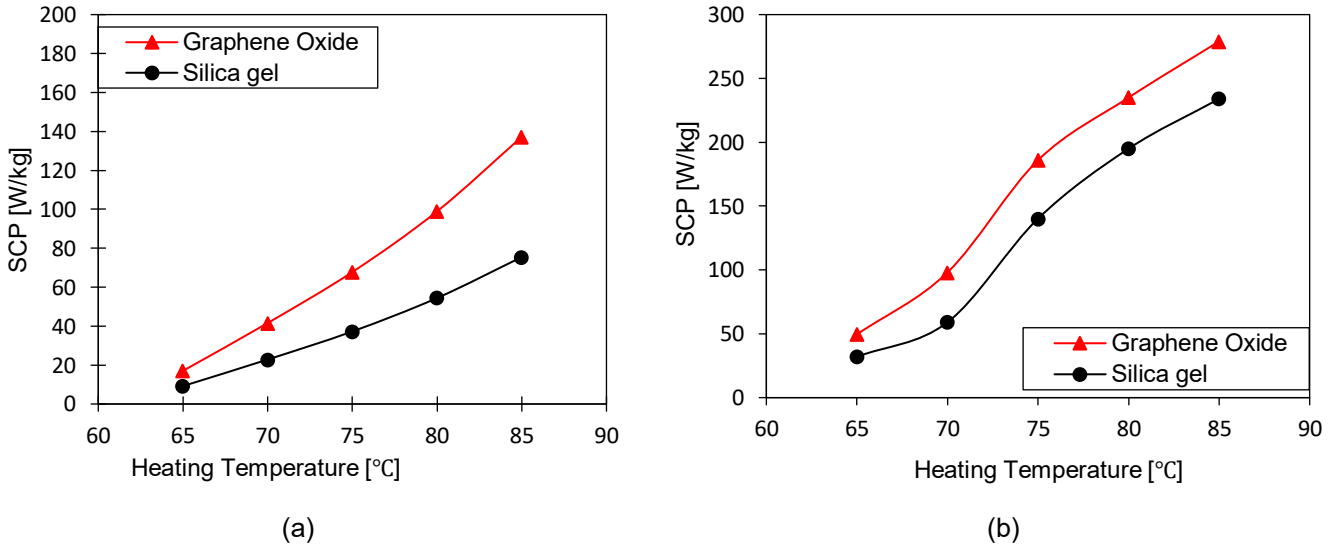

Figure 4.16: SCP at different heating temperatures for GO and SG at (a) Tev=12 ℃ and (b) Tev=30 ℃

Figure 4.17 and Figure 4.18 show the effect of regeneration (i.e., heat source) temperature on the COP and exergy efficiency of the system. Generally, increasing the heat source temperature increased the COP while the exergy efficiency decreased. Although increasing the heat source temperature while maintaining the cooling (i.e., heat sink) temperature increases the cyclic water uptake, cooling, and water production; it increases the heat transferred to the adsorbent bed during the regeneration process. Therefore, increasing the heat source temperature increased the energy conversion efficiency (COP) at the system level within the investigation temperature range. On the other hand, the higher the heat source temperature, the higher the exergy destruction in the desorption bed, which significantly influences the exergy efficiency at the system level causing its decrease.

As a result, the COP for GO increased by 29.5% (from 0.26 to 0.369) and for SG by 30.8% (from 0.173 to 0.25) at 12℃ evaporator temperature, while the increments at 30 ℃ were 49.4% (from 0.278 to 0.55) for GO and 52.2% (from 0.21 to 0.44) for SG by increasing the heat source temperature from 65°C to 85°C, respectively. The exergy efficiency for the GO-based system decreased by 42% (from 0.245 to 0.1402) and for the SG-based system by 44.5% (from 0.218 to 0.121 at 12℃ evaporator temperature, while the increments at 30℃ were 49.2% (from 0.248 to 0.126) for GO and 54.3% (from 0.248 to 0.101) for SG by increasing the heat source temperature from 65°C to 85°C, respectively.

The GO's advanced thermal response over SG led the GO-based system to attain higher water cyclic uptake/offtake and higher COP than the SG-based system. It results in COP for the GO-based system being, on average, 32.2% and 24% higher than the SG-based system for 12°C and 30°C evaporation temperatures. Even though the ratio between the produced cooling and heat added positively influences the exergy efficiency, increasing the heat source temperature has the opposite effect on the exergy destruction, specifically during the regeneration, which is higher in GO than SG, as previously quantified and demonstrated in Table 4-7. Such contradicting effects caused the exergy efficiency of the GO-based system averagely outperform that of the SG-based system by 17% and 13.7% for 12°C and 30°C evaporation temperatures. Furthermore, the average exergy efficiency increment was lower than the average COP increment by 9.2% and 9.8% for 12°C and 30°C evaporation temperatures. The reported results agree with the parametric studies undertaken by Cao and Chung [164] on a silica gel/water adsorption cooling system.

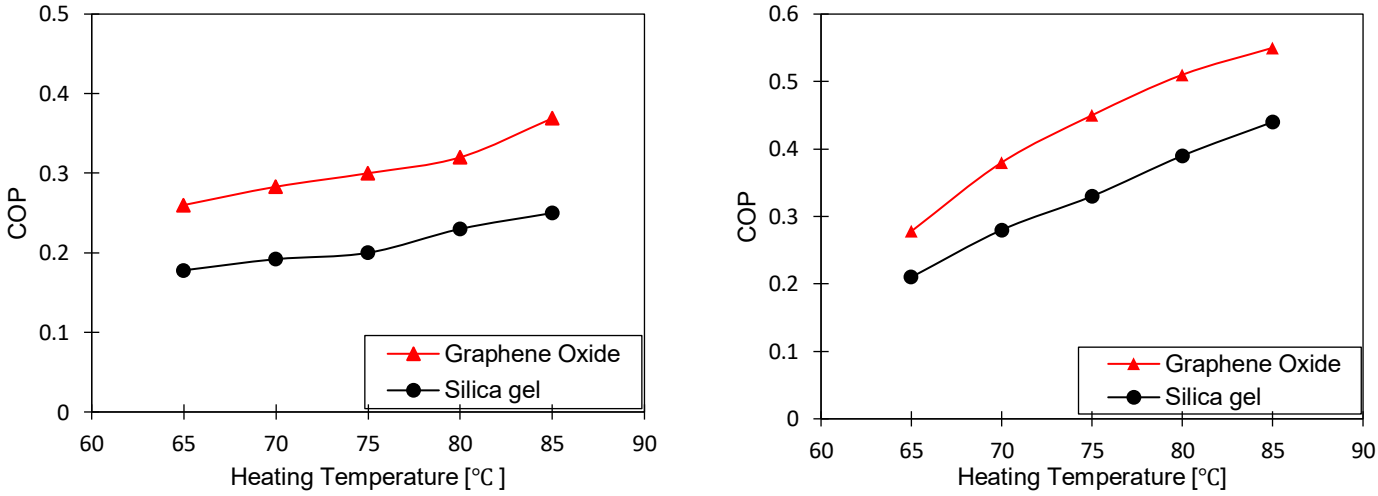

Figure 4.17: COP at different heating temperatures for GO and SG at (a) Tev=12 ℃ and (b) Tev=30 ℃

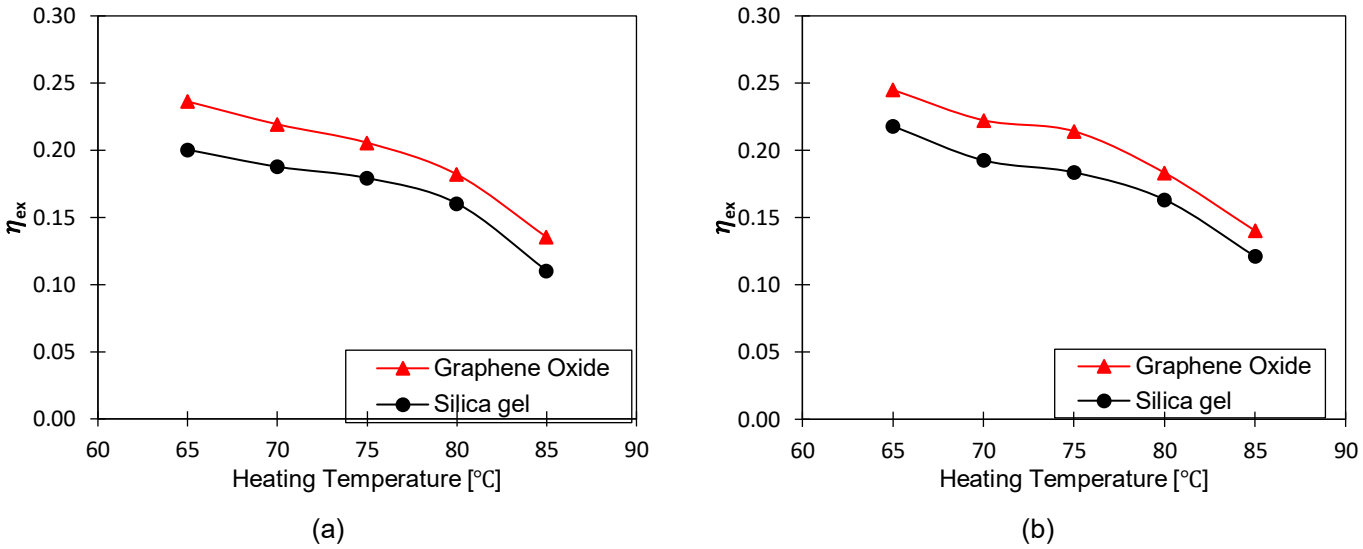

Figure 4.18: Exergy efficiency at different heating temperatures for GO and SG at (a) Tev=12 ℃ and (b) Tev=30 ℃

The SDWP potential of GO as an adsorbent was compared to that achieved by previously investigated adsorbents and is shown in table 10. Generally, even though the SDWP were obtained from different operating conditions, the achieved SDWP ranged from 4.5 to 24.9m^3/tonne/day. Furthermore, it was observed that GO achieved the second highest SDWP after Emim-Ac/syloid 72; composite, this indicates the GO's strong potential as an adsorbent, emphasising water desalination application. While graphene oxide exhibited superior adsorption characteristics, it is not widely available in the market as it might not the most cost-effective adsorbent. However, the widespread uptake of any new material might promote the large-scale manufacturing at better value for money, which could become financially competitive to the conventional materials such as silica gel and zeolite. In analogy, wider exploitation of GO will significantly promote its cost-effectiveness; this is in addition to the energy saving potential results from the advanced energy conversion efficiency.

Table 4-7. SDWP for different types of sorbents presented in the literature.

Adsorbent	Cycle time (s)	SDWP(m^3/tonne/day)	Application	Ref
Graphene Oxide	800	18.8	Cooling & desalination	This study
Silica gel	300	4.5	Desalination & cooling	[173]
Silica gel RD	-	7.5	Desalination	[29]
Silica gel A+++	1008	10	Desalination & cooling	[174]
AQSOA-ZO2	600	7.4	Desalination	[175]
COP-27 Ni MOF	1440	15	Desalination	[44]
Al fumarate MOF	900	8.2	Desalination & cooling	[176]
Emim-Ac/Syloid 72 FP	600	24.9	Desalination	[177]

4.6 Summary

This chapter presents the quantitative and qualitative analysis of utilising graphene oxide as a parent adsorbent for cooling and desalination and assess its influence on the system level's overall energy conversion potential under various operating conditions. The adsorption and thermal characteristics of graphene oxide were determined and benchmarked against the baseline silica gel adsorbent, which was modelled and coupled with a 2D Multiphysics computational model to envisage the heat and mass transfer performance at the adsorbent bed level. In addition, the influence of varying the heat source temperature, cycle time and evaporation temperature on the adsorbent bed and overall system performance was undertaken via energy and exergy analyses. The key findings of the chapter are below.

- The high thermal diffusivity of GO significantly influenced the thermal response of the adsorbent bed that advanced the cyclic water uptake at various evaporation temperatures, contradicting the equilibrium uptake cyclic predictions. Despite the faster heat transfer in the GO-based adsorbent bed increased exergy destruction, the exergy efficiency at the system level was availed. As a result, the SDWP, SCP, COP and exergy efficiency for the GO-based system was 40–44 .4%, 24.8–29.5%, 14.9–17.2% and 12–15.5% higher than the SG-based system when operated at 12-30°C.
- Increasing the cycle time increased the water uptake in both GO and SG since the adsorbent bed had a long time to reach closer to equilibrium uptake. As a result, the SDWP, SCP, COP and exergy efficiency for the GO-based system was higher than that of the SG-based system by 40%, 24.8%, 14.9% and 12% at 12°C evaporation temperature and by 44.4%, 29.5%, 17.2% and 15.5% at 30°C evaporation temperature. The GO-based system outperformed the SG-based system due to a higher thermal response, which led to higher cyclic water uptake.
- Increasing the heat source temperature increased the exergy destruction and reduced exergy efficiency but enhanced the SDWP, SCP and COP. Moreover, the GO-based system's exergy efficiency was higher than the SG-based system across the investigated heat source temperatures by 13.7% and 17%, on average, at 12°C and 30°C evaporation temperatures; this was despite the higher exergy destruction in the former system at the adsorbent bed level.

Overall, this study concludes that having an adsorbent with advanced thermal diffusivity will result in advanced adsorption performance at the component.

CHAPTER 5: STUDYING IONIC LIQUID AND A FEW LAYERED GRAPHENE SORPTION COMPOSITES.

5.1 Introduction

The research on composite adsorbents has indicated that composites improved their thermal conductivity and adsorption capacity. An investigation on activated carbon composite using graphene nanoplatelets showed an improvement in thermal conductivity of 23.5 times and an ethanol volumetric uptake 23% higher compared to pure activated carbon [178].On the other side hydrophilic IL have shown some high sorption properties and thermal stability, Experimental investigation on adsorption properties of silica-supported ionic liquid called EMIM-AC/Syloid 72 FP. A high SDWP of 47m^3 day^{-1} ton^{-1}, a coefficient of performance (COP) of 0.85 and a specific cooling power (SCP) of 600 Wkg^{-1} [95]. while GP and IL, performance in composites due to high thermal and sorption properties is known, there is hardly any literature on the development of composites combining the two (GP and IL) Therefore, the higher thermal diffusivity of GP and IL's thermal stability, solvation and low vapour pressure has stimulated the interest in developing and investigating GP and IL composites.

This chapter aims to develop a novel sorption composite comprised of GP host matrix and hydrophilic ILs 1-Ethyl-3-methylimidazolium methanesulfonate ($EMIMCH_3SO_3$) or 1-Ethyl-3-methylimidazolium chloride (EMIM Cl), as sorbents. The main aim of this research and its novelty is to develop an understanding of GP/IL composite for sorption cooling and desalination application and their impact on the enhancement of the heat and mass transfer properties of the sorption/desorption processes.

The chapter will cover the (1) experimental investigation of the thermal and physical properties of GP to ascertain their ability for use as a host matrix; (2) development of GP/IL composites and investigate their sorption and thermal characteristics and benchmark against baseline sorbent Silica gel; (3) investigate the impact of varying the IL concentration on the overall sorption and thermal performance of the composites; (4) experimentally and by 2D computational heat and mass transfer modelling, determine cyclic performance at material and component levels including energy conversion exergy efficiency

5.2 Materials

This chapter investigates a composite that comprises few-layered graphene (GP) and Ionic liquids (IL). The ILs, 1-Ethyl-3-methylimidazolium methane sulfonate ($EMIMCH_3SO_3$) and 1-Ethyl-3-methylimidazolium-chloride (EMIM Cl) were purchased from Acros organics and Sigma Aldrich, respectively. A host material for the IL was a few-layered pristine graphene platelets of 1-5 2D layers, commercially known graphene nanoplatelets obtained from Graphitene Ltd. The pristine GP was

selected for use as a host structure based on its experimentally determined superior thermal diffusivity of 22.3mm^2/s and high BET surface area of 56.8978m^2/g, compared to other graphene derivatives and Silica gel as shown in Figure 5.1 and Table 5-1. The composites were benchmarked against Fuji Silica gel (SG) of a widely used adsorbent of 0.18-1mm particle size.

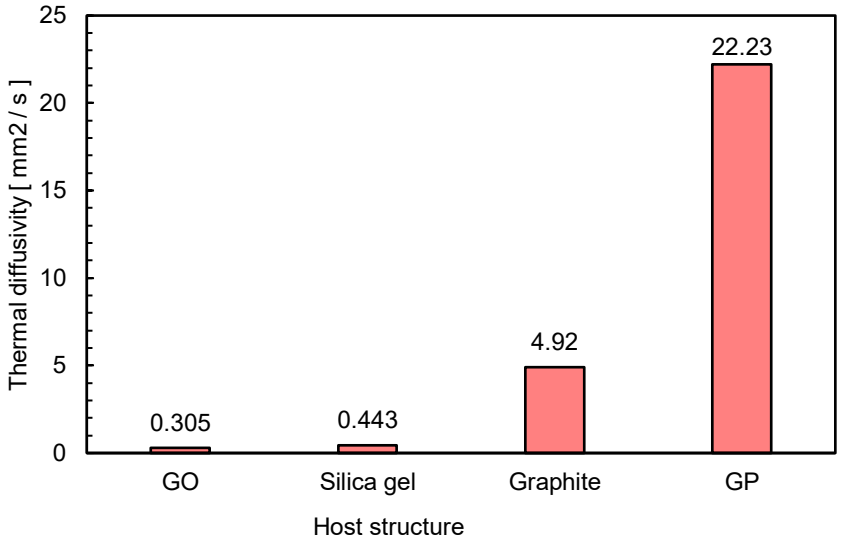

Figure 5.1:Comparison of thermal diffusivity of the host matrixes

Table 5-1 - Physical properties of pristine few-layered graphene platelets (GP and Graphite)

Nanoparticle	BET area (m^2/g)	Thermal diffusivity (mm^2/s)	Thermal conductivity (W/mK)
GP	56.8978	22.23	7.36
Graphite	22.5668	4.92	4.57

A simple two-bed sorption cooling and water desalination configuration was considered to determine the cyclic performance, as shown in Figure 2.3 (a) in Chapter 2. The two-bed system continuously supplies cooling and clean water, as one bed operates at each cycle.

5.2.1 Composite synthesis

There are two processes for developing composite adsorbents namely physical mixing or impregnation and chemical process. In impregnation process, a homogeneous mixture is formed by physically mixing all the composite constituent materials. The process involves the immersion of the parent adsorbent or host matrix into the organic salt or aqueous IL. The concentration and the amount of the IL determines whether interfacial or bulk deposition takes place within the composite. There are three impregnation approaches which can be used in composite development these include the Equilibrium deposition filtration (EDF), wet impregnation (WI), and Incipient wetness Impregnation. Table 5-2 gives a summary of the impregnation approaches.

Table 5-2: Impregnation Approaches

Method / Features	Equilibrium deposition filtration	Wet impregnation	Incipient wet impregnation
Concepts	▪ The Immersion of support matrix into a large volume of a very dilute aqueous solution occurs. This is followed by the equilibration of the suspension for several hours under stirring. The bulk of the deposition occurs interfacial during equilibration. ▪ After the equilibration, the filtration step is undertaken, and at this stage, it is anticipated that the non-interfacial-deposited IL is separated from those deposited at the interface and those non-deposited but restricted inside the pores.	▪ Involves the Immersion of support matrix into a large volume (higher than the pores volume of the support) of a concentrated aqueous solution of IL. ▪ No filtration is involved, and the deposition of IL on the pore surfaces occurs during the slow evaporation of the solvent of the impregnation solution.	▪ Involves the Immersion of support matrix into an aqueous solution of (Ionic Liquid) (IL) having the same volume as the pores volume of the support matrix at a suitable concentration. ▪ Small scale procedures in the lab do not include filtration since the support matrix encounters sufficient volume of the impregnating solution. ▪ Rapid liquid transfer inside the pores through capillary forces is anticipated although the IL movement might be slower.
Advantages and limitation	▪ The IL is highly dispersed into the pores. ▪ Limitation is that it cannot be applied for high IL loading.	▪ It is expected to allow high IL loading. ▪ The limitation is that excess aqueous solution /IL is expected to accumulate on the supporting matrix surfaces.	▪ Simple. ▪ Permits the deposition of the desired amount of IL on the surface of the matrix. ▪ Limitations on the capillary effect during impregnation due to the pore or interlayer size are prevalent
Deposition phenomenon	▪ The interfacial deposition is most prominent	▪ Interfacial/bulk deposition. occurs ▪ The impregnation conditions such as concentration and evaporation time can result in a dominance by one precipitation phenomenon over the other results.	▪ The bulk deposition is most prominent. ▪ In the case of very dilute aqueous solution, the interfacial deposition is more dominant.

The wet impregnation method was employed to develop the sorption composites due to its ability to attain a high level of Interfacial/bulk deposition onto the host matrix see Figure 5.2. Firstly, 1g of the host matrix was dried at 150°C for 12h. Ionic liquid's aqueous solutions were developed at a concentration of 10 wt% to 30 wt%. To enable the wet impregnation process, the total volume of the aqueous solution was 25mm^3, which sufficiently exceeded the volume of the dried matrix. Secondly, the dried host matrix was immersed into the aqueous solution and stirred for 1hr to attain a homogenous host matrix/aqueous solution mixture. Thirdly, the developed mixture was left to rest for an hour to ensure the complete impregnation of the host matrix. Finally, the excess solution was filtered, and the composite was dried gently at 150°C for 1hr. Table 5-3 shows the range of the developed composites based on different ionic liquid concentrations using a host matrix of few-layered graphene platelets.

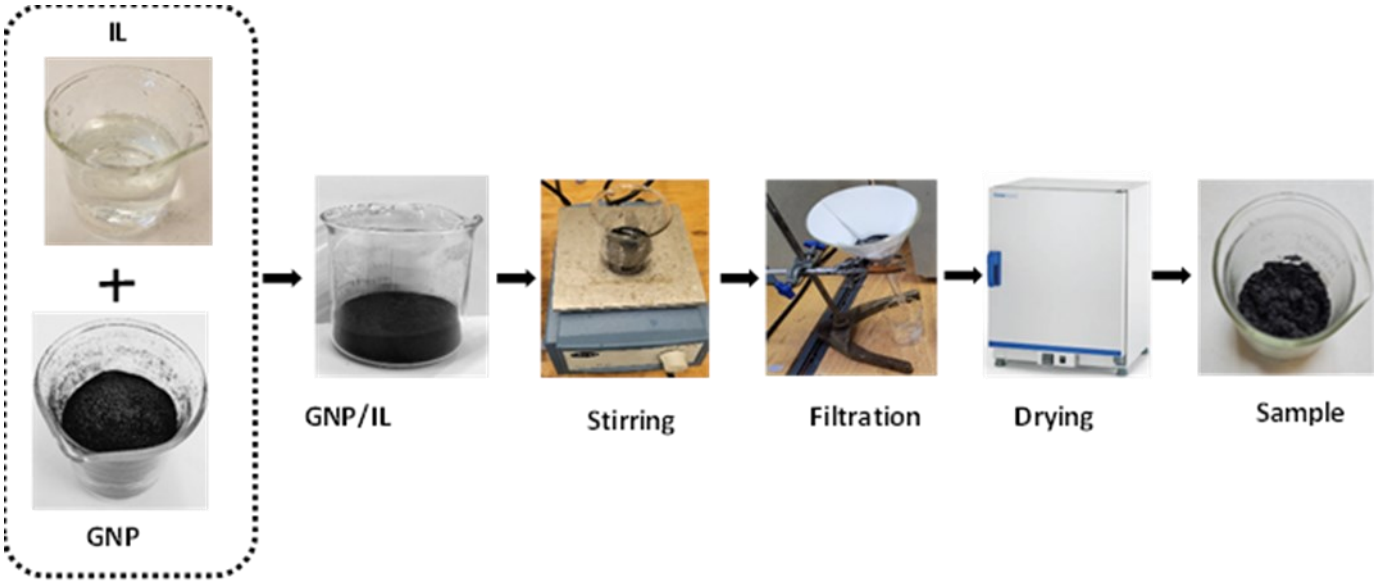

Figure 5.2: GNP/Il: composite making process.

Table 5-3 The range of composite developed

GP + [EMIMCl] composite		GP + [EMIMCH_3SO_3] composite	
Composite name	[EMIMCl] concentration	Composite name	[EMIMCH_3SO_3] concentration
GP-CL-10	10%	GP- CH_3SO_3-10	10%
GP-CL-20	20%	GP- CH_3SO_3-20	20%
GP-CL-30	30%	GP- CH_3SO_3-30	30%
GP-CL-40	40%	GP- CH_3SO_3-40	40%

5.3 Composites properties experimental analysis

5.3.1 SEM imaging

To understand the intercalation of the IL into the host scanning electronic microscope (SEM) was used. Figure 5.3 shows the SEM images for the developed composites impregnated with different concentrations of IL. Figure 5.3a-e indicate an uneven surface and cavities for the composites with an ionic liquid concentration of 30% and less for both (EMIMCl) and $EMIMCH_3SO_3$. The cavities indicate that the composites are highly heterogeneous and have a high possibility of the IL being confined into the host matrixes' interlayer spaces; hence, no over-impregnation occurred. However, ionic liquid concentration above 30% led to accumulating ILs on the surface of the host material, as shown in Figure 5.3 g-h of 40% IL concentration. The host matrix is smooth and fully covered with the ionic liquid, indicating the host matrix's over-impregnation. Due to the over-impregnation, the 40% IL concentration composite was not further investigated.

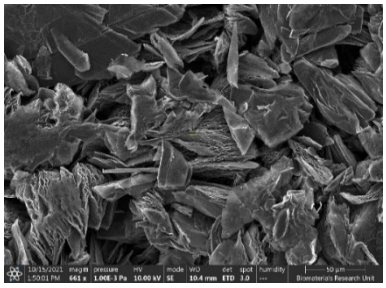

Pristine GP

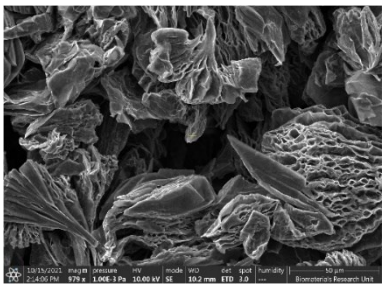

GP-CL-10

(a)

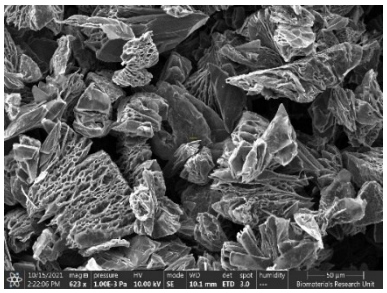

GP-CH_3SO_3-10

(b)

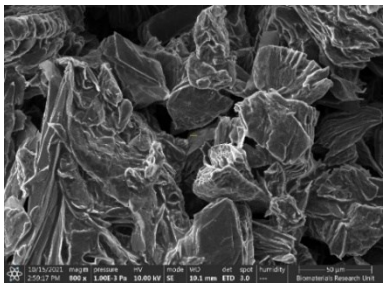

GP-CL-20

(c)

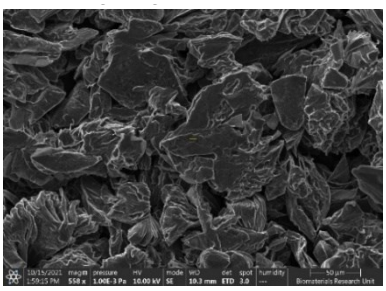

GP-CH_3SO_3-20

(d)

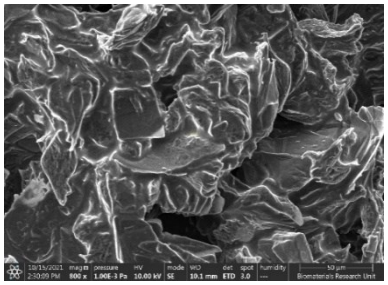

GP-CL-30

(e)

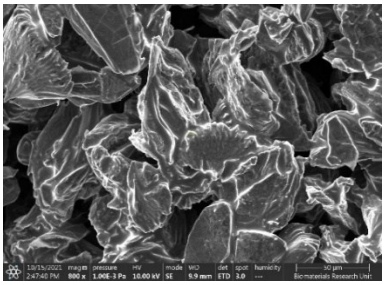

GP-CH_3SO_3-30

(f)

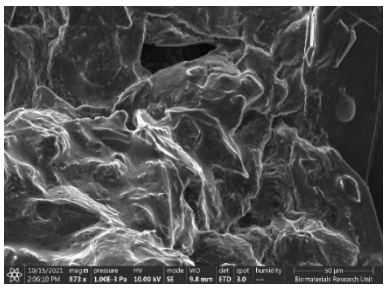

GP-CL-40

(g)

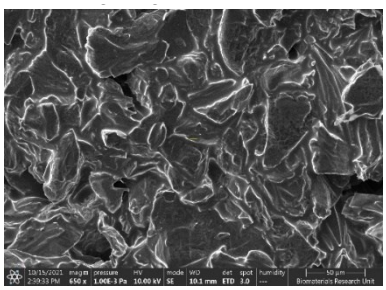

GP-CH_3SO_3-40

(h)

Figure 5.3 - SEM image of pristine graphene and few-layered graphene nano platelets/ Ionic liquid composites

5.3.2 XRD crystallographic analysis

The prepared composites were subjected to powder XRD analysis to examine the crystal structure of the GP in the composites, as shown in Figure 5.4. The diffraction of every sample shows the structure characteristic of graphite indicated by the diffraction peak 002 at 2 θ =26.4-26.6°, and 100 and 101 peaks at 2 θ =42.3-42.4° and 44.4-44.6°, respectively.

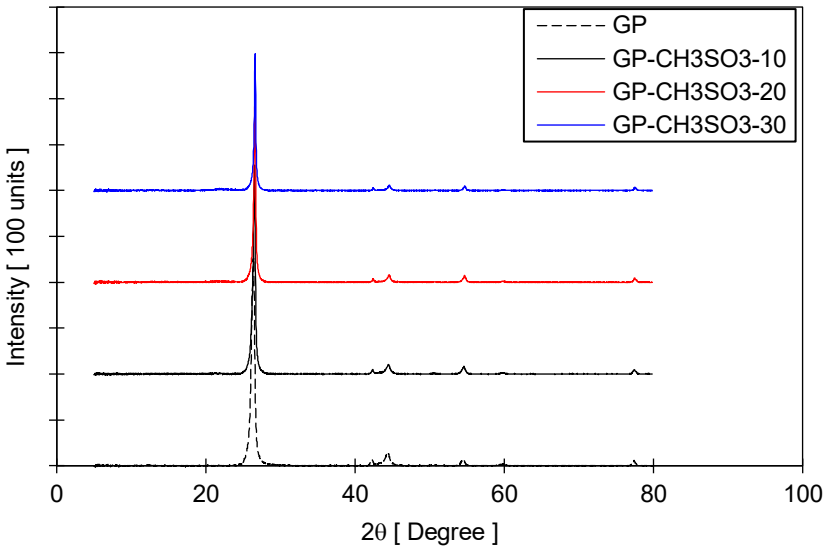

(a)

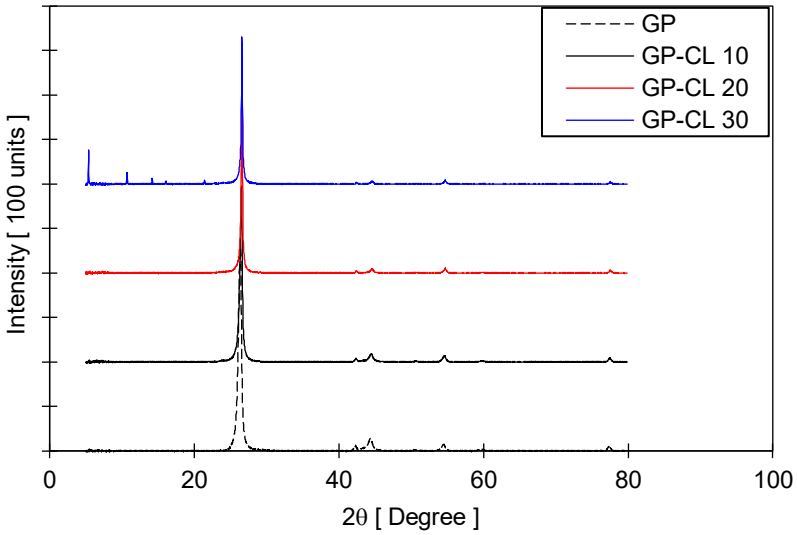

(b)

Figure 5.4: XRD results of the developed composites of (a) GP-CH_3SO_3 and (b) GP-CL.

The peaks of the pristine GP are slightly smaller than that of its composites with the ILs; the latter increases with the content of ILs towards that of perfect graphite. The characteristic diffraction angle increases imply that the impregnation of the ILs does not change the layered crystal structure of the GP but plays a role in driving the GP structure towards perfection. Furthermore, the GP-CL-30

composites show a series of diffraction peaks at 2θ = 5.39, 10.72, 14.19 16.36 and 21.42 °, which may indicate that some (EMIMCl) molecules have intercalated into the graphene layers at the surface of GP.

5.3.3 Ionic liquid contents

The ionic liquid contents in the composite was measured using a Thermogravimetric Analyser (TGA).The ionic liquid content of the developed composites was determined by Equation (5.1), and the results are shown in Figure 5.5. It can be seen from Figure 5.5 that the greater the weight percentage of ionic liquid in the aqueous solution during graphene impregnation, the higher the ionic liquid content of the composites. The results also show that an increase of final ionic liquid content in the composites was not linear with the increasing fraction of ionic liquid in the aqueous impregnation solution, suggesting that the host matrix approaches Figure 5.5, and this aligns with findings in the SEM experimentation. The test also showed that no inorganic residues were observed in any of the composites or raw materials.

$$\text{IL content} = \frac{\text{mass}_{IL}}{\text{mass}_{GP}} \times 100 \qquad (5.1)$$

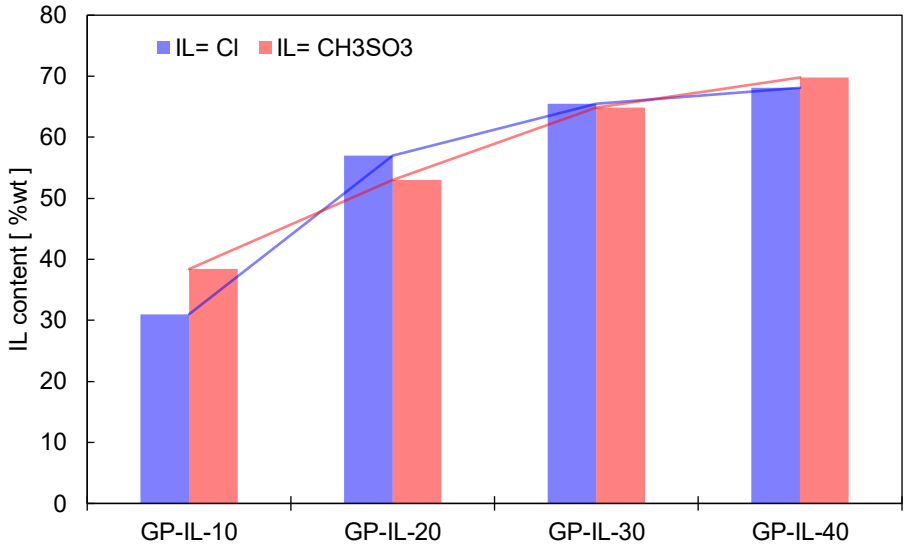

Figure 5.5: ILs content in the developed composites

5.4 Composites heat transfer properties.

The thermal characteristics of the composite were determined using the LFA following the procedure given in Chapter 3.

Table 5-4 shows the experimentally determined thermal diffusivity of the composites compared to the SG benchmark. There was a significant increase in thermal diffusivity in all the composites compared to SG due to the presence of, primarily, GP. It can also be observed that the 10%wt composite had the highest thermal diffusivity, followed by the 20% wt, and the 30% wt composites showed the least. The 10%wt composite had the highest thermal diffusivity because it had the lowest IL content; therefore, the impact of the relatively lower thermal diffusivity of IL, concerning GP, was experienced less in the 10 % than the other composites with higher IL concentrations. It agrees with the findings on the thermal diffusivity of IL by Zhao et al [179], which reported IL of lower thermal diffusivity than GP but higher than metal salts. It highlights the benefit of investigating ILs as a replacement for the conventionally used metal salts to support the sorption simultaneously with the heat transfer characteristics.

The thermal diffusivity test temperature range of 25–100℃ showed the impact of temperature on the thermal diffusivity of the composites. The composites of up to 65 %wt IL content (i.e., GP-Cl-30 and GP-CH_3SO_3-30) remained stable under high temperatures of up to 100 ℃, even though the thermal diffusivity decreases slightly with increasing temperature, unlike SG, which remains constant at that temperature range. On the other hand, composites of IL content above 65%wt experienced a separation of the impregnated ionic liquids at the higher temperature, which supports the earlier discussion about composites' over-impregnation when utilising high IL concentration (i.e., GP-Cl-40 and GP-CH_3SO_3-40). It also could be worsened by the thermal expansion of the IL at temperatures above 55°C at high IL concentrations above the 30% threshold. Therefore, the temperature range for thermal diffusivity measurement for GP-Cl-30 and GP-CH_3SO_3-30 narrowed to 25-55°C. However, it does not stand as limiting the adsorbent's usability at higher temperatures up to 30%wt range. Remarkably, during regeneration at 85°C, which exceeds the 55°C threshold, the IL within the composite retains its water capture capacity intact, while the composite cools down to 30°C for the subsequent adsorption cycle, the IL contracts and returns to its original state within the host graphene nanoplatelet (GNP) matrix, highlighting the reversible and robustness of the adsorption process. Therefore, the composite investigation was limited to up to GP-Cl-30 and GP-CH3SO3-30, which remained feasible.

Figure5.6 shows the influence of temperature on the composite's thermal diffusivity.

Table 5-4 - The thermal diffusivity values of the developed composites

Material	Thermal diffusivity (mm^2/s)	Temperature range (°C)	Material	Thermal diffusivity (mm^2/s)	Temperature range (°C)
Silica gel (exp)	0.365	Room temp	Silica gel [180]	0.312	Room temp
GP-CL-10	9.96	25-100	GP-CH_3SO_3-10	11.84	25-100
GP-CL-20	6.78	25-100	GP-CH_3SO_3-20	6.40	25-100
GP-CL-30	5.98	25-55	GP-CH_3SO_3-30	5.92	25-55
GP-CL-40	3.95	25-55	GP-CH_3SO_3-40	3.45	25-55

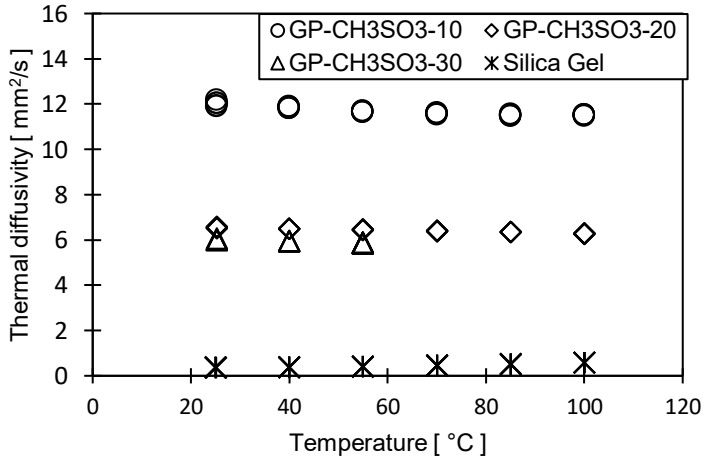

(a)

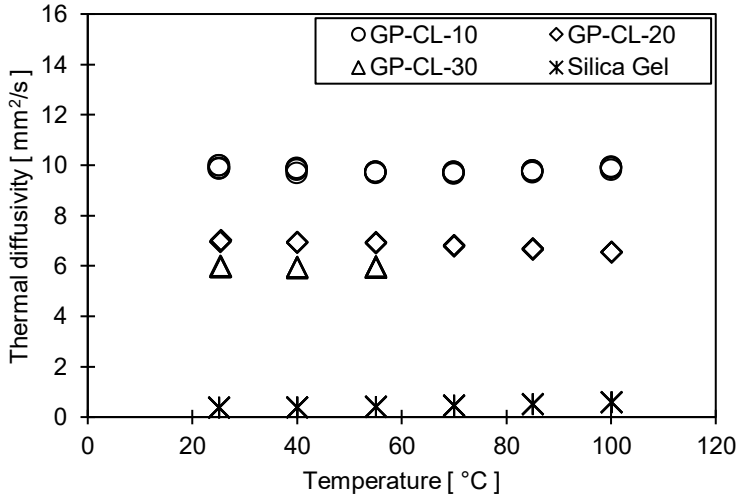

(b)

Figure5.6: Temperature dependant thermal diffusivity of the developed composites:(a) GP/EMIMCH_3SO_3, and (b) GP/EMIMCl composites compared with SG

5.5 Composites adsorption properties

The adsorption characteristics of the composites were determined using the DVS following the procedure given in the methodology Chapter 3. Figure 5.7 shows the experimentally measured equilibrium adsorption uptake for the GP-CL-10-30 and GP- CH_3SO_3-10-30 composites.

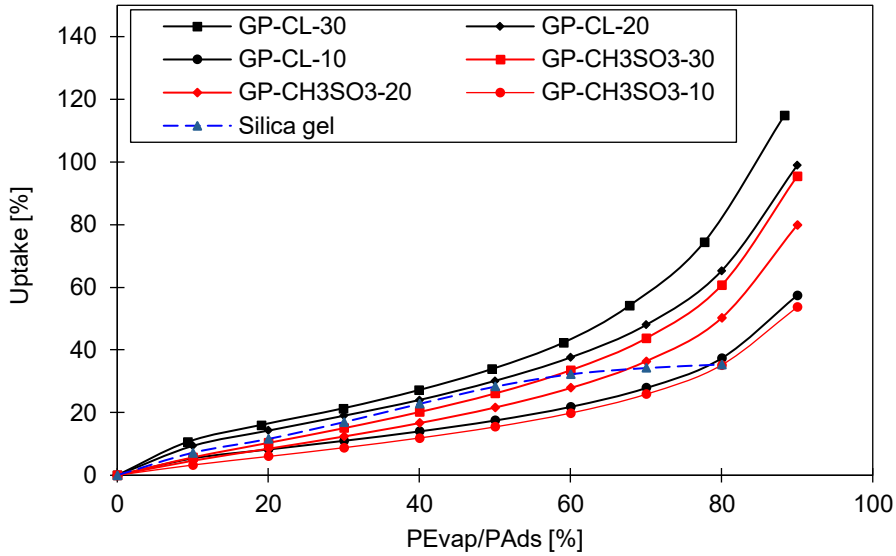

Figure 5.7:The adsorption isotherms for the developed composite and Fuji silica gel benchmark

The composites' gravimetric adsorption and desorption cycles were performed for 20 cycles. The pressure ratio P_{evap}/P_{bed} alternated between 0% and 90% extremes to determine the composite stability. All composites showed a slightly low uptake in the first cycle and maintained a stable uptake percentage until the last cycle. The percentage difference between the highest and lowest uptake was less than 1 %, which shows that the developed composites are highly stable. Figure 5.8 shows the gravimetric stability tests for the composites with IL content below 65% (i.e., GP-Cl-30 and GP-CH_3SO_3-30) during adsorption and desorption.

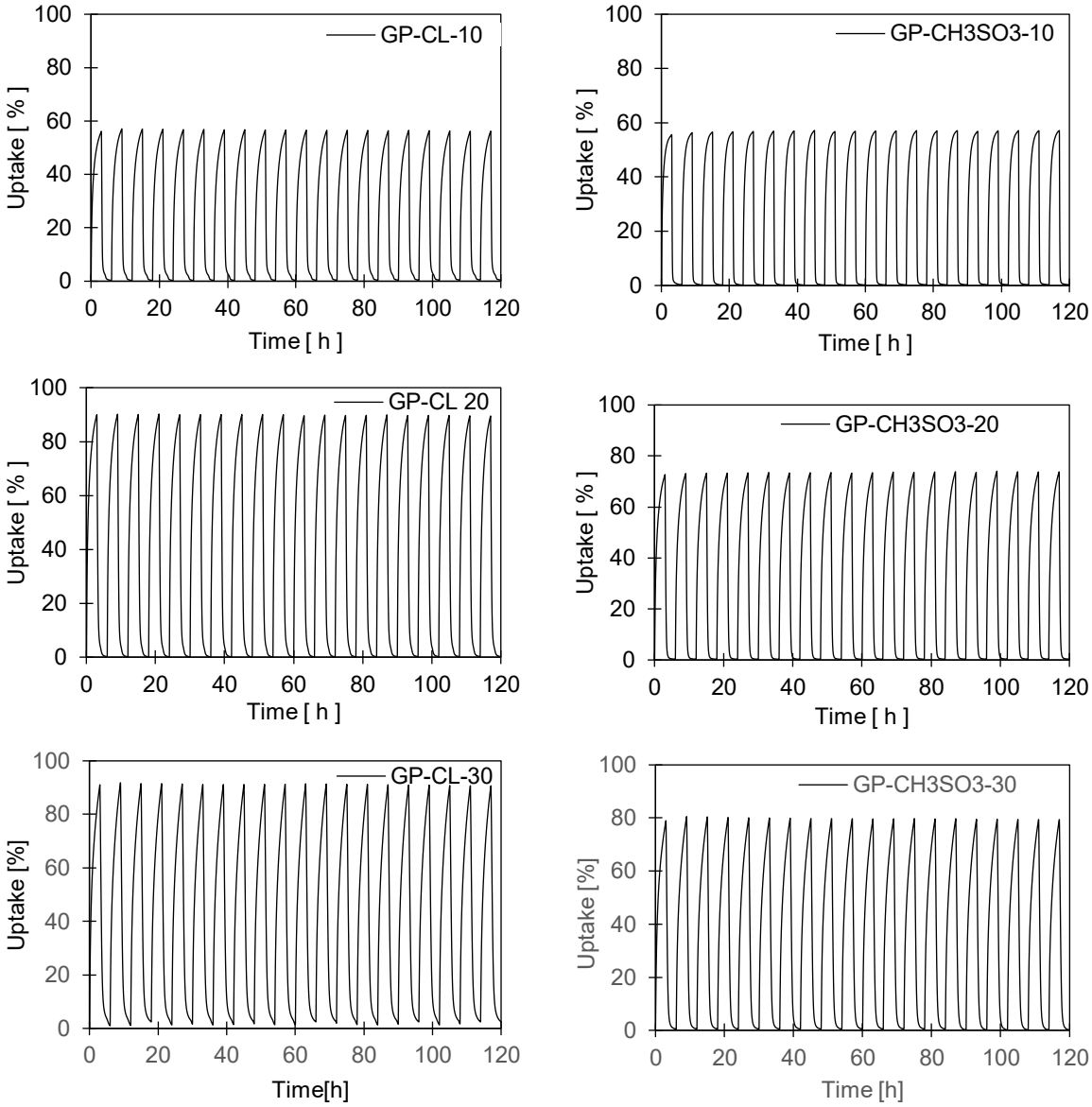

Figure 5.8: Gravimetric water adsorption/desorption cycles for selected composites GP-CL-10- GP-CL-30, GP-and GP-CH_3SO_3-10 -GP-CH_3SO_3-30 (stability test)

5.5.1 Isotherm modelling

Empirical modelling was employed to simulate the adsorption isotherms, which is more straightforward and reliable to implement. Many empirical isotherm models have been developed to determine the isotherms based on several properties such as the heat of adsorption, temperature-dependent saturation, amount of loading to create a monolayer coverage per unit volume of the packing media (solid saturation loading) and adsorption equilibrium constant [32, 119, 141]. Examples of such models include Sips, Dubinin-Astakhov, Tóth, Henry, Freundlich, Langmuir, Temkin and Hill-de Boer; each broadly suits a specific isotherm type. In this study, the developed composites showed type II isotherm with water, which can be modelled using the Dubinin-Astakhov (D-A) adsorption isotherms model, as stated by equation (5.2) [181]. D-A model was preferred in

fitting the experimentally measured adsorption isotherm because of its ability to linearize adsorption data at varied pressure ranges while accurately relating the equilibrium pressure and adsorbed amount by the composites over the entire range of the micropore filling. Considering the heterogeneity of the developed composites and the restriction on the calculated maximum adsorption by the micropore filling in the composite, it was possible to obtain information about the micropore structure owing to the n exponent parameter of the D-A to fully describe the isotherms. Furthermore it is one of the most utilised isotherm model for modelling type II adsorption isotherms data [182].

$$q = q_o \exp\left[-\left\{\frac{RT}{E} \ln\left(\frac{P}{P_s}\right)\right\}^n\right] \quad (5.2)$$

Where q (kg/kg) denotes adsorption uptake at a given temperature and corresponding pressure ratio; q_o is the equilibrium uptake (kg/kg); E is the characteristic energy of adsorption ($KJmol^{-1}$); P_s (kPa) is the saturation pressure at corresponding temperature and the index n is the structural heterogeneity coefficient.

In modelling the experimental isotherm data, a nonlinear optimisation method was employed for optimising the D-A model parameters for all the developed composite/water pairs. Table 5-5 shows the parameters of the D-A model employed in isotherm experimental data modelling with a regression parameter (R2) of 0.9998. The developed isotherm model agrees well with the experimental adsorption isotherm of 0.05 mean deviation, as shown in

Figure **5.9**.

The results show that GP-CL-30 has the highest equilibrium water uptake while CH_3SO_3-10 showed the least. The higher equilibrium water uptake in the GP-CL-30 is attributed to the high IL content in the composite. More IL content in the host matrix led to higher uptake, which agrees with the findings by Askalany et al [183] in their study of silica gel/IL composites for desalination. The high uptake in the GP-CL-30 compared to all the GP-CH_3SO_3 shows that the CL-based IL interacts highly with water (i.e., solvation), resulting in higher water uptake. It was also observed that all the studied composites have significantly higher equilibrium uptake than baseline adsorbent silica gel, with the highest GP-CL-30 showing a 78% enhancement. This can be attributed to the adsorption characteristics of IL, which allows more water sorption.

Table 5-5: Parameters of the D-A model for the fitted isotherm data for the composites

Adsorbent	D-A model fitting parameters			RMSD [%]
	Maximum uptake [$kgkg^{-1}$]	Characteristics energy [$kJkg^{-1}$]	Heterogeneity parameter [-]	
GP-CL-10	0.89	52.67	0.69	2.57
GP-CL-20	1.50	55.36	0.72	4.65
GP-CL-30	1.70	50.63	0.68	5.01
GP-CH3-SO3-10	0.75	55.18	0.78	2.13
GP-CH3-SO3-20	1.13	50.90	0.77	3.38
GP-CH3-SO3-30	1.41	48.32	0.74	3.68

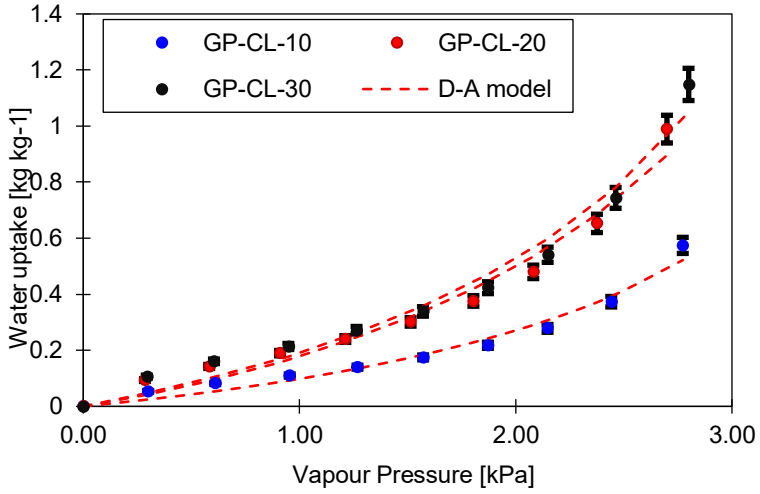

(a)

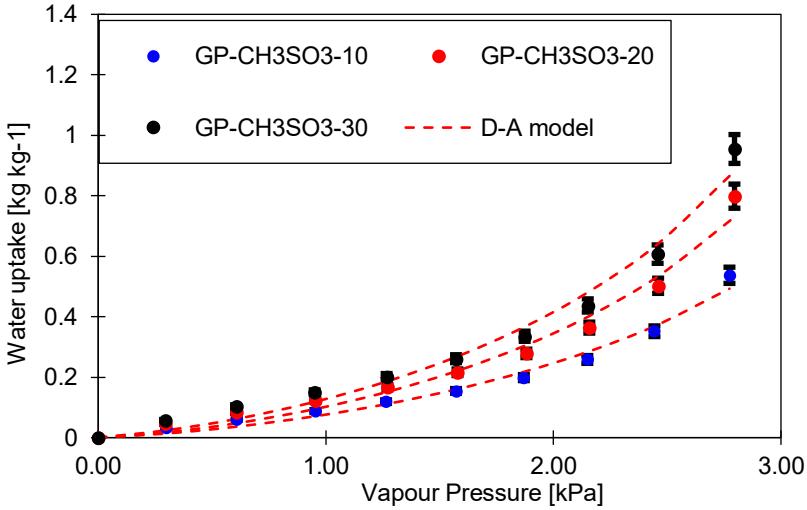

(b

Figure 5.9: Experimental isotherm of composites fitted with the D-A model (a) GP-[EMIM][Cl] and (b) GP- CH_3SO_3

5.5.2 Adsorption Kinetics

The adsorption kinetics were determined using the (LDF) model presented in Chapter 3, as shown in equation (3.2).

The LDF model's coefficients are given in Table 5-6.

Table 5-6: The empirical constants for the LDF

Parameter	value		Unit
	GP/IL composite	Silica gel	
D_{so}	4.4E-4	2.54E-4	m^2/s
E_a	48.32-55.36	42	kJ/mol
R_p	2.9 E-4	0.16E-5	m

5.5.3 Isosteric heat of sorption

The isosteric heat of sorption was determined using the C-S-K equation covered in Chapter 3. The calculated isosteric heat for the developed composites is furnished in Table 5-7.

Table 5-7: Isosteric heat of sorption of the developed composites

Material	Heat of sorption (J/mol)	Material	Heat of sorption (J/mol)
Pure EMIM-Cl	31905	Pure EMIM CH_3SO_3	31605
GP-CL-10	26525	GP-CH_3SO_3-10	26634
GP-CL-20	26549	GP-CH_3SO_3-20	26528
GP-CL-30	26571	GP-CH_3SO_3-30	26514
Fuji silica gel	26078	Fuji silica gel [184]	26790

As shown in Figure 5.10, the isosteric heat of adsorption or adsorption enthalpy decreases with increasing uptake. It is because the initial adsorbate molecules adsorb onto the high-energy sorption sites, releasing high amounts of heat energy and resulting in a higher adsorption enthalpy. On the other hand, when the uptake increases, high-energy sites are saturated with adsorbates, the water molecules get adsorbed onto the sites possessing lower energy, and thus the adsorption enthalpy is seen gradually decreasing.

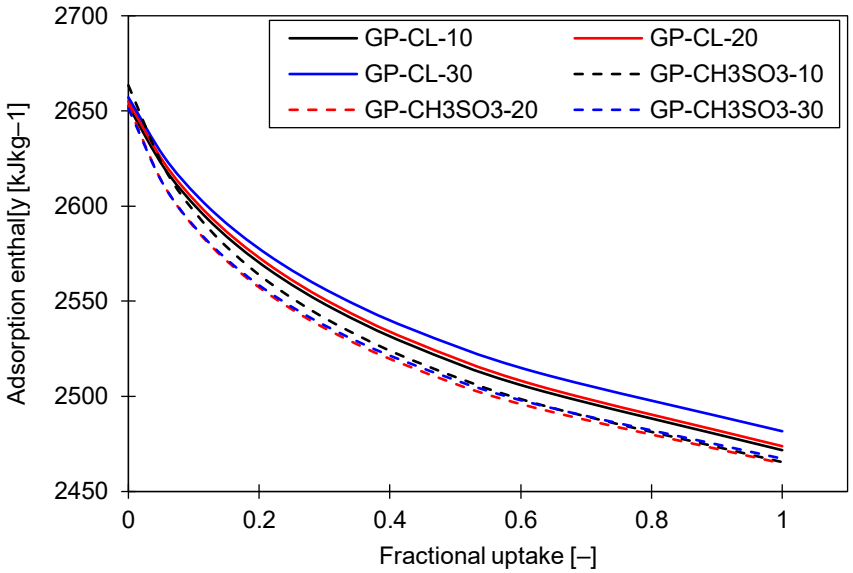

Figure 5.10:Isosteric heat of adsorption of the developed composites

5.6 Composites performance analysis

5.6.1 Material-level cyclic performance

The material-level cyclic performance based on the adsorption isotherms was performed to understand the cyclic water uptake potential of the developed composites and benchmark them against SG, as shown in Figure 5.11-Figure 5.12. Figure 5.11 shows the experimental isotherm curves and the cycle operation at the evaporator temperature of 12°C, condensation temperature 35°C and desorption 85℃. The mostly impregnated composites yet stable, i.e., GP-CH_3SO_3-30 and GP-CL-30, were investigated. Investigating the evaporating temperature of <25°C (P_v=1.4 kPa) depicts the potential cyclic performance when GP-CH_3SO_3 inferiors that for silica gel and the opposite in case of evaporating temperature ≥25°C (P_v=3.2).

At the low vapour pressure end of 1.4kPa corresponding to an evaporator temperature of 12℃, the net cyclic equilibrium uptake for SG, GP-CH_3SO_3-30 and GP-CL-30 was 0.15 kg/kg, 0.13 kg /kg and 0.18kg/kg respectively. SG outperformed GP-CH_3SO_3-30 regarding the net cyclic water uptake shown by distance 1-4, while GP-CL-30 outperforms SG. The two isotherms SG and GP-CH_3SO_3-30 at 35℃ adsorption temperatures intersect at a vapour pressure of 3.2kPa, which makes GP-CH_3SO_3-30 outperforms SG if the evaporation takes place above 25℃. As shown in Figure 5.12, considering the evaporator, condenser, adsorption, and desorption temperatures of 25℃, 35℃, 35℃ and 85℃, the cyclic equilibrium uptake utilising GP-CH_3SO_3-30 and GP-CL-30 outperformed that for SG by 38% and 54%, respectively. In practical terms, a low evaporator temperature requirement

might be less concern when utilising desalination, and freshwater production is highly prioritised over cooling, meaning that high evaporator temperature is acceptable. These findings agree with the reported results in the literature by Lian et al [86] and Banda et al [185].

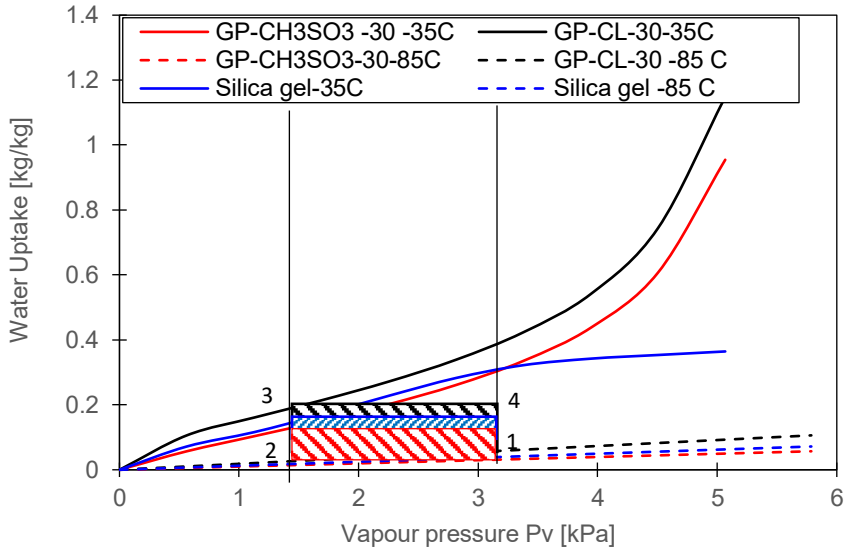

Figure 5.11: Comparison of GP-CH_3SO_3-30 and GP-CL-30 and SG at 35℃, condensation and 85℃, regeneration temperatures for 12 ℃ evaporation temperature

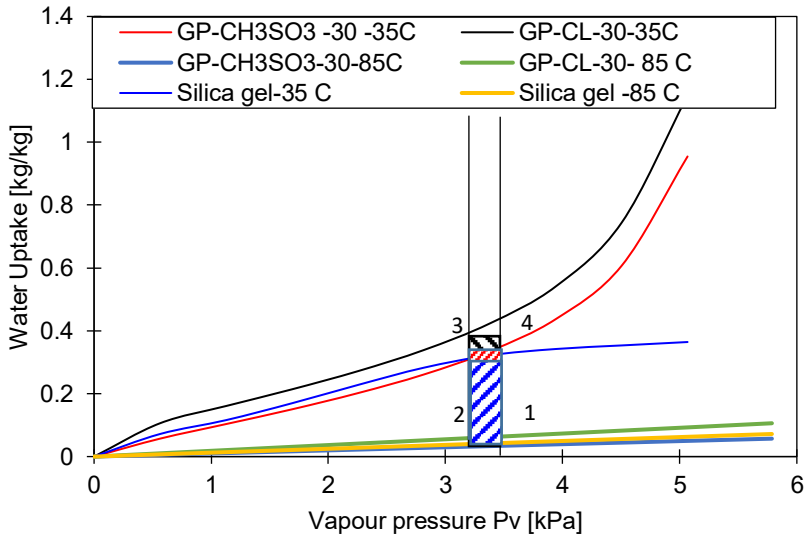

Figure 5.12: Comparison of GP-CH_3SO_3-30 and GP-CL-30 and SG at 35℃, condensation and 85℃, regeneration temperatures for 25℃ evaporation temperature

5.6.2 Component-level cyclic performance

The previous isotherm cyclic analysis considered the material-level equilibrium sorption performance but overlooked the influence of the material's thermal performance, specifically at the component level (i.e., adsorbent bed). Therefore, 2D dynamic heat and mass transfer performance at the

adsorbent bed level was undertaken to envisage the influence of the adsorption and thermal characteristics of the developed composites compared to the SG benchmark. The mostly impregnated composites yet stable, i.e., GP-CH_3SO_3-30 and GP-CL-30, were investigated. The cycle time of 800s, including the 30s preheating/precooling time, was considered in this analysis. The simulated geometry was a circular finned tube heat exchanger packed with adsorbent materials. Figure 5.13 shows the simulated finned tube adsorbent bed, the axisymmetric computational domain and the mesh replicating the simulated geometry. The computational domain considered was half the space between two fins. Table 5-8 and

Table ***5-9*** give the geometry dimensions and operating conditions.

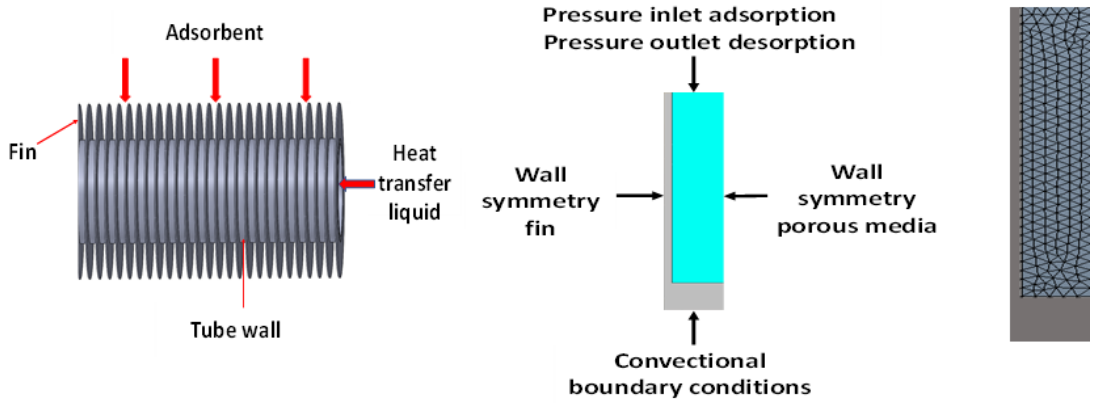

Figure 5.13 - Schematic and geometry of the simulated adsorbent bed

Table 5-8; Dimensions for the simulation model

Parameter	**Value**
Tube outer diameter (d_0)	27 mm
Tube inner diameter (d_i)	24 mm
Fin height (h_f)	10 mm
Fin thickness (δ)	0.54 mm
Fin pitch (p)	3.8 mm
length of the finned tube (l)	500 mm

Table 5-9:Operating conditions and parameters for the simulation

Parameter	Value	Unit
$M_{GP/IL}$	0.43	*kg*
M_{SG}	0.22	*kg*
M_{hex}	2.02	*kg*
T_{evap}	12-25	℃
T_{cond}	35	℃
T_{cw}	35	℃
T_{des}	85	℃
T_{ads}	35	℃
T_{chw}	35	℃
$\dot{m}_{ads/des}$	0.036	kg/s
$\dot{m}_{evap}$	0.018	kg/s
$\dot{m}_{cond}$	0.048	kg/s
t_{cycle}	800	s

Figure 5.14 and Figure 5.15 show cyclic dynamic changes in the adsorbent bed's temperature and water uptake/offtake by utilising evaporator temperatures 12°C and 25°C, similar to the evaporator temperatures utilised for analysing the potential cyclic performance based on the adsorption isotherms. Although silica gel outperformed GP-CH_3SO_3-30 based on the isotherm cyclic performance at 12°C evaporator temperature, its low thermal diffusivity hindered the utilisation of such an adsorption potential as determined by the component level analysis. Therefore, the developed composite, GP-CH_3SO_3-30 and GP-CL-30, outperformed SG at the component level, utilising evaporator temperatures 12℃ and 25℃ by 75% and 79% in terms of water production over the complete cycle. It is primarily due to the relatively faster thermal response of the composites, which is demonstrated by the dynamic temperature profile in Figure 5.14 (a-d) At an evaporator temperature of 25 ℃, the cumulative advanced adsorption and thermal characteristics of developed composites led to a higher water production by 82% and 85% over the entire cycle as shown in Figure 5.14(a-d) and confirmed in Figure 5.15(a-d). Such findings align with previously published research by Elsheniti et al [2]. The colourmaps contours for the dynamic temperature profiles and dynamic water uptake in Figure 5.14 and Figure 5.15 respectively, present the simulated average sorbent temperature and uptake for a full adsorption/desorption cycle. The time allocated for each colourmap are for the full adsorption and desorption cycle.

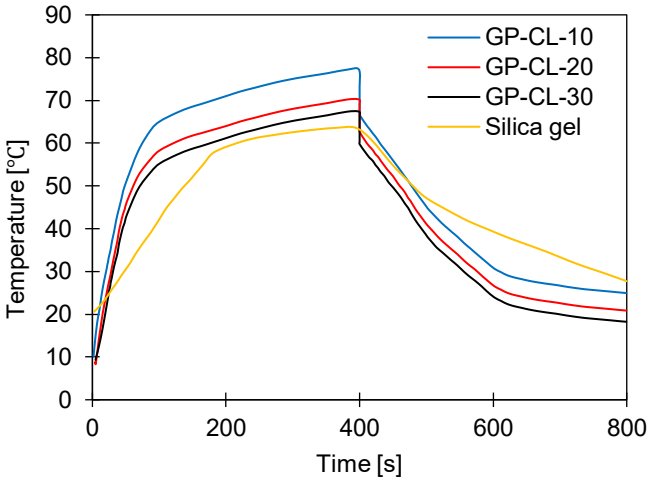

(a) Te= 12°C

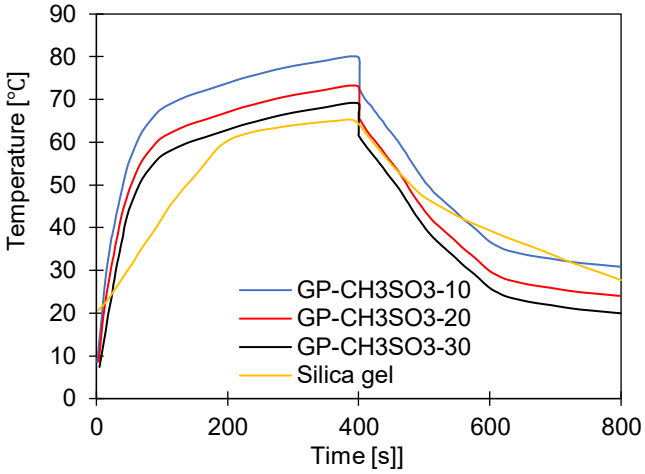

(b) Te= 12°C

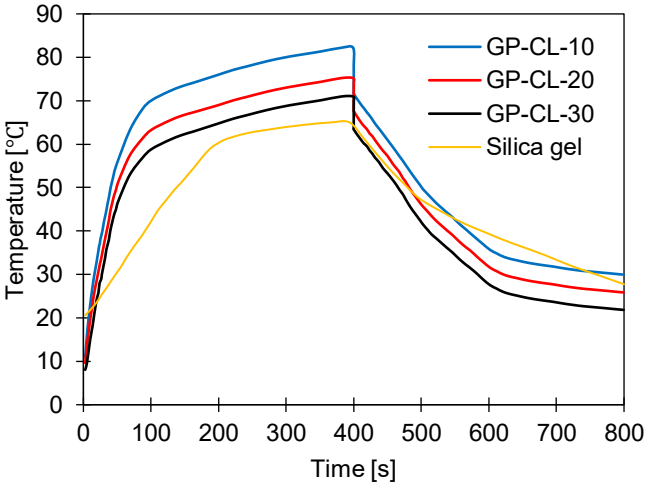

(c) Te= 25°C

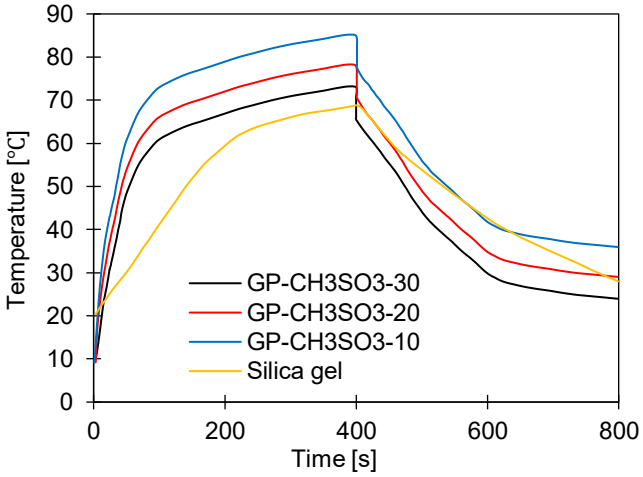

(d) Te= 25°C

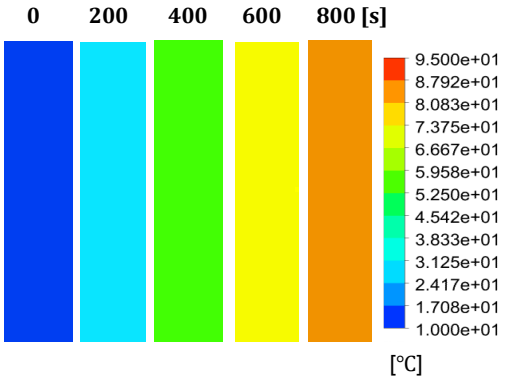

(e) GP-CL-30 & Te= 12°C

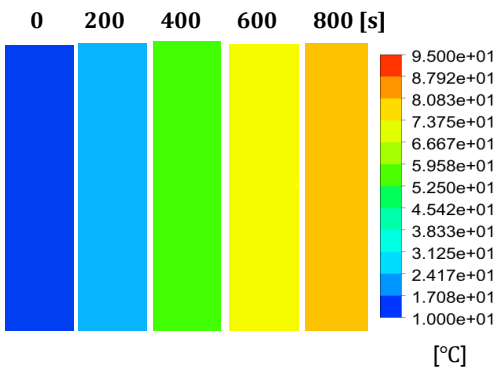

(f) GP-CL-20 & Te=12°C

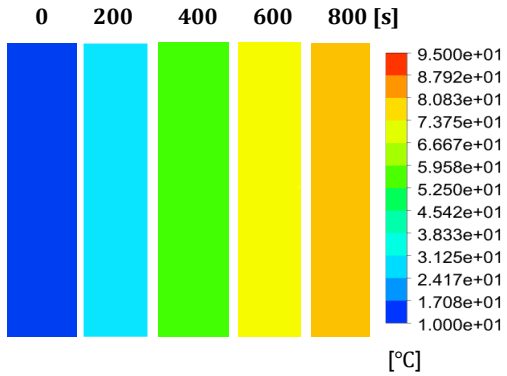

(g) GP-CL-10 & Te= 12°C

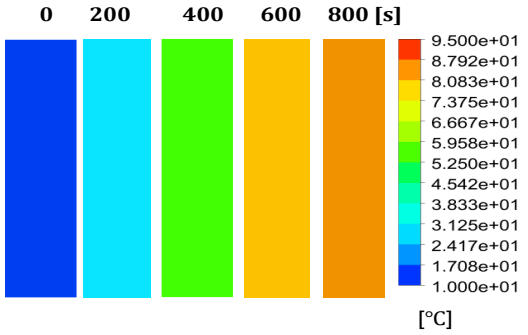

(h) GP-CH_3SO_3-30 & Te = 12°C

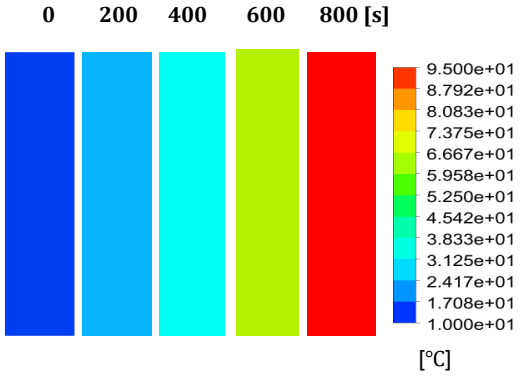

(i) GP-CH_3SO_3-20 & Te= 12°C

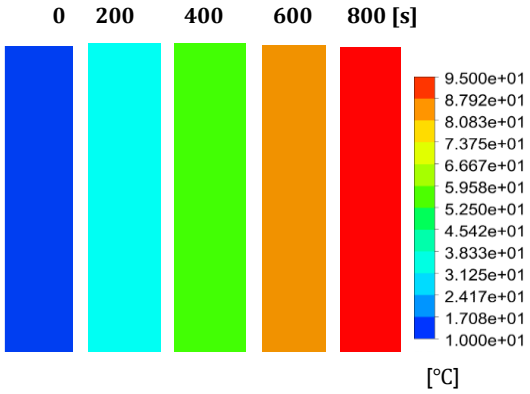

(j) GP-CH_3SO_3-10 & Te= 12°C

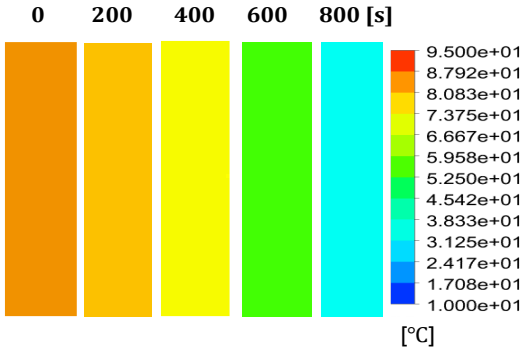

(k) GP-CL-30 & Te= 12°C

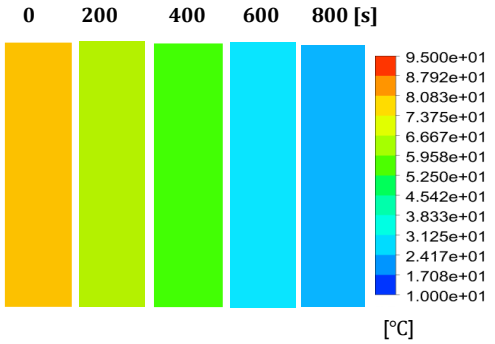

(l) GP-CL-20 & Te= 12°C

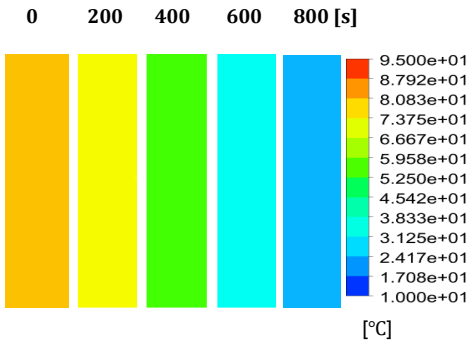

(m) GP-CL-10 & Te= 12°C

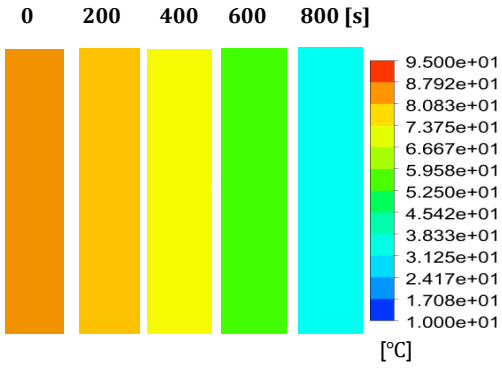

(n) GP-CH_3SO_3-30 & Te= 12°C

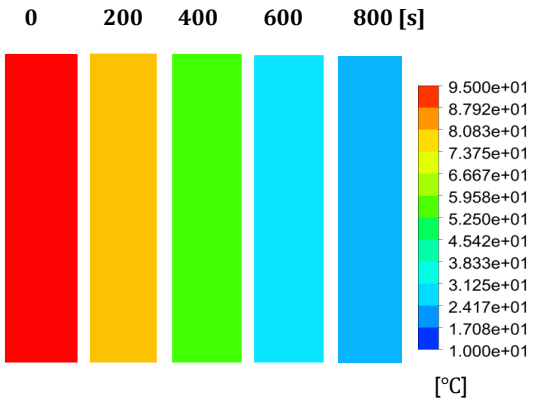

(o) GP-CH_3SO_3-20 & Te= 12°C

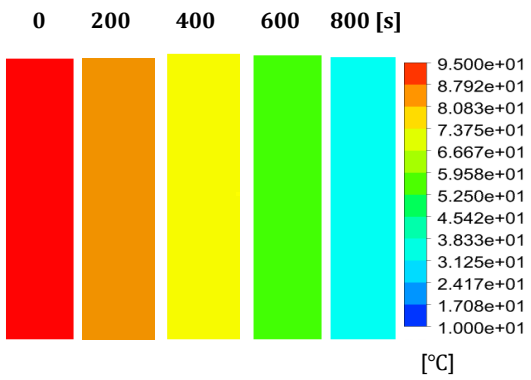

(p) GP-CH_3SO_3-10 & Te= 12°C

Figure 5.14: Dynamic temperature profiles for GP-Cl-10-30 and GP-CH_3SO_3 – 10-30.

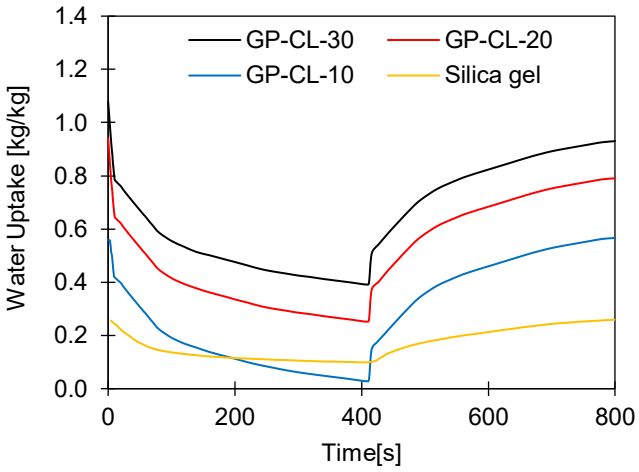

(a) Te= 12°C

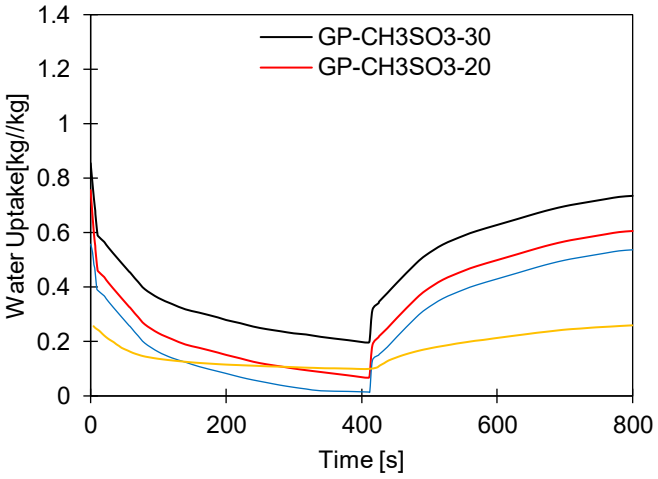

(b) Te=12°C

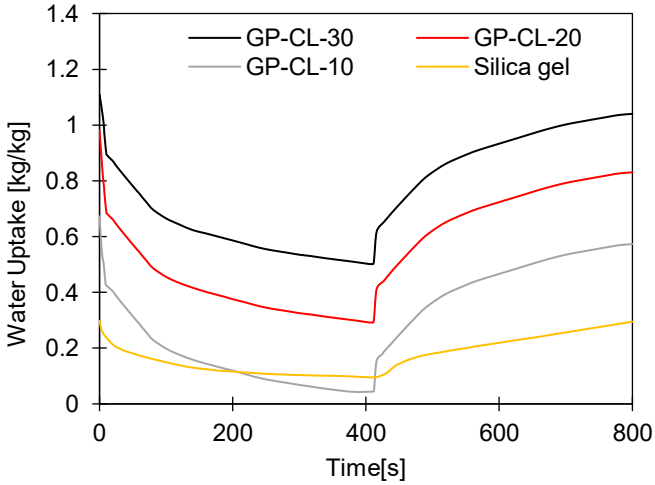

(c) Te=25°C

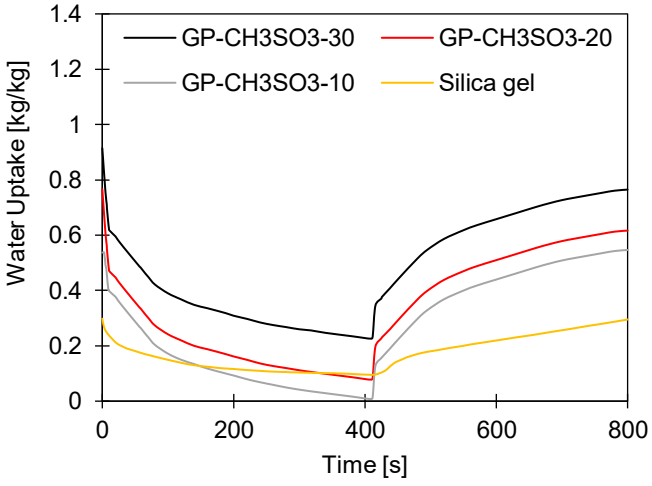

(d) Te=25°C

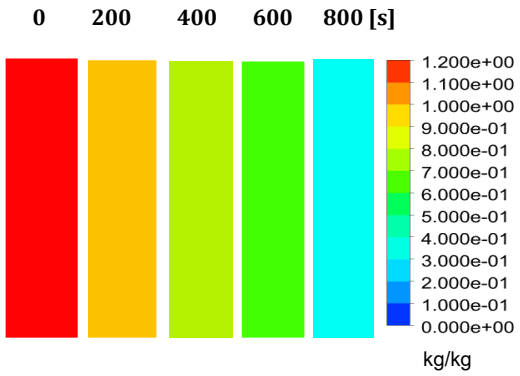

(e) GP-CL-30 & Te=12°C

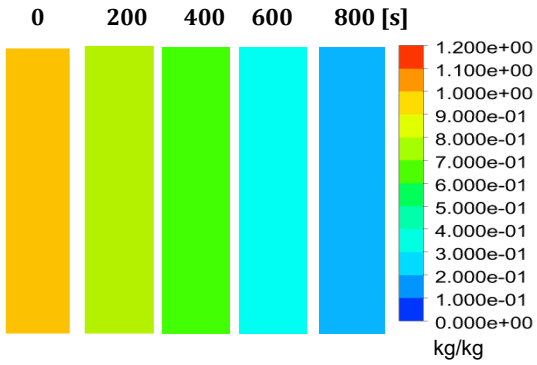

(f) GP-CL-20 & Te=12°C

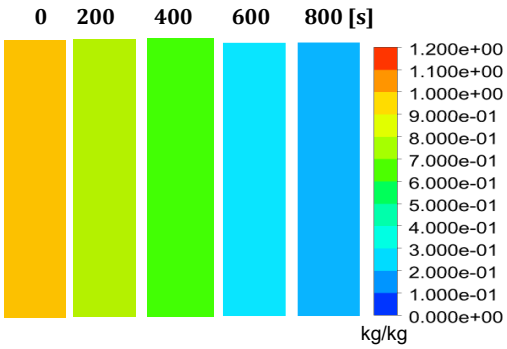

(g) GP-CL-10 & Te=12 °C

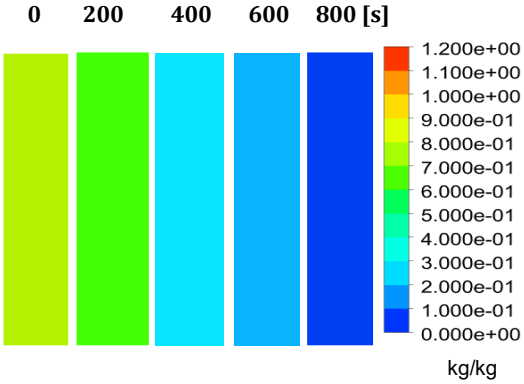

(h) GP-CH_3SO_3-30 & Te= 12°C

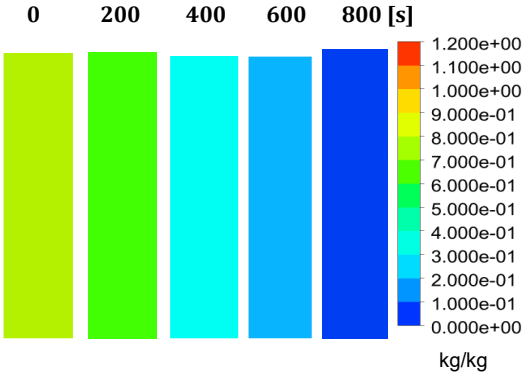

(i) GP-CH_3SO_3-20 & Te= 12°C

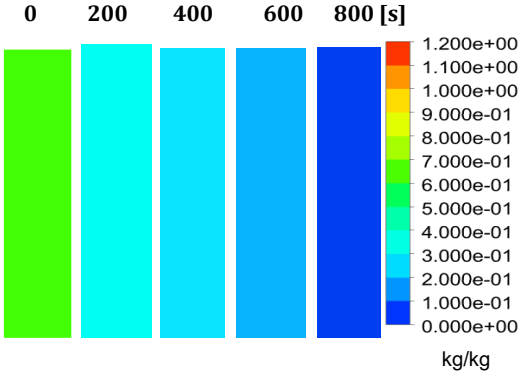

(j) GP-CH_3SO_3-10 & Te= 12°C

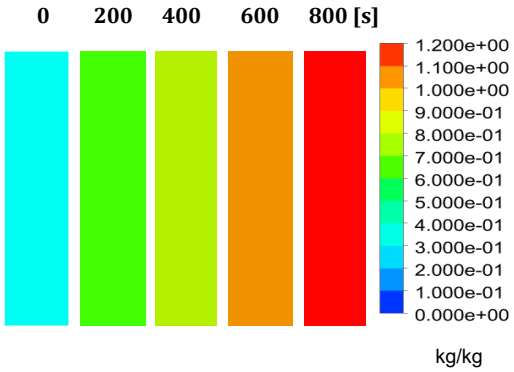

(k) GP-CL-30 & Te=12°C

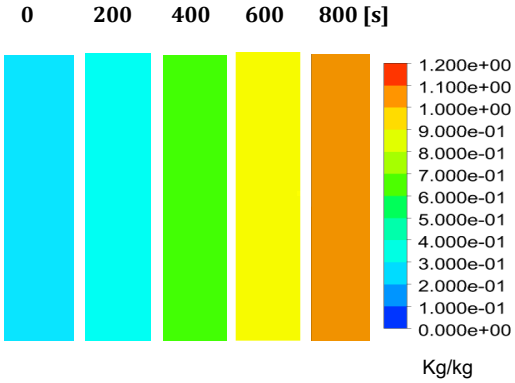

(l) GP-CL-20 & Te= 12°C

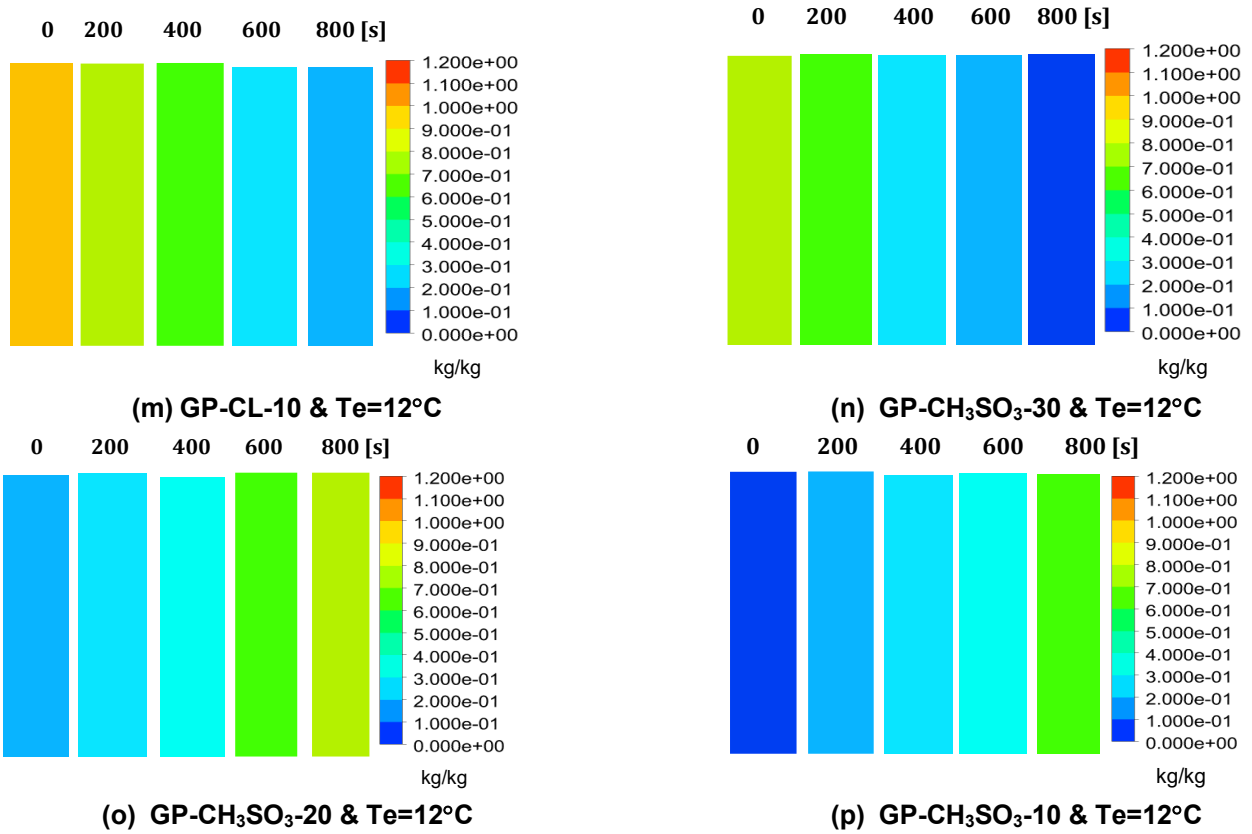

Figure 5.15: Dynamic Uptake profiles for GP-Cl-10-30 and GP-CH_3SO_3-10-30.

5.7 System performance indicators

The system level performance was analysed based on the impact of the composites thermal and adsorption properties on the SDWP, SCP, COP, and Exergy efficiency at two evaporator temperatures of 12 and 25℃. Further investigation was carried out to assess the effect of cycle time and change of heating water temperature.

5.7.1 Exergy analysis

The exergy analysis to establish the energy degradation of each component of the adsorption cooling and desalination system during the adsorption/desorption processes utilising the consolidated GP/IL composites/water pair benchmarking them against SG/water. The exergy efficiency and exergy destruction for all the consolidated GP/IL composites and SG systems are shown in Table 5-10.The obtained exergy results indicated that of all the components, the adsorbent bed had the highest exergy destruction. Under the investigated desorption and adsorption operating conditions of 85 and 35°C respectively. The GP-CL-10-CP1 based composite had the highest exergy destruction of 6.60 kW and 7.77kW during desorption and adsorption respectively. The SG based system experienced the same trend where the exergy destruction for the desorption and adsorption processes were 6. kW and 7.05kW, respectively

Table 5-10: Exergy destruction for GP/Il composites and Silica gel

Component/Process	GPCL30	GPCL20	GPCL10	$CH_3SO_3$30	$CH_3SO_3$20	$CH_3SO_3$10	Silica gel
	Exergy destruction (kW)						
Adsorption at 35 °C	6.11	6.22	6.60	6.35	6.43	6.36	6.
Desorption at 85 °C	7.15	7.34	7.77	7.25	7.5	7.45	7.11
Condenser at 35 °C	1.204	1.212	1.225	1.210	1.218	1.230	1.18
Evaporator at 25 °C	1.308	1.321	1.378	1.302	1.328	1.386	1.3
System overall	15.772	16.093	16.973	16.112	16.486	16.426	15.59
	Exergy efficiency (%)						
	33.9%	31.8	28.7	30	27.2	25.2	23.6

5.7.2 The effect of cycle time

The effect of cycle time on the adsorbent bed's performance was investigated for an 800s cycle, including 30s switching time each and evaporation temperatures of 12 and 25℃, as shown in Figure 5.14. The heating and cooling water inlet temperatures were maintained at 35°C and 85°C, respectively. There was a steep rise in temperature observed in the 100s followed by gradual rise in all the developed composites-based system unlike the temperature rise in the SG based system which was gradual from the onset. The gradual temperature rise, in the composite-based systems was due heat build-up in the adsorbent bed. During the adsorption process, the temperature drop was sudden in the first few seconds in the case of the composite-based system than in the SG-based system, followed by a gradual reduction in temperature. The observe pattern of the influence of cycle time on the adsorbent bed agrees with the findings of Li et al [172].

The influence of varying cycle time was also investigated on the overall systems' performance as shown in Figure 5.16 -Figure 5.19. In most cases, it was observed that SDWP, SCP, COP and exergy efficiency in all the composite based systems increased with increasing cycle time as the systems approached the equilibrium conditions. The overall system performance enhancement was attributed to the increase in the cyclic water uptake by extending the adsorption/desorption time, which positively influenced the clean water and cooling production.

The average increase in SDWP, SCP, COP and exergy efficiency were 78%, 62.5%,43% and 44% when utilising GP-CL-30 compared to SG at 25°C evaporation temperature. The increase in the overall system performance reflects a faster thermal response of all developed composites (GP-IL) that enhanced the overall cyclic water uptake/offtake hence the water and cooling production. The exergy efficiency which is a function of the ratio between useful outcomes and heat input to the system increases with cycle time .as the heat transfer is given more time to complete the adsorption

desorption process and the system becomes more efficient in producing more water up to the optimal cycle time. It was observed that the exergy efficiency was high in all the GP/IL composite based system compared to SG based system. Moreover, the GP-IL composites-based system's exergy efficiency outperformed the SG-based system due to their superior thermal properties resulting in high energy conversion from the heat input to produce cooling and clean water. The increase in cycle time had the effect of increasing the heat added to the system and in return caused an increase in the cooling and water production hence increase the COP. A similar effect was observed on the exergy efficiency. This agrees with the findings of Cao and Chung [164].

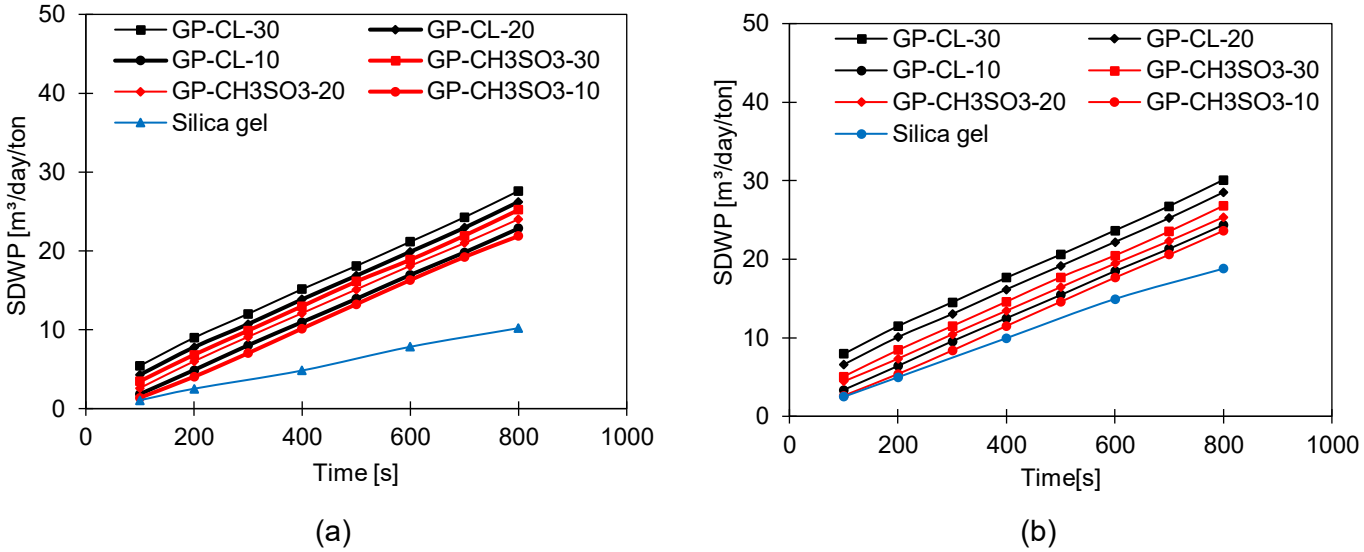

Figure 5.16: The effect of changing cycle time on SDWP for developed composites and SG at Tev= 12℃ and (b) Tev= 25℃

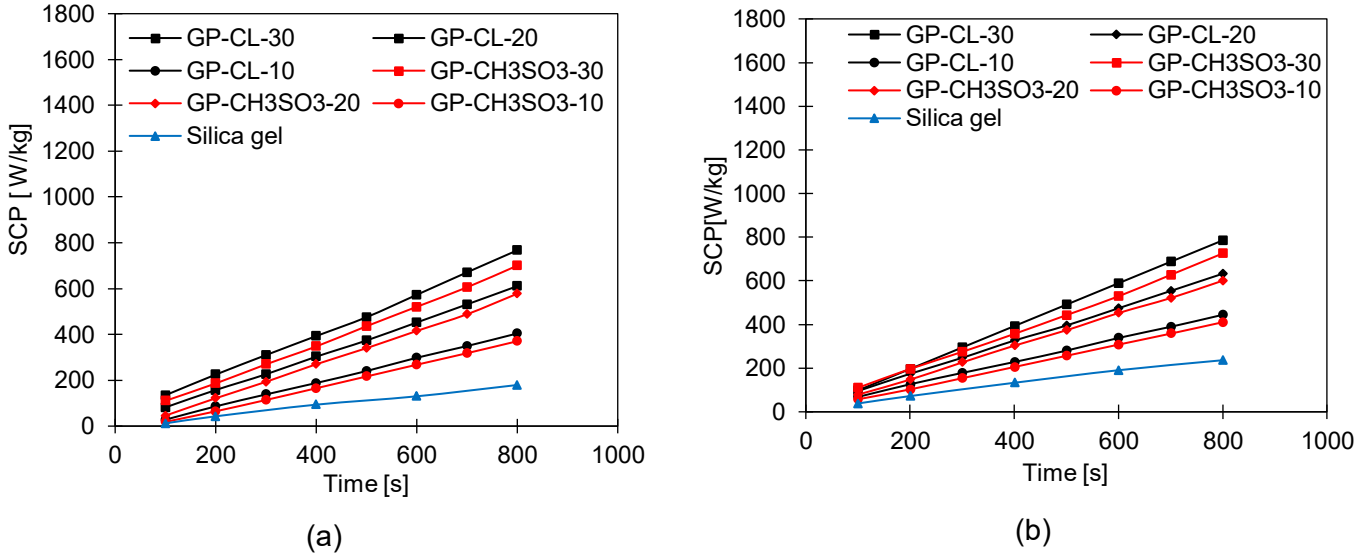

Figure 5.17: The effect of changing cycle time on SCP for developed composites and SG at (a) Tev= 12℃ and (b) Tev= 25℃

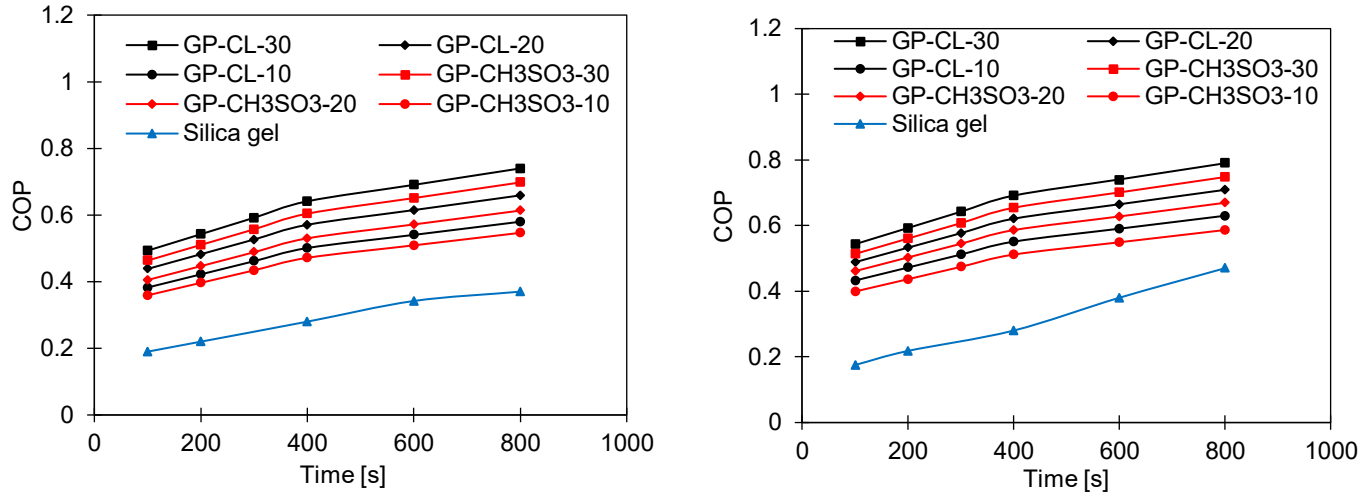

Figure 5.18:The effect of changing cycle time on COP for developed composites and SG at (a) Tev=12 ℃ and (b) Tev= 25 ℃

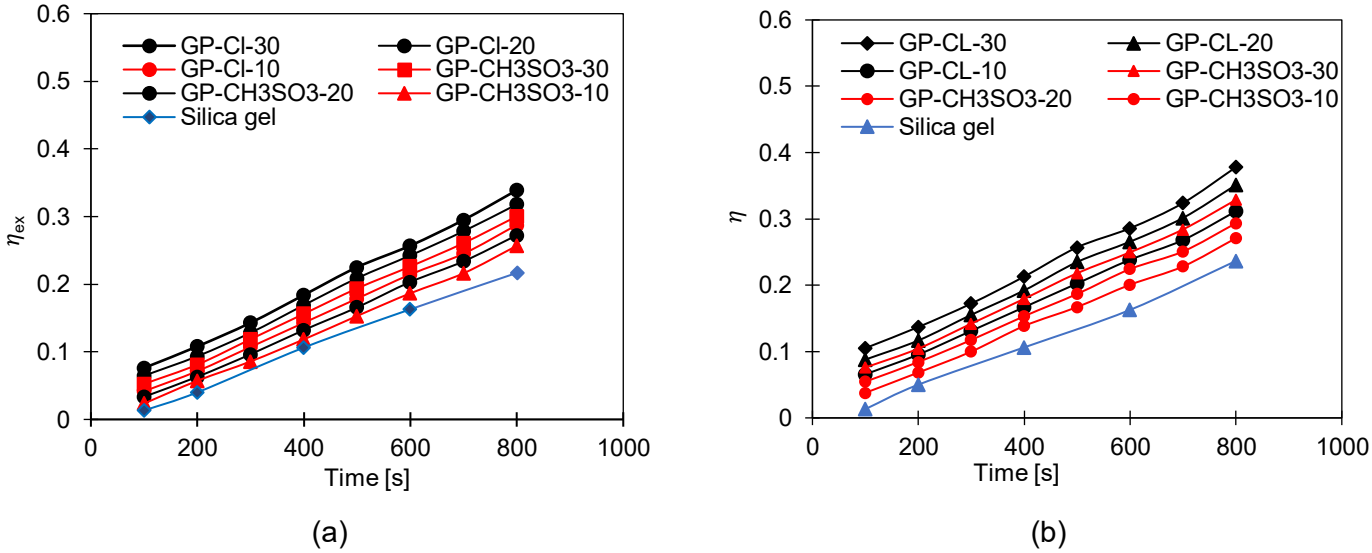

Figure 5.19; The effect of changing cycle time on exergy efficiency for developed composites and SG at (a) Tev=12 ℃ and (b) Tev= 25 ℃

5.7.3 The effect of heat source temperature

Varying the heat source temperature from 60 to 85°C at evaporator temperature of 12 and 25°C, at cooling temperature of 35°C, condensation temperature 35°C and cycle time 800s was investigated. Figure 5.20 shows the effect of increasing heating water temperature on the SDWP. Increasing the heat source temperature from 60℃ to 85℃ had the effect of increasing the SDWP for all the developed composites including GP- CL-30 based system which had the highest increase by 64% (from 8.6 to 24.2m^3/day/ton), and SG-based system by 65% (from 3 to 8.6m^3/day/ton). All the GP-IL-based system showed SDWP higher than the SG-based system on average by 60%. The same trend was observed on the 25℃ evaporator temperature where GP-CL-30 based system had the

highest increase by 57% (from 11 to 25.6 m^3/day/ton while SG had an increase of 80% from (from 2.3 to 12.1m^3/day/ton). Overall, the developed composites-based systems and particularly the highest performer GP-CL-30 had higher SDWP than SG by 51%.

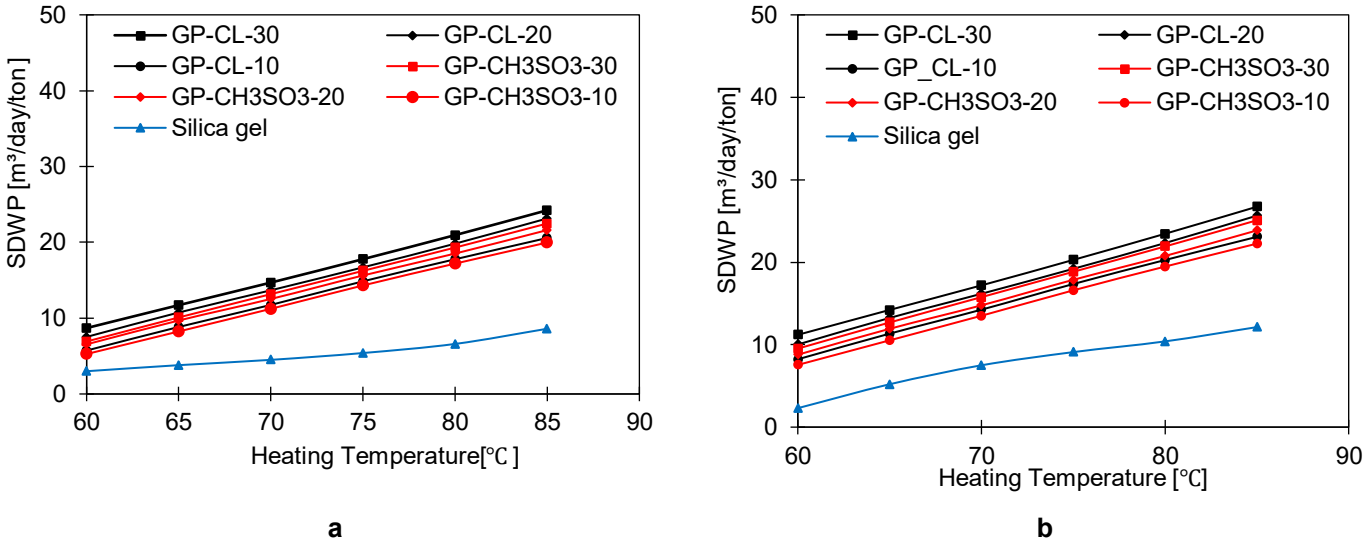

Figure 5.20: SDWP at different heating water temperatures at (a) Tev= 12 ℃ and (b) Tev= 25 ℃

Figure 5.21 shows the effect of increasing heating water temperature on the SCP. Alongside the SDWP trends, the developed composites GP- Cl-30 based system outperformed all the developed composites and the SG-based system averagely by 65% at an evaporator temperature of 30℃ and reassure the advancement of the GP-IL based system for water desalination at high evaporation temperature, as previously investigated. Overall, the better performance of the GP-CL-30 based system and other developed composites compared to the SG-based system across the investigated temperature range is credited to the advanced thermal diffusivity, resulting in higher thermal response at the component level in conjunction with the presence of IL which has a high impact on the adsorption capacity resulting in a higher cyclic water uptake/offtake rate at the system level. Increasing the heat source temperature from 60℃ to 85℃ increased the SCP for all the developed composite-based systems by averagely 36% and the SG-based system by 55% (from 430 to 670W/kg) at 25℃ evaporation temperature. These findings for SDWP and SCP agree with the study by Youssef et al [46] in their investigation of the influence of the heating water temperature on the SDWP for adsorption water desalination system.

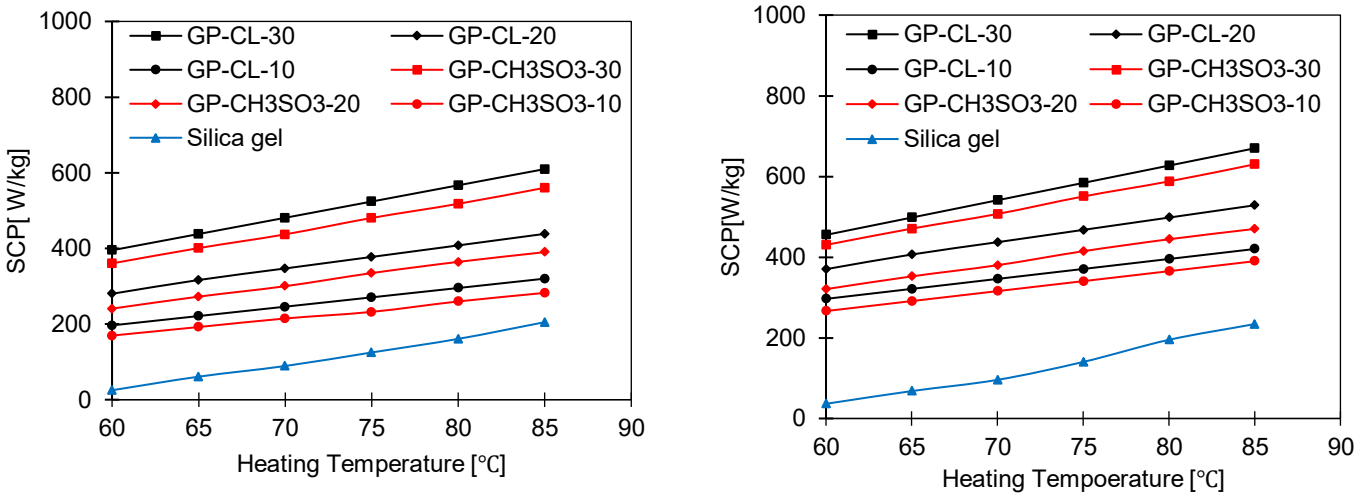

Figure 5.21: SCP at different heating temperatures for developed composites and SG at (a) Tev= 12℃ and (b) Tev= 25℃

Figure 5.22 show the effect of varying the regeneration (heat source) temperature on the COP of the system. In most cases, increasing the heat source temperature resulted in an increase of the COP. Increasing the heat source temperature while maintaining the cooling (heat sink) temperature has the effect of increasing the cyclic water uptake, cooling, and water production hence increases the heat transfer in the adsorbent bed during the regeneration process. Consequently, increasing the heat source temperature improved the energy conversion efficiency (COP) at the system level within the investigation temperature range.

Correspondingly, the COPs for GP-CL-30 increased by 33% (from 0.51 to 0.77), for the SG-based system by 46% (from 0.22 to 0.41) at 12℃ evaporator temperature while the COP increases at 25℃ evaporator temperature were 32.5% for GP-CL-30 (from 0.56 to 0.83) and 63% for SG (from0.16 to 0.44) when the heat source temperature from 60°C to 85°C respectively overall COP of the developed composite GP-CL-30 is higher than SG by 44% at 12℃ evaporator temperature and 47% at 25℃ evaporator temperature. This is attributed to the high thermal responses of the composite based system resulting in high water uptake. There was a decrease in exergy efficiency as heat source increases in all the composite and SG based systems. This was attributed to higher regenerative temperatures which tend to increase the thermodynamic irreversibility in desorption process causing higher exergy destruction and reduce the systems overall exergy efficiency. In some cases, higher regenerative temperature may exceed the optimal operating temperature of the adsorbent material causing a reduction in the desorption rate and decrease in overall system exergy efficiency. The exergy for GP-CL-30 decreased by 33% (from 0.31 to 0.15, for the SG-based system by 66% (from 0.22 to 0.071) at 12℃ evaporator temperature while exergy decrease at 25℃

evaporator temperature was 36% for GP-CL-30 (from 0.35 to 0.189) and 70% for SG (from 0.2 to 0.06).

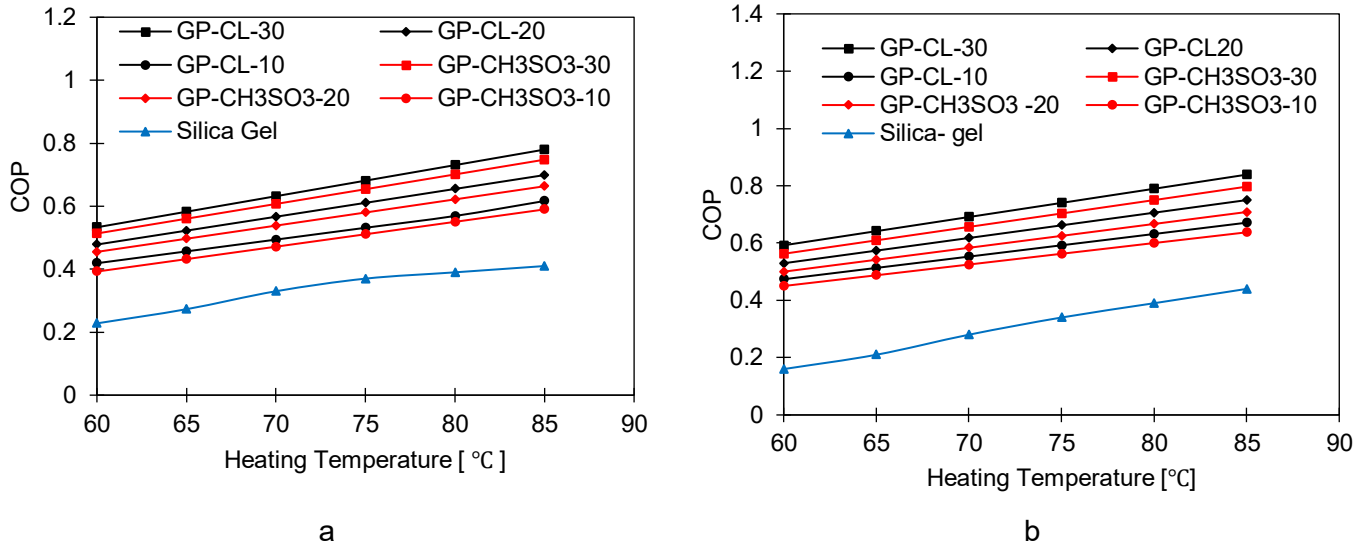

Figure 5.22: COP at different heating temperatures for developed composites and SG at (a) Tev= 12℃ and (b) Tev= 25℃

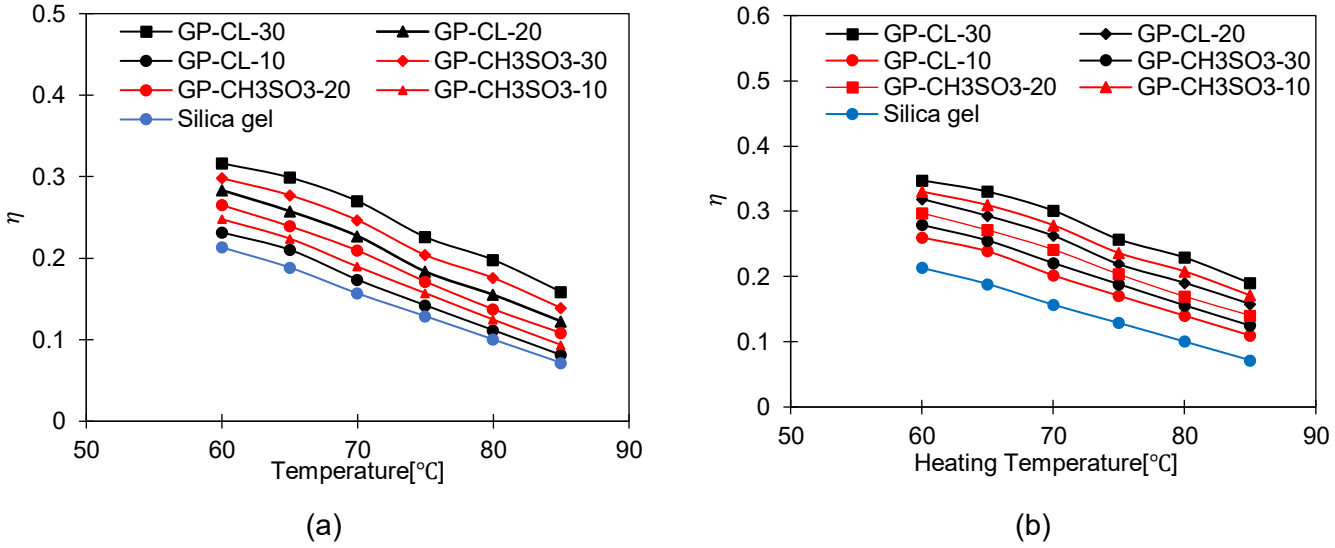

Figure 5.23: Exergy efficiency at different heating temperatures for developed composites and SG at (a) Tev= 12℃ and (b) Tev= 25℃

5.8 Conclusion

The purpose of the chapter study was to analyse the use of powder form composite utilising GP and IL as an adsorbent for cooling and desalination. Eight composites were initially synthesised using GP as the host matrix material as well as a thermal conductivity enhancer combined with two ILs (EMIMCL and EMIM CH_3SO_3) of different concentration ranging from 10 wt% to 30 wt%. The 40% wt composites were not further investigated as it was observed that it was over impregnated due to high concentration of IL SEM and XRD analysis were performed to understand the structure of the

material and interactions of the atoms making up the composites. The adsorption and thermal characteristics of GP-IL composites were determined and benchmarked against the baseline silica gel adsorbent, which was modelled and coupled with a 2D Multiphysics computational model to predict the heat and mass transfer performance at the adsorbent bed (component level). In addition, the influence of varying the cycle time and heat source temperature on the adsorbent bed and system level overall performance was undertaken via energy and exergy analyses: The key findings of the study are concluded below.

- ILs have high impact on the water uptake of the composites. In composites 30% wt and below, full impregnation took place without altering the high BET surface area and maintaining the thermal properties of the GP host material. The equilibrium adsorption water uptake increased with increase in IL concentration as shown in the GP-CL-30 which was a 78% enhancement to the baseline Silica gel. The results also showed that at material level, the high concentration EMIM CL is more effective in terms water solvation compared to the EMIM CH_3SO_3 and had the effect of increasing water uptake the most.
- The high thermal diffusivity of GP significantly influenced the thermal response of developed composite at component level. The GP10 wt % IL composites showed superior thermal diffusivity with the highest value of 11.84mm^2/s for the GP-CH_3SO_3-10 which was 394 times higher than Silica gel. This showed that the thermal diffusivity of GP was affected less by 10 wt % concentration compared to 20 wt% and 30wt %. Despite the faster heat transfer in the GP-IL based adsorbent bed with lower concentrations, they had increased exergy destruction, the exergy efficiency at the system level was availed. As a result, the SDWP, SCP, COP and exergy efficiency for the GP-CL-30 based system was 60%, 70.5%, 38.5% and 36% higher than the SG-based system when operated at 25°C.
- Increasing the cycle time had the effect of increasing the water uptake in the developed GP-IL composites and SG due to the adsorbent bed taking a long time to reach closer to equilibrium uptake. Consequently, the SDWP, SCP and COP for the GP-CL-30-based system which was the highest performing composite was higher than that of the SG-based system by 65%, 76% and 49% at 12°C evaporator temperature and by 59%, 70%, and 49% at 25 °C evaporation temperature respectively. The GP-CL-30 based system outperformed the SG-based system due to the higher water uptake capacity of IL and a higher thermal response, which led to higher cyclic water uptake.
- The effect of increasing the heat source temperature was to increase the regenerative temperature and had the effect of enhancing the SDWP, SCP and COP as the source temperature increased. The developed GP- IL -30 which had the highest performance of

all the developed composite had higher SDWP, SCP, COP than SG by 51-62%, 55-64% ,44-47% when operating at evaporator temperature range of 12-25°C.

In terms of the composite synthesis and maintaining the structure of the host material, the most effective concentration of IL to enhance the thermal properties of the host material and the equilibrium uptake, this investigation concluded that the GP-CL-30 composite is the most suitable among the investigated material. These enhanced characteristics of the synthesized components can play a significant role in the next generation adsorption desalination and cooling applications.

CHAPTER 6: SYNTHESIS AND PERFORMANCE ANALYSIS OF GRAPHENE/IONIC LIQUID CONSOLIDATED COMPOSITES

6.1 Introduction

Of late, researchers have worked on enhancing the thermal and adsorption properties of adsorbents by developing consolidated composites using various additives such as Expanded graphite (EG), Expanded natural graphite (ENG), Expanded graphite treated with sulphuric acid (ENG-TSA) and binders Polyvinyl alcohol (PVA), Polytetrafluoroethylene (PTFE), Polymerised ionic liquid (PIL),polyvinylpyrrolidone(PVP), gelatine, hydroxyethyl cellulose (HEC)[4, 109, 110, 178, 186-189]. Four different binders namely PVA, PVP, (HEC) and gelatine were investigated to find out the most appropriate binders for silica gel composite synthesis for application in adsorption cooling. The findings showed that the PVP and PVA where the most suitable binders for composite synthesis for adsorption cooling application since they had the least negative effect on the porous properties of the host material [109].

Studies on silica gel and PVP composites showed a 78.6% increase in thermal conductivity compared to pure silica gel [36].Investigation on a composite made of 50% Maxsorb III, 20% expanded graphite and 10% PVA binder, yielded a thermal conductivity 11 times higher and further test indicated an improved adsorption uptake by 51% [4, 190]. Consolidated composite made from activated carbon and expanded natural graphite with a ENG-TSA binder were investigated, and the findings showed an improved thermal conductivity of 34.2 W $m^{-1}K^{-1}$ which was 150 times higher compared to granular activated carbon [191]. The studies on consolidated has shown that consolidated composites had improved thermal and adsorption properties compared to ordinary adsorbents such as activated carbon. However, there is still a need to develop consolidated composites with both improved thermal properties and adsorption capacity to enhance the poor heat and mass transfer associated with adsorption systems.

The reported literature and findings from previous Chapter 5 has indicated that IL has excellent physicochemical properties that could make them excellent adsorbents and on the other hand GP has been proven to enhance thermal properties when added to adsorbents. While there are notable improvements on the thermal properties on many consolidated composites involving various additives and conventional adsorbents, there is hardly a study recorded involving IL and GNP and binder consolidated composites. Therefore, this chapter presents the investigation of a novel IL based consolidated composite adsorbent employing ILs, GP and PVA binder for cooling and desalination application and explore its impact on the system level's energy conversion prospective by means of exergy analysis and overall performance by virtue of energy analysis – operating under various conditions. Accordingly, the objectives are to (1) To develop a GP/IL consolidated composite

employing a PVA binder. (2) Experimentally investigate the thermal and adsorption characteristics of the developed consolidated composite (3) Envisage the heat transfer and water uptake of the consolidated composite using CFD simulation tool and benchmark it against a baseline adsorbent Silica gel. (4) Investigate the impact of PVA binder concentration (2%, 5% and 10%) and different compressional force (1MPa, 1.5 MPa and 2MPa) used in the development of the composites on the thermal and adsorption properties of the developed composites.

6.2 Materials

GNP, IL and PVA were used for developing the consolidated composites. Two ILs, Ethyl-methylimidazolium-chloride (EMIM Cl) and Ethyl-methylimidazolium methane sulfonate (EMIM CH_3SO_3) were sourced from Sigma Aldrich. The host material for the IL was a few-layered pristine graphene platelets of 1-5 layers, commercially known graphene nanoplatelets obtained from Graphitene ltd. The pristine GP was selected for use as a host material because it possesses superior thermal diffusivity of 22.3mm^2/s and high BET surface area of 56.8978m^2/g compared to other graphene derivatives. The PVA was procured from ThermoFisher Scientific UK. The PVA binder was selected Benchmarking of the composite was performed against a widely used adsorbent Fuji Silica gel (SG) of 0.18-1mm particle size.

The consolidated composites GP-CL-30 and GP- CH_3SO_3-30 both of 30% concentration were selected for further investigation as consolidated composite based on their overall adsorption performance as powder composites for cooling and water desalination application in Chapter 5. This study involves the analysis of the performance of the developed composites on a two-bed adsorption desalination and cooling system shown in Figure 2.3 (a) in Chapter 2 at both component and system level. The basic structure of the adsorption of the desalination and cooling system under study consists of two finned adsorbent beds packed with adsorbent material as the main component, evaporator, and condenser. The driving force of the adsorption cooling and water desalination system is the heat transfer between the sorbent and the heat transfer fluid (HTF) through the finned bed and the interaction between the adsorbent and water vapour during adsorption/desorption.

6.2.1 Synthesis of the consolidated IL/GNP composites

There are two processes for developing composite adsorbents namely physical mixing or impregnation and chemical process. The impregnation process was employed in making the consolidated tablets. In the impregnation process, a homogeneous mixture was formed by physically mixing all the composite constituent materials. The synthesis process involved several steps shown in Figure 6.1. The first step involved heating 1g of the host material GNP in an oven at 150℃ for 12hours to remove the moisture and some impurities. Secondly, the IL was mixed with pure water to form aqueous solution at 30 wt% concentration regarded the optimal concentration, where there

are no changes in the adsorption and thermal properties of the developed powder composites as indicated in Chapter 5. The host matrix from the oven was mixed with the IL aqueous solution and stirred for 1 hour until a homogeneous mix was achieved and allowed to rest for an hour. The binder solution was prepared by mixing PVA with pure water to come up with various binder concentrations of 2, 5 and 10%. To facilitate dissolving of PVA heat was supplied at 90℃. The binder solution was added to the GNP/IL mixture and was compressed in a consolidated composites mould. Weights were placed on top of the mould to supply the required compressional pressures of 1MPa, 1.5MPa and 2MPa.Table 6-1 and Table 6-2 show the range of composite developed. Finally, the compressed composite samples were dried in an oven at 150℃ for 12hours. Multiple GNP/IL samples were developed with dry sample masses ranging between 0.2 to 0.3g. and the sample diameter was 12.7mm while the thickness was 2.5mm.

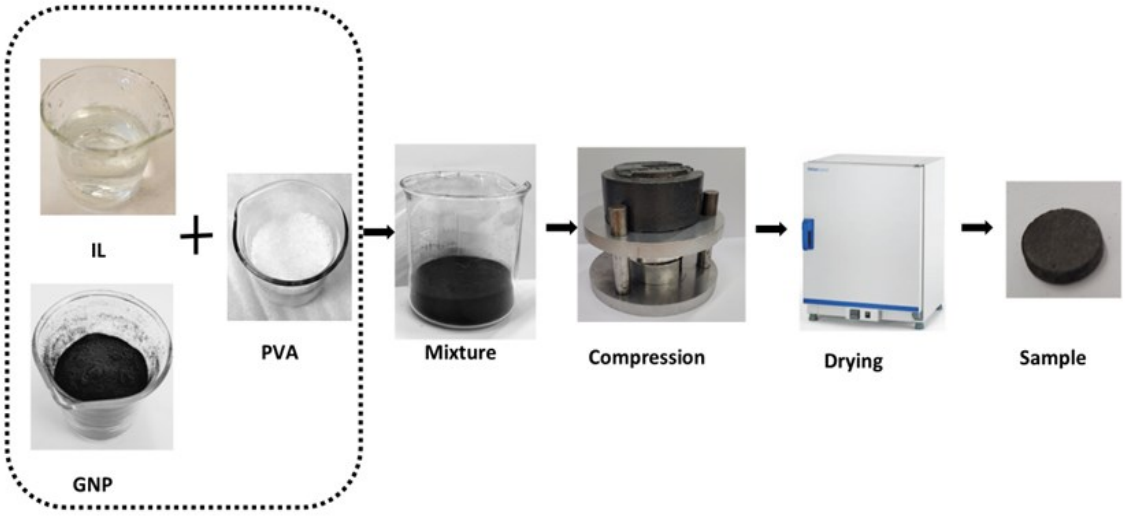

Figure 6.1: Steps in the composite synthesis

Table 6-1:GP-CL-30 Composites range, pressure and PVA concentration values

Composite name	Pressure (MPa)	PVA concentration (%)
GP-CL-30-CP1	1	2
GP-CL-30-CP2	1	5
GP-CL-30-CP3	1	10
GP-CL-30-CP4	1.5	2
GP-CL-30-CP5	1.5	5
GP-CL-30-CP6	1.5	10
GP-CL-30-CP7	2	2
GP-CL-30-CP8	2	5
GP-CL-30-CP9	2	10

Table 6-2: GP/ CH_3SO_3-30 Composite range, pressures and PVA concentration.

Composite name	Pressure (MPa)	PVA concentration (%)
GP- CH_3SO_3-30-CP 1	1	2
GP- CH_3SO_3-30-CP 2	1	5
GP- CH_3SO_3-30-CP 3	1	10
GP- CH_3SO_3-30-CP 4	1.5	2
GP- CH_3SO_3-30-CP 5	1.5	5
GP- CH_3SO_3-30-CP 6	1.5	10
GP- CH_3SO_3-30- CP 7	2	2
GP- CH_3SO_3-30- CP 8	2	5
GP- CH_3SO_3-30 -CP 9	2	10

6.2.2 Compression mould system

The compression mould in Figure 6.2, was designed and modelled using SolidWorks. The purpose of producing the composite in the desired tablet/pellet form was to meet the relevant dimensions acceptable to the Laser Flash Analyser for the thermal tests. The compression mould was made from aluminium and comprised of a top press plate, bottom press plate, support bracket, mould, and guide pins equispaced at 120°. The GP/IL composite mixture is placed in mould plate between the bottom pinned plate and the top pinned plate. The weights are placed on the top pinned plate to give the required compressional pressure. The compressional pressure is calculated using equation (6.1).

$$Pressure = F/A \tag{6.1}$$

Where A is the cross-sectional area of the pins (m^2) and F the force applied (N). F is calculated from Newtons second law of motion which is a relationship between the force applied to an object, its mass and acceleration due to gravity (g) given in equation(6.2)

$$F= mg \tag{6.2}$$

Where m is mass (kg) and g is the acceleration due to gravity (ms^{-2})

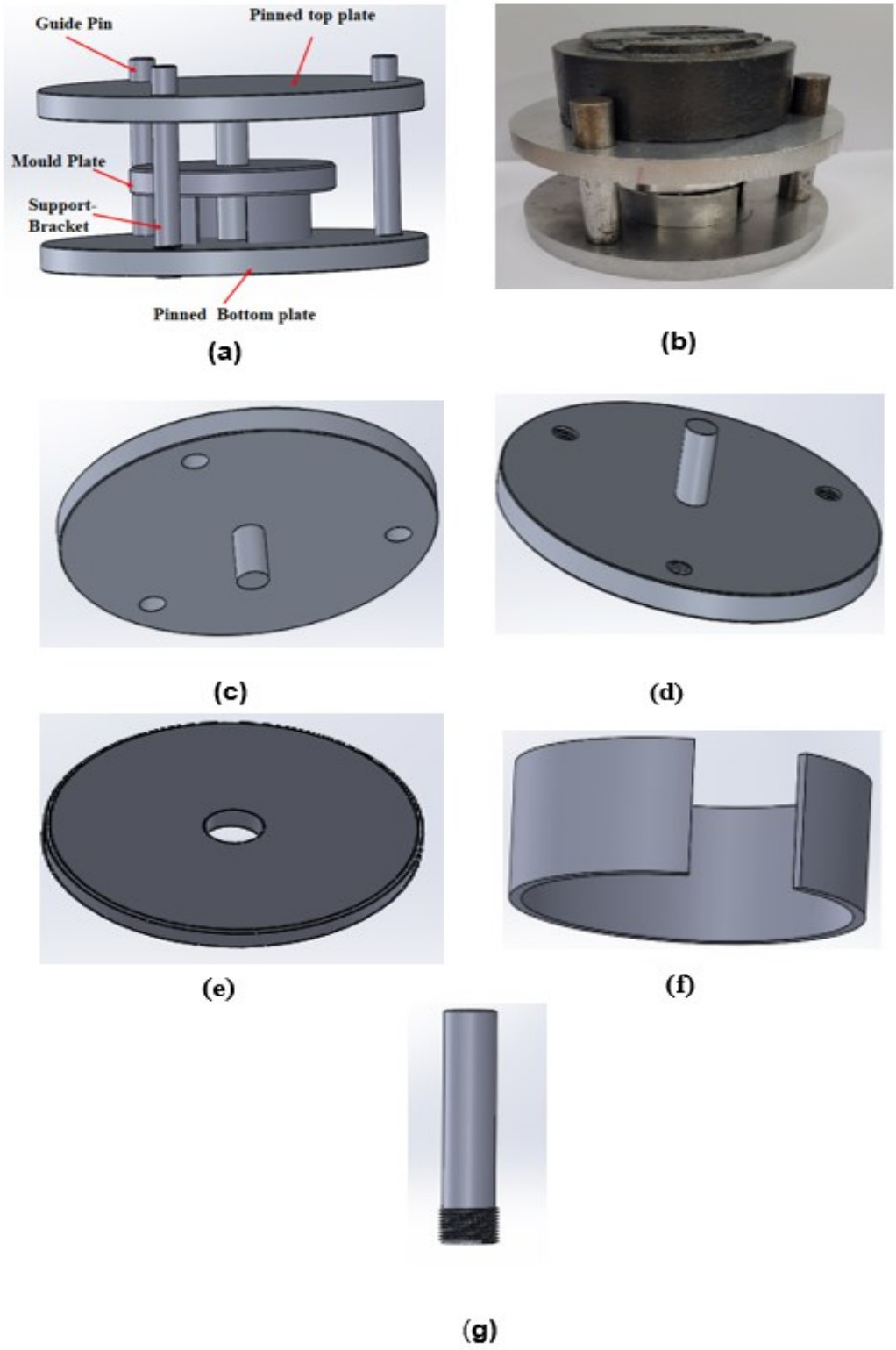

Figure 6.2 The compression mould (a) mould assembly (b) Mould with weights, (c)Pinned top plate (c) Pinned bottom plate (d) support bracket (e)mould plate (f) support bracket (g) guide pin

6.3 Heat transfer properties

Thermal properties of the composite were measured using the LFA, following the methodology in Chapter 3. The composites were developed cylindrical in shape with a small thickness of 2.5mm so that they can fit in the LFA sample holder. The thermal diffusivities of the developed consolidated composites compared to SG are presented in Table 6-3 and Table 6-4.

Table 6-3: GP-CL-30 thermal GP-diffusivity

Material	**Thermal diffusivity (mm^2/s)**
GP-CL-30-CP1	3.679
GP-CL-30-CP2	3.479
GP-CL-30-CP3	2.734
GP-CL-30-CP4	3.694
GP-CL-30-CP5	3.54
GP-CL-30-CP6	3.362
GP-CL-30-CP7	4.652
GP-CL-30-CP8	3.922
GP-CL-30-CP9	3.779
Silica gel	0.365

Table 6-4:GP- CH3SO3-30 thermal diffusivity

Composite name	**Thermal diffusivity (mm^2/s)**
GP- CH_3SO_3-30-CP 1	3.517
GP- CH_3SO_3-30-CP 2	3.052
GP- CH_3SO_3-30-CP 3	2.073
GP- CH_3SO_3-30-CP 4	3.582
GP- CH_3SO_3-30-CP 5	3.475
GP- CH_3SO_3-30-CP 6	2.482
GP- CH_3SO_3-30- CP 7	4.431
GP- CH_3SO_3-30- CP 8	3.895
GP- CH_3SO_3-30 -CP 9	3.619
Silica gel [192]	0.312

6.4 1 The effect of compressional pressure on thermal diffusivity

The thermal diffusivities of all the developed consolidated composites were higher than that of SG. The GP-CL-30-CP7 had the highest thermal diffusivity which was 12.7 times higher than SG. The thermal test for both GP-CL-30 and GP-CH_3SO_3-30 composite showed that the compressional pressure applied during the synthesis of the consolidated composites had an impact on their thermal diffusivities. As indicated by the thermal test results in tables 4 and 5, the highest compressional pressure applied (2MPa) for both GP-CL-30-CP7 and GP- CH_3SO_3-30- CP 7 composites resulted in the highest thermal diffusivity followed by the 1.5 MPa and the 1MPa compressional pressure yielding the least. The increase in thermal diffusivity of consolidated composite tablets with increasing compressional pressure is attributed to low void spaces caused by the compression resulting in reduced porosity and better contact between particles which allows efficient heat transfer. This agrees with the findings of Wu et al [193], in their study of composite bricks made from silica gel and copper nano powder and PVA binder that compression close intraparticle space and improve contact area increasing the heat transfer The other effect of increasing the compressional force is increasing the overall density of the composite tablets resulting in increase in thermal diffusivity.

6.5.2 Effect of PVA binder on the composite thermal diffusivity

The thermal test results revealed that the PVA concentration influences the overall thermal diffusivity of the composites. The composite that had the highest thermal diffusivities (GP-CL-30-CP7 and GP-CH_3SO_3-30-CP7) had the least concentration of PVA (2%) followed by those with 5% PVA concentration and the least being the ones with 10% PVA concentration. The corresponding decrease in thermal diffusivity with increasing PVA binder concentration shows that a higher binder concentration will have an insulation effect on the composites which hinders the heat transfer. Conversely, a lower binder concentration means there is less binder material present in the composite which tends to allow rapid movement of heat through the composite. The thermal results indicating that less binder concentration of 2% has less effect on the thermal properties is in agreement with the findings by Younes et al [109] in their investigation of silica gel composites with polymer binders.

6.5 Adsorption characteristics modelling

6.5.1 Isotherms

The consolidated composite isotherms were classified as type II adsorption isotherms and the Dubnin-Astakhov (D-A) was considered as the most suitable model to experimentally determined isotherms fully. The D-A model is presented in equation (6.3) introduced in Chapter 5.

$$q = q_o \exp\left[-\left\{\frac{RT}{E} \ln\left(\frac{P}{P_s}\right)\right\}^n\right] \quad (6.3)$$

Modelling of the consolidated experimental isotherms data was performed using a nonlinear optimization method for D-A model parameters. Table 6-4 and Table 6-5 shows the D-A model fitting parameters with a root mean square deviation (RMSD) of less than 5%. Figure 6.3 shows the experimentally determined equilibrium adsorption isotherms for the GP-CL-30-CP1-9 and GP-CH_3SO_3-30-CP1-9 consolidated composites. The developed isotherm Figure 6.4 model had a good agreement with the experimental adsorption isotherm with a regression parameter (R^2) of 0.998.

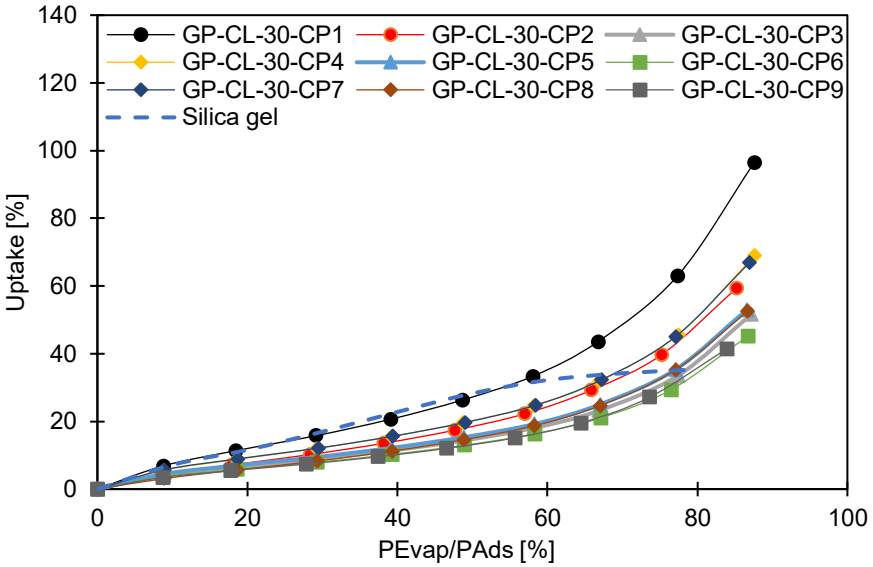

(a)

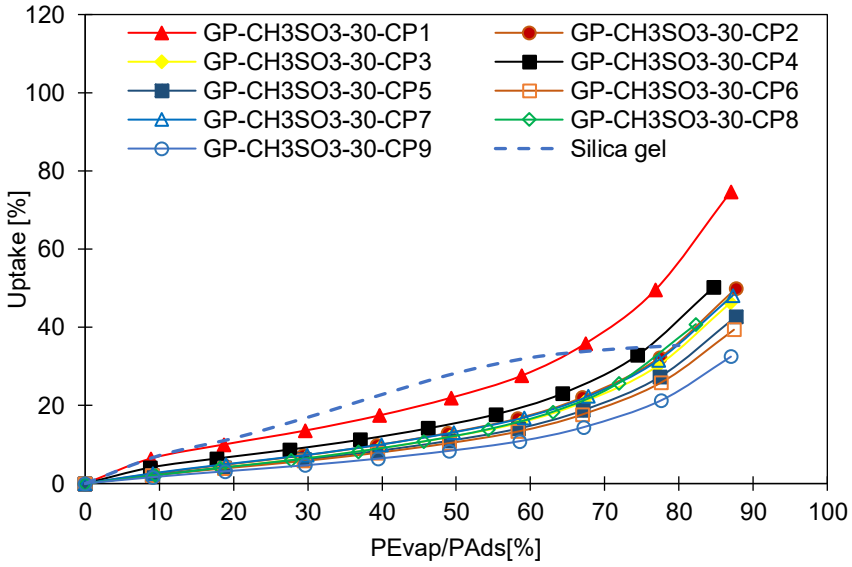

(b)

Figure 6.3 The adsorption isotherms for the consolidated composites and silica gel

Table 6-5: GP-CL-30 composite model fitting parameters.

Adsorbent	D-A model fitting parameters			RMSD [%]
	Maximum uptake [$kgkg^{-1}$]	Characteristics energy [$kJkg^{-1}$]	Heterogeneity parameter [-]	
GP-CL-30-CP1	0.62	50.626	0.68	2.80
GP-CL-30-CP2	0.657	50.626	0.68	2.33
GP-CL-30-CP3	1.01	50.626	0.68	2.69
GP-CL-30-CP4	0.79	50.626	0.68	2.31
GP-CL-30-CP5	1.12	50.626	0.68	3.33
GP-CL-30-CP6	1.03	50.626	0.68	2.96
GP-CL-30-CP7	0.67	50.626	0.68	1.91
GP-CL-30-CP8	0.84	50.626	0.68	2.57
GP-CL-30-CP9	0.75	50.626	0.68	2.61

Table 6-6: GP-CH3SO3-30 D-A fitting model parameters

Adsorbent	D-A model fitting parameters			RMSD [%]
	Maximum uptake [$kgkg^{-1}$]	Characteristics energy [$kJkg^{-1}$]	Heterogeneity parameter [-]	
GP-CH_3SO_3-30-CP1	0.845	48.321	0.74	2.21
GP-CH_3SO_3-30-CP2	0.65	48.321	0.74	1.82
GP-CH_3SO_3-30-CP3	0.75	48.321	0.74	1.92
GP-CH_3SO_3-30-CP4	0.61	48.321	0.74	1.55
GP-CH_3SO_3-30-CP5	0.49	48.321	0.74	1.38
GP-CH_3SO_3-30-CP6	0.70	48.321	0.74	1.86
GP-CH_3SO_3-30 -CP7	0.73	48.321	0.74	1.85
GP-CH_3SO_3-30-CP8	0.66	48.321	0.74	2.17
GP-CH_3SO_3-30-CP9	1.48	48.321	0.74	3.95

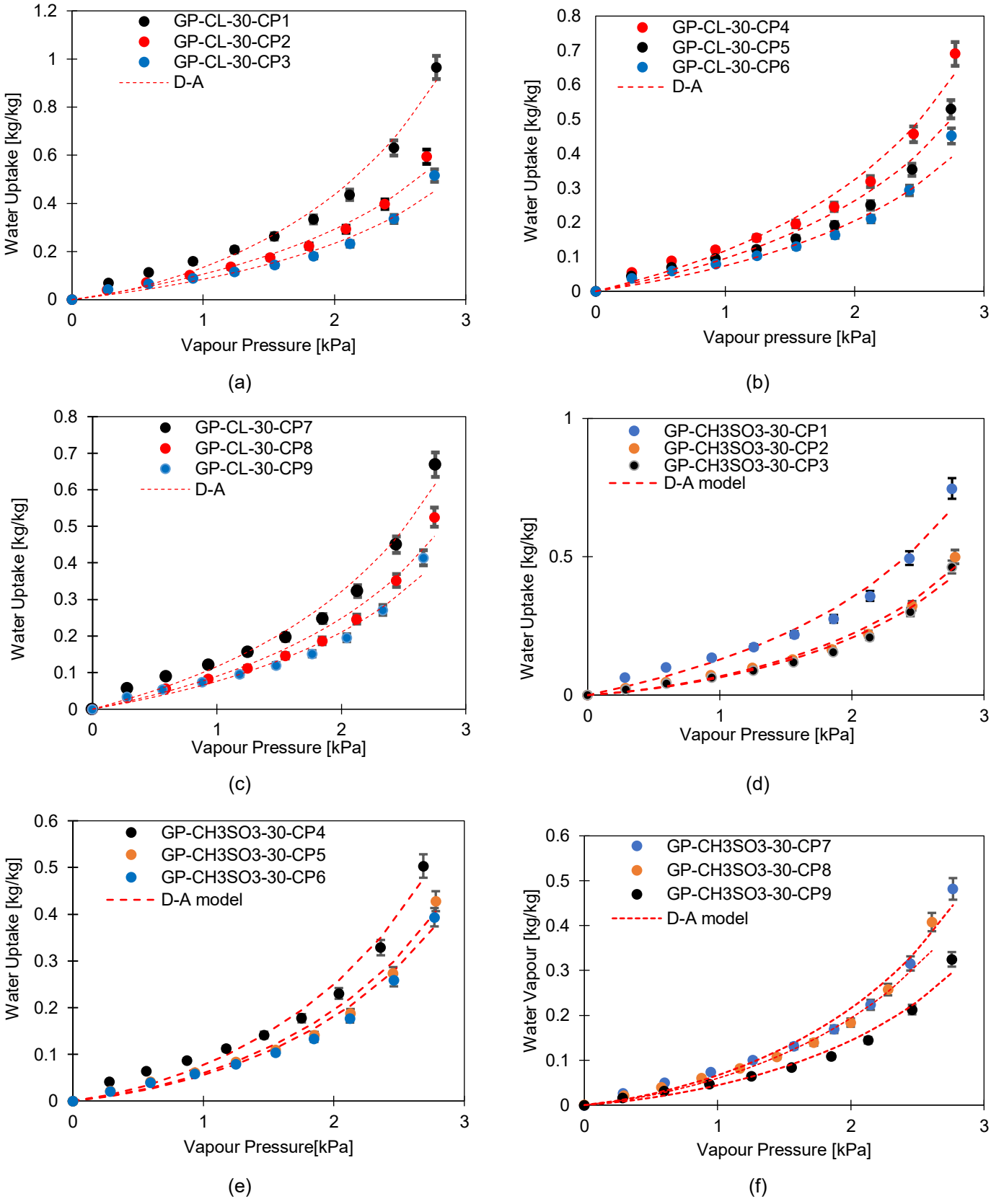

Figure 6.4 : Experimental Isotherm fitted with D-A model.

6.6 Isosteric heat of sorption

The calculated isosteric heat for the developed consolidated composite presented in Table 6-7

Table 6-7: GP-CL-30 and GP-CH3SO3-30 Heat of sorption.

Material	**Heat of sorption (J/mol)**	**Material**	**Heat of sorption (J/mol)**
GP-CL-30-CP1	26547	GP-CH_3SO_3-30-CP1	26424
GP-CL-30-CP2	26596	GP-CH_3SO_3-30-CP2	26641
GP-CL-30-CP3	26572	GP-CH_3SO_3-30-CP3	26720
GP-CL-30-CP4	26646	GP-CH_3SO_3-30-CP4	26398
GP-CL-30-CP5	26609	GP-CH_3SO_3-30-CP5	26640
GP-CL-30-CP6	26566	GP-CH_3SO_3-30-CP6	26631
GP-CL-30-CP7	26576	GP-CH_3SO_3-30-CP7	26587
GP-CL-30-CP8	26533	GP-CH_3SO_3-30-CP8	26767
GP-CL-30-CP9	26663	GP-CH_3SO_3-30-CP9	26635
Fuji silica gel	26078	Fuji silica gel [184]	26790

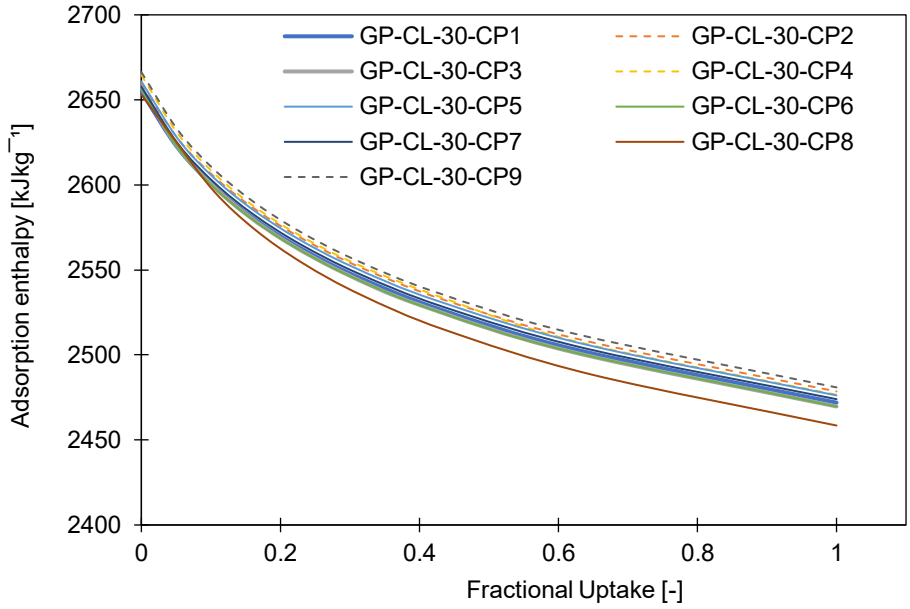

(a)

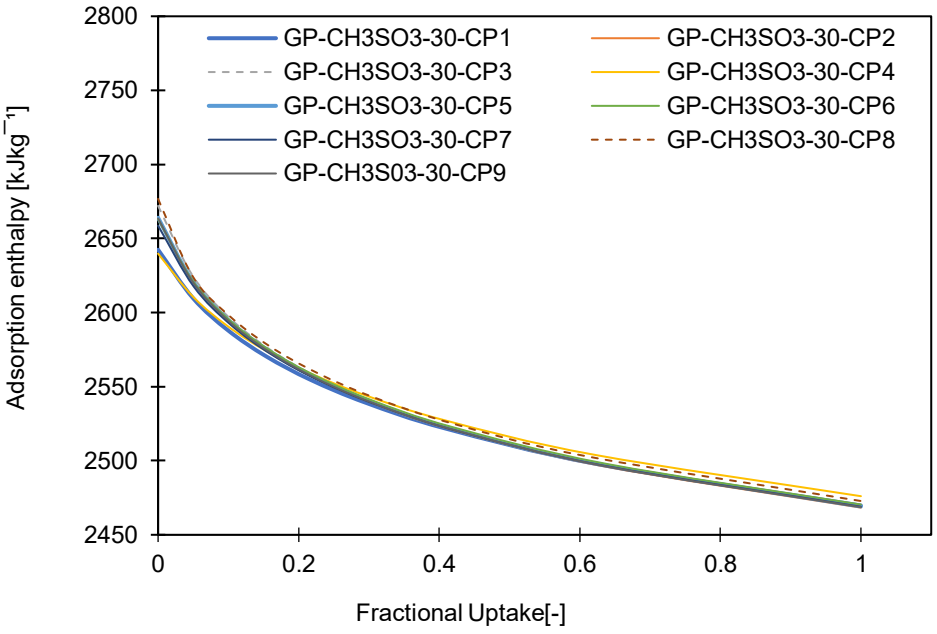

(b)

Figure 6.5 The isosteric heat for the developed consolidated isotherm (a) GP-CL-30-CP1-9 (b) GP-CH_3SO_3-30-CP1-9

The isosteric heat of adsorption for both GP-CL-30-CP1-9 and GP- CH_3SO_3-30-CP1-9 consolidated composites showed the same trend of decreasing as the uptake increases as shown in Figure 6.5.and b. The higher isosteric heat of sorption is realized at the initial stages where the adsorbate molecules are adsorbed on to higher energy sorption sites, giving out higher heat energy and hence higher adsorption enthalpy. However, as the water uptake increases the high energy sites got

saturated resulting in the water molecules being adsorbed on to those available sites possessing lower energy resulting in the gradual decrease in adsorption energy.

6.7 Consolidated composite cyclic performance.

The water uptake potential of the developed composites was determined by performing a cyclic analysis of the experimentally developed isotherms comparing them with baseline adsorbent silica gel as shown in Figure 6.6a and b. This analysis was based on the ambient temperature of 35°C and regeneration temperature of 85°C. The evaporator temperatures used in this analysis were 12°C and 30°C. corresponding to vapour pressure of 1.4kPa and.4.2kPa respectively [170]. At 12°C evaporator temperature the net cyclic water uptake is 0.169kg_w/kg_{ads} for SG, 0.157kg_w/kg_{ads} for GP-CL-30-CP1 and 0.132kg_w/kg_{ads} for GP-CH_3SO_3-30-CP1. At 4.2kPa corresponding to higher evaporator temperature of 30°C, the CH_3SO_3-30-CP1 isotherm intersect the SG isotherm and the net cyclic equilibrium uptake for GP-CL-30-CP1 and CH_3SO_3-30-CP1 is higher by 34% and 29% respectively, as shown in Figure 6.6b. This shows that at higher vapour pressures and higher evaporator temperatures more freshwater production is prioritised more than cooling.

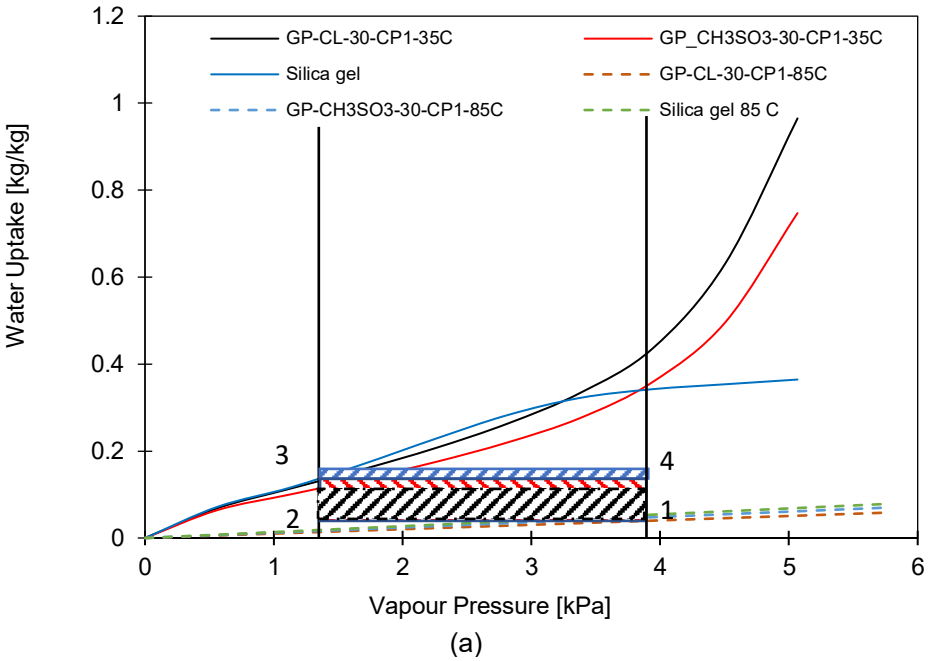

Figure 6.6: Comparison of the GP-CL-10-30, GP- CH_3SO_3-10-30 and SG at 35℃, condensation and 85℃, regeneration temperatures (a) 12 ℃ evaporation temperature and (b) 30℃ evaporation temperature

6.8 Component level Thermal performance

While the cyclic analysis established the water uptake potential of the consolidated composites, it did not show the effect of the thermal performance of all the materials on the adsorbent bed. That being so, the Multiphysics modelling of the adsorbent described in Chapter 3 was employed to further investigate the combined impact of the thermal and adsorption characteristics at component level. The simulation was performed for an 800 s cycle time inclusive of 30 s switching time. Although the

isotherm cyclic performance analysis showed that SG outperformed the composites at low evaporator temperatures and vapour pressure, the simulation indicated that the consolidated composites performed better than SG in terms of the thermal response and adsorption capacity. The dynamic temperature profiles in Figure 6.7 show changes taking place in the adsorbent bed at 12℃ and 30℃ evaporator temperatures. The outcome of the simulation shows excellent performance of all consolidated composites compared to SG over the entire cycle. At evaporator temperature of 12℃, the performance of the is 70% and 68% for the highest performing GP-CL-30-CP1 and CH_3SO_3-30-CP1 composites. This attributed to the superior thermal diffusivity of the composites which effectively improves the thermal response of the composites**.** Figure 6.8 shows that employing the evaporator temperature of 30℃ and HTF at 35℃, resulted in a significant improvement in the thermal and adsorption capacity of the composite with an uptake increase between 60-75%. The colourmaps contours for the dynamic temperature profiles and dynamic water uptake in Figure 6.7 and Figure 6.8 respectively, represent the average sorbent temperature and uptake for a full cycle which include the adsorption/desorption process. The parameters and conditions used for the modelling are shown in Table 6-8.

Table 6-8:simulation parameters and conditions

Parameter	Value	Unit
$M_{GP/IL}$	0.2	kg
M_{SG}	0.22	kg
M_{hex}	2.02	kg
Ads/des bed flow rate	0.036	kg/s
Cond flow rate	0.018	kg/s
Evap flow rate	0.048	kg/s
T_{des}	65-85	℃
T_{ads}	35	℃
T_{chw}	35	℃
T_{evap}	12 -30	℃
T_{cw}	35	℃
T_{cond}	35	℃
Cycle time	800	s

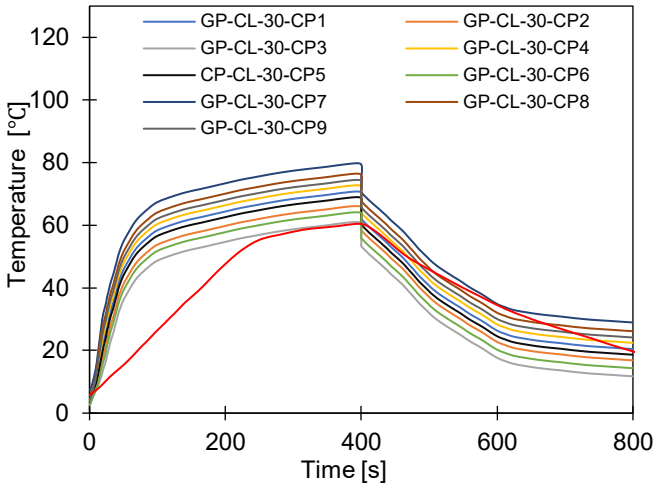

Te =12°C

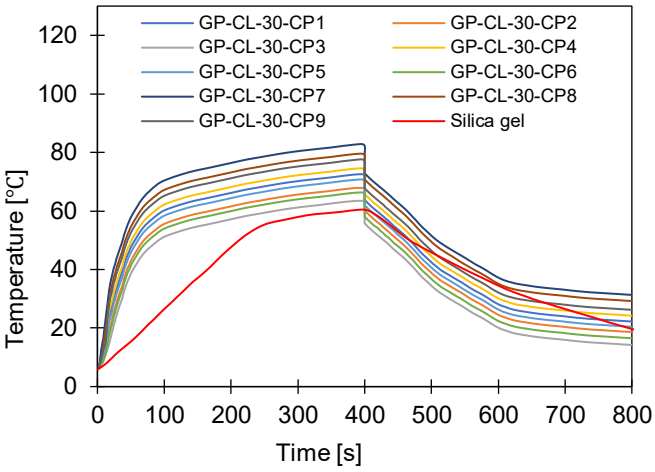

Te =30°C

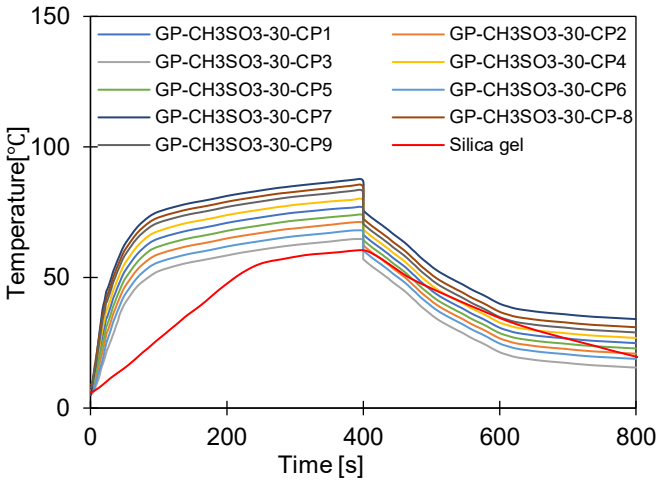

Te =12°C

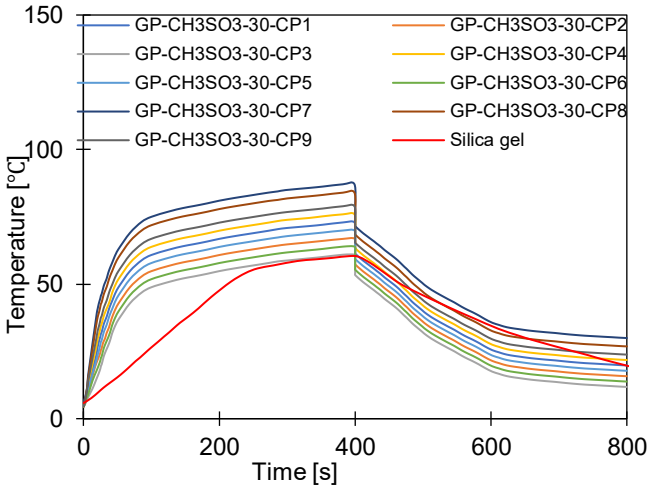

Te =30°C

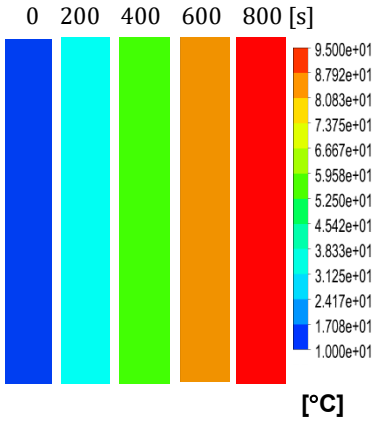

GP-CL-30-CP1 & T_e=12°C

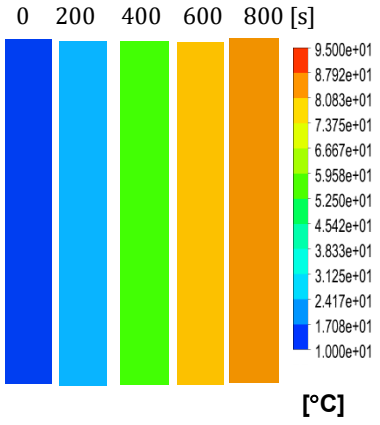

GP-CL-30-CP2 & T_e=12°C

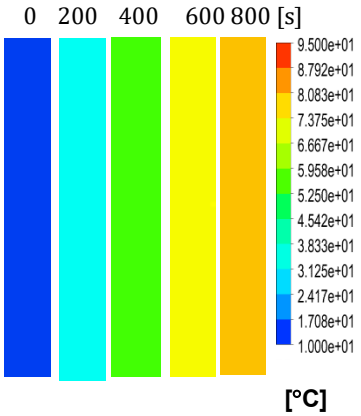

GP-CL-30-CP3 & T_e=12°C

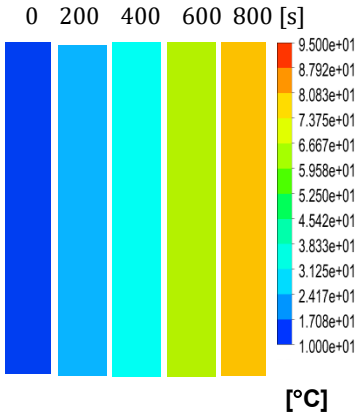

GP-CL-30-CP4 & T_e=12°C

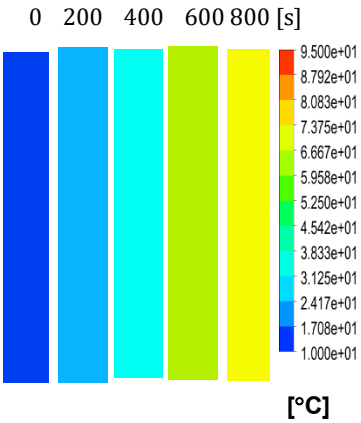

GP-CL-30-CP5 & T_e=12°C

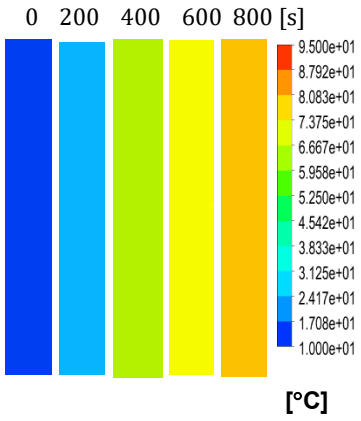

GP-CL-30-CP6 & T_e=12°C

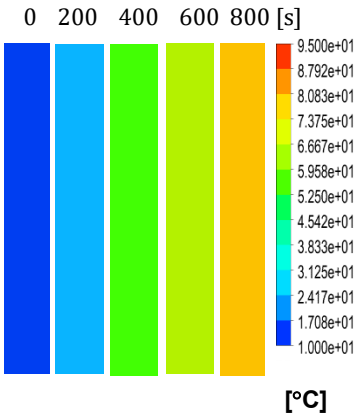

GP-CL-30-CP7 & T_e=12°C

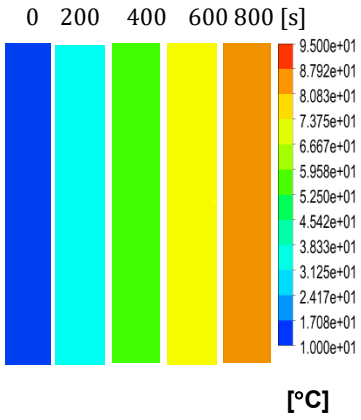

GP-CL-30-CP8 & T_e=12°C

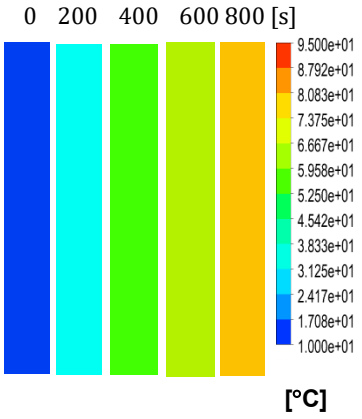

GP-CL-30-CP9 & T_e=12°C

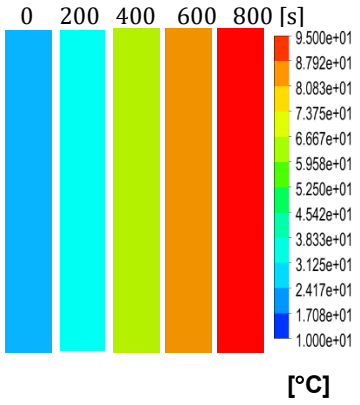

GP-CH_3SO_3-30-CP1 & T_e=12°C

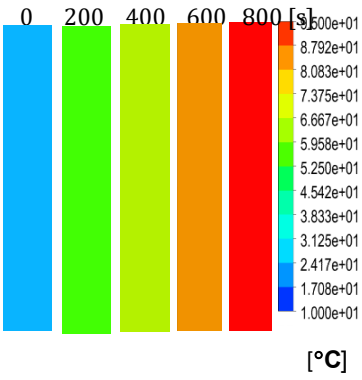

GP-CH_3SO_3-30-CP2 & T_e=12°C

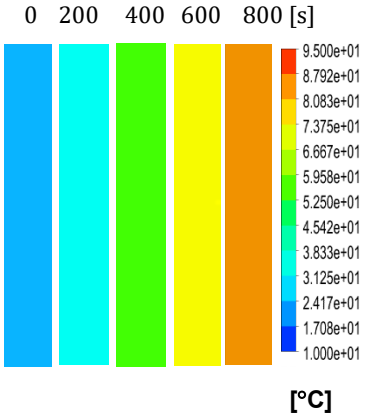

GP-CH_3SO_3-30-CP3 & T_e=12°C

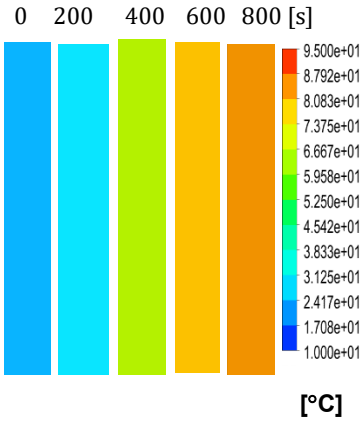

GP-CH_3SO_3-30-CP4 & T_e=12°C

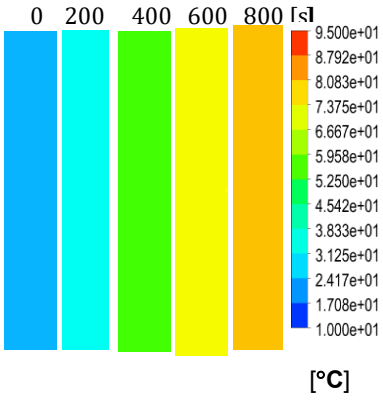

GP-CH_3SO_3-30-CP5 & T_e=12°C

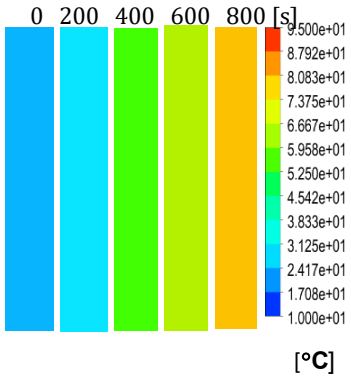

GP-CH_3SO_3-30-CP6 & T_e=12°C

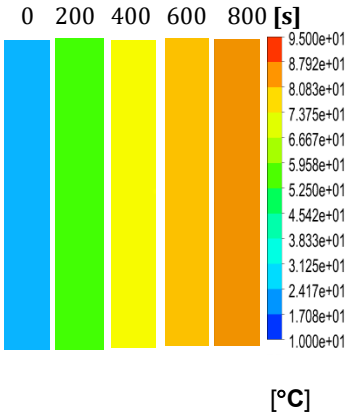

GP-CH_3SO_3-30-CP7 & T_e=12°C

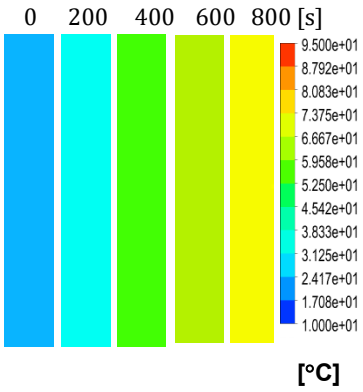

GP-CH_3SO_3-30-CP8 & T_e=12°C

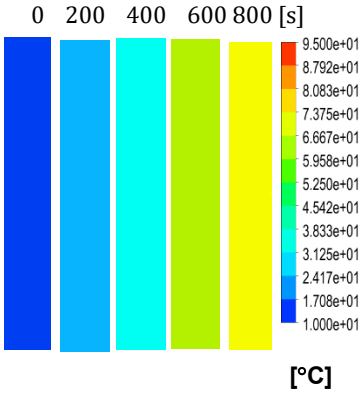

GP-CH_3SO_3-30-CP9 & T_e=12°C

Figure 6.7: Dynamic temperature profiles for GP-CL-30-CP1-9 and GP-CH_3SO_3-30-CP1-9

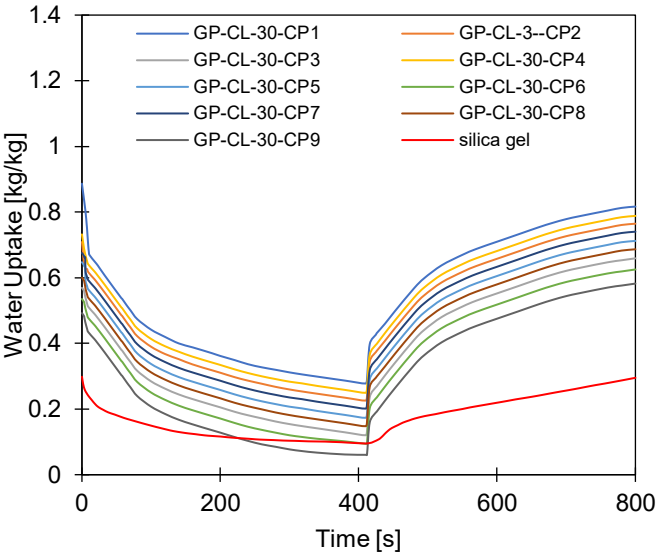

(a)

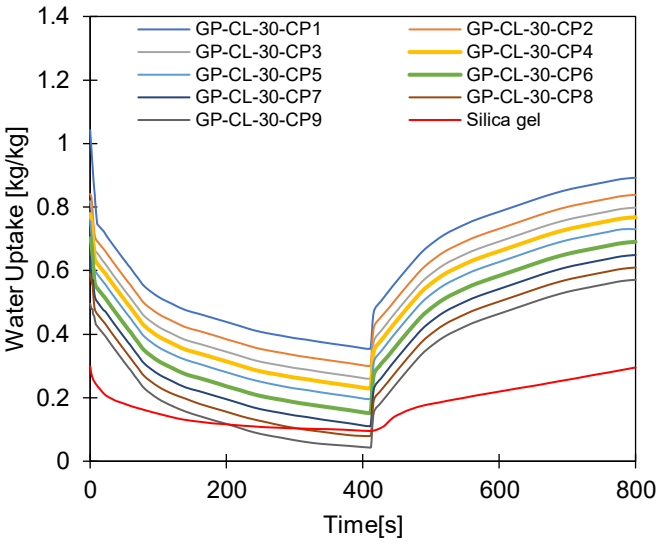

(b)

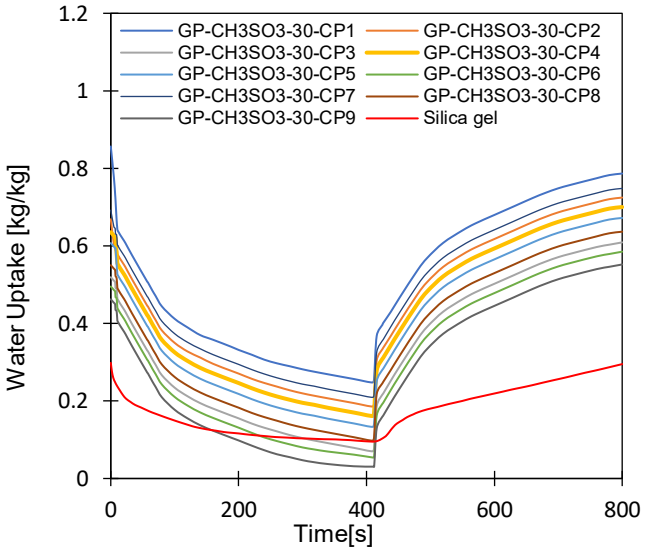

(c)

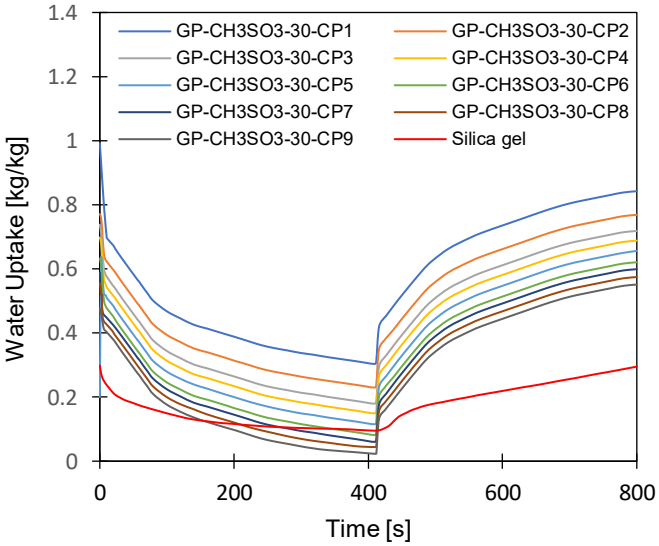

(d)

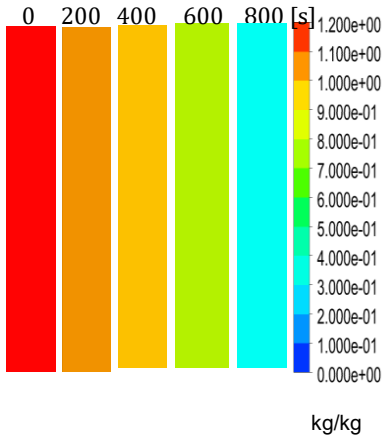

GP-CL-30-CP1 & T_e=12°C

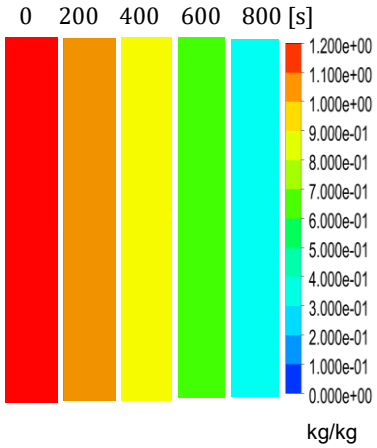

GP-CL-30-CP2 & T_e=12°C

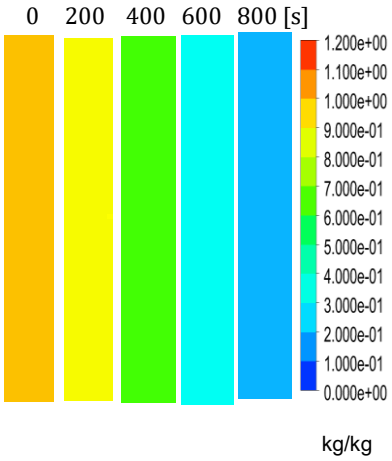

GP-CL-30-CP3 & T_e=12°C

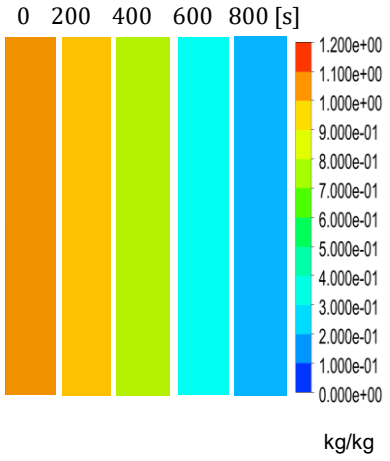

GP-CL-30-CP4 & T_e=12°C

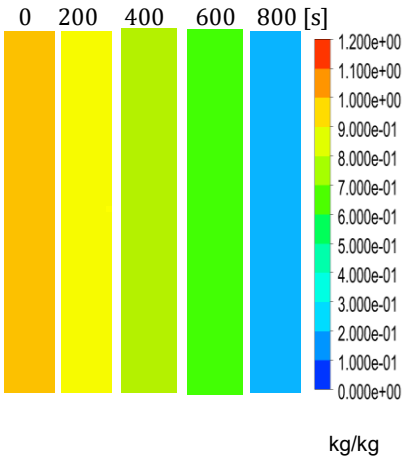

GP-CL-30-CP5 & T_e=12°C

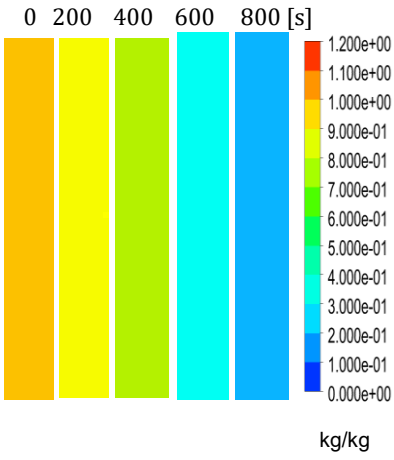

GP-CL-30-CP6 & T_e=12°C

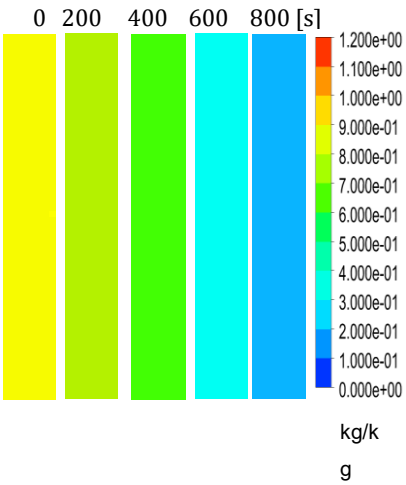

GP-CL-30-CP7 & T_e=12°C

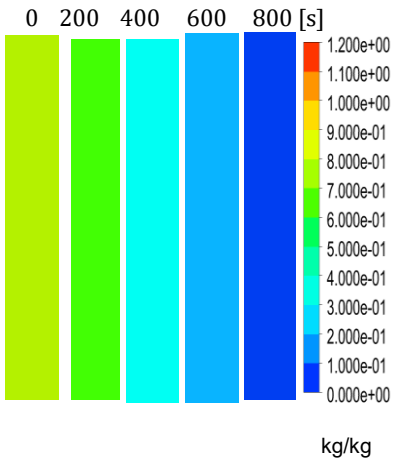

GP-CL-30-CP8 & T_e=12°C

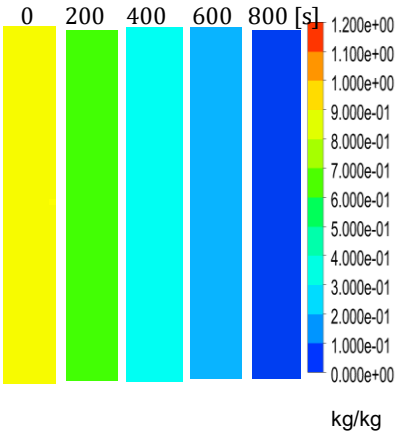

GP-CL-30-CP9 & T_e=12°C

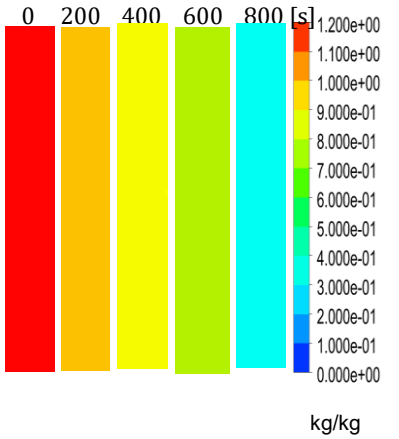

GP-CH_3SO_3-30-CP1 & T_e=12°C

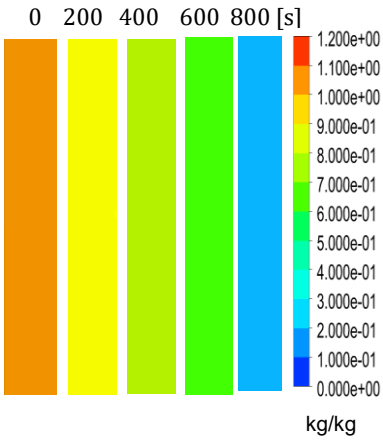

GP-CH_3SO_3-30-CP2 & T_e=12°C

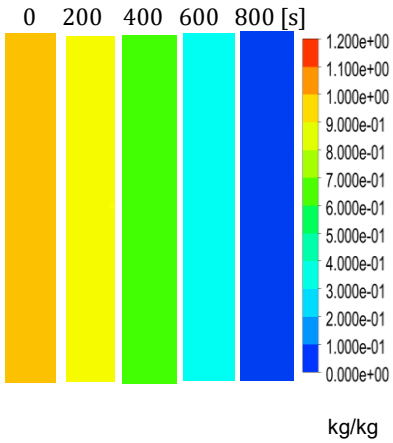

GP-CH_3SO_3-30-CP3 & T_e=12°C

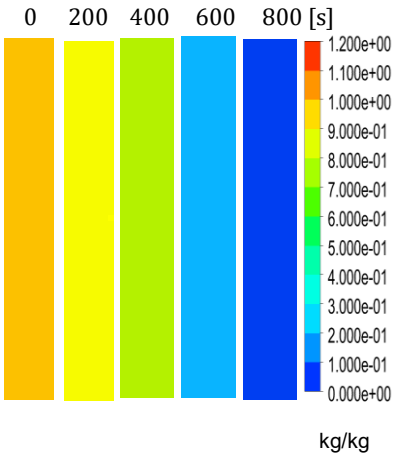

GP-CH_3SO_3-30-CP4 & T_e=12°C

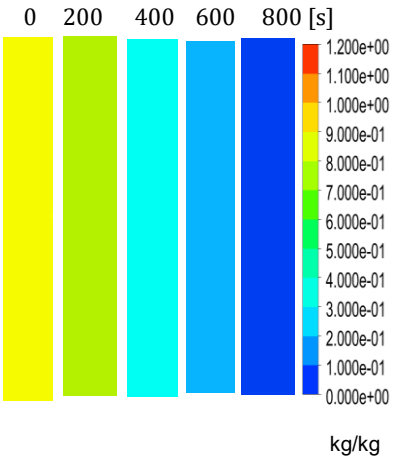

GP-CH_3SO_3-30-CP5 & T_e=12°C

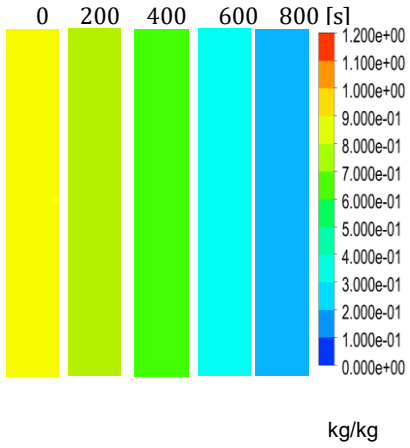

GP-CH_3SO_3-30-CP6 & T_e=12°C

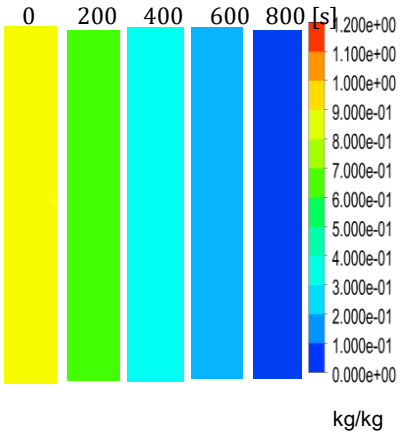

GP-CH_3SO_3-30-CP7 & T_e=12°C

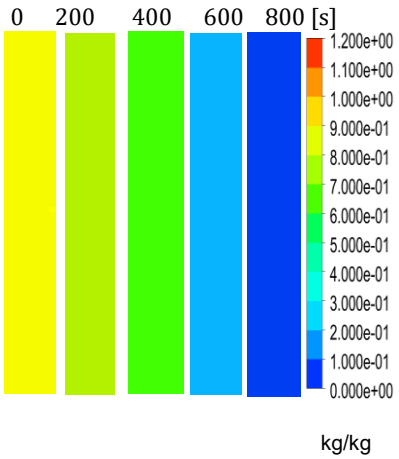

GP-CH_3SO_3-30-CP8 & T_e=12°C

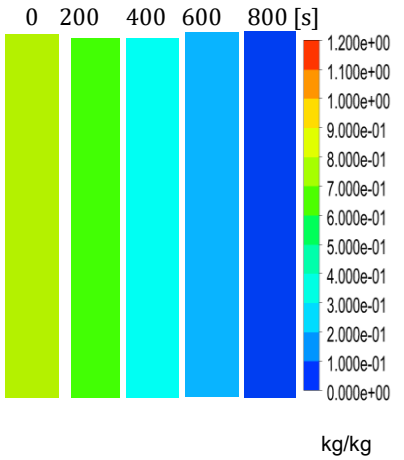

GP-CH_3SO_3-30-CP9 & T_e=12°C

Figure 6.8: - Dynamic uptake profiles for GP-CL-30-CP1-9 and GP-CH_3SO_3-30-CP1-9

6.8.1 Exergy destruction

The adsorption cooling and desalination system was analysed for its energy conversion ability while utilising the GP-CL-30 and GP-CH_3SO_3-30, composites as the adsorbents in comparison to silica gel. The Exergy destruction of each component was determined, and the exergy efficiency of the system was obtained based on the performance of the adsorbent and their impact on the component heat and mass transfer capability using the exergy equations laid down in methodology Chapter 3. The exergy destruction of each component is given in Table 6-9 and

Table 6-10. The obtained exergy destruction showed that the desorption process utilises most of the energy in adsorption system, and the adsorbent bed has the highest exergy destruction as it is at centre of the adsorption/desorption process. Of the two processes in the adsorbent bed, desorption process has the highest exergy destruction due to the high regenerative temperatures involved during the process. At material level the GP-CL-30 and GP-CH_3SO_3-30, have higher exergy destruction compared to SG owing their high thermal properties which allows more heat transfer to take place during the adsorption/desorption processes to facilitate more water uptake and cooling. While the SG exergy destruction is low compared to the developed composite its poor heat transfer properties resulting in less water uptake and cooling being produces explains the low exergy efficiency of 16.6% compared to 42.2% of the highest performing composite GP-CL-30-CP1 as less energy is used for useful work in water and cooling production. These findings are in agreement with Cao et al [164] utilising the SG/water adsorption pair.

Table 6-9: Exergy destruction of GP-CH3SO3-30 and Silica gel

Component/Process	CH3SO3-30									Silica gel
	CP1	CP2	CP3	CP4	CP5	CP6	CP7	CP8	CP9	
	Exergy destruction (kW)									
Adsorption at 35 °C	6.05	6.88	6.55	6.21	6.70	6.87	7.4	7.26	7.19	7.17
Desorption at 85 °C	8.58	8.20	8.82	8.76	8.38	8.01	9.35	9.14	8.95	9.5
Condenser at 35 °C	1.12	1.2	1.22	1.21	1.22	1.3	1.3	1.0	1.1	1.2
Evaporator at 30 °C	1.31	1.05	1.00	1.16	1.08	1.01	1.28	1.24	1.2	1.3
System overall	17.1	17.3	18.7	17.6	17.4	17.5	19.3	18.6	18.44	19.17
	Exergy efficiency (%)									
	40.9	37.2	30.8	38.8	34.3	29.7	35.8	32.8	28.6	16.6

Table 6-10 Exergy destruction of GP-CL-3-0 composites and Silica gel

Component/Process	GP-CL-30									Silica gel
	CP1	CP2	CP3	CP4	CP5	CP6	CP7	CP8	CP9	
	Exergy destruction (kW)									
Adsorption at 35 °C	6.37	6.69	6.04	6.87	6.48	6.20	7.41	7.24	7.01	7.17
Desorption at 85 °C	8.29	8.94	8.53	8.60	8.50	8.71	9.10	8.91	8.72	9.5
Condenser at 35 °C	1.11	1.08	1.01	1.12	1.09	1.04	1.22	1.17	1.15	1.2
Evaporator at 30 °C	1.27	1.2	1.1	1.31	1.22	1.16	1.43	1.39	1.35	1.3
System overall	17.0	17.9	16.7	17.9	17.3	19.2	17.4	18.7	18.23	19.17
	Exergy efficiency (%)									
	42.2	39.0	32	40.4	36	29.9	37.5	34.5	28.7	16.6

High exergy destruction was experienced in the adsorbent bed due to large temperature difference with the bed that occurs between the adsorbent and heat transfer fluid as the adsorption/desorption processes begin. The temperature differences are attributed to irreversibility due to heat transfer processes resulting in high exergy destruction throughout the whole cycle. On the other hand, the exergy destruction during desorption is higher than adsorption due to the high heat supplied which is the required energy input for desorption.

At material level, it can be observed that all the GP/IL composites-based systems had high exergy destruction compared to the SG based system. This is attributed to the thermal properties of the composites mainly the high thermal diffusivity which increases the rate of heat transfer within the adsorbent bed (component level). While the same temperature of heating water inlet temperature was employed, the low thermal diffusivity of SG reduced the exergy destruction at the expense of heat and mass transfer and therefore low clean water production and cooling. The overall energy conversion process at system level was reflected by the exergy efficiency. The determined exergy

efficiency showed that all the GP/IL composite based systems had higher exergy efficiency with the highest being GP-CL-30-CP1 with 33.9% compared to 16.6% of SG. The high exergy efficiency indicated a more efficient energy conversion by the GP/IL based systems which effectively produced more clean water and cooling. This also reflects the impact of the superior thermal properties of the consolidated composites.

6.8.2 The effect of cycle time

The performance of adsorption system is dependent on the duration of a complete adsorption/desorption cycle (cycle time). A computational modelling investigation of the effect of cycle time on the adsorbent bed performance was carried out for two cycle times 400s and 800s with a switching time of 30s operating at12℃ and 30℃ evaporator temperatures as shown in Figure 6.9, Figure 6.10, Figure 6.11 and Figure 6.12. The cooling temperature inlet water temperature was 35°C while the heating temperature was 85°C.

The observed results showed that the net cyclic water uptake for the 400s cycle operating at 30°C evaporator temperature was higher for all the GP/IL composites compared to that of SG. GP-CL-30-CP1 composite based system had the highest net cyclic uptake of 0.95kg_w/kg_{ads} while that of SG based system was 0.2 kg_w/kg_{ads}. The same trend was observed for the 800s cycle where the GP-CL-30-CP1based system had the highest net cyclic uptake of 0.74kg_w/kg_{ads} compared to 0.24kg_w/kg_{ads} for SG based system. The results show that the cyclic uptake is influenced by the adsorbent's thermal. In this case, the GP-CL-30-CP1 has a faster thermal response than SG response leading to a quick temperature change within the adsorbent bed of the GP-CL-30-CP1 based system hence capture of more adsorbate.

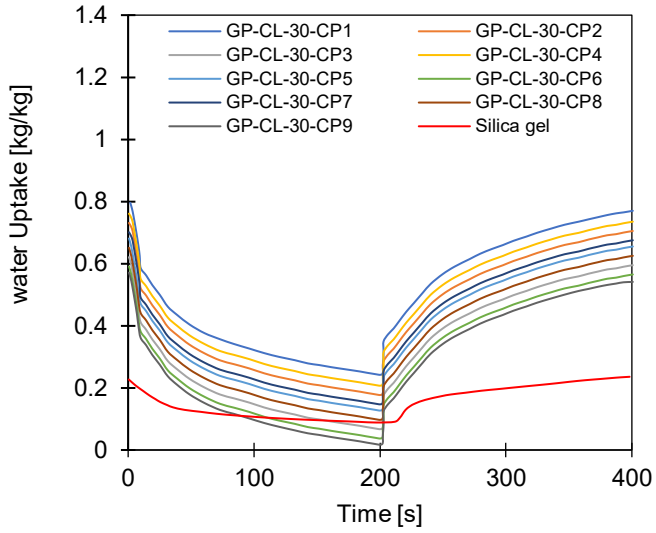
GP-CL-30-CP1
GP-CL-30-CP2
GP-CL-30-CP3
GP-CL-30-CP4
GP-CL-30-CP5
GP-CL-30-CP6
GP-CL-30-CP7
GP-CL-30-CP8
GP-CL-30-CP9
Silica gel
water Uptake [kg/kg]
Time [s]

(a)

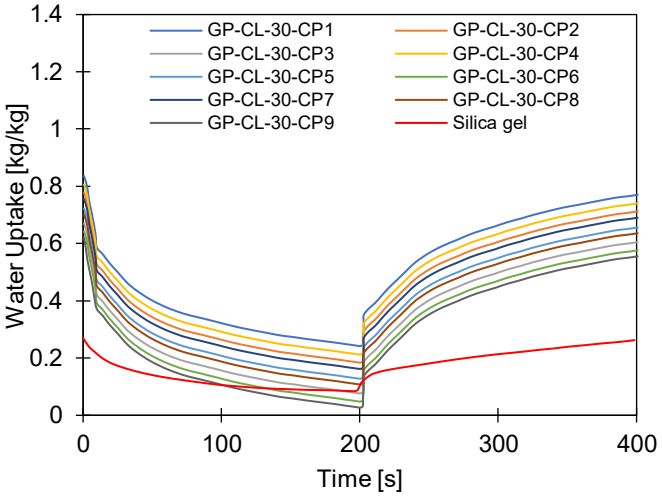
GP-CL-30-CP1
GP-CL-30-CP2
GP-CL-30-CP3
GP-CL-30-CP4
GP-CL-30-CP5
GP-CL-30-CP6
GP-CL-30-CP7
GP-CL-30-CP8
GP-CL-30-CP9
Silica gel
Water Uptake [kg/kg]
Time [s]

(b)

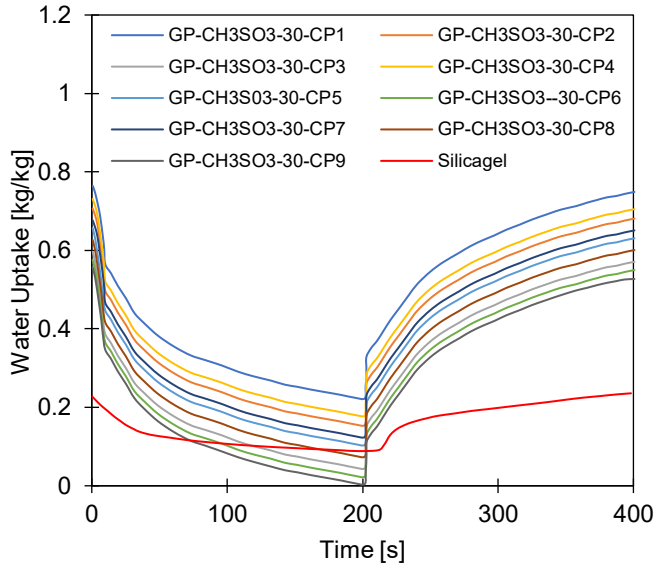
GP-CH3SO3-30-CP1
GP-CH3SO3-30-CP2
GP-CH3SO3-30-CP3
GP-CH3SO3-30-CP4
GP-CH3S03-30-CP5
GP-CH3SO3--30-CP6
GP-CH3SO3-30-CP7
GP-CH3SO3-30-CP8
GP-CH3SO3-30-CP9
Silicagel
Water Uptake [kg/kg]
Time [s]

(c)

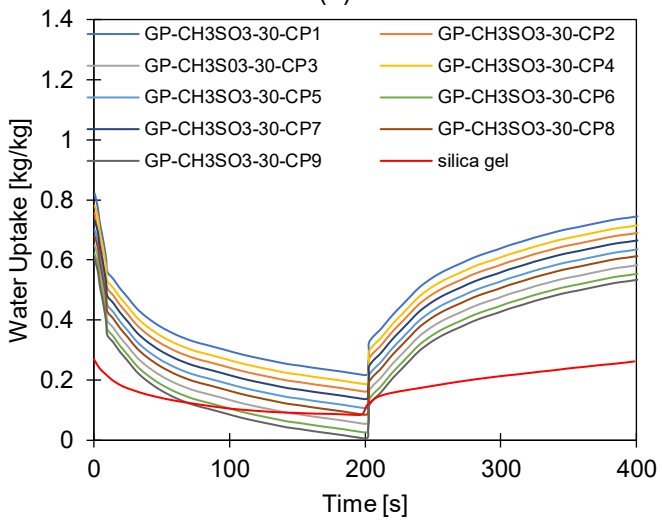
GP-CH3SO3-30-CP1
GP-CH3SO3-30-CP2
GP-CH3S03-30-CP3
GP-CH3SO3-30-CP4
GP-CH3SO3-30-CP5
GP-CH3SO3-30-CP6
GP-CH3SO3-30-CP7
GP-CH3SO3-30-CP8
GP-CH3SO3-30-CP9
silica gel
Water Uptake [kg/kg]
Time [s]

(d)

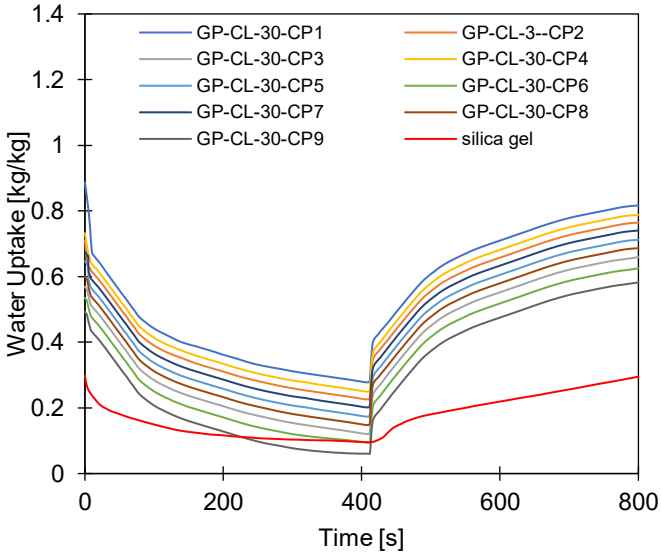
GP-CL-30-CP1
GP-CL-3--CP2
GP-CL-30-CP3
GP-CL-30-CP4
GP-CL-30-CP5
GP-CL-30-CP6
GP-CL-30-CP7
GP-CL-30-CP8
GP-CL-30-CP9
silica gel
Water Uptake [kg/kg]
Time [s]

(e)

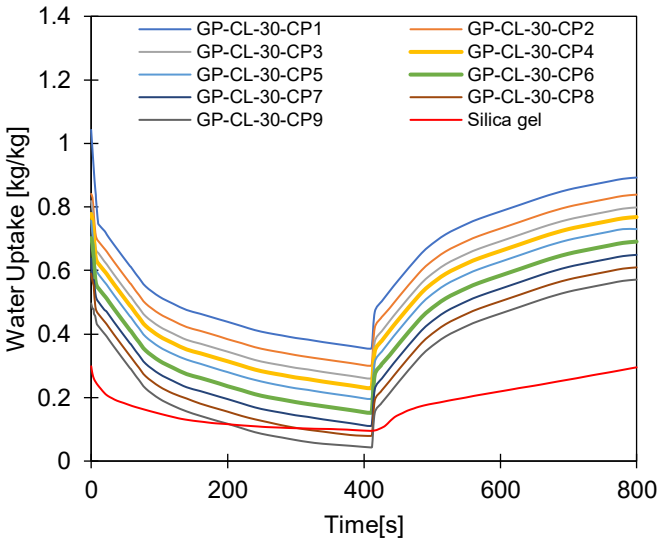
GP-CL-30-CP1
GP-CL-30-CP2
GP-CL-30-CP3
GP-CL-30-CP4
GP-CL-30-CP5
GP-CL-30-CP6
GP-CL-30-CP7
GP-CL-30-CP8
GP-CL-30-CP9
Silica gel
Water Uptake [kg/kg]
Time[s]

(f)

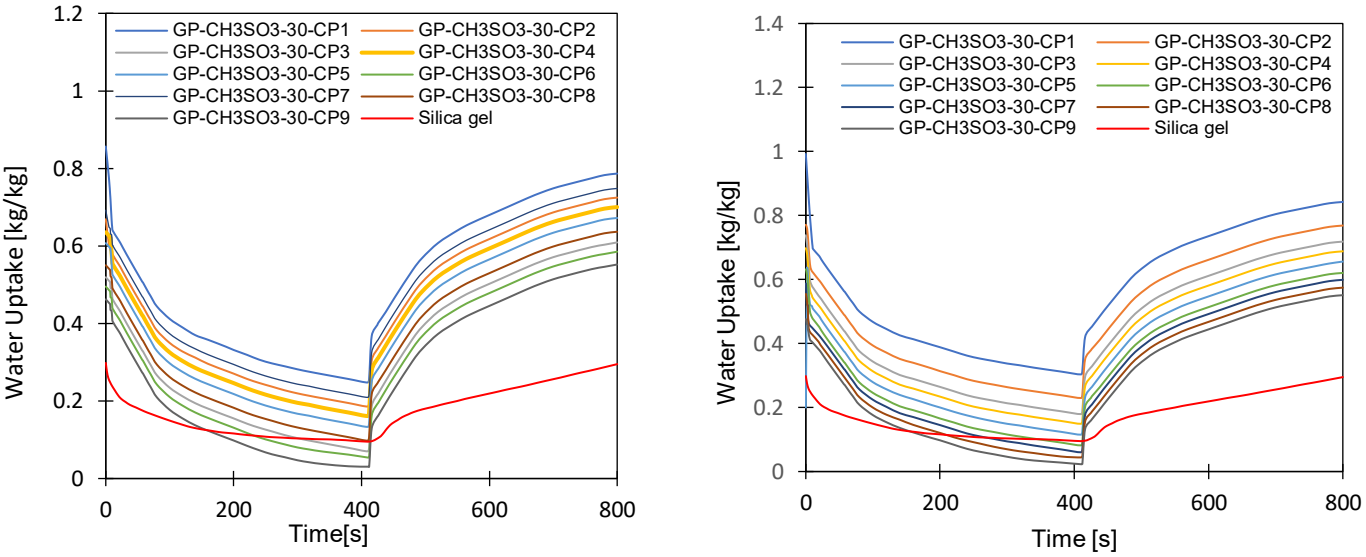

Figure 6.9: Dynamic water uptake profiles for GP-CL-30 CP1 to CP9 and-CH_3SO_3-30 CP1 toCP9at (a) T_{ev}=12°C temperature t_{cycle}=400s; (b) T_{ev}=30°C temperature t_{cycle}=400s; (c) T_{ev}=12°C temperature t_{cycle}=400s (d) T_{ev}=30°C temperature t_{cycle}=400s; (e) T_{ev}=12°C temperature t_{cycle}=800s, (f) T_{ev}=30°C temperature t_{cycle}=800s; (g)T_{ev}=12°C temperature t_{cycle}=800s (h) T_{ev}=30°C temperature t_{cycle}=800s

It can be observed that the net cyclic temperature rises for 400s cycle time at 30°C evaporator temperature was high in the GP/IL based systems. The highest net cyclic temperature was 65°C for GP-CL-30-CP1 based system compared to 51°C for SG. The same trend was observed on the 800s cycle where the GP-CL-30 -CP1 based system had a net cyclic temperature rise of 75°C compared to 58°C for SG. The dynamic temperature profile of the GP/IL based system show a steep temperature rise during the 100s for both the 400s and 800s indicating their ability to stabilise and reach the desired temperature faster hence better control of the systems operating conditions and improved cyclic performance, while the temperature rises of dynamic profile of the SG was less steep and gradual.

The same trend was observe operating at 12°C evaporation temperature, where the net cyclic water uptake for GP-CL-30-CP1 based system, the highest performing composite was 0.42kg_w/kg_{ads} and 0.10kg_w/kg_{ads} for SG based system. The similar trend was observed on the 800s cycle time systems where the net cyclic uptake was high in all the GP/IL composite systems with the GP-CL-30-CP1 based system registering 0.4942kg_w/kg_{ads} while that of SG based system was 0.12 kg_w/kg_{ads}. On the other hand, the net cyclic temperature rise was 76°C and 62°C for GP-CL-30-CP1 based system and SG based system respectively, operating at 400s cycle time and 12°C evaporating temperature. The trend of the dynamic temperature profile for both the 400s and 800s had a steep rise for the first 100s indicating a rapid temperature rise at the initial stage due to increase in heat released in the adsorbent bed followed by a period of little change (plateau) in all the composites including the GP-

CL-30-CP1 based system. The plateau on the dynamic temperature profile for composite based system can be attributed to the balance between the heat dissipated and heat generated resulting in a relatively stable profile. The SG based system exhibited gradual cyclic temperature rise. A steep temperature drop for the first few seconds at the early stages of adsorption for GP/IL composites was observed and it was attributed quick heat transfer within the adsorbent bed causing a rapid temperature to drop. The net cyclic uptake and net cyclic temperature rise was higher in the 800s cycle time than the 400s cycle time at both the 12°C and 30°C evaporator temperatures. This showed that the 800s cycle time was the optimal cycle time to allow for thorough adsorption to take place. The findings on the effect of cycle time agrees with Li et al [172].

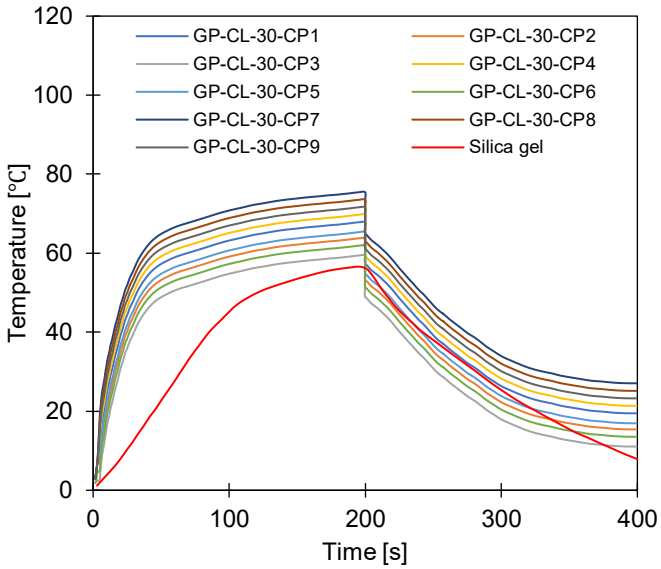

(a)

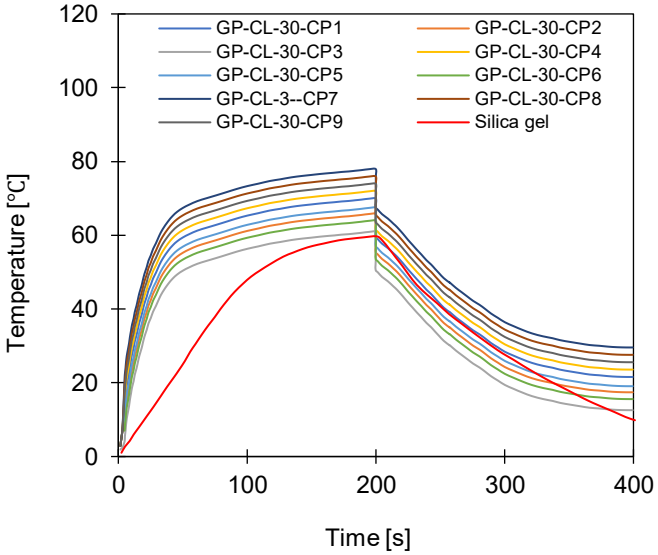

(b)

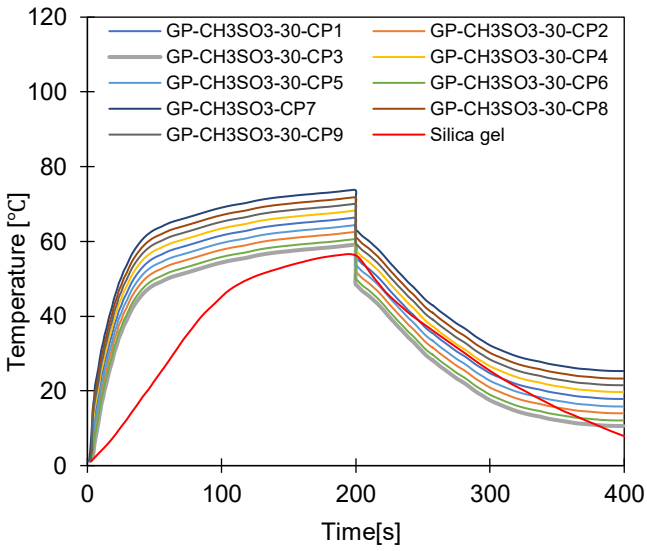

(c)

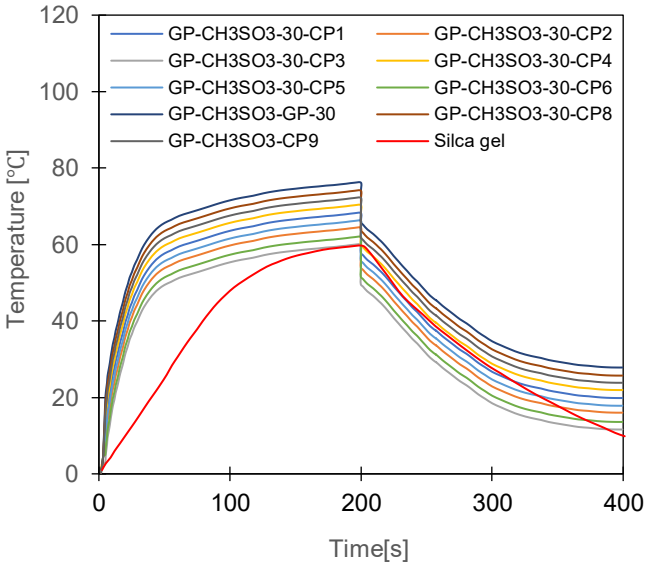

(d)

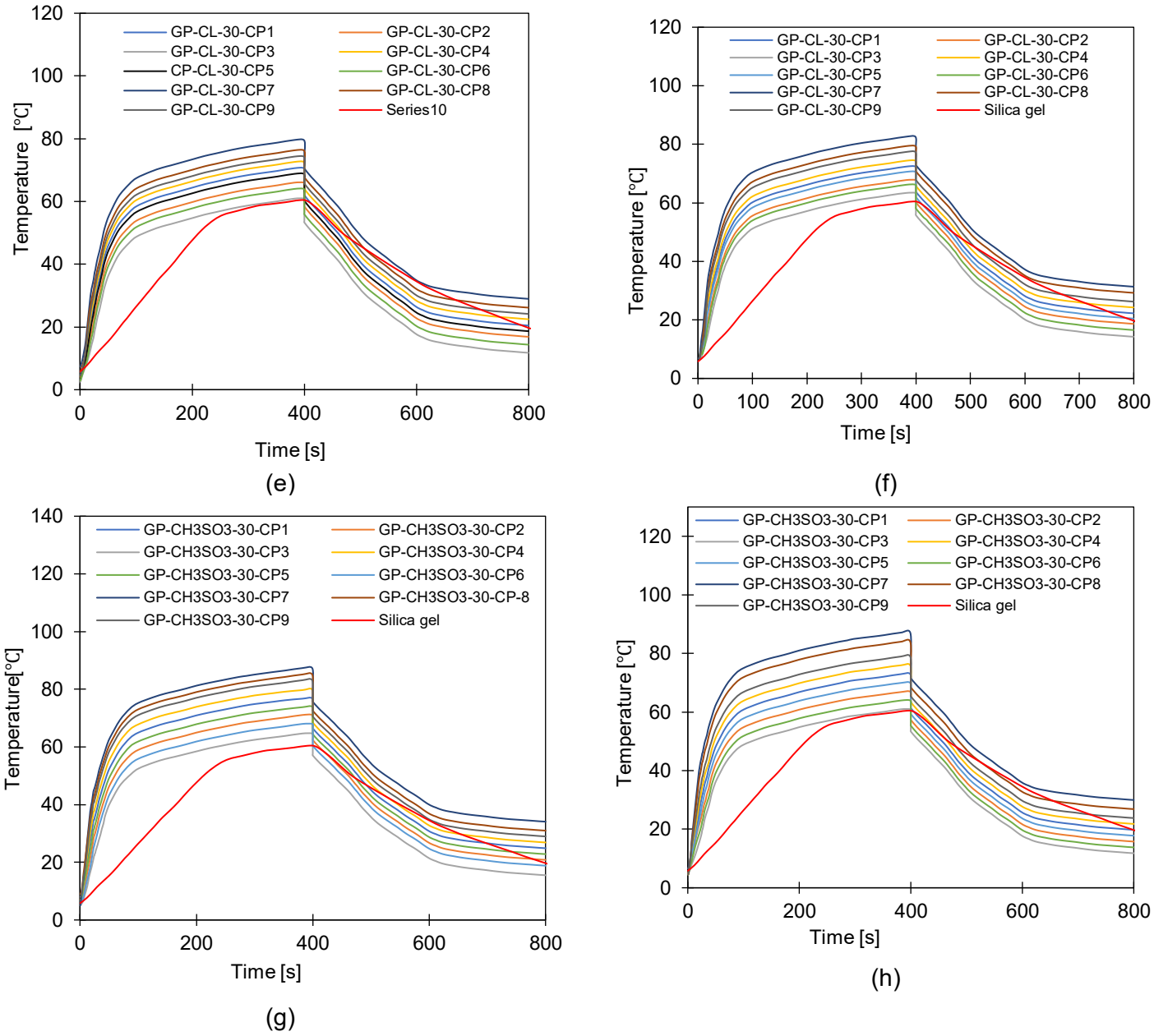

Figure 6.10: Dynamic temperature profiles for GP-CL-30 CP1-9 at (a) T_{ev}=12°C temperature t_{cycle}=400s; (b) T_{ev}=30°C temperature t_{cycle}=400s; (c) T_{ev}=12°C temperature t_{cycle}=400s; (d) T_{ev}=30°C temperature t_{cycle}=400s. (e) T_{ev}=12°C temperature t_{cycle}=800s; (d) T_{ev}=30°C temperature t_{cycle}=800s. (g) T_{ev}=12°C temperature t_{cycle}=800s; (d) T_{ev}=30°C temperature t_{cycle}=800s.

Further investigation was performed on the influence of varying the cycle time on the system performance as shown in Figures 6.11- 6.14. The observed results showed that an increase in cycle time, increased the SDWP, SCP, COP and the exergy efficiency in all the GP/IL composites-based systems and SG based system. This increase in the system performance can be attributed to giving enough time for adsorption/desorption to take place hence increasing the overall clean water production. A longer cycle time also allows complete adsorption and release of more heat resulting in a high specific cooling power. if there is no further increase in energy input the specific cooling power increases thus increasing the COP of the system. Increasing the cycle time allows more time

for effective energy conversion and utilisation hence enhance the exergy efficiency. The GP/IL composites-based system operating at 12°C outperformed SG based system. The highest performing composite GP-CL-30-CP1 showed higher SDWP, SCP, COP and exergy efficiency than SG based system by 53%, 29%,18% and 21,5%. Operating at 30°C evaporation temperature, an increase in SDWP, SCP, COP, and exergy efficiency for the GP-CL-30-CP1 based system were 57%, 32%, 20% and 24 % respectively compared to SG based system.

The improved overall system performance was attributed to the impact of the high thermal and adsorption properties of the GP/IL composites which was reflected in the rapid thermal response of the highest performing composite GP-CL-30-CP1 to give the highest overall cyclic water uptake and cooling. Furthermore, GP-CL-30-CP1 based system showed a higher exergy efficiency compared to SG based systems. The higher exergy efficiency of the GP-CL-30-CP1 based system indicated improved heat transfer capability of the adsorbent leading to more utilisation of the energy hence increased cooling and water production. In addition, high adsorption capacity and fast adsorption rate contributed to the efficient achievement of adsorption equilibrium and allows the storage of more energy in the adsorption phase thus enhance the exergy efficiency of the system.

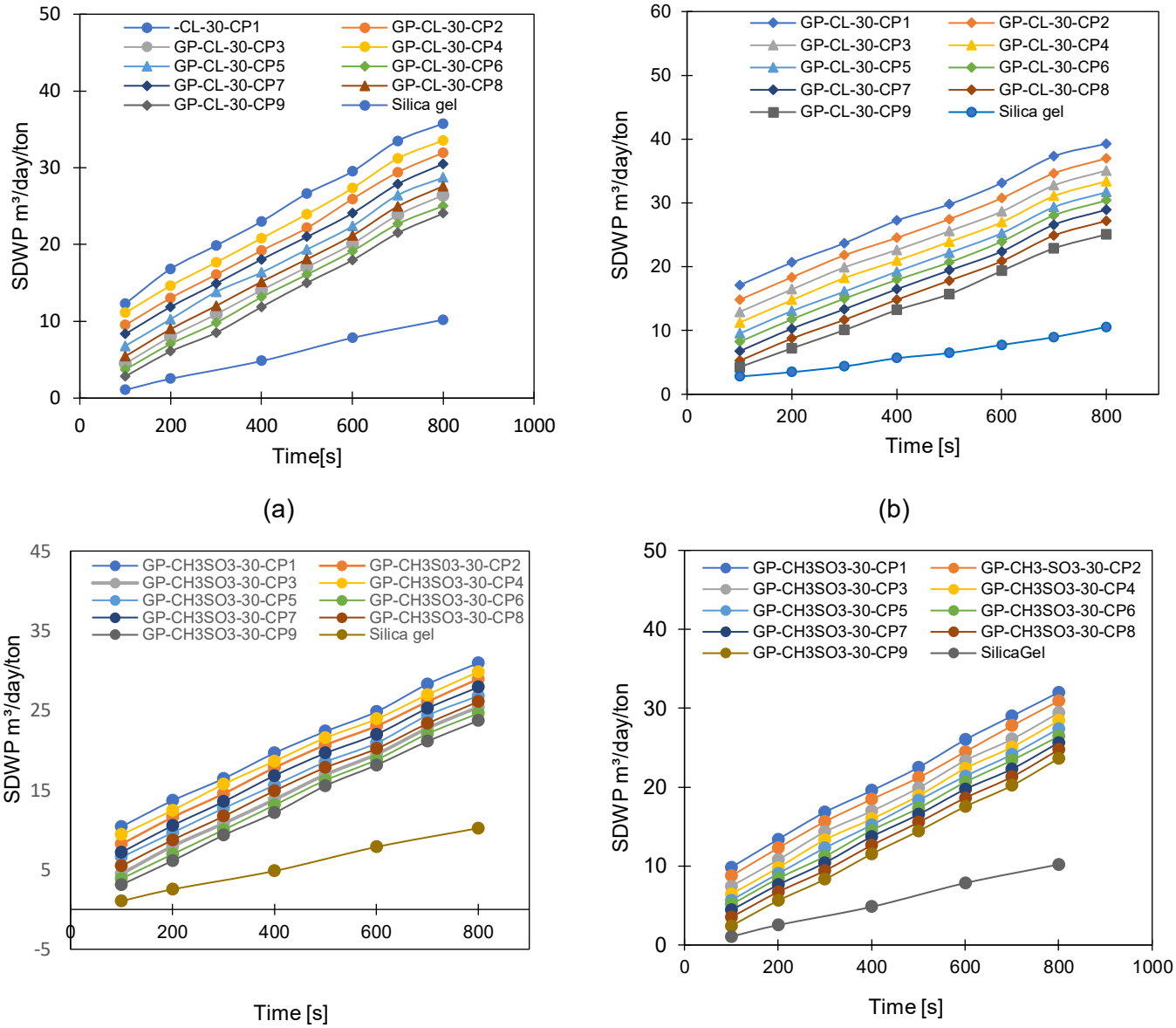

Figure 6.11: The effect of changing cycle time on SDWP for GP-Cl-30 – CP1 -9 and SG, at (a) T_{ev}=12 ℃ and (b) T_{ev}=30 ℃ and for GP-CH_3SO_3-30-CP1-9 and SG at (c) T_{ev}=12 ℃ and (d) T_{ev}=30 ℃

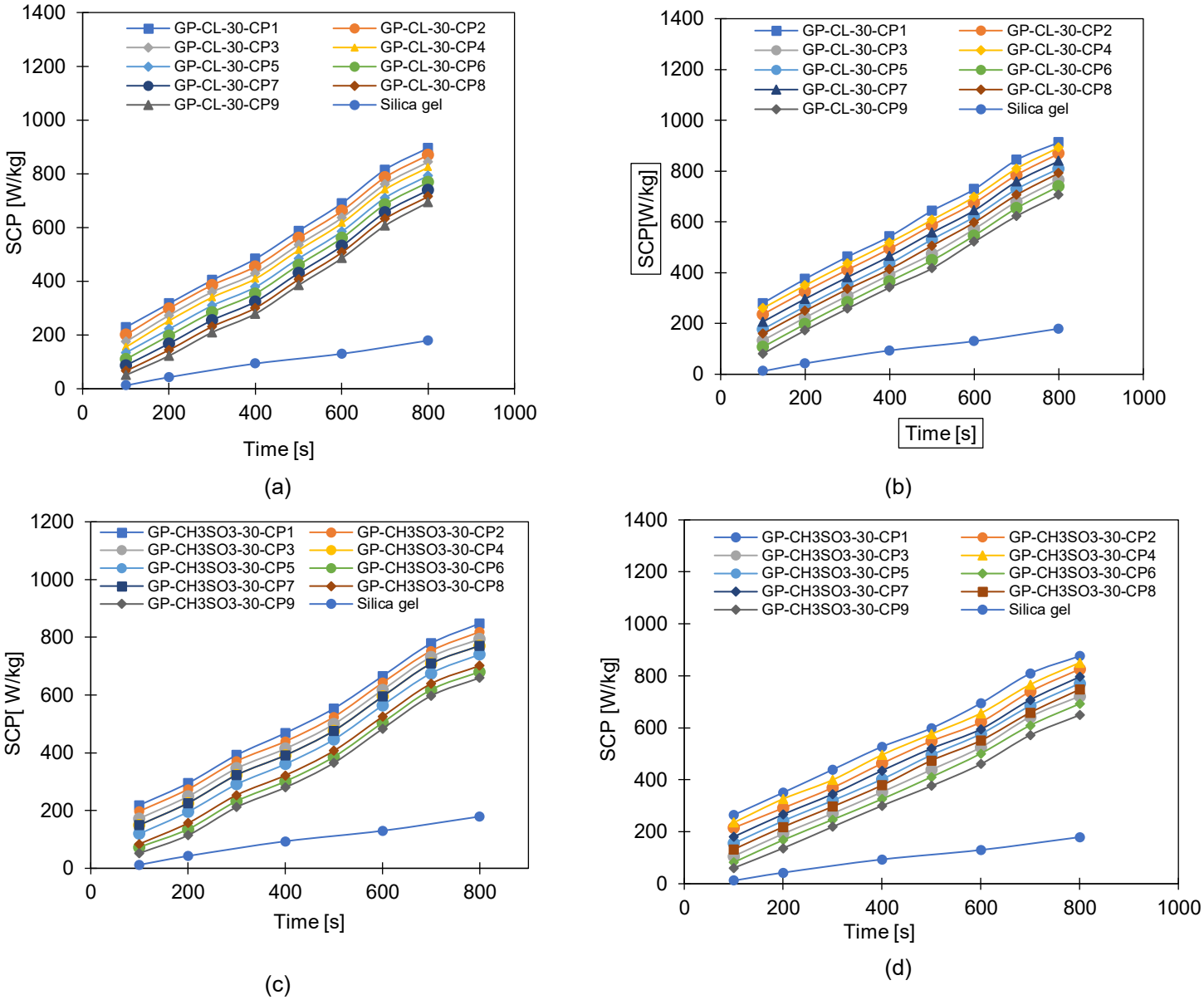

Figure 6.12: The effect of changing cycle time on SCP for GP-CL-30 CP1-CP9 and SG at(a) T_{ev}=12 ℃ and (b) T_{ev}=30 ℃ and GP-CH_3SO_3-30 CP1-CP9 and SG at (c) T_{ev}=12 ℃ and (d) T_{ev}= 30℃

The effect of increasing the cycle time at both the 12°C and 30°C evaporation temperatures was prominent in the GP/IL composite based systems than SG based system. As the cooling and water production increased so did the heat addition to the system causing an increase in COP. Similarly, the exergy increase was perceived as a ratio of the useful work in producing the desired outcome to the total heat added to the system. The observed results agree with previous work by Cao and Chung [164], which studied the influence of cycle time on the performance of the silica gel/water adsorption cooling system.

The changes in the system performance by varying the cycle time from 400 s to 800 s and across the investigated range (100 - 800 s) are quantified and summarised in Table 9.

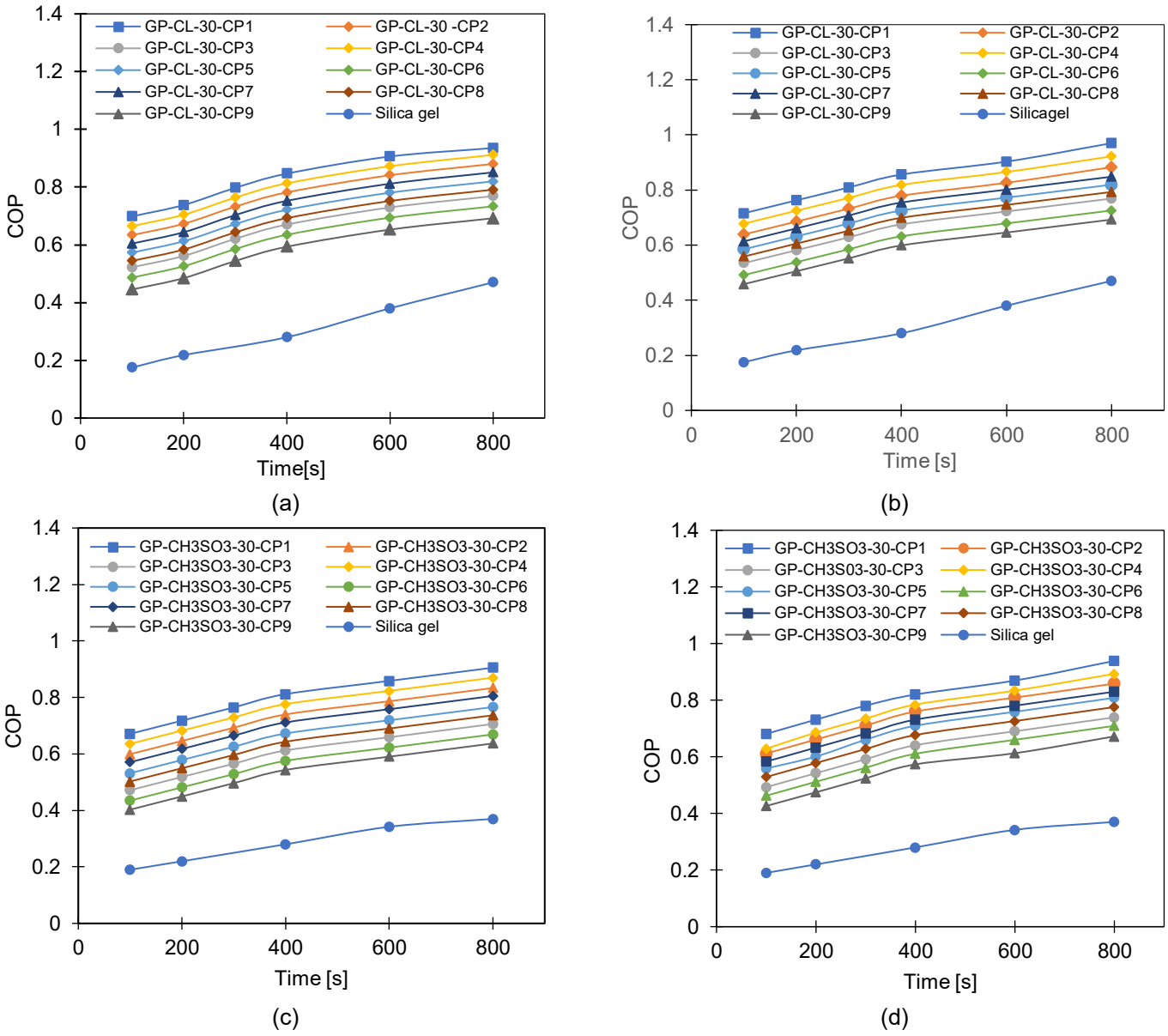

Figure 6.13: The effect of changing cycle time on COP for GP-CL-30 CP1-CP9 and SG at (a) T_{ev}=12 ℃ and (b) T_{ev}=30 ℃ and GP-CH_3SO_3-30 CP1-CP9 and SG at (c) T_{ev}=12 ℃ and (d) T_{ev}=30 ℃

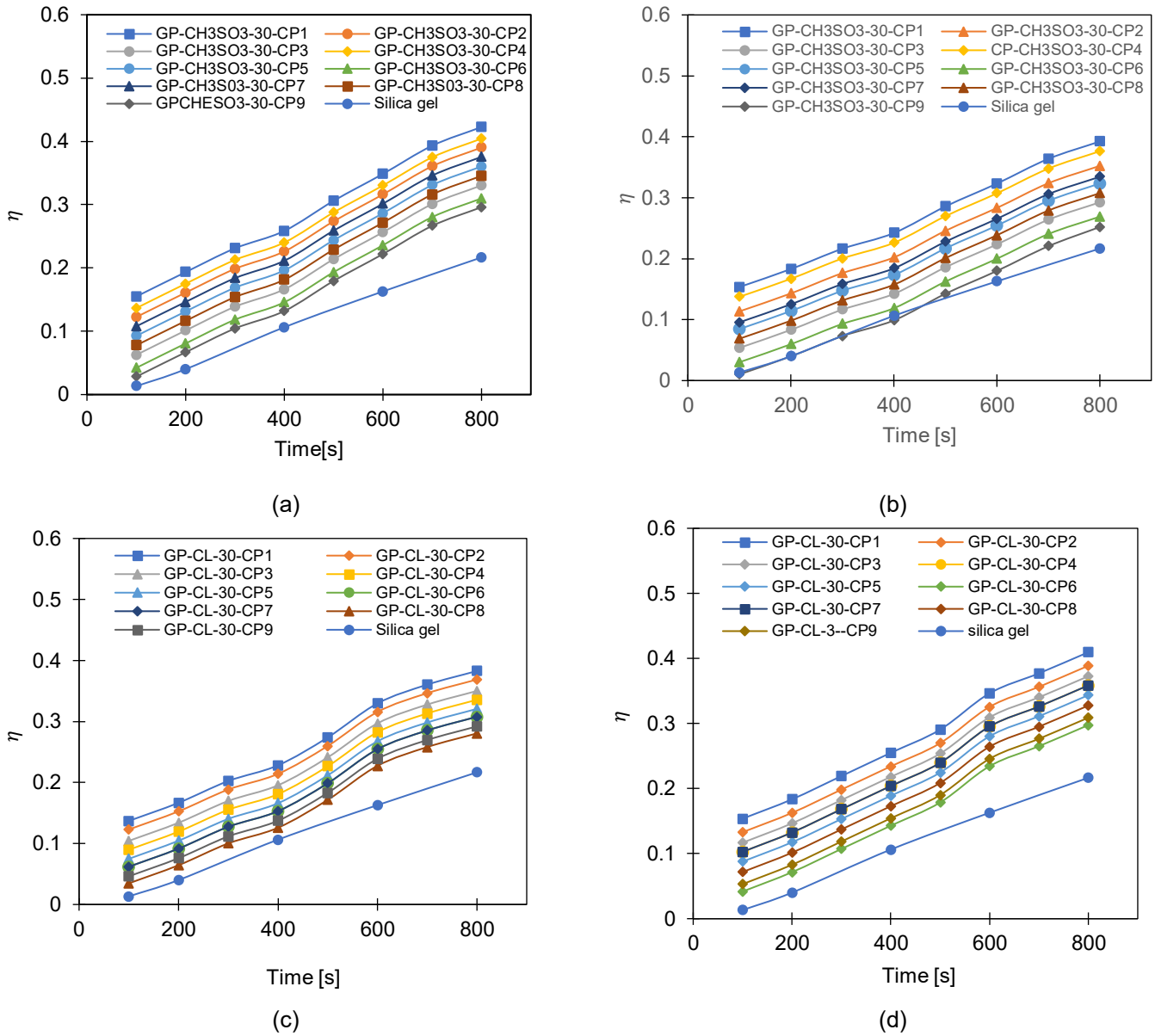

Figure 6.14: The effect of changing cycle time on Exergy efficiency for GP-CH_3SO_3-30 CP1-CP9 (a) T_{ev}=12 ℃, (b) T_{ev}=30 ℃ and GP-CL-30 CP1-CP9 and SG at (c) T_{ev}=12 ℃ and (d) T_{ev}=30 ℃

6.8.3 Effect of heat source temperature

The impact of varying the heat source temperature from 60℃ to 85℃ operating at evaporation temperature of 12℃ and 30°C, and maintaining the cooling water temperature, condensation temperature and cycle time at 35°C, 35°C and 800s respectively. The effect of increasing heating water temperature on the SDWP is shown in Figure 6.15. At 12℃ evaporation temperature, the increase in heat source temperature from 60℃ to 85℃ lead to an increase in the SDWP for the highest performing composite GP-CL-30-CP1 based system by 60% from (from 9 to 33m^3/day/ton) and by 53% (from 3.1 to 6.6m/day/ton) for the SG-based system.

An increase in SDWP for all the GP/IL composites and SG based systems was also observed with increasing heating water temperature from 60℃ to 85°C, operating at 30℃ evaporation temperature. GP-CL-30-CP1 based system had an increase of 77% (from 10 to 34.6m^3/day/ton), and SG-based system by 73% (from 5.2 to 19.5m^3/day/ton). GP-CL-30-CP1 based system performed better than SG based system on average by 42%.

The effect of increasing the heating water temperature from on the SCP is shown in figure 6.20. The results showed that the GP-CL-30-CP1 based system outperformed the SG based system by 32% operating at 12℃ evaporation temperature and by 40% operating at 30℃ evaporation temperature. The improved performance of GP-CL-30-CP1 confirmed the superiority of the thermal and adsorption properties of the GP/IL composites as observed in the SDWP performance. The higher cyclic water uptake performance of the GP/IL composites at system level, including the highest performing GP-CL-30-CP1 based system is attributed to composite material's high thermal response and faster adsorption rate which allows the attainment of equilibrium faster allowing it to capture more adsorbate at component level compared to SG. Increasing the heating water temperature from 60℃ to 85°C enhanced the SCP for GP-CL-30-CP1 based system operating by 305% (from 260 to 912.2W/kg) and SG-based system by 200.8% (from 9.2 to 75.47W/kg when operating at 12℃ evaporation temperature. The observed results in which system performance increases in terms of SDWP and SC with heat source temperature increases agrees with findings by Youssef et al [46], in their investigation of the influence of the heating water temperature on the SDWP for the water adsorption desalination system.

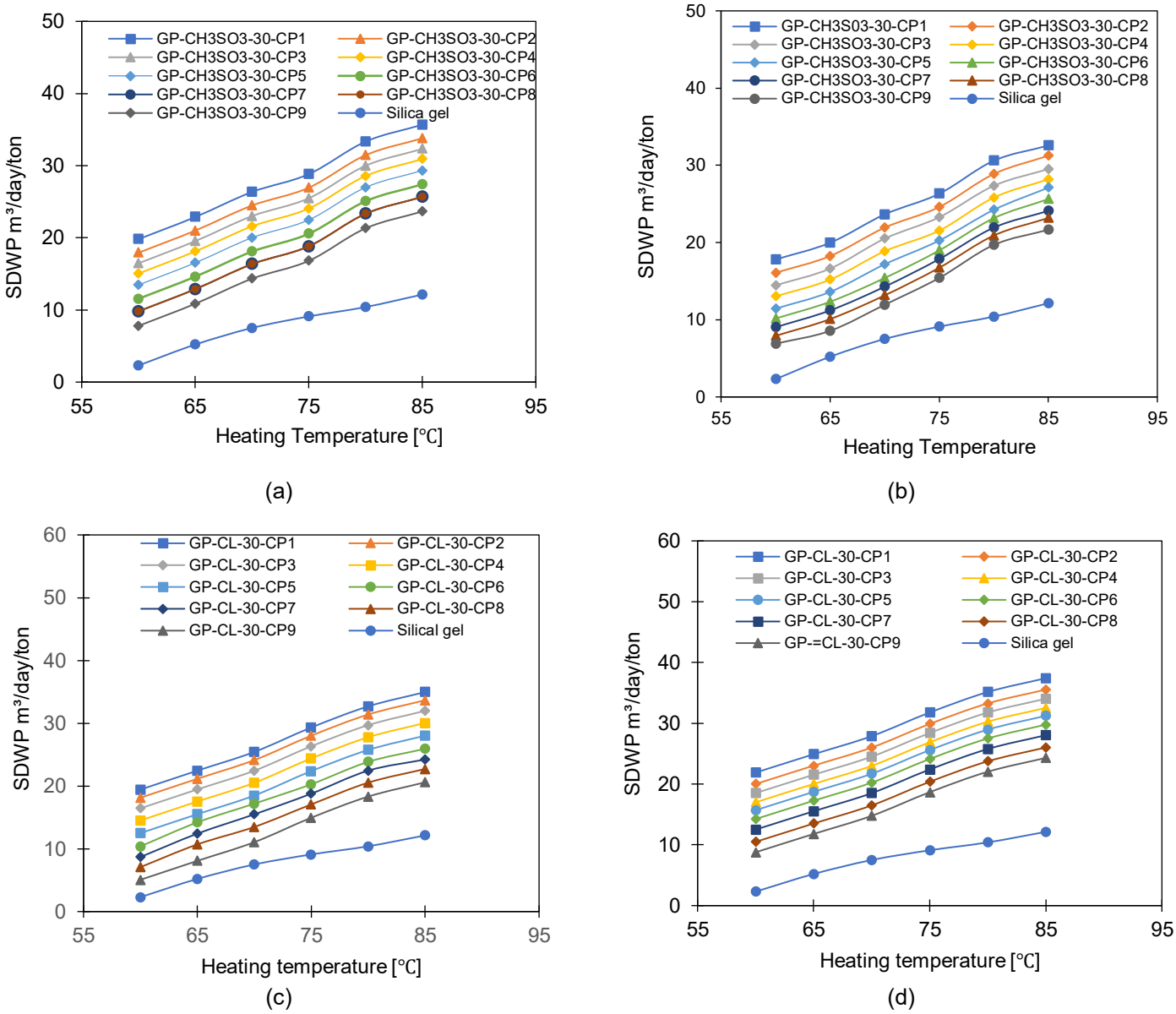

Figure 6.15: SDWP at different heating water temperatures for GP-CH_3SO_3-30 CP1-CP9 and SG at (a) T_{ev}=12 ℃ and (b) T_{ev}=30 ℃ and GP-CL-30 CP1-CP9 and SG at (c) T_{ev}=12 ℃ and (d) T_{ev}=30 ℃

The impact of heating water temperature increase on the COP and exergy of the system is shown in Figure 6.16 and Figure 6.17. It was observed that increasing the heat source temperature had an effect of increasing the COP while decreasing the exergy efficiency. The increase in COP was attributed to the increasing temperature difference between the heat source and the constant temperature cooling water allowing more cyclic water uptake at component level hence more water and cooling production. At material level the thermal properties of the adsorbent contributed to the efficient heat transfer in the adsorbent bed leading to an increased system COP.As for the exergy efficiency, increasing the heat source temperature leads to higher exergy destruction due to high temperature differences between the heat source and cooling medium thus reducing the system's exergy efficiency.

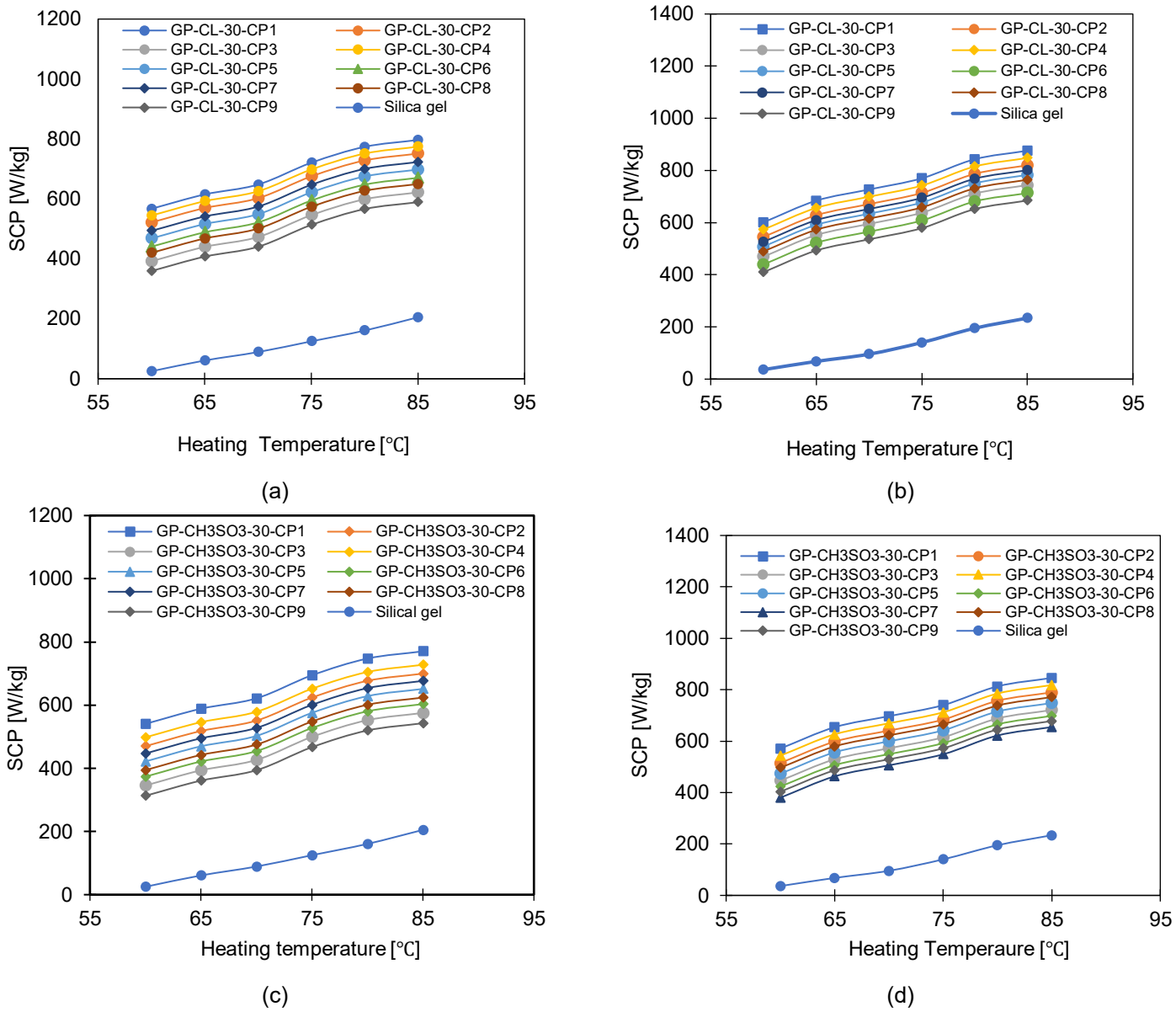

Figure 6.16: SCP at different heating temperatures for GP-CL-30 CP1-CP9 at (a) T_{ev}=12 ℃ and (b) T_{ev}=30 ℃ and GP-CH_3SO_3-30 CP1-CP9and SG at (c) T_{ev}=12 ℃ and (d) T_{ev}=30 ℃

Correspondingly, the COP of GP-CL-30-CP1 based system improved by102% (from 0.40 to 0.85) and for SG by 40.8% (from 0.154 to 0.40) operating at 12℃ evaporator temperature, whilst at 30℃ evaporation temperature an improvement of 79.4% (from 0.478 to 0.75) for GP-CL-30-CP1 based system and 72.5% (from 0.261 to 0.65) for SG based system when the heat source temperature was increased from 60°C to 85°C, respectively. On the other hand the decrease in exergy efficiency for the GP-CL-30-CP1 based system was by 42% (from 0.405 to 0.32) and for the SG-based system by 44.5% (from 0.218 to 0.121 operating at 12℃ evaporation temperature, while at 30℃ the decrease was by 29.6% (from 0.248 to 0.126) for GP-CL-30-CP1 based system and 74.3% (from 0.248 to 0.101) for SG based systems when the heat source temperature increased from 60°C to 85°C, respectively. The improved COP observed for the GP-CL-30-CP1based system which was on

average 40% and 37% higher than the SG based systems operating at 12°C and 30°C evaporation temperatures respectively was due the superior thermal and adsorption properties of GP-CL-30-CP1 compared to SG resulting in more efficient heat transfer and increase adsorption capacity to produce more water and cooling. The average COP for GP-CL-30-CP1based system was 76% and 70% high compared to SG based system operating at 12°C and 30°C evaporation temperatures. Although high regeneration temperature increases heat input during desorption and enhance exergy efficiency, it also leads to high exergy destruction impacting negatively on the exergy efficiency. The GP-CL-30-CP1 has a higher exergy efficiency due to its high adsorption capacity and rapid thermal response resulting in high energy conversion rate to produce more cooling and water. On the other hand, SG has low exergy efficiency caused by its inefficiencies in heat transfer and low adsorption capacity resulting in less cooling and water production than GP-CL-30-CP1 when the same heat source temperature is applied. These findings are in agreement with the parametric investigation undertaken by Cao and Chung [164], on a silica gel/water adsorption cooling system.

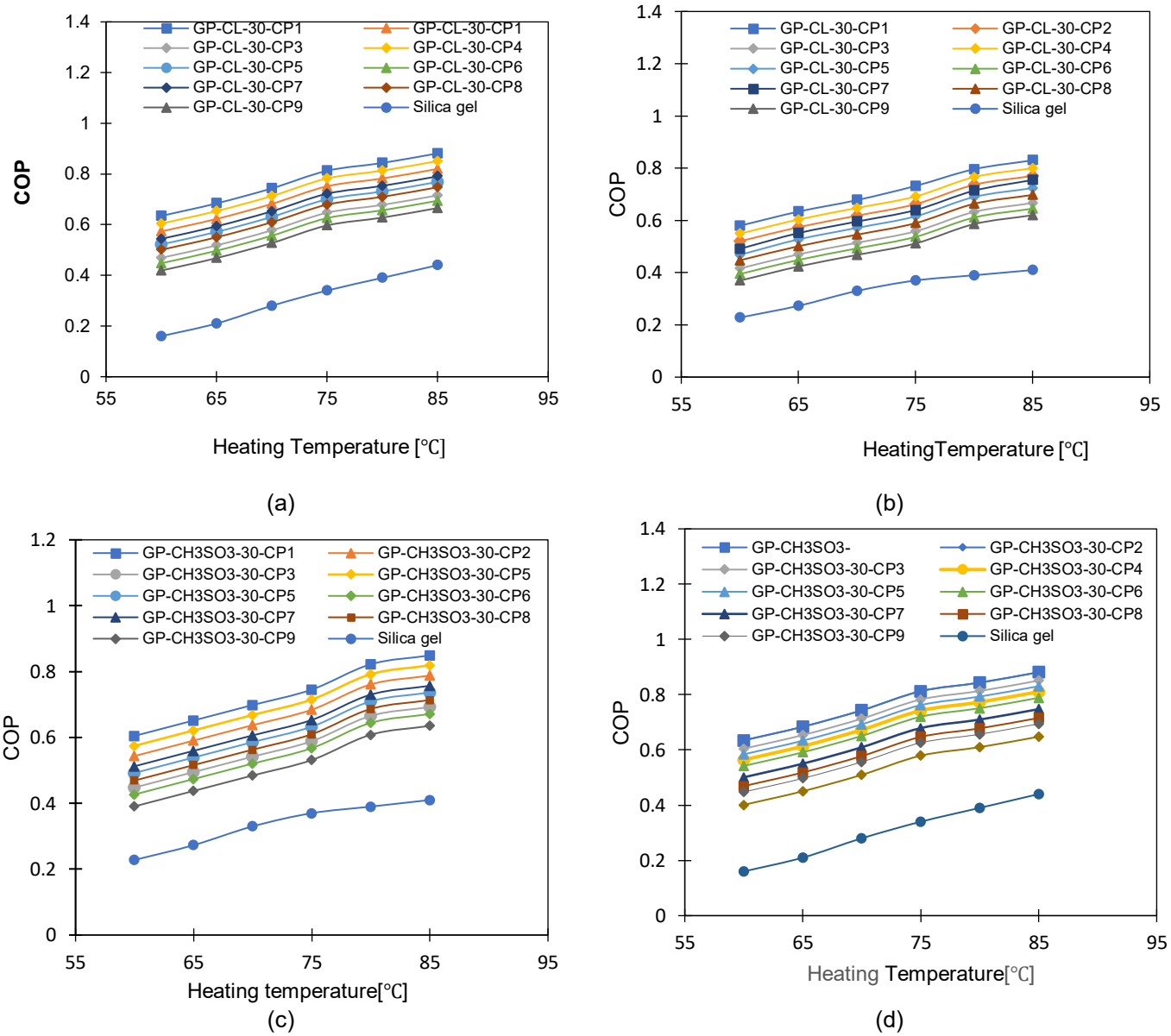

Figure 6.17: COP at different heating temperatures for GP-CL-30 CP1-CP9(a)Tev=12 ℃ and (b) Tev=30 ℃ and GP-CH3SO3-30 CP1-CP9 and SG at (c) T_{ev}=12 ℃ and (d) T_{ev}=30 ℃

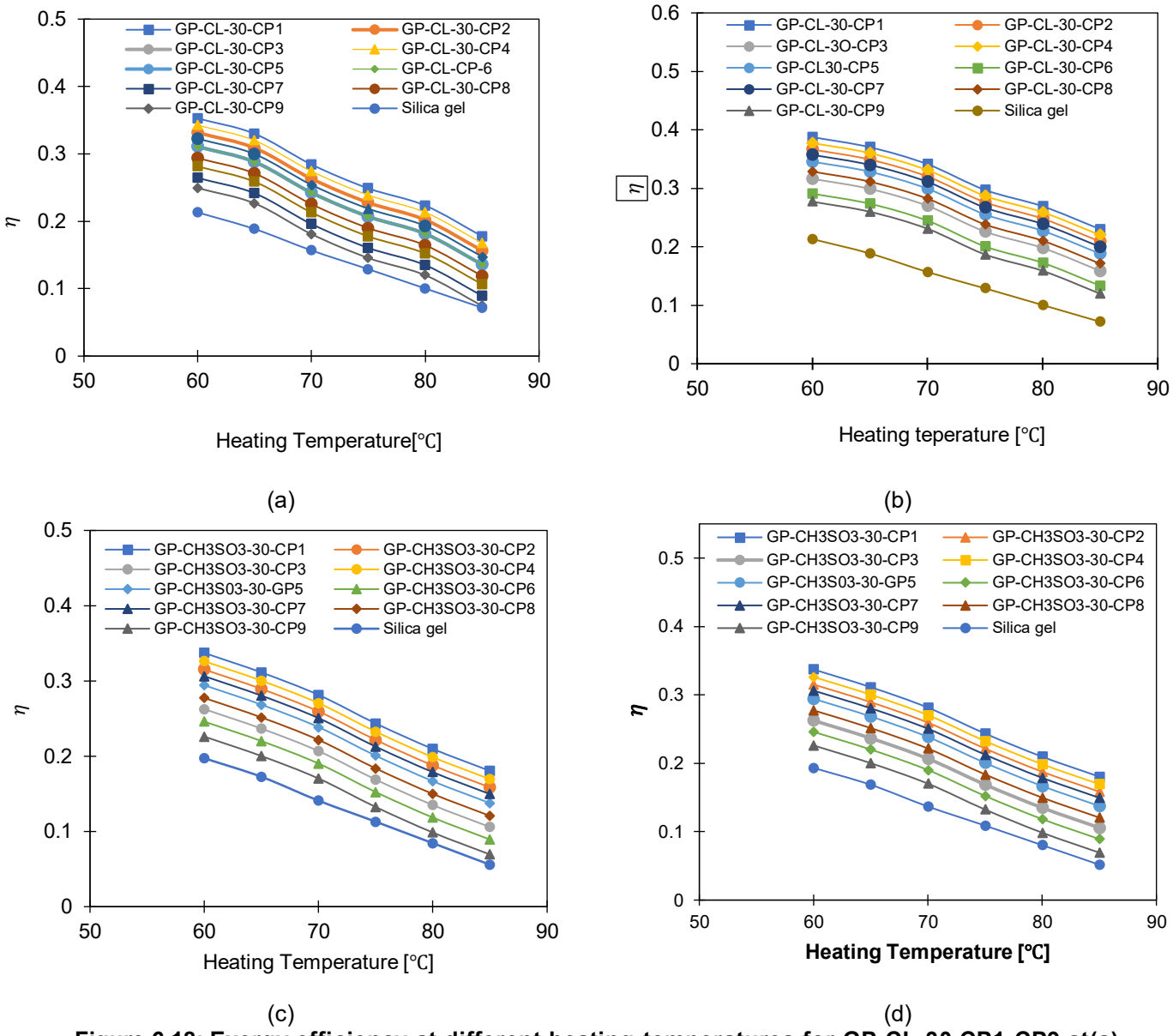

Figure 6.18: Exergy efficiency at different heating temperatures for GP-CL-30 CP1-CP9 at(a) T_{ev}=12 ℃ and (b) T_{ev}=30 ℃ and GP-CH3SO3-30 CP1-CP9 and SG at (c) T_{ev}=12 ℃ and (d) T_{ev}=30 ℃

6.9 Summary

This chapter presents the experimental and computational modelling investigation of GP/IL consolidated composites for use as adsorbents for cooling and desalination from their development utilising graphene nanoplatelets and Ionic liquids, to analysing their impact at component and system levels as well as overall energy conversion performance operating at various conditions. The determined thermal and adsorption characteristics of the developed GP/IL composites were benchmarked silica gel a baseline adsorbent. A 2D Multiphysics computational model was employed to analyse the impact of the GP/IL composites' heat transfer and mass transfer properties at adsorbent bed level. Furthermore, the effect of varying the evaporation temperature, cycle time and

heat source temperature on the adsorbent bed and system performance including energy conversion and exergy analysis was performed. The key findings are:

Key findings of the chapter are below.

- All the GP/IL composites had high thermal diffusivity compared to SG and GP-CL-30-CP7 had the highest. The higher thermal diffusivity coupled with high adsorption capacity had a significant influence on the thermal response of the adsorbent bed resulting in high cyclic water uptake operating at two different evaporation temperature. The high thermal properties in the GP/IL composites resulted in enhanced heat transfer which resulted in effective energy conversion thereby improve the exergy efficiency compared to SG.
- Enhanced heat transfer capabilities contribute to a more effective utilization of the available energy, improving exergy efficiency.
- The high thermal diffusivity of GP-CL-30-CP1 significantly influenced the thermal response of the adsorbent bed that advanced the cyclic water uptake at various evaporation temperatures, contradicting the equilibrium uptake cyclic predictions. Despite the faster heat transfer in the GP-CL-30-CP1 -based adsorbent bed increased exergy destruction, the exergy efficiency at the system level was availed. As a result, the SDWP, SCP, COP, and exergy efficiency for the GP-CL-30-CP1 -based system was 75–85.4%, 84–93%, 65-87.2% and 45–70.5% higher than the SG-based system when operated at 12-30°C.
- Increasing the cycle time increased the water uptake in both GP-CL-30-CP1 and SG since the adsorbent bed had a long time to reach closer to equilibrium uptake. As a result, the SDWP, SCP, COP, and exergy efficiency for the GP-CL-30-CP1 based system was higher than that of the SG-based system by 80%, 75%, 65% and 62% at 12°C evaporation temperature and by 95%, 75%, 76% and 68% at 30°C evaporation temperature. The GP-CL-30-CP1 based system outperformed the SG-based system due to a higher thermal response, which led to higher cyclic water uptake.
- Increasing the heat source temperature increased the exergy destruction and reduced exergy efficiency but enhanced the SDWP, SCP and COP. Moreover, the GP-CL-30-CP1 -based system's exergy efficiency was higher than the SG-based system across the investigated heat source temperatures by 80.7% and 70%, on average, at 12°C and 30°C evaporation temperatures; this was despite the higher exergy destruction in the former system at the adsorbent bed level.

Overall, this study concludes that having an advanced thermal diffusivity adsorbent material is crucial to exploit the advanced adsorption performance at the component level.

CHAPTER 7: CONCLUSION AND RECOMMENDATIONS

7.1 Introduction

Adsorption cooling and water desalination emerged as an alternative technology for providing fresh water and cooling in areas experiencing high temperatures. In addition, adsorption systems have the advantages of producing both clean water and cooling at the same time However, low heat and mass transfer in adsorption reactors lead to low energy conversion efficiency, which has caused them not to meet the demand for environmentally friendly cooling and water desalination systems. The problems associated with the adsorption systems highlights the motivation for research and innovative ways to improve the freshwater output and improve cooling efficiency. This chapter presents a summary of this PhD research findings highlighting the original contributions undertaken. In addressing the objectives of the study point by point response to the set objectives is given. An outline of the future work and is given.

7.2 Responses to objectives

Objective #1: To carry out a literature review on experimental and theoretical work carried out on adsorption desalination and cooling technology.

The literature review indicated that adsorption cooling and water desalination systems are highly regarded as the alternative to conventional cooling and water desalination systems owing to their ability to utilise low grade heat source such as waste heat, renewable solar and geothermal energies. The literature also revealed that:

a. Apart from saving energy and providing clean water and cooling simultaneously, the adsorption cooling and desalination systems has shown its viability in mitigating climate change using environmentally friendly materials and refrigerants. This has made it so attractive in this age where global warming needs to be addressed. This motivated the further research into these user friendly materials.
b. Although the adsorption cooling and water desalination systems have many advantages compared to conventional systems, they are characterised by Low heat and mass transfer in the current adsorption systems – leading to low energy conversion efficiency, hence poor clean water, and cooling production. This has been the main issue which has stalled their commercialisation and needed to be addressed. Therefore, the need to enhance the heat and mass transfer in adsorbent beds.
c. The adsorbents are key components of an efficient adsorption cooling and water desalination system. However, conventional adsorbents, such as silica gel and zeolite, have limited adsorption capacity and poor thermal characteristics. This has been the Achilles heel of the

performance of the adsorption cooling and water desalination systems. Researchers devoted their efforts to developing new parent adsorbents and composites of advanced adsorption and thermal characteristics. An example of advanced tuneable parent adsorbents is metal-organic frameworks (MOF). Despite these qualities, many MOFs are highly unstable, making them problematic to utilise in real-life applications. This highlighted the need for new adsorbent with improved thermal and adsorption properties.

d. A two bed system is the commonly used basic system for producing continuous clean water and cooling. Most recorded studies on adsorption systems focussed on enhancing the adsorption system performance by applying new adsorbents, adsorbent-bed heat exchange designs and adsorption cycle layouts. However, the poor heat transfer at the material level remains challenging. This indicated the need for computational investigation of the adsorbent bed to understand the impact of the adsorbents at component and system levels.

Objective #2: Investigate novel approaches to enhance the adsorption/desorption processes at the adsorption reactor/bed level.

The novelty aspect of the presented research is the use of highly thermal diffusive parent adsorbent to improve the heat and mass transfer in the adsorption bed. This involved the investigation of new adsorbent materials such as Graphene oxide, developing new composites using materials with high thermal properties (GNP)blended with Ionic liquid (IL) with attractive adsorption properties and synthesis of consolidated composites of GNP/IL with PVA binder. The numerical computation of the new adsorbents allowed an analysis of the influence of these adsorbents on the system's efficiency under various operating conditions benchmarking them with baseline adsorbent Silica gel to be performed. All the investigated adsorbent materials in this study performed better than silica gel in terms of thermal properties and adsorption capacity.

Objective #3 To develop and validate a 2D CFD modelling tool to predict the heat and mass transfer during adsorption/desorption processes in the adsorbent bed.

A 2D computational fluid dynamics (CFD) model was developed using Ansys Fluent to envisage the heat and mass transfer performance at the adsorbent bed level. The model was validated using experimental data provide in the literature. The model has proved to be a useful tool by accurately predicting the transient changes in adsorption /desorption process. This made it possible to study the influence of varying the heat source temperature, cycle time and evaporation temperature on the adsorbent bed and overall system performance. By undertaking energy and exergy analyses when utilising the new adsorbents packed in the adsorbent bed, it was possible to have insights into the efficiency of the energy conversion and help to optimise adsorbent bed performance. The dynamic temperature and water uptake profiles indicated how the thermal properties (thermal diffusivity)

influenced the thermal response of the adsorbent that advanced the cyclic water uptake at various evaporation temperatures, contradicting the equilibrium uptake cyclic predictions.

Objective #4: Study capabilities of new adsorbent materials to substitute traditional adsorbents through characterisation of new adsorbent materials Multi-layered Graphene derivatives.

An experimental investigation of the adsorption and thermal characteristics of Graphene Oxide as a new water sorbent for cooling cum desalination application and benchmark it against the baseline silica gel adsorbent was performed. This included the thermal test to obtain the thermal diffusivity using LFA and the adsorption characterisation using the DVA. The obtained thermal test results showed that graphene oxide enhances thermal performance by 44% compared to silica gel. While the adsorption performance of GO was enhanced by up to 57% compared to SG. The developed 2D Multiphysics computational model was successfully used to envisage the heat and mass transfer performance at the adsorbent bed level. The performance of the adsorption cooling and desalination cycle was investigated by various operating conditions such as varying the heat source temperature, cycle time and evaporation temperature on the adsorbent bed and overall system performance by undertaking energy and exergy analyses when utilising graphene oxide and silica gel. It was noted that these operating conditions influences the adsorption cooling and water desalination system's performance. Furthermore, graphene oxide, compared to silica gel as a parent adsorbent, enhanced the system's specific daily water production by up to 44.4%, the specific cooling power by up to 29.5%, the coefficient of performance by up to 17.2% and the exergy efficiency by up to 15.8%. The significance of this findings implies that GO can be utilised as an adsorbent where more water is a priority at evaporator temperature above 12℃.

Objective #5: Develop new Graphene nanoplatelets and Ionic liquid composites and investigate the adsorption and thermal characteristics of the developed composites benchmarking against traditional baseline adsorbent silica gel.

New composites were developed from Graphene nanoplatelets and Ionic liquid. The physical and thermal properties of GP was experimentally investigated to ascertain its suitability as a host matrix. The results showed that GP has a BET surface area of 56.8978 m^2/g, thermal diffusivity of 22.3mm^2/s and thermal conductivity of 7.36(W/mK) which are all considered very high compared with the baseline adsorbent silica gel. This indicated that GP is suitable to be used as a host matrix and with high thermal diffusivity, it can improve the heat transfer properties of composites. The new GP/IL composites were synthesised using the wet impregnation method. The adsorption characteristics and thermal properties of the developed composites were experimentally investigated and compared with silica gel. The results showed higher thermal diffusivity than the baseline adsorbent silica gel and the highest thermal diffusivity was 11.84 mm^2/s for GP-CH_3SO_3-10, 394 times higher than silica

gel. Water adsorption characteristics of the composites were carried out, and the cumulative advanced adsorption and thermal characteristics of the developed composites showed a higher cyclic performance by up to 82% and 85% respectively than that of the baseline silica gel. Further investigation on the system performance indicator results utilising the developed composites showed that the GP-IL composites performed better than SG in terms of the SDWP, SCP and COP. With the highest performer GP-CL- 30 having enhanced SDWP, SCP and COP than SG by 65%, 70% and 49% respectively. The GP-CL-30 composite is the optimal composite adsorbent for application as an adsorbent material to have a high impact on adsorption cooling and water desalination The significance of the findings is that novel adsorbent enhanced characteristics of the synthesized components can play a significant role in the next generation adsorption desalination and cooling applications."

Objective #6: Develop consolidated IL/GP composites using a binder and investigate the impact of various binder concentration and compressional pressure on the adsorption and thermal characteristics and compare with silica gel.

New GP/IL consolidated composites were developed comprising of GP host matrix, ILs (EMIMCH3SO3) and (EMIMCl), individually and PVA binder at various concentration (2, 5 and 10%). The composites were compressed under three different pressures (1, 1.5 and 2MPa). Eighteen composites CL-30-CP1-9 and GP-CH_3SO_3-30-CP1-9 were developed. The determined thermal and adsorption characteristics of the developed GP/IL composites were benchmarked against silica gel. The outstanding thermal diffusivity of GNP significantly improved the thermal response of the developed composite materials. In comparison to SG, all GP/IL composites exhibited notably high thermal diffusivity values particularly, the composite denoted as GP-CL-30-CP7. The influence of low PVA concentration of 2% binder material in the composite facilitated rapid movement of heat through the composite. On the other hand, the highest compression pressure of 2 MPa had great influence in reducing void spaces allowing better contact between particles to give efficient heat transfer. The highest thermal diffusivity value of 4.65mm^2/s was obtained, representing 12.7 times as large as SG. The SDWP, SCP, COP, and exergy efficiency for the GP-CL-30-CP1 based system were higher than that of the SG-based system by 80%, 75%, 65% and 62% at 12°C evaporation temperature and by 95%, 75%, 76% and 68% at 30°C evaporation temperature. GP-CL-30-CP1 was the most suitable composite for cooling and water desalination productivity especially where desalination is more preferred to cooling due to its overall performance at system level.

7.3 Future Work

The tremendous potential of GO as an adsorbent is a steppingstone to further research around the use of graphene derivatives. The methodology and model developed in this study could be used to explore the development of other novel materials and evaluate their heat and mass transfer at the material level for adsorption system applications, such as cooling, desalination and heat storage. This has the potential of testing a wide range of material combinations.

In addition to envisaging the heat and mass of the developed materials at component level using the CFD dynamic tool, it is worthy confirming the mass transfer performance of the materials developed by performing the permeability tests and large temperature jump tests. This will help to have more understanding of the new materials' adsorption properties. This requires collaboration with other institutions with the permeability test equipment and the large temperature jump instruments.

The design and layout of an adsorbent bed are pivotal to the overall performance of the adsorption systems. Another potential area of improvement is further modelling to optimise the heat exchanger design for the new materials to find acceptable trade-offs for all the design choices such as the geometry, fin height and fin spacing.

Lastly, the material investigated in this study could be tested on a large scale system, whether experimentally or through simulations to showcase their economic feasibility and feasibility for commercialisation. This requires collaboration with industrial partners to provide the testing facilities.

References

1. Saha, B.B., et al., *Fundamental and application aspects of adsorption cooling and desalination.* Applied Thermal Engineering, 2016. **97**: p. 68-76.
2. Elsheniti, M.B., et al., *Performance of a solar adsorption cooling and desalination system using aluminum fumarate and silica gel.* Applied Thermal Engineering, 2021. **194**: p. 117116.
3. Hua, W.S., H.J. Xu, and W.H. Xie, *Review on adsorption materials and system configurations of the adsorption desalination applications.* Applied Thermal Engineering, 2022. **204**: p. 117958.
4. El-Sharkawy, I.I., et al., *A study on consolidated composite adsorbents for cooling application.* Applied Thermal Engineering, 2016. **98**: p. 1214-1220.
5. Jribi, S., et al., *Corrected adsorption rate model of activated carbon–ethanol pair by means of CFD simulation.* International Journal of Refrigeration, 2016. **71**: p. 60-68.
6. Dong, Y., M. Coleman, and S.A. Miller, *Greenhouse Gas Emissions from Air Conditioning and Refrigeration Service Expansion in Developing Countries.* 2021. **46**(1): p. 59-83.
7. Choudhury, B., et al., *An overview of developments in adsorption refrigeration systems towards a sustainable way of cooling.* Applied Energy, 2013. **104**: p. 554-567.
8. Heredia-Aricapa, Y., et al., *Overview of low GWP mixtures for the replacement of HFC refrigerants: R134a, R404A and R410A.* International Journal of Refrigeration, 2020. **111**: p. 113-123.
9. Bengtsson, P. and T. Eikevik, *Reducing the global warming impact of a household heat pump dishwasher using hydrocarbon refrigerants.* Applied Thermal Engineering, 2016. **99**: p. 1295-1302.
10. Tso, C.Y., et al., *Experimental performance analysis on an adsorption cooling system using zeolite 13X/CaCl2 adsorbent with various operation sequences.* International Journal of Heat and Mass Transfer, 2015. **85**: p. 343-355.
11. Gong, L.X., et al., *Experimental study on an adsorption chiller employing lithium chloride in silica gel and methanol.* International Journal of Refrigeration, 2012. **35**(7): p. 1950-1957.
12. El-Sharkawy, I.I., et al., *Experimental investigation on activated carbon–ethanol pair for solar powered adsorption cooling applications.* International Journal of Refrigeration, 2008. **31**(8): p. 1407-1413.

13. Bai, S., et al., *Study of the salinity effects on the cooling and desalination performance of an adsorption cooling cum desalination system with a novel composite adsorbent.* Applied Thermal Engineering, 2020. **181**: p. 115879.

14. Jribi, S., et al., *CFD simulation and experimental validation of ethanol adsorption onto activated carbon packed heat exchanger.* International Journal of Refrigeration, 2017. **74**: p. 345-353.

15. Shaaban, M., et al., *Performance investigation of adsorption cooling and desalination systems employing thermally enhanced copper foamed bed coated with SAPO-34 and CPO-27 (Ni).* Applied Thermal Engineering, 2022. **205**: p. 118056.

16. Woo, S.-Y., et al., *Silica gel-based adsorption cooling cum desalination system: Focus on brine salinity, operating pressure, and its effect on performance.* Desalination, 2019. **467**: p. 136-146.

17. Thu, K., et al., *Performance investigation of a waste heat-driven 3-bed 2-evaporator adsorption cycle for cooling and desalination.* International Journal of Heat and Mass Transfer, 2016. **101**: p. 1111-1122.

18. Elsayed, E., et al., *CPO-27(Ni), aluminium fumarate and MIL-101(Cr) MOF materials for adsorption water desalination.* Desalination, 2017. **406**: p. 25-36.

19. Shiklomanov, I.A., *Appraisal and Assessment of World Water Resources.* Water International, 2000. **25**(1): p. 11-32.

20. Dhakal, N., et al., *Is desalination a solution to freshwater scarcity in developing countries?* Membranes, 2022. **12**(4): p. 381.

21. Rezk, A., G. Gediz Ilis, and H. Demir, *Experimental study on silica gel/ethanol adsorption characteristics for low-grade thermal driven adsorption refrigeration systems.* Thermal Science and Engineering Progress, 2022. **34**: p. 101429.

22. Gordon, J.M., et al., *The electro-adsorption chiller: a miniaturized cooling cycle with applications to micro-electronics.* International Journal of Refrigeration, 2002. **25**(8): p. 1025-1033.

23. Alsaman, A.S., et al., *Performance evaluation of a solar-driven adsorption desalination-cooling system.* Energy, 2017. **128**: p. 196-207.

24. Wang, L., et al., *Rational design, synthesis, adsorption principles and applications of metal oxide adsorbents: a review.* Nanoscale, 2020. **12**(8): p. 4790-4815.

25. Gabelman, A.J.C.E.P., *Adsorption basics: part 1.* 2017. **113**(7): p. 48-53.

26. Khalfaoui, M., et al., *New theoretical expressions for the five adsorption type isotherms classified by BET based on statistical physics treatment.* Journal of Colloid and Interface Science, 2003. **263**(2): p. 350-356.

27. Youssef, P.G., S.M. Mahmoud, and R.K. Al-Dadah, *Numerical simulation of combined adsorption desalination and cooling cycles with integrated evaporator/condenser.* Desalination, 2016. **392**: p. 14-24.

28. Zhang, Y., V. Palomba, and A. Frazzica, *Understanding the effect of materials, design criteria and operational parameters on the adsorption desalination performance – A review.* Energy Conversion and Management, 2022. **269**: p. 116072.

29. Ng, K.C., et al., *Solar-assisted dual-effect adsorption cycle for the production of cooling effect and potable water.* International Journal of Low-Carbon Technologies, 2009. **4**(2): p. 61-67.

30. Ali, E.S., et al., *Recycling brine water of reverse osmosis desalination employing adsorption desalination: A theoretical simulation.* Desalination, 2017. **408**: p. 13-24.

31. Sadri, S., M. Ameri, and R. Haghighi Khoshkhoo, *A new approach to thermo-economic modeling of adsorption desalination system.* Desalination, 2018. **428**: p. 69-75.

32. Kim, Y.-D., K. Thu, and K.C. Ng, *Adsorption characteristics of water vapor on ferroaluminophosphate for desalination cycle.* Desalination, 2014. **344**: p. 350-356.

33. Alsaman, A.S., et al., *A state of the art of hybrid adsorption desalination–cooling systems.* Desalination, 2016. **58**: p. 692-703.

34. Freni, A., et al., *Thermal conductivity of selective water sorbents under the working conditions of a sorption chiller.* Applied Thermal Engineering, 2002. **22**(14): p. 1631-1642.

35. Poyelle, F., J.-J. Guilleminot, and F. Meunier, *Experimental Tests and Predictive Model of an Adsorptive Air Conditioning Unit.* Industrial & Engineering Chemistry Research, 1999. **38**(1): p. 298-309.

36. Sharafian, A., et al., *Thermal conductivity and contact resistance of mesoporous silica gel adsorbents bound with polyvinylpyrrolidone in contact with a metallic substrate for adsorption cooling system applications.* International Journal of Heat and Mass Transfer, 2014. **79**: p. 64-71.

37. Vasiliev, L., D. Mishkinis, and L. Vasiliv Jr, *Multi-effect complex compound/ammonia sorption machines.* 1996.

38. Lu, Z.S. and R.Z. Wang, *Performance improvement and comparison of mass recovery in CaCl2/activated carbon adsorption refrigerator and silica gel/LiCl adsorption chiller driven by low grade waste heat.* International Journal of Refrigeration, 2013. **36**(5): p. 1504-1511.

39. Wang, D.C., et al., *Study of a Novel Silica gel-Water Adsorption Chiller: Part I. Design and Performance Prediction.* Int. J. Refrigeration, 2005. **28**(7): p. 1073.

40. Lai, H.-M., *An enhanced adsorption cycle operated by periodic reversal forced convection.* Applied Thermal Engineering, 2000. **20**(7): p. 595-617.

41. Oliveira, R.G., R.Z. Wang, and C. Wang, *Evaluation of the cooling performance of a consolidated expanded graphite–calcium chloride reactive bed for chemisorption icemaker.* International Journal of Refrigeration, 2007. **30**(1): p. 103-112.

42. Wang, K., et al., *Composite adsorbent of CaCl2 and expanded graphite for adsorption ice maker on fishing boats.* International Journal of Refrigeration, 2006. **29**(2): p. 199-210.

43. Mitra, S., et al., *Performance evaluation of a two-stage silica gel+ water adsorption based cooling-cum-desalination system.* International journal of refrigeration, 2015. **58**: p. 186-198.

44. Youssef, P.G., et al., *Experimental investigation of adsorption water desalination/cooling system using CPO-27Ni MOF.* Desalination, 2017. **404**: p. 192-199.

45. Al-Dadah, R., et al., *Metal-organic framework materials for adsorption heat pumps.* Energy, 2020. **190**: p. 116356.

46. Youssef, P.G., S.M. Mahmoud, and R.K.J.I.J.o.E. Al-Dadah, Chemical, Ecological, Geological Engineering, *Effect of evaporator temperature on the performance of water desalination/refrigeration adsorption system using AQSOA-ZO2.* International Journal of Environment,Chemical,Ecological,Geological Engineering, 2015. **9**: p. 679-83.

47. Alsaman, A.S., et al., *Experimental investigation of porous carbon for cooling and desalination applications.* npj Clean Water, 2023. **6**(1): p. 4.

48. Tamainot-Telto, Z. and R.E. Critoph, *Monolithic carbon for sorption refrigeration and heat pump applications.* Applied Thermal Engineering, 2001. **21**(1): p. 37-52.

49. Wang, K., et al., *Effective thermal conductivity of expanded graphite–CaCl2 composite adsorbent for chemical adsorption chillers.* Energy Conversion and Management, 2006. **47**(13): p. 1902-1912.

50. Pons, M., D. Laurent, and F. Meunier, *Experimental temperature fronts for adsorptive heat pump applications.* Applied Thermal Engineering, 1996. **16**(5): p. 395-404.

51. Zheng, X., et al., *Thermal conductivity, pore structure and adsorption performance of compact composite silica gel.* International Journal of Heat and Mass Transfer, 2014. **68**: p. 435-443.

52. Eun, T.-H., et al., *Enhancement of heat and mass transfer in silica-expanded graphite composite blocks for adsorption heat pumps: Part I. Characterization of the composite blocks.* International Journal of Refrigeration, 2000. **23**(1): p. 64-73.

53. Restuccia, G., A. Freni, and G. Maggio, *A zeolite-coated bed for air conditioning adsorption systems: parametric study of heat and mass transfer by dynamic simulation.* Applied Thermal Engineering, 2002. **22**(6): p. 619-630.

54. Al Mers, A., et al., *Optimal design study of cylindrical finned reactor for solar adsorption cooling machine working with activated carbon–ammonia pair.* Applied Thermal Engineering, 2006. **26**(16): p. 1866-1875.

55. Ji, X., et al., *Structure optimization and performance experiments of a solar-powered finned-tube adsorption refrigeration system.* Applied Energy, 2014. **113**: p. 1293-1300.

56. Demir, H., M. Mobedi, and S.J.i.j.o.r. Ülkü, *The use of metal piece additives to enhance heat transfer rate through an unconsolidated adsorbent bed.* international Journal of Refrigeration-Revue Internationale DuFroid, 2010. **33**(4): p. 714-720.

57. Sztekler, K., et al. *Effect of Metal Additives in the Bed on the Performance Parameters of an Adsorption Chiller with Desalination Function*. Energies, 2021. **14**, DOI: 10.3390/en14217226.

58. Pino, L., et al., *Composite materials based on zeolite 4A for adsorption heat pumps.* Adsorption, 1997. **3**(1): p. 33-40.

59. Wang, L.W., et al., *The performance of two adsorption ice making test units using activated carbon and a carbon composite as adsorbents.* Carbon, 2006. **44**(13): p. 2671-2680.

60. Teo, H.W.B., A. Chakraborty, and B. Han, *Water adsorption on CHA and AFI types zeolites: Modelling and investigation of adsorption chiller under static and dynamic conditions.* Applied Thermal Engineering, 2017. **127**: p. 35-45.

61. Lior, N., *Advances in water desalination*. Vol. 1. 2012: John Wiley & Sons.

62. Alghoul, M.A., et al., *Advances on multi-purpose solar adsorption systems for domestic refrigeration and water heating.* Applied Thermal Engineering, 2007. **27**(5): p. 813-822.

63. Askalany, A.A., et al., *A review on adsorption cooling systems with adsorbent carbon.* Renewable and Sustainable Energy Reviews, 2012. **16**(1): p. 493-500.

64. Faysal Hossain, M.D., N. Akther, and Y. Zhou, *Recent advancements in graphene adsorbents for wastewater treatment: Current status and challenges.* Chinese Chemical Letters, 2020. **31**(10): p. 2525-2538.

65. Li, T.X., et al., *A combined double-way chemisorption refrigeration cycle based on adsorption and resorption processes.* International Journal of Refrigeration, 2009. **32**(1): p. 47-57.

66. Srivastava, N.C. and I.W. Eames, *A review of adsorbents and adsorbates in solid–vapour adsorption heat pump systems.* Applied Thermal Engineering, 1998. **18**(9): p. 707-714.

67. Young, K., *Metal Hydrides☆*, in *Reference Module in Chemistry, Molecular Sciences and Chemical Engineering*. 2018, Elsevier.

68. Askalany, A.A., et al., *An overview on adsorption pairs for cooling.* Renewable and Sustainable Energy Reviews, 2013. **19**: p. 565-572.

69. Aristov, Y.I., *Challenging offers of material science for adsorption heat transformation: A review.* Applied Thermal Engineering, 2013. **50**(2): p. 1610-1618.

70. Ng, K.C., et al., *Adsorption desalination: An emerging low-cost thermal desalination method.* Desalination, 2013. **308**: p. 161-179.

71. Kulakowska, A., et al. *Effect of Metal and Carbon Nanotube Additives on the Thermal Diffusivity of a Silica Gel-Based Adsorption Bed*. Energies, 2020. **13**, DOI: 10.3390/en13061391.

72. Ng, K.C., et al., *Experimental investigation of the silica gel–water adsorption isotherm characteristics.* Applied Thermal Engineering, 2001. **21**(16): p. 1631-1642.

73. Zheng, X., et al., *Performance study of composite silica gels with different pore sizes and different impregnating hygroscopic salts.* Chemical Engineering Science, 2014. **120**: p. 1-9.

74. El Gamal, M., et al., *Bio-regeneration of activated carbon: A comprehensive review.* Separation and Purification Technology, 2018. **197**: p. 345-359.

75. Alsaman, A.S., et al., *Composite adsorbent materials for desalination and cooling applications: A state of the art.* 2022. **46**(8): p. 10345-10371.

76. Sayılgan, Ş.Ç., M. Mobedi, and S. Ülkü, *Effect of regeneration temperature on adsorption equilibria and mass diffusivity of zeolite 13x-water pair.* Microporous and Mesoporous Materials, 2016. **224**: p. 9-16.

77. Chan, K.C., et al., *Performance predictions for a new zeolite 13X/CaCl2 composite adsorbent for adsorption cooling systems.* International Journal of Heat and Mass Transfer, 2012. **55**(11): p. 3214-3224.

78. Grisel, R.J.H., S.F. Smeding, and R.d. Boer, *Waste heat driven silica gel/water adsorption cooling in trigeneration.* Applied Thermal Engineering, 2010. **30**(8): p. 1039-1046.

79. Shi, B., et al., *Mathematical and CFD modelling for a rectangular finned tube adsorption bed for automotive cooling system.* Proc. of ICAE, 2013.

80. Khan, N.A., Z. Hasan, and S.H. Jhung, *Beyond pristine metal-organic frameworks: Preparation and application of nanostructured, nanosized, and analogous MOFs.* Coordination Chemistry Reviews, 2018. **376**: p. 20-45.

81. Moumen, E., L. Bazzi, and S. El Hankari, *Metal-organic frameworks and their composites for the adsorption and sensing of phosphate.* Coordination Chemistry Reviews, 2022. **455**: p. 214376.

82. Tatlier, M., *Performances of MOF vs. zeolite coatings in adsorption cooling applications.* Applied Thermal Engineering, 2017. **113**: p. 290-297.

83. Küsgens, P., et al., *Characterization of metal-organic frameworks by water adsorption.* Microporous and Mesoporous Materials, 2009. **120**(3): p. 325-330.

84. Yuan, S., et al., *Stable Metal–Organic Frameworks: Design, Synthesis, and Applications.* Advanced Materials, 2018. **30**(37): p. 1704303.

85. Eddaoudi, M., et al., *Zeolite-like metal–organic frameworks (ZMOFs): design, synthesis, and properties.* Chemical Society Reviews, 2015. **44**(1): p. 228-249.

86. Lian, B., et al., *Extraordinary water adsorption characteristics of graphene oxide.* 2018. **9**(22): p. 5106-5111.

87. Ren, S., P. Rong, and Q. Yu, *Preparations, properties and applications of graphene in functional devices: A concise review.* Ceramics International, 2018. **44**(11): p. 11940-11955.

88. Lee, X.J., et al., *Review on graphene and its derivatives: Synthesis methods and potential industrial implementation.* Journal of the Taiwan Institute of Chemical Engineers, 2019. **98**: p. 163-180.

89. Johnson, D.J. and N. Hilal, *Can graphene and graphene oxide materials revolutionise desalination processes?* Desalination, 2021. **500**: p. 114852.

90. Oliveira, R.G., et al., *Novel composite sorbent for resorption systems and for chemisorption air conditioners driven by low generation temperature.* Renewable Energy, 2009. **34**(12): p. 2757-2764.

91. Carmona, M., E. Pérez, and M. Palacio, *Experimental evaluation of porosity, axial and radial thermal conductivity, of an adsorbent material composed by mixture of activated carbon,*

expanded graphite and lithium chloride. Applied Thermal Engineering, 2019. **150**: p. 456-463.

92. Fayazmanesh, K., S. Salari, and M. Bahrami, *Effective thermal conductivity modeling of consolidated sorption composites containing graphite flakes.* International Journal of Heat and Mass Transfer, 2017. **115**: p. 73-79.

93. Askalany, A.A., et al., *Effect of improving thermal conductivity of the adsorbent on performance of adsorption cooling system.* Applied Thermal Engineering, 2017. **110**: p. 695-702.

94. Wang, L.W., et al., *Study of thermal conductivity, permeability, and adsorption performance of consolidated composite activated carbon adsorbent for refrigeration.* Renewable Energy, 2011. **36**(8): p. 2062-2066.

95. Askalany, A.A., et al., *Water desalination by silica supported ionic liquid: Adsorption kinetics and system modeling.* Energy, 2022. **239**: p. 122069.

96. Tanashev, Y.Y., A.V. Krainov, and Y.I. Aristov, *Thermal conductivity of composite sorbents "salt in porous matrix" for heat storage and transformation.* Applied Thermal Engineering, 2013. **61**(2): p. 401-407.

97. Tso, C.Y. and C.Y.H. Chao, *Activated carbon, silica-gel and calcium chloride composite adsorbents for energy efficient solar adsorption cooling and dehumidification systems.* International Journal of Refrigeration, 2012. **35**(6): p. 1626-1638.

98. Aristov, Y.I., et al., *Reallocation of adsorption and desorption times for optimisation of cooling cycles.* International Journal of Refrigeration, 2012. **35**(3): p. 525-531.

99. Maruyama, T., *Chapter 6 - Carbon nanotubes*, in *Handbook of Carbon-Based Nanomaterials*, S. Thomas, et al., Editors. 2021, Elsevier. p. 299-319.

100. Tlili, I., et al., *Investigation of thermal characteristics of carbon nanotubes: Measurement and dependence.* Journal of Molecular Liquids, 2019. **294**: p. 111564.

101. Dellago, C., M.M. Naor, and G. Hummer, *Proton Transport through Water-Filled Carbon Nanotubes.* Physical Review Letters, 2003. **90**(10): p. 105902.

102. Kinloch, I.A., et al., *Composites with carbon nanotubes and graphene: An outlook.* Science, 2018. **362**(6414): p. 547-553.

103. Rocky, K.A., et al., *Recent advances of composite adsorbents for heat transformation applications.* Thermal Science and Engineering Progress, 2021. **23**: p. 100900.

104. Gordeeva, L.G. and Y.I. Aristov, *Composites 'salt inside porous matrix' for adsorption heat transformation: a current state-of-the-art and new trends.* International Journal of Low-Carbon Technologies, 2012. **7**(4): p. 288-302.

105. Restuccia, G., et al., *Selective water sorbent for solid sorption chiller: experimental results and modelling.* International Journal of Refrigeration, 2004. **27**(3): p. 284-293.

106. Hanif, S., M. Sultan, and T. Miyazaki, *Effect of relative humidity on thermal conductivity of zeolite-based adsorbents: Theory and experiments.* Applied Thermal Engineering, 2019. **150**: p. 11-18.

107. Rouhani, M., W. Huttema, and M. Bahrami, *Thermal conductivity of AQSOA FAM-Z02 packed bed adsorbers in open and closed adsorption thermal energy storage systems.* International Journal of Refrigeration, 2019. **105**: p. 158-168.

108. Rocky, K.A., et al., *Zeolite-graphene composite adsorbents for next generation adsorption heat pumps.* Microporous and Mesoporous Materials, 2021. **313**: p. 110839.

109. Younes, M.M., et al., *Synthesis and characterization of silica gel composite with polymer binders for adsorption cooling applications.* International Journal of Refrigeration, 2019. **98**: p. 161-170.

110. Pal, A., et al., *Ionic liquid as a new binder for activated carbon based consolidated composite adsorbents.* Chemical Engineering Journal, 2017. **326**: p. 980-986.

111. Toor, M. and B. Jin, *Adsorption characteristics, isotherm, kinetics, and diffusion of modified natural bentonite for removing diazo dye.* Chemical Engineering Journal, 2012. **187**: p. 79-88.

112. Donohue, M.D. and G.L. Aranovich, *Classification of Gibbs adsorption isotherms.* Advances in Colloid and Interface Science, 1998. **76-77**: p. 137-152.

113. Rouquerol, J., et al., *Adsorption by powders and porous solids: principles, methodology and applications*. 2013: Academic press.

114. Yahia, M.B., et al., *Models for Type VI Adsorption Isotherms from a Statistical Mechanical Formulation.* Adsorption Science & Technology, 2013. **31**(4): p. 341-357.

115. Zhang, P.J.K.G., *Adsorption and desorption isotherms.* 2016.

116. Lowell, S. and J.E. Shields, *Powder surface area and porosity (Vol. 2)*. 2013, Springer Science & Business Media London, UK.

117. Malek, A. and S.J.A.J. Farooq, *Comparison of isotherm models for hydrocarbon adsorption on activated carbon.* 1996. **42**(11): p. 3191-3201.

118. Zhang, P. and L. Wang, *Extended Langmuir equation for correlating multilayer adsorption equilibrium data.* Separation and Purification Technology, 2010. **70**(3): p. 367-371.

119. Foo, K.Y. and B.H. Hameed, *Insights into the modeling of adsorption isotherm systems.* Chemical Engineering Journal, 2010. **156**(1): p. 2-10.

120. Elmorsi, T.M., *Equilibrium Isotherms and Kinetic Studies of Removal of Methylene Blue Dye by Adsorption onto Miswak Leaves as a Natural Adsorbent %J Journal of Environmental Protection.* 2011. **Vol.02No.06**: p. 11.

121. Günay, A., E. Arslankaya, and İ. Tosun, *Lead removal from aqueous solution by natural and pretreated clinoptilolite: Adsorption equilibrium and kinetics.* Journal of Hazardous Materials, 2007. **146**(1): p. 362-371.

122. Dąbrowski, A., *Adsorption — from theory to practice.* Advances in Colloid and Interface Science, 2001. **93**(1): p. 135-224.

123. Ayawei, N., et al., *Adsorption of congo red by Ni/Al-CO3: equilibrium, thermodynamic and kinetic studies.* 2015. **31**(3): p. 1307.

124. Ghosal, R. and D.M. Smith, *Micropore characterization using the Dubinin-Astakhov equation to analyze high pressure CO2 (273 K) adsorption data.* Journal of Porous Materials, 1996. **3**(4): p. 247-255.

125. Sharafian, A. and M. Bahrami, *Assessment of adsorber bed designs in waste-heat driven adsorption cooling systems for vehicle air conditioning and refrigeration.* Renewable and Sustainable Energy Reviews, 2014. **30**: p. 440-451.

126. Zhang, L.Z., *Design and testing of an automobile waste heat adsorption cooling system.* Applied Thermal Engineering, 2000. **20**(1): p. 103-114.

127. Li, M., et al., *Metal foam packed adsorbent bed boosting the performance of the adsorption-based desalination and cooling system.* Energy Conversion and Management, 2022. **254**: p. 115250.

128. Niazmand, H., H. Talebian, and M. Mahdavikhah, *Bed geometrical specifications effects on the performance of silica/water adsorption chillers.* International Journal of Refrigeration, 2012. **35**(8): p. 2261-2274.

129. Hong, S.W., O.K. Kwon, and J.D. Chung, *Application of an embossed plate heat exchanger to adsorption chiller.* International Journal of Refrigeration, 2016. **65**: p. 142-153.

130. Mohsen, O.A., M.A.R. Muhammed, and B.O. Hasan, *Heat Transfer Enhancement in a Double Pipe Heat Exchanger Using Different Fin Geometries in Turbulent Flow.* Iranian

Journal of Science and Technology, Transactions of Mechanical Engineering, 2021. **45**(2): p. 461-471.

131. McCague, C., et al., *Lab-scale sorption chiller comparison of FAM-Z02 coating and pellets.* Applied Thermal Engineering, 2020. **173**: p. 115219.

132. Saleh, M.M., et al., *Experimental testing of wire finned heat exchanger coated with aluminium fumarate MOF material for adsorption desalination application.* Thermal Science and Engineering Progress, 2022. **28**: p. 101050.

133. Wang, L., D. Zhu, and Y. Tan, *Heat Transfer Enhancement on the Adsorber of Adsorption Heat Pump.* Adsorption, 1999. **5**(3): p. 279-286.

134. Jahan, I., et al., *Experimental study on the influence of metal doping on thermophysical properties of porous aluminum fumarate.* Heat transfer Engineering, 2021. **42**(13-14): p. 1132-1141.

135. Parker, W., R. Jenkins, and C. Butler, *Flash method of determining thermal diffusivity, heat capacity, and thermal conductivity.* Journal of Applied Sciences

1961. **32**(9): p. 1679-1684.

136. Wang, X.L., H.T. Chua, and L.Z. Gao, *A thermogravimetric analyzer for condensable gas adsorption under subatmospheric conditions.* Journal of Thermal Analysis and Calorimetry, 2007. **90**(3): p. 935-940.

137. Wang, X., et al., *Investigation on the isotherm of silica gel+water systems.* Journal of Thermal Analysis and Calorimetry, 2004. **76**(2): p. 659-669.

138. Lin, C.-I. and L.-H. Wang, *Rate equations and isotherms for two adsorption models.* Journal of the Chinese Institute of Chemical Engineers, 2008. **39**(6): p. 579-585.

139. Llano-Restrepo, M. and M.A. Mosquera, *Accurate correlation, thermochemistry, and structural interpretation of equilibrium adsorption isotherms of water vapor in zeolite 3A by means of a generalized statistical thermodynamic adsorption model.* Fluid Phase Equilibria, 2009. **283**(1): p. 73-88.

140. Stoeckli, F., T. Jakubov, and A. Lavanchy, *Water adsorption in active carbons described by the Dubinin–Astakhov equation.* Journal of the Chemical Society, Faraday Transactions, 1994. **90**(5): p. 783-786.

141. Malek, A. and S. Farooq, *Comparison of isotherm models for hydrocarbon adsorption on activated carbon.* AIChE Journal, 1996. **42**(11): p. 3191-3201.

142. Jahan, I., et al., *Energy efficient green synthesized MOF-801 for adsorption cooling applications.* Journal of Molecular Liquids, 2022. **345**: p. 117760.

143. Chakraborty, A., et al., *On the thermodynamic modeling of the isosteric heat of adsorption and comparison with experiments.* Applied Physics Letters, 2006. **89**(17): p. 171901.

144. Anderson, J.D. and J. Wendt, *Computational fluid dynamics*. Vol. 206. 1995: Springer.

145. Chhanwal, N., et al., *Computational fluid dynamics (CFD) modeling for bread baking process—a review.* 2012. **5**: p. 1157-1172.

146. Jeong, W. and J. Seong, *Comparison of effects on technical variances of computational fluid dynamics (CFD) software based on finite element and finite volume methods.* International Journal of Mechanical Sciences, 2014. **78**: p. 19-26.

147. Niazmand, H. and I. Dabzadeh, *Numerical simulation of heat and mass transfer in adsorbent beds with annular fins.* International Journal of Refrigeration, 2012. **35**(3): p. 581-593.

148. Jafari, A., et al., *Application of CFD technique to simulate enhanced oil recovery processes: current status and future opportunities.* Petroleum Science, 2020. **17**(2): p. 434-456.

149. Tu, J., et al., *Computational fluid dynamics: a practical approach*. 2023: Elsevier.

150. Denton, J.D., *Some Limitations of Turbomachinery CFD*. 2010. p. 735-745.

151. Jin, Y. and A.V.J.P.o.F. Kuznetsov, *Turbulence modeling for flows in wall bounded porous media: an analysis based on direct numerical simulations.* Physics of Fluids, 2017. **29**(4): p. 045102.

152. Nimvari, M., et al., *Numerical simulation of turbulent reacting flow in porous media using two macroscopic turbulence models.* Computers & Fluids, 2013. **88**: p. 232-240.

153. Jiao, S., Z.J.A.A.M. Xu, and Interfaces, *Selective gas diffusion in graphene oxides membranes: a molecular dynamics simulations study.* ACS Appl Mater Interfaces, 2015. **7**(17): p. 9052-9059.

154. Xia, B., D.-W.J.C. Sun, and e.i. agriculture, *Applications of computational fluid dynamics (CFD) in the food industry: a review.* Computers and Electronics in Agriculture, 2002. **34**(1-3): p. 5-24.

155. Khanam, M., et al., *Numerical investigation of small-scale adsorption cooling system performance employing activated carbon-ethanol pair.* Energies, 2018. **11**(6): p. 1499.

156. *Ansys Preprocessor*, in *The Finite Element Method and Applications in Engineering Using Ansys®*, E. Madenci and I. Guven, Editors. 2006, Springer US: Boston, MA. p. 83-148.

157. Albaik, I., et al., *Numerical and experimental investigation of multiple heat exchanger modules in cooling and desalination adsorption system using metal organic framework.* Energy Conversion and Management, 2022. **251**: p. 114934.

158. Sosnowski, M., J. Krzywanski, and R. Scurek, *A Fuzzy Logic Approach for the Reduction of Mesh-Induced Error in CFD Analysis: A Case Study of an Impinging Jet.* Entropy, 2019. **21**(11): p. 1047.

159. Ozen, M. *Meshing workshop*. Academia 2014; Available from: https://www.academia.edu/download/51822095/MESHING_WORKSHOP_2014.pdf.

160. Winterton, R.H., *Where did the Dittus and Boelter equation come from?* International journal of heat mass transfer, 1998. **41**(4-5): p. 809-810.

161. Otowa, T., R. Tanibata, and M. Itoh, *Production and adsorption characteristics of MAXSORB: High-surface-area active carbon.* Gas Separation & Purification, 1993. **7**(4): p. 241-245.

162. El-Sharkawy, I.I., et al., *Adsorption of ethanol onto parent and surface treated activated carbon powders.* International Journal of Heat and Mass Transfer, 2014. **73**: p. 445-455.

163. Sharifzadeh, M., M. Ghazikhani, and H. Niazmand, *Temporal exergy analysis of adsorption cooling system by developing non-flow exergy function.* Applied Thermal Engineering, 2018. **139**: p. 409-418.

164. Cao, N.V. and J.D.J.E.T. Chung, *Exergy analysis of adsorption cooling systems based on numerical simulation.* Energy Technology, 2019. **7**(1): p. 153-166.

165. Chua, H., et al., *Entropy generation analysis of two-bed, silica gel-water, non-regenerative adsorption chillers.* 1998. **31**(12): p. 1471.

166. Thu, K., et al., *Entropy generation analysis of an adsorption cooling cycle.* International Journal of Heat and Mass Transfer, 2013. **60**: p. 143-155.

167. Liu, C., et al., *Recent Advance on Graphene in Heat Transfer Enhancement of Composites.* ES Energy & Environment, 2018. **2**: p. 31-42.

168. Choi, Y.R., et al., *Role of oxygen functional groups in graphene oxide for reversible room-temperature NO2 sensing.* Carbon, 2015. **91**: p. 178-187.

169. Liu, L., et al., *Sorption equilibria, kinetics, and temperature-swing adsorption performance of polyethyleneimine-impregnated silica for post-combustion carbon dioxide capture.* Separation and Purification Technology, 2021. **266**: p. 118582.

170. Rogers, G.F.C. and Y.R. Mayhew, *Thermodynamic and transport properties of fluids*. 5th ed. 1995: John Wiley & Sons.

171. Baiju, V. and C.I.J.o.S.E. Muraleedharan, *Energy and exergy analysis of solar hybrid adsorption refrigeration system.* International Journal of Sustainable Engineering, 2013. **6**(4): p. 289-300.

172. Li, M., et al., *Computational fluid dynamic study on adsorption-based desalination and cooling systems with stepwise porosity distribution.* Desalination, 2021. **508**: p. 115048.

173. Wang, X. and K.C. Ng, *Experimental investigation of an adsorption desalination plant using low-temperature waste heat.* Applied Thermal Engineering, 2005. **25**(17): p. 2780-2789.

174. Thu, K., et al., *Performance investigation on a 4-bed adsorption desalination cycle with internal heat recovery scheme.* Desalination, 2017. **402**: p. 88-96.

175. Youssef, P.G., S.M. Mahmoud, and R.K. Al-Dadah, *Performance analysis of four bed adsorption water desalination/refrigeration system, comparison of AQSOA-Z02 to silica-gel.* Desalination, 2015. **375**: p. 100-107.

176. Elsayed, E., et al., *Experimental testing of aluminium fumarate MOF for adsorption desalination.* Desalination, 2020. **475**: p. 114170.

177. Askalany, A., et al., *Silica-Supported Ionic Liquids for Heat-Powered Sorption Desalination.* ACS Applied Materials & Interfaces, 2019. **11**(40): p. 36497-36505.

178. Pal, A., et al., *Activated carbon and graphene nanoplatelets based novel composite for performance enhancement of adsorption cooling cycle.* Energy Conversion and Management, 2019. **180**: p. 134-148.

179. Zhao, Y., et al., *Measurements of ionic liquids thermal conductivity and thermal diffusivity.* Journal of Thermal Analysis and Calorimetry, 2017. **128**(1): p. 279-288.

180. Chua, H.T., et al., *Adsorption Characteristics of Silica Gel + Water Systems.* Journal of Chemical & Engineering Data, 2002. **47**(5): p. 1177-1181.

181. Muttakin, M., et al., *Theoretical framework to evaluate minimum desorption temperature for IUPAC classified adsorption isotherms.* International Journal of Heat Mass Transfer, 2018. **122**: p. 795-805.

182. Rupam, T.H., et al., *Thermodynamic property surfaces for various adsorbent/adsorbate pairs for cooling applications.* International Journal of Heat and Mass Transfer, 2019. **144**: p. 118579.

183. Askalany, A.A., A. Freni, and G. Santori, *Supported ionic liquid water sorbent for high throughput desalination and drying.* Desalination, 2019. **452**: p. 258-264.

184. Mitra, S., et al., *Modeling study of two-stage, multi-bed air cooled silica gel+water adsorption cooling cum desalination system.* Applied Thermal Engineering, 2017. **114**: p. 704-712.

185. Banda, H., et al., *Experimental and computational study on utilising graphene oxide for adsorption cooling and water desalination.* Applied Thermal Engineering, 2023. **229**: p. 120631.

186. Oliveira, R.G. and R.Z. Wang, *A consolidated calcium chloride-expanded graphite compound for use in sorption refrigeration systems.* Carbon, 2007. **45**(2): p. 390-396.

187. Cacciola, G., G. Restuccia, and L. Mercadante, *Composites of activated carbon for refrigeration adsorption machines.* Carbon, 1995. **33**(9): p. 1205-1210.

188. Xu, S.Z., et al., *A zeolite 13X/magnesium sulfate–water sorption thermal energy storage device for domestic heating.* Energy Conversion and Management, 2018. **171**: p. 98-109.

189. Li, S.L., et al., *Study on the adsorption isosteres of the composite adsorbent CaCl2 and expanded graphite.* Energy Conversion and Management, 2011. **52**(2): p. 1501-1506.

190. El-Sharkawy, I.I., et al., *Adsorption of ethanol onto parent and surface treated activated carbon powders.* International Journal of Heat and Mass Transfer, 2014. **73**: p. 445-455.

191. Wang, L.W., et al., *Development of thermal conductive consolidated activated carbon for adsorption refrigeration.* Carbon, 2012. **50**(3): p. 977-986.

192. Chua, H.T., et al., *Adsorption characteristics of silica gel+ water systems.* Chemical Engineering Data, 2002. **47**(5): p. 1177-1181.

193. Wu, C.-H., et al., *Enhancing the thermal conductivity of the heat exchanger in a noncompressive system as a means of energy efficiency improvement of the system.* International journal of green energy, 2009. **6**(5): p. 490-507.